Tropical Climate Variability from the Last Glacial Maximum to the Present

by

Kristina Ariel Dahl

B.A. Boston University, 1999

Submitted to the MIT/WHOI Joint Program in partial fulfillment of the requirements for the degree of

Doctor of Philosophy

at the

MASSACHUSETTS INSTITUTE OF TECHNOLOGY

and the

WOODS HOLE OCEANOGRAPHIC INSTITUTION

September, 2005

Signature of Author .....

Joint Program in Oceanography
Massachusetts Institute of Technology
and Woods Hole Oceanographic Institution
May 20, 2005

Certified by .....

Dr. Delia Oppo
Thesis Supervisor
Woods Hole Oceanographic Institution

Accepted by .....

Dr. Gregory Hirth
Chair, Joint Committee for Marine Geology and Geophysics
Associate Scientist
Woods Hole Oceanographic Institution

Tropical Climate Variability from the Last Glacial Maximum to the Present

by

Kristina Ariel Dahl

Submitted to the Department of Marine Geology and Geophysics,
Massachusetts Institute of Technology–Woods Hole Oceanographic Institution,
Joint Program in Oceanography
on May 20, 2005, in partial fulfillment of the
requirements for the degree of
Doctor of Philosophy

Abstract

This thesis evaluates the nature and magnitude of tropical climate variability from the Last Glacial Maximum to the present. The temporal variability of two specific tropical climate phenomena is examined. The first is the position of the Intertropical Convergence Zone (ITCZ) in the Atlantic basin, which affects sea surface temperature (SST) and precipitation patterns throughout the tropical Atlantic. The second is the strength of the Indian Monsoon, an important component of both tropical and global climate.

Long–term variations in the position of the ITCZ in the Atlantic region are determined using both organic geochemical techniques and climate modeling. Upwelling in Cariaco Basin is reconstructed using chlorin steryl esters as proxies for phytoplankton community structure. We find that the diatom population was larger during the Younger Dryas cold event, indicating that upwelling was enhanced and the mean position of the ITCZ was farther south during the Younger Dryas than it is today. A climate simulation using an ocean–atmosphere general circulation model confirms these results by demonstrating that the ITCZ shifts southward in response to high–latitude cooling.

The climate of the Arabian Sea region is dominated by the Indian Monsoon. Results from modern sediments from a suite of cores located throughout the Arabian Sea suggest that wind strength is well represented by the accumulation rate and carbon isotopic composition of terrestrially–derived plant waxes in sediments. Arabian Sea SST patterns, reconstructed from a suite of sediment cores representing four time slices utilizing the Mg/Ca SST proxy, suggest that both the summer and winter monsoons were enhanced 8,000 yr BP relative to today while the summer monsoon was weaker and the winter monsoon stronger at 15,000 and 20,000 yr. These results are confirmed by a time–series reconstruction of SST on the Oman Margin that reveals that SST at this site is sensitive to both regional and global climate processes. The results of this thesis demonstrate that tropical climate, as evaluated by a number of different proxies as well as climate models, has varied substantially over the past 20,000 years and is closely coupled to climate at high–latitudes.

Acknowledgments

During my orientation to the Joint Program, I was told to look around the room at my classmates. These were the people, I was told, on whom I would be relying on for help, for friendship, and for inspiration for the next few years. I rolled my eyes impatiently and smugly assured myself that I didn't need anyone's help. I had no idea then that the community of Woods Hole is filled with people whose help with science, as well as with the rest of life, would be something I would come to treasure.

My Ph.D. adviser, Delia Oppo allowed me to follow my own interests and to develop my own projects without ever letting me stray too far down the wrong path. Our converstaions science, as well as those about balancing science and the rest of your life, have helped to shape my career and my priorities in many positive ways. Very early on in my graduate career, Bill Curry gave me the good advice to always focus on the questions I'm asking rather than the techniques I'm using. During the many moments of feeling bogged down in the details of work, his words echoed in my mind and reminded me of why I had come to graduate school in the first place. Each in their own way, the other members of my committee, Karen Bice, Konrad Hughen, and Julian Sachs, have influenced this work by sharing ideas, opinions, and enthusiasm. Dan Repeta was the first to offer me the opportunity to come to WHOI and for that opportunity I will always be grateful.

This thesis would have taken me double the time if not for the help of many assistants. Sean Sylva, Carl Johnson, Luping Zou, Rindy Ostermann, and Marti Jeglinski, and the whole Fye gang provided both technical and emotional support as I explored the murky waters of geochemistry. The members of the WHOI Academic Programs Office are bona fide miracle workers when it comes to navigating the Joint Program, and they pretty much knew my name before I did when I arrived in Woods Hole. Many thanks to Hugh Birmingham and the employees of Coffee Obsession, who, unbeknownst to them, witnessed the writing of much of this thesis.

The students of the Joint Program take it from being a great program in which to get a degree to being a great program in which to grow and have fun. I was fortunate to have several classmates whose interests also lie in the field of paleoclimate. These students, Rose Came, Mea Cook, Dave Lund, and Matt Makou, have been inspiring to learn and work with as we all begin our careers in the same field. Almost from day one in the Joint Program, Rachel Wisniewski, Helen White, and Cara Santelli became my good friends and confidants. Together we've hosted barbeques, designed costumes for a plethora of P–parties, and spent hours strolling on the bike path talking about life. Carmina Mock, Beckett Coppola, Pascale Poussart, and the many many students who have come to my yoga classes have, for the past few years, been inspiring me to smile, to be patient, and to teach. Many thanks also go to Rhea Workman, Mea Cook, and John McGrath, three exceptionally insightful and kind people whose conversations about the pursuit of happiness will always stick with me.

I would not have made it through graduate school without the support of a few very important people. Dave Ting was the first person to encourage me to apply to graduate school, and assured me that if he could make it through MIT, so could I. His enthusiasm for science and learning was truly inspiring. Once in graduate school, Falk Feddersen

encouraged me to stay there while hearing out my fantasies of becoming a professional chef and a yoga teacher. His unwavering belief in me, whether I am a scientist or a triathlete by trade, continues to be a source of strength. Most of all, I thank my family for always making sure that I knew that I could be anything I wanted to be and that they would be there cheering me on.

This work was funded by the National Science Foundation (OCE02–20776 and OCE03–34598 to D. Oppo), a Schlanger Ocean Drilling Program Fellowship, a WHOI Watson Fellowship, and a Fye Teaching Fellowship.

Contents

Chapter 1

Introduction

The tropics, delimited by the Tropic of Cancer to the north and the Tropic of Capricorn to the south, cover 50% of Earth's surface area. While this balmy band of latitude is generally known for its relatively stable year–round climate, the tropics are, in fact, home to some of the most dramatic and influential climatic processes that take place on Earth. Phenomena such as the El Niño Southern Oscillation (ENSO) and the Asian monsoon system have climatically and societally relevant impacts not only within the tropical regions in which they occur, but also throughout extratropical regions (*Webster*, 1987; *Lau and Nath*, 1996; *Klein et al.*, 1999).

The exact nature of the climatic interactions occurring between the tropics and extratropics remains an open question. Over the course of the glacial–interglacial cycles of the past 800,000 years, the high latitudes have experienced much larger fluctuations in climate than the low latitudes. This pattern of large changes within high latitudes and small changes in the tropics was demonstrated most effectively by the CLIMAP study of 1981, a study of global sea surface temperatures at the Last Glacial Maximum (~20,000 years ago; *CLIMAP Project Members*, 1981). The CLIMAP study led to the widely held belief that the high latitudes were the drivers of climate change while the tropics were simply passive recorders of the propagation of high latitude signals to lower latitudes (*e.g. Porter and An*, 1995). In the past decade, however, that view has been challenged by a growing number of studies suggesting that tropical climate undergoes much larger changes than implied by CLIMAP (*e.g. Hostetler and Mix*, 1999) and by a growing understanding of the propagation of tropical climate signals into higher latitudes (*Trenberth et al.*, 1998). This has led some to suggest that global climate can be driven by tropical processes (*Cane*, 1998; *Clement and Cane*, 1999; *Clement et al.*, 2001). The contrast between the results of the CLIMAP study and those of subsequent studies has fueled much research into the nature and variability of tropical climate.

Until recently, paleoclimate research was primarily focused on the high latitudes. Polar ice cores (*e.g. Petit et al.*, 1999) have provided very detailed records of Quaternary climate variability in the high latitudes while comparable resolution records of tropical climate variability are just beginning to emerge (*e.g. Haug et al.*, 2001; *Wang et al.*, 2001).

In order to evaluate the the relationship between tropical and extratropical climate on long (i.e. millennial to orbital) timescales, it is critical to develop high quality climate records from throughout the tropical region such that they can be compared to the wealth of information from the extratropics. This thesis focuses on two tropical climate phenomenon that are strongly connected to high latitude climate in the modern climate regime. Chapters 2 and 3 examine variations in the latitudinal position of the Intertropical Convergence Zone (ITCZ) in the tropical Atlantic during the Younger Dryas cold event. Chapters 4–6 focus on fluctuations in the strength of the Indian Monsoon from the Last Glacial Maximum (LGM) to the present.

1.1 Tropical Atlantic Climate and the ITCZ

The ITCZ is a band of low atmospheric pressure generated by the convergence of the trade wind systems of the northern and southern hemispheres. This band, which is characterized by high precipitation, migrates seasonally between 10°N and 5°S. During northern hemisphere (i.e. boreal) summer, the ITCZ is at its northermost position, and northern South America is relatively dry. High precipitation occurs in northern South America during boreal winter, when the ITCZ migrates into the southern hemisphere. Similar seasonal precipitation variations occur over the African continent, although the distribution of precipitation over land is highly dependent upon the geographic configuration of the continent. Over Africa, the ITCZ manifests itself as a latitudinally defined band over northern Africa during boreal summer and a 7–shaped region of relatively high precipitation during boreal winter.

The ITCZ preferrentially migrates to the warmer hemisphere such that when the Northern Hemisphere is cold, the ITCZ migrates into the Southern Hemisphere (*Broccoli et al.*, 2005). This migration can be observed today on seasonal timescales both in models and in nature and has been postulated to occur on longer (i.e. millennial to orbital) timescales (*Haug et al.*, 1998). If this is the case, then paleoclimate records of precipitation and/or trade wind strength throughout the tropical Atlantic should be able to detect long–term changes in the mean position of the ITCZ. Several studies have suggested that the mean

position of the ITCZ was further south than it is today during the Younger Dryas, a cold event that began about 13,000 years ago (13 ka) and lasted roughly 1300 years (*Hughen et al.*, 1996; *Lin et al.*, 1997; *Lea et al.*, 2003; *Hughen et al.*, 2004). This thesis presents two lines of evidence suggesting that, indeed, it is likely that the ITCZ was further south during the Younger Dryas than it is today.

1.1.1 Reconstructing the phytoplankton community of the Cariaco Basin during the Younger Dryas

The Cariaco Basin, located just north of Venezuela, is uniquely positioned to record changes in the position of the ITCZ. During boreal winter, strong trade winds induce upwelling and, in turn, strong primary productivity, in the basin. During boreal summer, the trade winds over the basin ease and upwelling ceases. These seasonal changes in upwelling and primary productivity are associated with seasonal variability in the types of phytoplankton that populate the upper water column (*de Miro*, 1971; *Ferraz-Reyes*, 1983; *Muller-Karger et al.*, 2001). Chapter 2 of this thesis utilizes a suite of organic biomarkers, chlorin steryl esters (CSEs), as tracers of the abundance of various phytoplanktonic classes, such as diatoms and dinoflagellates, through time. These compounds are widespread in marine and lacustrine environments and have been shown to be relatively resilient to diagenesis (*Talbot et al.*, 1999a, 2000, and references therein), making them ideal biomarkers. This work is the first to apply CSEs to the reconstruction of past environments. The data presented in Chapter 2 suggest that CSEs can yield valuable information about the structure of phytoplankton communities in the past. Furthermore, it is shown that, during the Younger Dryas cold event, the phytoplankton community in the Cariaco Basin underwent dramatic and rapid changes that imply significantly enhanced upwelling in the basin during the Younger Dryas. This scenario is consistent with a southward migration of the ITCZ during this time.

1.1.2 North Atlantic freshwater forcing as a driver of tropical Atlantic climate change

Chapter 3 presents further evidence for a southward shift of the ITCZ during North Atlantic cold events, this time as determined from the results of a modeling study. In this study, freshwater was applied to the North Atlantic region of a coupled ocean–atmosphere general circulation model. The motivation for perfoming such an experiment stems from the hypothesis that millennial–scale climate changes can be driven by rapid inputs of freshwater to the North Atlantic (*Broecker et al.*, 1985, 1988). Such freshwater inputs may weaken the formation of North Atlantic Deep Water (NADW) and, as a consequence, cause changes in climate by redistributing the heat normally transported via the NADW overturning cell. Historically, such modeling experiments have been unable to simulate large changes outside of the North Atlantic region. By performing an ensemble of three identical experiments, this study shows that climate change within the North Atlantic region does, indeed, have an effect on the climate of the tropical Atlantic. Specifically, when the North Atlantic cools, tropical Atlantic sea surface temperatures warm and the ITCZ shifts southward, altering precipitation patterns throughout South America and Africa. These changes are generally consistent with Younger Dryas climate reconstructions from throughout the tropical Atlantic basin, although the magnitude of change predicted by the model is smaller than that implied by the paleoclimate reconstructions.

1.2 The Indian Monsoon

The word "monsoon" is derived from the Arabic "mausem" meaning "season." All monsoons are characterized by a seasonal reversal in wind direction caused by differential heating between land and ocean. The Indian Monsoon is a particularly vigorous monsoon system due to the presence of the Tibetan Plateau, which serves to amplify the differential heating. During boreal summer, the Asian continent is heated more effectively than the Arabian Sea, causing a gradient from higher pressure over the ocean to lower pressure over the land. This pressure gradient drives moisture–laden winds from the southwest

over the Arabian Sea and onto the Asian continent, bringing heavy rain to India. During boreal winter, the pressure gradient is reversed and dry winds blow from the northeast from the continent to the Arabian Sea. The seasonal cycle of rains and droughts in monsoon–affected regions has a significant impact on the lives of millions of people, particularly those whose livelihood depends upon agriculture. Understanding the full range of monsoonal variability under a variety of climate regimes is critical to the development and sustainablity of monsoon–affected communities and cultures. This thesis examines the history of the Indian Monsoon from the LGM to the present using two different approaches.

1.2.1 Plant waxes as tracers of monsoon winds

Terrestrial plant leaf waxes, produced by all higher plants (*Gulz*, 1994), contain a suite of organic compounds that are ablated from living plants and delivered to the marine environment by wind (*e.g. Hadley and Smith*, 1989; *Ohkouchi et al.*, 1997; *Huang et al.*, 2000; *Rommerskirchen et al.*, 2003). Because the presence of these compounds in marine sediments indicates a terrestrial source, plant waxes can be used to reconstruct the strength and source of winds. Chapter 4 presents a quantification and carbon isotopic analysis of plant waxes in core–top (i.e. modern) sediments from throughout the Arabian Sea. As is evident from the map views contained within Chapter 4, these data suggest that plant waxes are delivered to the Arabian Sea by summer monsoon winds, winter monsoon winds, and summer northwesterly winds from the Arabian Peninsula/Mesopotamian region. The west–to–east carbon isotopic gradient of the plant waxes appears to be a good proxy for the strength and position of the summer monsoon winds. Determination of this gradient through time would therefore be a valid means by which to reconstruct summer monsoon winds.

1.2.2 Arabian Sea sea surface temperatures as tracers of monsoon strength

The summer monsoon winds over the Arabian Sea induce a strong coastal upwelling system offshore of Somalia and Oman. This upwelling depresses sea surface temperatures (SST) in the western Arabian Sea by 4°C relative to the eastern Arabian Sea. Recon-

structing this sea surface temperature gradient through time should then yield information about the strength of upwelling in the western Arabian Sea and, in turn, the strength of the summer monsoon winds. Chapter 5 of this thesis presents a time–slice view of Arabian Sea SST as a means of assessing this gradient. In this chapter, SST is determined via the Mg/Ca ratio of planktonic foraminifera from a suite of cores throughout the Arabian Sea for four distinct time intervals (0 ka, 8 ka, 15 ka, and 20 ka). In contrast to traditional paleoceanographic reconstructions of SST that focus on one site, these data yield snapshots of the regional response to climate changes upon which changes in monsoon strength are superimposed.

Chapter 6 presents time–series of SST from sediment cores on the Oman and Pakistan Margins. Both records again utilize the Mg/Ca SST proxy. The Oman Margin record spans the last 20 kyr and demonstrates large changes in SST, some of which are coherent with large climate changes in the North Atlantic region, suggesting a global forcing mechanism, others of which are likely to be driven purely by changes in the strength of the Indian Monsoon. This record suggests that the early to mid–Holocene was a time of a stronger than present summer monsoon. The Pakistan Margin time–series, spanning the time period from 5 ka to the present, records a decrease in the strength of the winter monsoon over this time period.

1.3 Future Directions

The results of this thesis paint a picture of tropical climate that is much more dynamic and variable than previously thought. This work is like most other scientific work in which we place one foot in front of the other, relying on a solid past in order to take a tiny step forward. Here, off balance and adjusting to our new view of the world, we find that there are a multitude of places for our other foot to land. The field of paleoclimate is relatively young. One could place her foot almost anywhere next and be certain of being on new ground. Each step brings us closer to answering some of the most challenging climate questions: Do changes in tropical climate propagate outside of their regional confines? How might these changes affect or be affected by ENSO? What does the future hold for

these wondrous climate processes?

Chapter 2

Reconstructing the phytoplankton community of the Cariaco Basin during the Younger Dryas cold event using chlorin steryl esters

This work originally appeared as:

Dahl, K. A., D. J. Repeta, and R. Goericke, Reconstructing the phytoplankton community of the Cariaco Basin during the Younger Dryas cold event using chlorin steryl esters, Paleoceanography, 19, PA1006, 2003PA000907, 2004.

Reconstructing the phytoplankton community of the Cariaco Basin during the Younger Dryas cold event using chlorin steryl esters

Kristina A. Dahl

Massachusetts Institute of Technology, Woods Hole Oceanographic Institution Joint Program in Oceanography and Ocean Sciences, Woods Hole, Massachusetts, USA

Daniel J. Repeta

Woods Hole Oceanographic Institution, Woods Hole, Massachusetts, USA

R. Goericke

Scripps Institution of Oceanography, La Jolla, California, USA

Received 1 April 2003; revised 13 October 2003; accepted 7 November 2003; published 29 January 2004.

[1] A record of the downcore distribution of chlorin steryl esters (CSEs) through the Younger Dryas was produced from Cariaco Basin sediments in order to assess the potential use of CSEs as recorders of the structure of phytoplankton communities through time. Using an improved high-performance liquid chromatography method for the separation of CSEs, we find significant changes in the distribution of CSEs during the Younger Dryas in the Cariaco Basin. During the Younger Dryas, enhanced upwelling in the Cariaco Basin caused an increase in the diatom population and therefore an increase in the relative abundance of CSEs derived from diatoms. In contrast, the dinoflagellate population, and therefore CSEs derived from dinoflagellates, decreased in response to the climate change during the Younger Dryas. These community shifts agree well with the shifts observed in the present day on a seasonal basis that result from the north-south migration of the Intertropical Convergence Zone over the Cariaco Basin. We also identify changes in the abundance of several CSEs that seem to reflect rapid warming and cooling events. This study suggests that CSEs are useful proxies for reconstructing phytoplankton communities and paleoenvironments. *INDEX TERMS:* 1055 Geochemistry: Organic geochemistry; 4267 Oceanography: General: Paleoceanography; 4855 Oceanography: Biological and Chemical: Plankton; *KEYWORDS:* Younger Dryas, Cariaco Basin, chlorin steryl esters

Citation: Dahl, K. A., D. J. Repeta, and R. Goericke (2004), Reconstructing the phytoplankton community of the Cariaco Basin during the Younger Dryas cold event using chlorin steryl esters, *Paleoceanography, 19*, PA1006, doi:10.1029/2003PA000907.

1. Introduction

[2] Chlorin steryl esters (CSEs) (Figure 1) consist of pyropheophorbide-a (a chlorophyll-a degradation product) and various sterols [e.g., *King and Repeta*, 1991]. Chlorophyll-*a* is the major photosynthetic pigment of all oxygenic photoautotrophs and can be used as a biomarker for phytoplankton-derived organic matter in sediments. Chlorophyll-*a* is rapidly degraded in the water column during zooplankton ingestion. One of the major degradation products is pyropheophorbide-*a*. Because chlorophyll-*a* degrades so rapidly and cannot be uniquely linked to a single class of phytoplankton, it cannot be used to track changes in the composition of the phytoplankton community through time.

[3] Sterols are a subset of the lipid class that has been well studied due to their ubiquity in algae and heterotrophs. Sterols that are geochemically important biomarkers have 27–30 carbon atoms and consist of a four-ring system onto which a variety of side chains are attached. The side chains, or R groups, attached to the ring structures allow for a wide range of sterol structures (Figure 2). Sterols have been utilized extensively because they exhibit the traits of good biomarkers: they are relatively refractory in the water column, and they can be traced back to known biological precursors [e.g., *Volkman*, 1986; *Volkman et al.*, 1993; *Meyers*, 1997; *Volkman et al.*, 1998]. The main issue confronting the use of sterols as biomarkers, however, is that sterols degrade at different rates. More specifically, 4-methyl sterols, found mainly in dinoflagellates [*Volkman et al.*, 1998], exhibit enhanced preservation relative to 4-desmethyl sterols [*Gagosian et al.*, 1980; *Wolff et al.*, 1986; *Harvey et al.*, 1989]. The free sterol distribution could therefore overestimate the dinoflagellate constituent of the phytoplankton community [e.g., *Pearce et al.*, 1998]. Furthermore, the ability to reconstruct the relative abundances of different phytoplankton classes could be affected by the amount of diagenesis that has taken place in the sediments.

0883-8305/04/2003PA000907$12.00

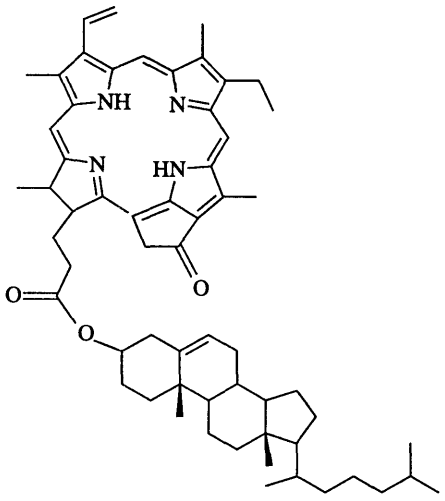

Figure 1. Structure of pyropheophorbide-*a* cholesteryl ester, a typical chlorin steryl ester.

While this problem may not be significant in recent sediments, it could become more significant in sediments heavily affected by diagenesis.

1.1. Formation of CSES in the Marine Environment

[4] Recent studies of zooplankton grazing and senescence-induced changes [*Harradine et al.*, 1996; *King and Wakeham*, 1996; *Talbot et al.*, 1999a, 1999b, 2000] have confirmed the finding of *King and Repeta* [1991, 1994] that CSEs are formed during zooplankton herbivory when the sterols produced by phytoplankton become esterified to pyropheophorbide-*a*, a chlorin. Several studies suggest that the conversion of sterols to CSEs occurs nonselectively during the grazing process [*King and Repeta*, 1991; *Harradine et al.*, 1996; *Talbot et al.*, 1999a]. That is, the structure of a sterol does not affect whether or not it esterifies to the pyropheophorbide-*a* molecule. Thus the distribution of CSE sterols reflects the sterols in algae that are grazed by herbivorous zooplankton and therefore the distribution of different classes (e.g., diatoms, dinoflagellates, red algae, etc.) of phytoplankton in the water column [e.g., *Pearce et al.*, 1998].

[5] After their formation in the water column, CSEs and other chlorins arrive at the seafloor via fecal pellets [*King*, 1993; *Talbot et al.*, 1999a]. Within sediments, CSEs exhibit enhanced preservation relative to both other chlorins [*Talbot et al.*, 1999a, and references therein] and free sterols [*King and Repeta*, 1991, 1994; *Talbot et al.*, 2000]. The enhanced preservation of CSE sterols relative to free sterols has been inferred from stanol/stenol ratios of the two groups of compounds [*King and Repeta*, 1991, 1994; *Pearce et al.*, 1998], which provide an estimate of the amount of degradation each type of compound has experienced [*Wakeham*, 1989]. CSE sterols have a low stanol/stenol ratio relative to free sterols, which indicates that they are less affected by microbial degradation [*King and Repeta*, 1991, 1994; *Pearce et al.*, 1998]. While several studies have now noted the enhanced preservation of CSE sterols relative to free sterols, a definitive mechanism for this phenomenon has not yet been demonstrated. As a result of their enhanced preservation, the distribution of CSE sterols in sediments reflects the distribution of water column sterols more closely than the sedimentary free sterol distribution does [*King and Repeta*, 1991, 1994; *Pearce et al.*, 1998]. Although CSEs do degrade once they reach the seafloor, the best available evidence suggests that the distribution of esterified sterols does not change during degradation; that is, there is no preferential degradation of a given CSE [*Talbot et al.*, 2000].

[6] CSEs exhibit the structural diversity of water column sterols while circumventing the problem of differential degradation that affects free sterol distributions. This feature of CSEs has prompted many to suggest that sedimentary CSEs could record the structure of phytoplankton communities through time [*King and Repeta*, 1994; *Harradine et al.*, 1996; *Pearce et al.*, 1998; *Talbot et al.*, 1999a]. However, only one study to date [*King and Repeta*, 1994] has made correlations between community structure and CSE sterol distributions. Our study evaluates the potential

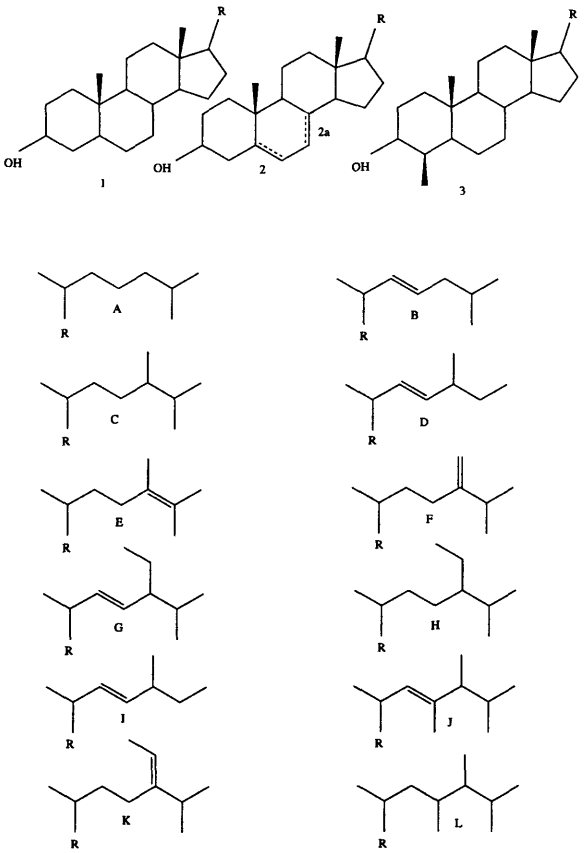

Figure 2. Sterol structures. R refers to the attachment point between the tetracyclic structure and the carbon chain.

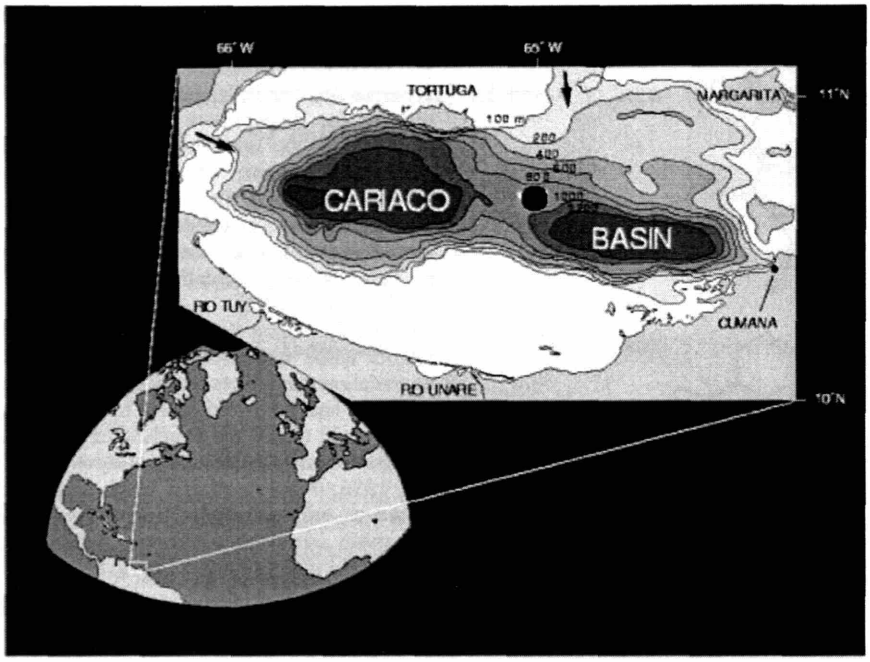

Figure 3. Location and bathymetry of the Cariaco Basin. The location of core 56-PC is shown as a black dot. Arrows indicate sills that control exchange with the Caribbean Sea. (Figure provided by K. Hughen.)

of CSE sterols as proxies for the phytoplankton community through time. In order to assess this possibility, we examined Younger Dryas-aged sediments from the Cariaco Basin, Venezuela.

1.2. Cariaco Basin: Setting and Background

[7] The Cariaco Basin is a small, anoxic, marine basin off the coast of Venezuela in the southern Caribbean Sea (Figure 3). Shallow (<146 m) sills separate the basin from the rest of the Caribbean Sea. The sills restrict flow to and from the basin and prevent oxygenation of deeper waters. Consequently, the basin has been anoxic below ~300 m for the past 12.6 kyr (^{14}C age; *Peterson et al.* [1991]). Owing to its latitude, the Cariaco Basin is subject to seasonal [*Peterson et al.*, 1991] and long-term [e.g., *Black et al.*, 1999; *Haug et al.*, 2001] fluctuations in the Intertropical Convergence Zone (ITCZ). During the Northern Hemisphere winter the ITCZ is at its farthest latitude south. Trade winds blow along the northern coast of South America, inducing upwelling and, subsequently, high production [*Muller-Karger et al.*, 2001]. During this upwelling season, diatoms dominate the phytoplankton community [*de Miro*, 1971; *Ferraz-Reyes*, 1983]. The ITCZ migrates northward during the Northern Hemisphere summer, causing trade winds and upwelling in the basin to diminish. Primary production during the nonupwelling season is lower [*Muller-Karger et al.*, 2001] and dominated by cyanobacteria and dinoflagellates [*Ferraz-Reyes*, 1983]. Sediments in the basin exhibit seasonal laminae, which are indicative of the basin's high sediment preservation potential. Furthermore, the lack of significant bioturbation and high deposition rates (20–100 cm/kyr; *Peterson et al.* [1991]) make the Cariaco Basin an ideal site for paleoceanographic reconstructions [*Lin et al.*, 1997].

[8] Much like the seasonal migrations of the ITCZ, longer-term (i.e., millennial-scale and longer) changes in trade wind strength cause changes in primary productivity and, most likely, phytoplankton community structure in the Cariaco Basin [*Haug et al.*, 1998]. The Younger Dryas is the most thoroughly researched millennial-scale climate event. Its timing is well constrained by radiocarbon dates from the varved sediments of the Cariaco Basin [*Hughen et al.*, 1996, 1998, 2000]. The Younger Dryas began about 13 kyr (calendar age) BP and lasted roughly 1300 years. It has been proposed that the Younger Dryas occurred as a result of a shutdown of North Atlantic Deep Water (NADW) formation [*Broecker et al.*, 1985; *Boyle and Keigwin*, 1987; *Broecker et al.*, 1988]. Such a change in thermohaline circulation would have caused changes in the meridional sea-surface temperature gradient and therefore the strength of trade winds and subsequent upwelling over the Cariaco Basin [*Hughen et al.*, 1996, and references therein]. Strengthening of the trade winds has been invoked as a mechanism to explain lithologic, climatologic, and faunal evidence from Younger Dryas-aged sediments from the basin [*Hughen et al.*, 1996; *Lin et al.*, 1997; *Lea et al.*, 2003].

[9] At the onset of the Younger Dryas, increases in trade wind intensity, and therefore upwelling, in the basin would have increased the concentration of nutrients in surface

waters. Under these high nutrient conditions, diatoms likely became the dominant primary producers [*Schrader et al.*, 1993]. Easing of the trade winds at the Younger Dryas termination should have shifted the dominant primary producers to cyanobacteria and dinoflagellates, as is observed during present-day Northern Hemisphere summer [*Ferraz-Reyes*, 1983]. If CSE sterols do indeed accurately reflect the phytoplankton community at the time of formation, then the assemblage of CSE sterols should undergo major changes at the onset and termination of the Younger Dryas in the Cariaco Basin. More specifically, we expected that the distribution should reflect an increase in the diatom population and a decrease in the dinoflagellate population during the Younger Dryas. As cyanobacteria do not produce large amounts of sterols, CSEs are unlikely to yield information regarding the abundance of this class of phytoplankton through time.

[10] *Werne et al.* [2000] performed a study of the distribution of free sedimentary sterols and a C_{37} alkenone in the Cariaco Basin during the Younger Dryas. These authors concluded that diatoms were the dominant primary producers during the Younger Dryas, while alkenone-producing coccolithophorids dominated during warm periods, such as the Holocene. While these shifts do exhibit the trends that one would expect, there are several uncertainties with this type of analysis. First, it has been widely noted that free sterols are more susceptible to selective degradation than are CSE sterols [*King and Repeta*, 1991, 1994; *Talbot et al.*, 1999a, 2000]. Second, although sterols and alkenones are both relatively refractory compound classes, it is expected that one class of lipids would undergo preferential degradation relative to the other [e.g., *Wakeham et al.*, 1997]. In contrast, CSEs all belong to the same class of compounds and therefore do not preferentially degrade relative to one another [*Talbot et al.*, 2000]. Because the Cariaco Basin is largely anoxic, it is unlikely that free sterol degradation and preferential degradation of one compound class over another will have a great effect on the accuracy of downcore records [*Wakeham and Ertel*, 1988]. In fact, *Werne et al.* [2000] noted that the highest accumulation rates of sterols (which are labile relative to alkenones) were found in the deepest sediment layers that they studied, which indicates that differential degradation is not a significant factor in the Cariaco Basin. Given the robustness of the free sterol record from the Cariaco Basin, the findings of *Werne et al.* [2000] provided an ideal backdrop for testing the potential of CSEs as proxies for phytoplankton community reconstructions.

2. Methods

2.1. Extraction and Isolation of CSES

[11] Core-top sediments were obtained from a box core taken from the center of the western basin of the Cariaco Trench (10°40N, 65°36′W, 700 m water depth) by the R/V *Iselin* [*Wakeham and Ertel*, 1988]. Pigments were extracted ultrasonically from ~300 g of wet sediment with acetone (3x, 400 mL each) followed by methylene choloride (3x, 400 mL each).

[12] Chlorin steryl esters were purified from the bulk extract using a combination of solid-phase extraction and reverse-phase high performance liquid chromatography (RP-HPLC). Solid-phase extraction was performed by packing a 6 cm diameter glass column with 75 g octadecylsilane (J.T. Baker, 40–140 mesh size) and eluting the pigments in several fractions, which were then further purified by RP-HPLC prior to structural identification. CSEs were purified on two Nucleosil C18 columns (Alltech, 3μm, 150 × 4 mm) connected in series. The CSEs were eluted isocratically with 25/75 (v/v) methylene chloride/acetonitrile at 1.5 mL/min and detected at 410 and 666 nm. In method development experiments this solvent composition provided an optimal separation of seventeen individual CSEs, which eluted between 25 and 65 min in our samples (Figure 4). Individual CSE peaks were collected manually as they eluted from the columns.

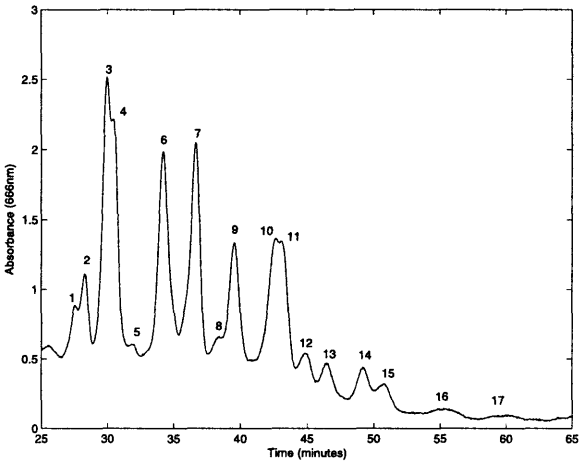

Figure 4. High-performance liquid chromatogram of the CSEs in a typical Cariaco Basin sample, showing the numbering scheme used in this study. Seventeen CSEs eluted between 25 and 65 min (refer to text for specific conditions). See Table 1 for CSE sterol identifications.

[13] Downcore samples are from piston core PL07-56PC in the Cariaco Basin [*Hughen et al.*, 1998]. This core was retrieved at 10°40.60′N, 64°57.70′W from 810 m water depth and has a sedimentation rate of ~50 cm/kyr. Samples (0.3 grams dry weight (gdw)) were taken every 10 cm from 300–800 cm across the Younger Dryas as determined from previous work [*Hughen et al.*, 1998]. The samples were freeze-dried overnight and extracted using automated solvent extraction (ASE) (100% methylene chloride, 1000 psi, 100°C). Total chlorins were quantified at 666 nm using UV/Vis spectrophotometry assuming an extinction coefficient of 5×10^4 L mol^{-1} cm^{-1}.

2.2. Sterol Identification

[14] CSE sterols were structurally identified for the bulk core-top sediment extraction using a combination of liquid chromatography-mass spectrometry (LC-MS) and Gas chromatography- mass spectrometry (GC-MS). LC-MS was performed on the individually collected CSEs from the core-top sediments in order to determine the molecular weight of the each CSE. The same columns and conditions

Table 1. Identification of CSE Sterols[a]

Peak	CSE Sterol Structure[b]	Precursor	MW	Basis[c]	Reference
1	24-norcholesta-5,22E-dien-3β-ol (2B)	dinoflagellates	887	G,L	*Goad and Withers* [1982] *Leblond and Chapman* [2002]
2	27-nor-24-methylcholesta-5,22E-dien-3β-ol (2I)	dinoflagellates	901	L	*Goad and Withers* [1982] *Mansour et al.* [1999]
3	24-methylcholesta-5,24(28)-dien-3β-ol (2F)	diatoms	915	L	*Barrett et al.* [1995, and references therein] *Volkman et al.* [1998]
4	cholesta-5,22E-dien-3β-ol (2B)	diatoms, red algae[d]	901	G,L	*Barrett et al.* [1995] *Véron et al.* [1998] *Volkman et al.* [1998]
5	24-methylene-cholest-5-en-3β-ol (2F)	many	915	L	*Goad* [1978, and references therein]
6	24-methylcholesta-5,22E-dien-3β-ol (2D)	diatoms, chryptophytes, coccolithophorids	915	G, L	*Volkman et al.* [1998] *Leblond and Chapman* [2002]
7	cholest-5-en-3β-ol (2A)	zooplankton, phytoplankton	903	G,L	*Volkman* [1986]
8	23,24-dimethylcholesta-5,22E-dien-3β-ol (2J)	diatoms, dinoflagellates	929	L	*Volkman et al.* [1993] *Leblond and Chapman* [2002]
	24-ethylcholesta-5,22E-dien-3β-ol (2G)	haptophytes, green and golden algae diatoms			*Volkman et al.* [1998] *Véron et al.* [1998]
	24-ethylcholesta-5,24(28)E-dien-3β-ol (2K)	haptophytes, prasinophytes			*Volkman et al.* [1994]
9	24-methylcholest-5-en-3β-ol (2C)	green algae	917	G,L	*Volkman* [1986] *Véron et al.* [1998]
10	24-ethylcholest-7-en-3β-ol (2aH) 24-ethylcholest-22-en-3β-ol (1G) 23,24-dimethylcholest-5-en-3β-ol (2K)	green algae, prasinophytes diatoms dinoflagellates	931	L	*Volkman et al.* [1998] *Véron et al.* [1998] *Volkman et al.* [1984] *Goad and Withers* [1982]
	23,24-dimethylcholest-22-en-3β-ol (1J)	green algae, prasinophytes			*Volkman et al.* [1998]
11	24-ethylcholest-5-en-3β-ol (2H)	many	931	G,L	*Volkman et al.* [1998]
12	24-ethylcholest-7-en-3β-ol (2aH) 24-ethylcholest-22-en-3β-ol (1G) 23,24-dimethylcholest-5-en-3β-ol (2K)	green algae, prasinophytes diatoms dinoflagellates	931	L	*Volkman et al.* [1998] *Véron et al.* [1998] *Volkman et al.* [1984] *Goad and Withers* [1982]
	23,24-dimethylcholesta-22-en-3β-ol (1J)	green algae, prasinophytes			*Volkman et al.* [1998]
13	4α,23,24-trimethylcholest-22E-en-3β-ol (3J) 4α,23,24-trimethylcholest-N-3β-ol[e]	dinoflagellates dinoflagellates	945	L	*Withers* [1987] *Volkman et al.* [1998]
14	4α,23,24-trimethylcholest-22E-en-3β-ol (3J) 4α,23,24-trimethylcholest-N-3β-ol[d]	dinoflagellates dinoflagellates	945	L	*Withers* [1987] *Volkman et al.* [1998]
15	23,24-dimethyl-5α(H)-cholestan-3β-ol (1L) 4α,24-dimethyl-5α-cholestan-3β-ol (3C)	dinoflagellates dinoflagellates	933	L	*Volkman et al.* [1998] *Robinson et al.* [1984] *Withers* [1987, and references therein]
16	4α,23,24-trimethyl-5α-cholestan-3β-ol (3L)	dinoflagellates	947	L	*Talbot et al.* [2000] *Leblond and Chapman* [2002]
17	unknown		ND		

[a]Sterol identifications for peaks shown in Figure 4. For peaks with uncertain sterol identities, all possible sterol identities, on the basis of molecular weight, are listed. These CSE sterols have not been firmly identified.
[b]Structure numbers refer to Figure 2.
[c]Basis refers to the methods used to identify the CSE sterol. L, LC-MS; G, GC-MS.
[d]The red algae that produce this sterol are generally not found in seawater [*Volkman*, 1986].
[e]N indicates that the position of the double bond is unknown.

were used for the LC-MS as described above for RP-HPLC. The instrument used was a Shimadzu HPLC fitted to a Finnegan MAT LCQ operated in the positive ion mode and using atmospheric pressure electrospray ionizaton.

[15] Individual CSEs, collected from core-top sediments by RP-HPLC, were then hydrolyzed to liberate the CSE sterols. GC-MS was then performed on the individual CSE sterols in order to determine the structure (and therefore the identity) of each sterol. We apply these identifications to our downcore record, assuming that the sterols present in the core-top sample will be present downcore. Given the uniformity of RP-HPLC retention times in our downcore record, this is assumption is likely a good one.

[16] For cases in which the identity of a sterol was uncertain despite LC-MS and GC-MS, we have made certain assumptions in order to make the identifications listed in Table 1. CSEs 2 and 4 have the same molecular weight. GC-MS of CSE sterol 4 enabled us to identify it as cholesta-5,22E-dien-3β-ol. Results from GC-MS of the total CSE sterol fraction revealed that the only other CSE sterol present in our samples with the same molecular weight was 27-nor-24-methylcholesta-5,22E-dien-3β-ol. This is there-

fore our identification of CSE sterol 2. This identification is consistent with the elution order of the CSEs during RP-HPLC. The identifications of CSEs 3 and 5 are based on their relative abundances in seawater. 24-methylcholesta-5,24(28)-dien-3β-ol is more abundant in seawater than 24-methylenecholest-5-en-3β-ol [*Volkman*, 1986]. By analogy with their relative peak areas, we have identified CSE sterols 3 and 5 as indicated in Table 1.

2.3. Data Analysis

[17] In order to determine the distribution of CSEs in each downcore sample, the area of each CSE peak in each chromatogram was determined using the HP Chemstation software's data analysis program. The areas were determined as follows: A baseline was drawn between the beginning of CSE 1 and the end of CSE 15. Vertical lines were then drawn between each of the peaks, using the lowest point of the valley between peaks when obvious, and the area was calculated. For cases in which no distinct minimum separated two CSEs this area of the two peaks were combined. This was done throughout the downcore record for peaks 1 and 2, peaks 3 and 4, and peaks 10 and 11. The downcore records of peaks 3 and 4 (as well as 10 and 11) are mirror images of one another, which is an artifact of the integration rather than a true signal. The resolvability of peaks 1 and 2 varied throughout the record. Combining the peaks of two CSEs has implications for the reconstruction of phytoplankton classes through time in that if the combined peaks do not have the same biological source, then the combined peak will be a reflection of multiple classes of phytoplankton. As will be shown in the "sterol identification" section of the results, this does not pose a significant problem in the interpretation of our record. Peaks 16 and 17 were not included in the integration because the peak heights were generally very low and the boundaries of the peaks were not consistently defined. The area of each peak was then divided by the total area of the CSEs in order to determine changes in the distribution of the CSEs relative to one another. The average error for two sets of integrations was 0.23 ± 0.095%.

[18] Principal component analysis was performed using Matlab software. For this analysis, peaks 1 and 2 (hereafter 1 + 2), peaks 3 and 4 (3 + 4), and peaks 10 and 11 (10 + 11), which were not well resolved, were combined so as to prevent the introduction of erroneous changes in the distribution of the CSEs with depth. Elemental CHN analysis was performed on ten samples throughout the core to determine changes in the organic carbon content of these sediments through the Younger Dryas. These analyses were performed using a Carlo Erba Elemental Analyzer (model 1108).

3. Results

3.1. Bulk Parameters

[19] Stadial events, such as the Last Glacial Maximum (LGM) and the Younger Dryas, are characterized by relatively low percentages of organic carbon in comparison to interstadial events (Figure 5b). The lowest organic carbon contents (<2%) occurred during the LGM. The

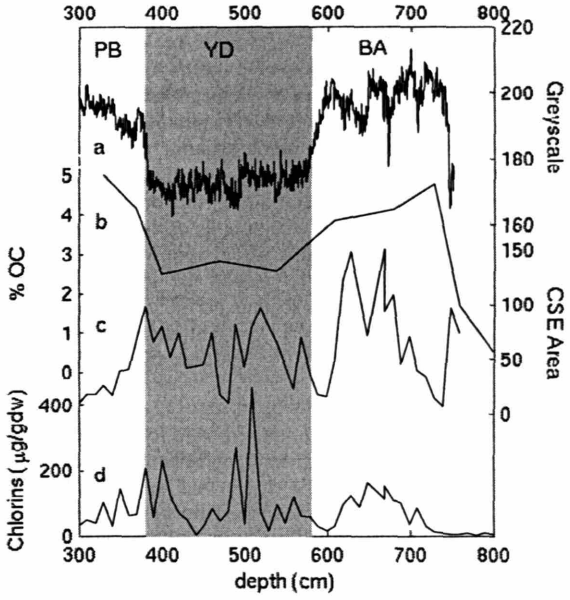

Figure 5. (a) Gray scale, (b) percent organic carbon, (c) total CSE area per gdw (arbitrary units), and (d) total chlorins versus depth. The Younger Dryas period is denoted by the shaded bar. PB, YD, and BA refer to the Preboreal, Younger Dryas, and Bølling/Allerød periods, respectively.

organic carbon content rose to 4–5% during the Bølling/Allerød warm period then dropped again to ~2.5% during the Younger Dryas. At the Younger Dryas termination the organic carbon content rose once again to 4–5%. These results are in good agreement with higher resolution data from a neighboring piston core, PL07-39PC (K. Hughen, personal communication, 2001). The shifts toward a lower percent organic carbon during stadials reflect a dilution of the organic carbon signal rather than a decrease in the preservation of organic carbon. During the Younger Dryas, increased productivity drove a roughly 3-fold increase in the bulk sedimentation rate [*Hughen et al.*, 1996]. The increased sedimentation of biogenic debris (i.e., diatom and foraminifera tests) during the Younger Dryas therefore diluted the organic carbon reaching the sediments. It should be noted, however, that the accumulation rate of organic carbon was elevated during the Younger Dryas relative to the Bølling/Allerød and Preboreal periods [*Werne et al.*, 2000] due to a decrease in the oxygen content of the water column [*Dean et al.*, 1999; *Lyons et al.*, 2003].

[20] Increased primary productivity during the Younger Dryas is also reflected in the gray scale record of this core, previously published by *Hughen et al.* [1996] (Figure 5a). Gray scale is a measure of the reflectivity of sediment. In the Cariaco Basin, gray scale is determined primarily by the relative inputs of terrestrial (dark) and biogenic (light) material and can therefore be used as a proxy for primary productivity. During the Younger Dryas the increase in sedimentation of biogenic material relative to

terrestrial material caused a decrease in the gray scale of the sediments.

[21] The concentration of total chlorins in the Cariaco Basin through time varies from nondetectable to 448 μg/gdw with an average value of 72 μg/gdw (Figure 5d). The ratio of chlorin concentration to percent organic carbon varies through time as well, which suggests that either there are different mechanisms controlling the preservation of chlorins and organic carbon in sediments or the contribution of CSEs to the total organic carbon pool varies through time. The total CSE area, defined as the integrated area under all of the CSE peaks in a given HPLC chromatogram, corresponds well to total chlorin concentration, determined by the absorbance at 666 nm, through time (Figure 5c).

3.2. CSE Fraction

[22] The CSE fraction is composed of at least 17 distinct CSEs (Figure 4), all of which have pyropheophorbide-*a* as the chlorin component. We did not find any CSEs with pyropheophorbide-*b* (CSEs b) as the chlorin component in our samples. As shown by *Talbot et al.* [1999b], sterols are incorporated into CSEs of pyropheophorbide-*a* and pyropheophorbide-*b* in equal proportions. The pigment precursor to pyropheophorbide-*b* (chlorophyll-*b*) is much less abundant in algae than the precursor to pyropheophorbide-*a* [e.g., *Svec*, 1991]. The concentrations of CSEs b are therefore generally lower than those of CSEs a, which have pyropheophorbide-*a* as their chlorin [*Gall et al.*, 1998; *Kowalweska et al.*, 1999; *Tani et al.*, 2002].

[23] The HPLC chromatogram shown in Figure 4 is typical of CSE distributions in core-top and downcore sample extracts. The largest peaks in each chromatogram are 3 + 4, 6, 7, 9, and 10 + 11. These CSEs, on average, constitute roughly 80% of the total CSEs. The remaining 12 CSE peaks are consistently smaller than those mentioned above and collectively constitute ~20% of the total CSE area.

3.3. Sterol Identification

[24] LC-MS data enabled us to identify the molecular weights of each CSE (Table 1). The molecular weights of the CSEs (i.e., the combined weight of the chlorin and the sterol of a given CSE) range from 887 to 947 Daltons and generally increase with retention time. These molecular weights correspond to sterols with carbon numbers of 26–30 and molecular weights of 352–412 Daltons. In general, the diunsaturated 5,24(28) sterols eluted before 5,22 sterols, and monounsaturated 5-stenols eluted after diunsaturated 5,24(28) and 5,22 sterols. Sterol identifications, made via a combination of LC-MS, GC-MS of individual CSE sterols, and GC-MS of a total CSE sterols sample, are shown in Table 1.

[25] In many cases the molecular weight alone is enough to make a definitive identification of the CSE sterol. Identifications based solely on LC-MS become problematic, however, given that several sterols can have the same molecular weight if they differ in structure simply by the position of a double bond. Because GC-MS was performed on just the CSE sterols, we were able to clarify many of the ambiguous LC-MS data. The combination of LC-MS and GC-MS allowed us to identify 10 out of the 17 CSEs.

[26] Our sterol identifications provide further justification for combining the peaks for CSEs 1 + 2 and CSEs 3 + 4. As shown in Table 1, CSE sterols 1 and 2 are both derived from dinoflagellates while CSE sterols 3 and 4 are both derived from diatoms. CSEs 10 and 11 are not derived from the same phytoplankton class; we therefore do not interpret CSEs 10 + 11 as a reflection of a given phytoplankton class.

3.4. Downcore CSE Records

[27] As shown in Figure 6, the relative percent of some CSEs varies very little (e.g., CSE 13, which varies between 2 and 3%) while the relative percent of others varies quite dramatically downcore (e.g., CSE 7, which varies between 12 and 24%). It is clear that the distribution of some CSEs changes through time and that these changes are often synchronous with changes in the climate of the Cariaco Basin (Figure 6).

[28] Five CSE peaks that vary significantly downcore, along with variations in gray scale from the same core, are shown in Figure 7. As mentioned above, gray scale can be used as a proxy for primary productivity in the Cariaco Basin. The gray scale record from this core correlates very well with the accumulation rate of the GISP2 ice core from central Greenland, which has been interpreted as a proxy for North Atlantic sea- surface temperature [*Kapsner et al.*, 1995; *Hughen et al.*, 2000]. This correlation implies that gray scale in the Cariaco Basin is a reflection of climate. We use gray scale here primarily as a reference for the rapid transitions into and out of the Younger Dryas. On the basis of our sterol identifications we can draw several conclusions about the nature of the phytoplankton community during the Younger Dryas in the Cariaco Basin.

[29] CSEs 1 + 2 decrease in abundance during the Younger Dryas (Figure 7a). The mean abundance of CSEs 1 + 2 during the Younger Dryas is significantly different from the mean abundance during the Bølling/Allerød and Preboreal periods at the 99% confidence level, as determined by a *t* test for two sample populations. Furthermore, CSEs 1 + 2 may reflect some of the centennial-scale variability during the Bølling/Allerød that can be seen clearly in the pattern of gray scale. CSE sterols 1 and 2 (24-nor-cholesta-5,22E-dien-3β-ol and 27-nor-24-methyl-cholesta-5,22E-dien-3β-ol, respectively) are produced by dinoflagellates [*Goad and Withers*, 1982; *Mansour et al.*, 1999; *Leblond and Chapman*, 2002]. We can therefore infer from Figure 7a that the relative abundance of dinoflagellates in the Cariaco Basin is high during warm weak trade wind intervals and low during cold increased trade wind intervals such as the Younger Dryas. The decrease is gradual over the Bølling/Allerød-Younger Dryas transition. At the Younger Dryas-Preboreal transition, however, CSEs 1 + 2 increase very rapidly. The downcore relationship between CSEs 1 + 2 and gray scale is consistent with the observation that the dinoflagellate population increases during the nonupwelling (lower productivity) season in the Cariaco Basin today [*Peterson et al.*, 1991].

[30] Figure 7b shows the distribution of CSEs 3 + 4 through the Younger Dryas. The sterols of CSE 3 (24-methylcholesta-5,24(28)-dien-3β-ol) and CSE 4 (cho-

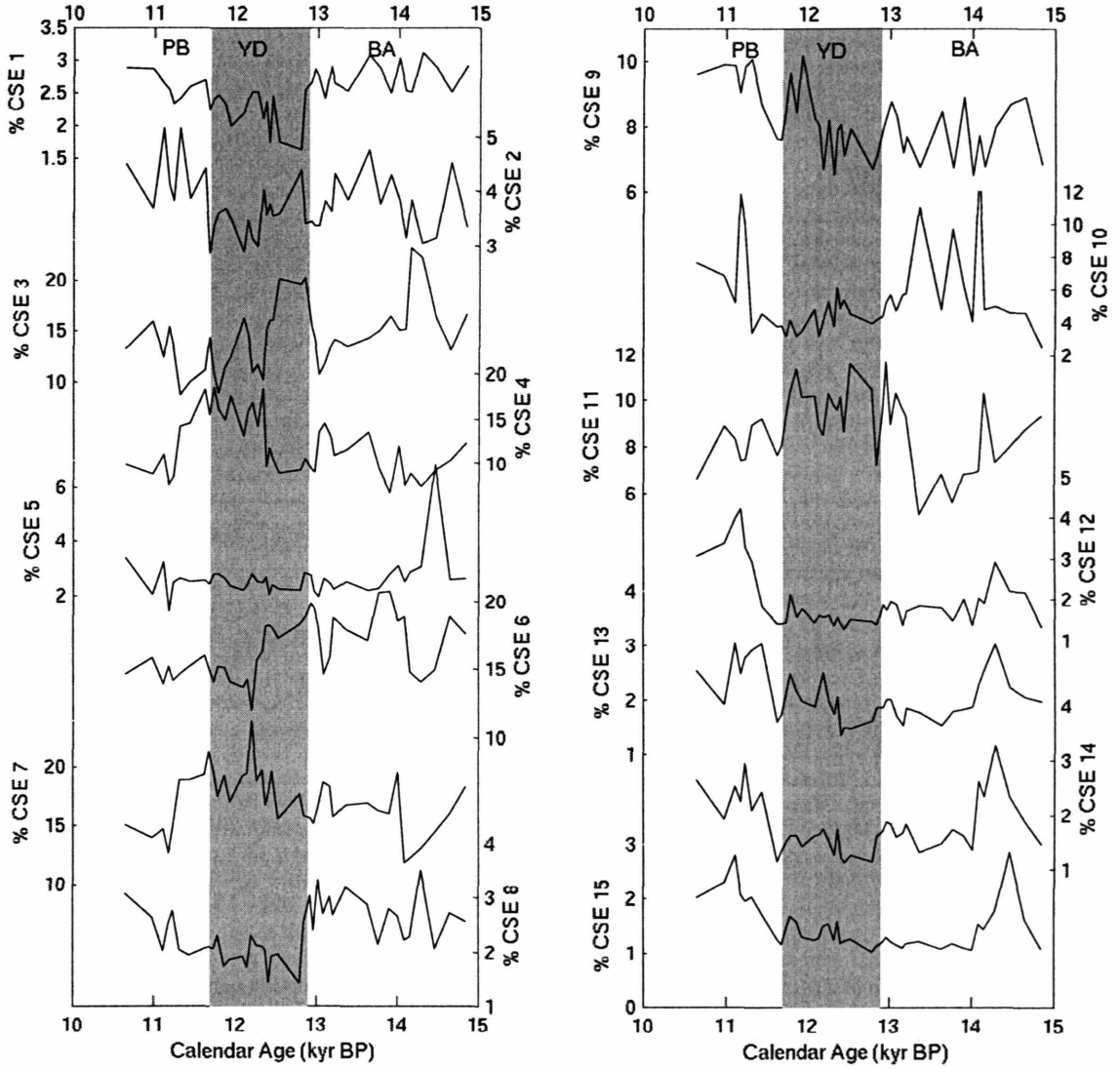

Figure 6. Downcore changes in the relative percentage of each CSE relative to the total CSE area through time. CSE numbers refer to the peaks in Figure 4. The Younger Dryas period is represented by the shaded bar. BA and PB refer to the Bølling/Allerød and Preboreal periods, respectively.

lesta-5,22E-dien-3β-ol) are both abundant in diatoms [e.g., *Barrett et al.*, 1995; *Véron et al.*, 1998; *Volkman et al.*, 1998]. CSEs 3 + 4 increased in abundance during the Younger Dryas and decreased during the Preboreal period. The increase in abundance at the onset of the Younger Dryas was very rapid, while the decrease coming out of the Younger Dryas lagged slightly behind that of the increase in gray scale. The mean abundance of CSEs 3 + 4 during the Younger Dryas is different from that of the Bølling/Allerød and Preboreal periods at the 99% confidence level. This downcore distribution suggests that the diatom population of the Cariaco Basin increased during the Younger Dryas, which was expected a priori, given that the increase in trade wind intensity and upwelling during the Younger Dryas would have favored the growth of diatoms just as it does during the present-day upwelling season [*Peterson et al.*, 1991].

[31] CSE 6 shows an interesting pattern of high abundance during the Bølling/Allerød and the first half of the Younger Dryas followed by a rapid decrease about halfway through the Younger Dryas (Figure 7c). The abundance stays relatively low throughout the rest of the Younger Dryas and the Preboreal period. CSE sterol 6 is 24-methylcholesta-5,22E-dien-3β-ol, a sterol that is found in many types of phytoplankton including diatoms and coccolithophorids [*Volkman et al.*, 1998, and references therein].

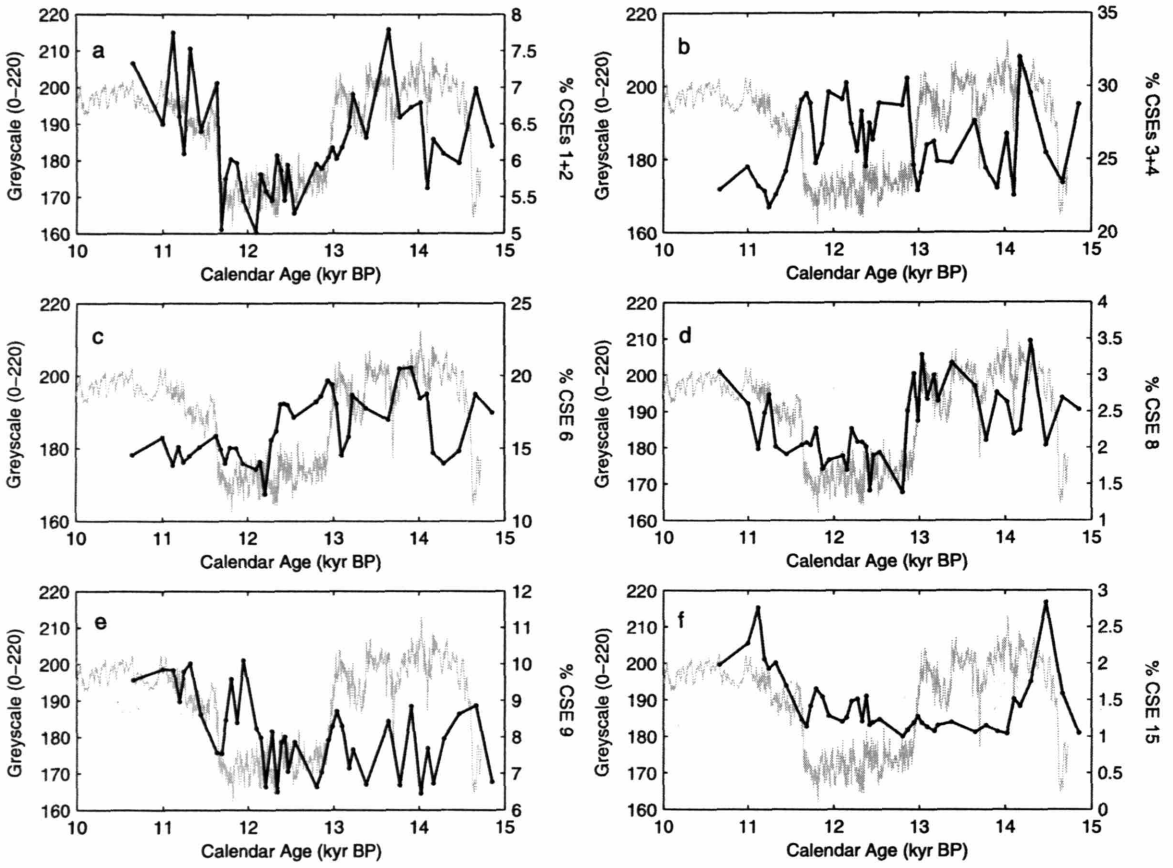

Figure 7. Changes in the relative percentage of different CSEs (black) and gray scale (gray) in core PL07-56PC. (a) CSEs 1 + 2, (b) CSEs 3 + 4, (c) CSE 6, (d) CSE 8, (e) CSE 9, and (f) CSE 15.

[32] The relative percentage of CSE 9 (24-methylcholest-5-en-3β-ol), derived from green algae [*Volkman*, 1986], generally increases from low during the Bølling/Allerød to high during the Preboreal period (Figure 7e). Much of this increase takes place during the second half of the Younger Dryas. Interestingly, this trend is opposite that of CSE 6, which shows a decrease in abundance in the middle of the Younger Dryas. CSE 9 also undergoes major changes in relative abundance at each climate transition. During transitions into interstadials (stadials) the relative percent of CSE 9 increases (decreases). While higher-resolution data is needed, this relationship appears to hold true for the centennial-scale variability exhibited in the gray scale record during the Bølling/Allerød.

[33] CSEs 8 and 15 remain unidentified. It is evident from their downcore trends, however, that they may be useful climate proxies (Figures 7d and 7f). CSE 8, which could originate from a number of different classes of phytoplankton, including dinoflagellates and diatoms, exhibits a rapid decrease in abundance at the onset of the Younger Dryas but does not respond rapidly to the warming at the end of the Younger Dryas. This CSE might therefore be a useful indicator of rapid cooling and/or increased upwelling events. Although CSE 15 has also not been identified, all of the sterols that are consistent with its molecular weight are dinoflagellate sterols (Table 1). CSE 15 (as well as CSEs 12 and 14, Figure 6) responds rapidly to warming events or decreases in upwelling intensity but does not appear to respond to cool increased upwelling events such as the Younger Dryas. Shifts in the abundance of these CSEs take place not only at rapid climate transitions (e.g., the Bølling/Allerød-Younger Dryas transition) but also within "stable" climate regimes (e.g., the rapid decrease in the abundance of CSE 15 during the Bølling/Allerød). Thus the biological sources of CSEs 8 and 15 are responding to changes in the environment of the Cariaco Basin that are not reflected in the gray scale record. Identification and downcore analysis of these CSE sterols would therefore allow for reconstruction of specific aspects of the paleoenvironment that cannot be inferred from gray scale changes. In addition, the downcore records of CSEs 1 + 2 and CSE 15 are markedly different from one another despite the fact that each of these CSEs originates from dinoflagellates. That different sterols, each presumably being produced by different species of dinoflagellates, can exhibit independent trends suggests that the

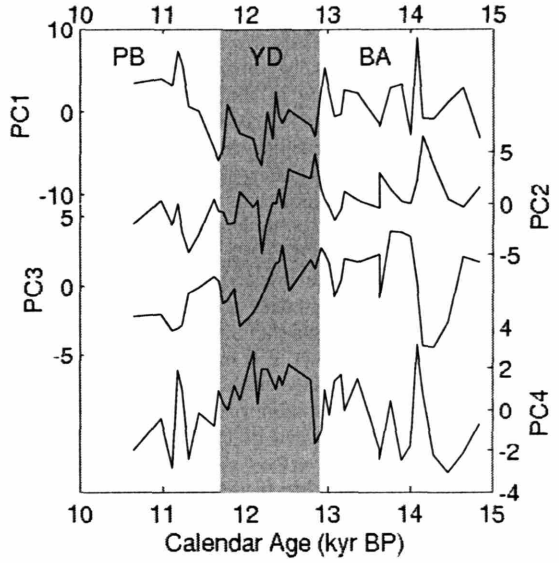

Figure 8. Principal components 1–4 plotted through time. the younger Dryas is defined by the shaded bar. BA and PB refer to the Bølling/Allerød and Preboreal periods, respectively.

suite of CSEs can offer a very in-depth detailed view of paleoenvironments.

3.5. Principal Component Analysis

[34] Principal component analysis of the downcore CSEs demonstrated that 94% of the total variance in the data set could be explained by four principal components (PCs). These four PCs are shown plotted against age in Figure 8. PC1, which explains 46.1% of the variance, becomes more negative during the Younger Dryas. This reflects a greater influence of CSEs 3 + 4 (diatoms) and 7 (many sources) during this time. Positive values of PC1, such as those that occur during the Bølling/Allerød and Preboreal periods, reflect a greater influence of CSEs 6 and 10 + 11, both of which come from a number of different phytoplankton sources. PC2, explaining 18.8% of the variance, shows a generally decreasing trend from the Bølling-Allerød to the Preboreal period. This decrease represents a trend from a greater influence of CSEs 3 + 4 (diatoms), 6, and 7 (many sources) to a greater influence of CSE 9 (green algae). PC3, which explains 18.6% of the variance, becomes more positive at the onset of the Bølling-Allerød, which reflects an increase in the influence of CSEs 6 and 7 (many sources) and a decrease in the influence of CSEs 3 + 4 (diatoms) and 9 (green algae). PC4 explains 10.6% of the variance and has very positive values during the Younger Dryas. These positive values reflect an increased influence of CSEs 10 + 11 and 7 (many sources) and a decreased influence of CSEs 1 + 2 (dinoflagellates) and 5 (diatoms). The results of the PCA therefore support the results of the downcore distribution trends. The increased influence of diatom CSEs and the decreased influence of dinoflagellate CSEs during the Younger Dryas (Figure 8) support the trends seen in the downcore CSE records. Furthermore, the trend toward a greater influence of green algae is consistent with a generalized warming and/or decreased upwelling in the Cariaco Basin since the LGM.

4. Discussion

[35] The successful application of CSEs as biomarkers requires the identification each CSE sterol as well as the generation of accurate downcore records of the CSE distribution. With respect to both of these requirements, the results presented here represent an important step toward successful reconstruction of phytoplankton communities. One of the main benefits of our approach is that it can be performed using relatively small (0.3 gdw) samples. In addition, the analyses can be done very quickly using automated RP-HPLC technology. In contrast, the use of gas chromatography (GC) to do such work would require larger samples and longer preparation time for several reasons. Prior to GC analysis, CSEs would have to be purified using RP-HPLC, yielding the same information we have utilized for this study. Owing to their high molecular weights, the CSEs would then need to be hydrolyzed in order to liberate the CSE sterols. Furthermore, given the sensitivity of the GC-MS we have been using, we estimate that we would need to start with double the amount of sediment.

[36] In this study, we have doubled the previous number of CSEs [*King and Repeta*, 1994] that can be separated by optimizing the HPLC solvent composition and the columns. By only resolving about half of the CSEs reported in this study, earlier studies could not represent the full suite of phytoplankton sterols. Furthermore, substantial coelution prevented accurate determination of the relative contribution of each CSE. Our improved separation represents a critical step toward accurate reconstruction of phytoplankton communities through time. With further method development and more complete CSE sterol identification, our ability to reconstruct phytoplankton communities will continue to improve.

[37] One limitation of using CSE sterols or free sterols as indicators of phytoplankton communities is that most sterols do not have a single biological precursor. For example, 24-methylcholesta-5,22E-dien-3β-ol (CSE 6) has been identified not only in diatoms, but also in haptophytes and cryptophytes [*Goad and Withers*, 1982; *Volkman*, 1986; *Volkman et al.*, 1998]. Furthermore, the sterol composition in a given class of phytoplankton can be diverse. As shown by *Volkman et al.* [1998], while some diatoms contain an abundance of 24-methylcholesta-5,24(28)-dien-3β-ol, others have cholesterol as their major sterol. Still others contain only cholesta-5,24-dien-3β-ol [*Barrett et al.*, 1995], which demonstrates there may not be a single definitive sterol biomarker for diatoms. With further method development and statistical analysis of trends within groups of CSEs downcore, however, CSEs could be very powerful biomarkers.

[38] There is evidence that zooplankton may preferentially take up certain sterols during the CSE formation process. A culture study by *Talbot et al.* [2000] showed that copepods discriminated against 4-methyl sterols (predominantly from

dinoflagellates) during CSE production. It has been observed that the abundance of 4-methyl sterols is lower in CSE sterols than in free sterols [*King and Repeta*, 1991; *Eckardt et al.*, 1992; *King and Repeta*, 1994; *Pearce et al.*, 1998]. As a result, it is possible that the distribution of CSEs will underestimate the contribution of dinoflagellates to the community of the overlying water column [*Talbot et al.*, 2000]. However, the discrimination against 4-methyl sterols may depend upon the setting [*Pearce et al.*, 1998]. Reconstructions of the dinoflagellate population using free sterols have the opposite problem: 4-methyl sterols are more refractory than 4-desmethyl sterols, which could lead to an overestimation of the dinoflagellate contribution to the phytoplankton community. In this study, we have used 4-desmethyl sterols (24-norcholesta-5,22E-dien-3β-ol and 27-nor-24-methylcholesta-5,22E-dien-3β-ol, CSEs 1 + 2), as opposed to the more traditional 4-methyl sterol, dinosterol, as dinoflagellate indicators. Using these 4-desmethyl sterols, we see evidence for changes in the dinoflagellate community through time in the direction that we would expect. This may be a potential solution to the problem of 4-methyl sterol exclusion from CSE formation, although it is clear from a comparison of CSEs 1 + 2 and CSE 15 that different dinoflagellate biomarkers can yield different results.

[39] Our results are broadly consistent with paleoceanographic studies of the Cariaco Basin during the Younger Dryas. *Peterson et al.* [1991] showed that the relative abundance of the planktonic foraminifer *Globigerina bulloides*, which is commonly used as a proxy for upwelling conditions [*Duplessy et al.*, 1981; *Ganssen and Sarnthein*, 1983; *Prell*, 1984; *Prell and Campo*, 1986], was higher during the Younger Dryas than during the Bølling/Allerød and the Preboreal periods. Further evidence for increased upwelling in the Cariaco Basin during the Younger Dryas comes from oxygen isotopes of several taxa of planktonic foraminifera [*Lin et al.*, 1997]. Our finding of an increased abundance of diatoms during the Younger Dryas is consistent with an increase in upwelling in the basin.

[40] *Werne et al.* [2000] also demonstrated that diatoms increased in abundance during the Younger Dryas through the use of free sterols and other organic biomarkers. Similar to our results for CSEs 6 and 9, *Werne et al.* [2000] found that significant changes in the phytoplankton community took place in the middle of the Younger Dryas. *Werne et al.* [2000] observed a decrease in the diatom and dinoflagellate populations during the Younger Dryas, while in this study we find a decrease in the relative abundance of CSE 6, which is derived from a variety of phytoplankton classes including diatoms and coccolithophorids. While the specific classes involved in this decrease may differ between this study and that of *Werne et al.* [2000], the biomarkers used in both studies suggest that phytoplankton community reconstructions potentially record changes in environmental conditions that take place during periods of seemingly stable climate. In contrast to our observations of a strong decrease in the relative abundance of dinoflagellates during the Younger Dryas, *Werne et al.* [2000] found relatively little change in the dinoflagellate population through time. There are several potential reasons why this discrepancy exists. First, *Werne et al.* [2000] use dinosterol (4α,23,24-trimethylcholest-22E-en-3β-ol, CSE 13 or 14) as their sole indicator of dinoflagellates, whereas we use a suite of CSE sterols (1 + 2 and 15) as dinoflagellate indicators. Given the fact that CSEs 1 + 2 and CSE 15 show such different trends, it is apparent that using different dinoflagellate biomarkers can yield different results. Second, free 4-methyl sterols, such as dinosterol, are known to exhibit enhanced preservation relative to free 4-desmethyl sterols [*Gagosian et al.*, 1980; *Wolff et al.*, 1986; *Harvey et al.*, 1989]. Thus changes in the diagenetic conditions of the water column or sediments could alter the abundance of dinosterol relative to other sterols. Given the anoxic nature of the Cariaco Basin, however, it is unlikely that this is the reason for the discrepancy between the two records. In more oxic settings this would become a more likely scenario.

[41] The differing approaches of this study and that of *Werne et al.* [2000] each have their strengths. For example, *Werne et al.* [2000] were able to detect large changes in the coccolithophorid population by using an alkenone biomarker for coccolithophorids and by assuming that their sterol and alkenone biomarkers would not have experienced differential degradation. Unfortunately, there is no CSE sterol that uniquely corresponds to coccolithophorids; therefore our study cannot yield information regarding coccolithophorid populations. Through the use of CSEs, however, we have been able to detect changes in the green algae population; a phytoplankton class that was not identified by *Werne et al.* [2000].

5. Conclusions

[42] In this study, we have examined the paleoceanographic potential of chlorin steryl esters. We find that during the Younger Dryas cold event in the Cariaco Basin, the phytoplankton community shifted such that there were fewer dinoflagellates and more diatoms than there were during the Bølling/Allerød warm period. These shifts are consistent with both the seasonal shifts in productivity in the basin today and the hypothesis that trade wind-induced upwelling in the Cariaco Basin increased during the Younger Dryas. The ability to detect these changes in the downcore distribution of CSEs has been made possible via optimization of the separation of CSEs using RP-HPLC. These results represent an important step in the development of CSEs as paleoenvironmental indicators. As we continue to improve the separation as well as the identifications of the CSE sterols, the nature of these downcore distribution changes will become more salient and CSEs may become more robust proxies for environmental conditions through time.

[43] **Acknowledgments.** The authors would like to thank Sean Sylva and Leah Houghton for assistance with sample analysis. Konrad Hughen graciously provided samples from the Cariaco Basin. We would also like to thank Julian Sachs for thoughtful discussions and encouragement. The comments of John Volkman and two anonymous reviewers greatly improved this manuscript. This work was supported by the Chemical Oceanography Division of the National Science Foundation and a WHOI Watson Fellowship (to KAD).

References

Barrett, S. M., J. K. Volkman, G. A. Dunstan, and J.-M. LeRoi (1995), Sterols of 14 species of marine diatoms (Bacillariophyta), *J. Phycol.*, *31*, 360–369.

Black, D. E., L. C. Peterson, J. T. Overpeck, A. Kaplan, M. N. Evans, and M. Kashgarian (1999), Eight centuries of North Atlantic Ocean atmosphere variability, *Science*, *286*, 1709–1713.

Boyle, E. A., and L. D. Keigwin (1987), North Atlantic thermohaline circulation during the last 20,000 years linked to high latitude surface temperature, *Nature*, *330*, 35–40.

Broecker, W. S., D. Peteet, and D. Rind (1985), Does the ocean-atmosphere system have more than one stable mode of operation?, *Nature*, *315*, 21–25.

Broecker, W. S., M. Andree, W. Wolli, H. Oeschger, G. Bonani, J. Kennett, and D. Peteet (1988), A case in support of a melt-water diversion as the trigger for the onset of the Younger Dryas, *Paleoceanography*, *3*, 1–9.

Dean, W. E., D. Z. Piper, and L. C. Peterson (1999), Molybdenum accululation in Cariaco basin sediment over the past 24 k.y.: A record of water-column anoxia and climate, *Geology*, *27*, 507–510.

de Miro, M. D. (1971), Los foraminiferos vivos y sedimentados del margen continental de Venezuela (resumen), *Acta Geol. Hisp.*, *4*, 102–106.

Duplessy, J. C., A. W. H. Be, and P. L. Blanc (1981), Oxygen and carbon isotopic composition and biogcographic distribution of planktonic foraminifera in the Indian Ocean, *Palaeogeogr. Palaeoclimatol. Palaeoecol.*, *33*, 9–46.

Eckardt, C. B., G. E. S. Pearce, B. J. Keely, G. Kowalewska, R. Jaffe, and J. R. Maxwell (1992), A widespread and abundant chlorophyll transformation pathway in the aquatic environment, *Org. Geochem.*, *19*, 217–277.

Ferraz-Reyes, E. (1983), Estudio del fitoplankton el la cuenta Tuy–Cariaco, Venezuela, *Bol. Inst. Oceanogr. Univ. Oriente*, *22*, 111–124.

Gagosian, R. B., S. O. Smith, C. L. Lee, J. W. Farrington, and N. E. Frew (1980), Steroid transformations in recent marine sediments, in *Advances in Organic Geochemistry 1979*, edited by A. G. Douglas and J. R. Maxwell, pp. 407–419, Pergamon, New York.

Gall, V. C.-L., A. Rosell-Mele, and J. R. Maxwell (1998), Data report: Characterization of distributions of photosynthetic pigments in sapropels from holes 966D and 969C, *Proc. Ocean Drill. Program Sci. Results*, *160*, 297–302.

Ganssen, G., and M. Sarnthein (1983), Stable isotope composition of foraminifers: The surface and bottom water record of coastal upwelling, in *Coastal Upwelling: Its Sediment Record, Part A: Responses of the Sedimentary Regime to Present Coastal Upwelling*, *NATO Conf. Ser.*, vol. 10A, edited by E. Seuss and J. Thiede, pp. 99–124, Plenum, New York.

Goad, L. J. (1978), The sterols of marine invertebrates, in *Marine Natural Products: Chemical and Biological Perspectives*, vol. II, edited by P. J. Scheuer, pp. 75–172, Academic, San Diego, Calif.

Goad, L. J., and N. Withers (1982), Identification of 27-nor-(24R)-24-methylcholesta-5,22-dien-3β-ol and brassicasterol as the major sterols of the marine dinoflagellate *Gymnodium simplex*, *Lipids*, *17*, 853–858.

Harradine, P. J., P. G. Harris, R. N. Head, R. P. Harris, and J. R. Maxwell (1996), Steryl chlorin esters are formed during zooplankton herbivory, *Geochim. Cosmochim. Acta*, *12*, 2265–2270.

Harvey, H. R., S. C. M. O'Hara, G. Eglinton, and E. D. S. Corner (1989), The comparative fate of dinosterol and cholesterol in copepod feeding: Implications for a conservative molecular biomarker in the marine water column, *Org. Geochem.*, *14*, 635–641.

Haug, G. H., T. F. Pedersen, D. M. Sigman, S. E. Calvert, B. Nielsen, and L. C. Peterson (1998), Glacial/interglacial variations in production and nitrogen fixation in the Cariaco Basin during the last 580 kyr, *Paleoceangraphy*, *13*, 427–432.

Haug, G. H., K. A. Hughen, D. M. Sigman, L. C. Peterson, and U. Röhl (2001), Southward migration of the Intertropical Convergence Zone through the Holocene, *Science*, *293*, 1304–1308.

Hughen, K. A., J. T. Overpeck, L. C. Peterson, and S. Trumbore (1996), Rapid climate changes in the tropical Atlantic region during the last deglaciation, *Nature*, *380*, 51–54.

Hughen, K. A., J. T. Overpeck, S. J. Lehman, M. Kashgarian, J. Southon, L. C. Peterson, R. Alley, and D. M. Sigman (1998), Deglacial changes in ocean circulation from an extended radiocarbon calibration, *Nature*, *391*, 65–68.

Hughen, K. A., J. R. Southon, S. J. Lehman, and J. T. Overpeck (2000), Synchronous radiocarbon and climate shifts during the last deglaciation, *Science*, *290*, 1951–1954.

Kapsner, W. R., R. B. Alley, C. A. Schuman, S. Anadakrishnan, and P. M. Grootes (1995), Dominant influences of atmospheric circulation on snow accumulation in Greenland over the past 18,000 years, *Nature*, *373*, 52–54.

King, L. L. (1993), Chlorophyll diagenesis in the water column and sediments of the Black Sea, Ph.D. thesis, *WHOI-93-04*, Mass. Inst. of Technol. Woods Hole Oceanogr. Inst., Woods Hole, Mass.

King, L. L., and D. J. Repeta (1991), Novel pyropheophorbide steryl esters in Black Sea sediments, *Geochim. Cosmochim. Acta*, *55*, 2067–2074.

King, L. L., and D. J. Repeta (1994), Phorbin steryl esters in Black Sea sediment traps and sediments: A preliminary evaluation of their paleooceanographic potential, *Geochim. Cosmochim. Acta*, *58*, 4389–4399.

King, L. L., and S. G. Wakeham (1996), Phorbin steryl ester formation by macrozooplankton in the Sargasso Sea, *Org. Geochem.*, *24*, 581–585.

Kowalweska, G., B. Winterhalter, H. M. Talbot, and J. Maxwell (1999), Chlorins in sediments of the Gotland Deep (Baltic Sea), *Oceanologia*, *41*, 81–97.

Lea, D. W., D. K. Pak, L. C. Peterson, and K. A. Hughen (2003), Synchroneity of tropical and high-latitude Atlantic temperatures over the last glacial termination, *Science*, *301*, 1361–1364.

Leblond, J., and P. J. Chapman (2002), A survey of the sterol composition of the marine dinoflagellates Karenia brevis, Karenia mikimotoi, and Karlodinium micrum: Distribution of sterols within other members of the lass Dinophyceae, *J. Phycol.*, *38*, 670–682.

Lin, H.-L., L. C. Peterson, J. T. Overpeck, S. E. Trumbore, and D. W. Murray (1997), Late Quaternary climate change from $\delta^{18}O$ records of multiple species of planktonic foraminifera: High-resolution records from the anoxic Cariaco Basin, Venezuela, *Paleoceanography*, *12*, 415–427.

Lyons, T., J. P. Werne, D. J. Hollander, and R. W. Murray (2003), Contrasting sulfur geochemistry and Fe/Al and Mo/Al ratios across the last oxic-to-anoxic transition in the Cariaco Basin, Venezuela, *Chem. Geol.*, *195*, 131–157.

Mansour, M. P., J. K. Volkman, A. E. Jackson, and S. I. Blackburn (1999), The fatty acid and sterol composition of five marine dinoflagellates, *J. Phycology*, *35*, 710–720.

Meyers, P. (1997), Organic geochemical proxies of paleoceanographic, paleolimnologic, and paleoclimatic processes, *Org. Geochem.*, *27*, 213–250.

Muller-Karger, F., et al. (2001), Annual cycle of primary production in the Cariaco Basin: Response to upwelling and implications for vertical export, *J. Geophys. Res.*, *106*, 4527–4542.

Pearce, G. E. S., P. J. Harradine, H. M. Talbot, and J. R. Maxwell (1998), Sedimentary sterols and steryl chlorin esters: Distribution differences and significance, *Org. Geochem.*, *28*, 3–10.

Peterson, L. C., J. T. Overpeck, N. G. Kipp, and J. Imbrie (1991), A high-resolution Late Quaternary upwelling record from the anoxic Cariaco Basin, Venezuela, *Paleoceanography*, *6*, 99–119.

Prell, W. L. (1984), Variation of monsoonal upwelling: A response to changing solar radiation, in *Climate Processes and Climate Sensitivity*, *Maurice Ewing Ser.*, vol. 5, edited by J. Hansen and T. Takahashi, pp. 48–57, AGU, Washington, D. C.

Prell, W. L., and E. V. Campo (1986), Coherent response of Arabian Sea upwelling and pollen transport to late Quaternary monsoonal winds, *Nature*, *323*, 526–528.

Robinson, N., G. Eglinton, S. C. Brassell, and P. A. Cranwell (1984), Dinoflagellate origin for sedimentary 4α-methylsteroids and 5α(H)-stanols, *Nature*, *308*, 439–442.

Schrader, H., N. Swanberg, A. K. Lycke, M. Paetzel, T. Schrader, and T. Schrader (1993), Diatom-inferred productivity changes in the eastern equatorial Pacific: The Quaternary record of ODP Leg 111, Site 677, *Hydrobiologia*, *269/270*, 137–151.

Svec, W. A. (1991), The distribution and extraction of the chlorophylls, in *The Chlorophylls*, edited by H. Scheer, pp. 89–102, CRC Press, Boca Raton, Fla.

Talbot, H. M., R. N. Head, R. P. Harris, and J. R. Maxwell (1999a), Distribution and stability of steryl chlorin esters in copepod faecal pellets from diatom grazing, *Org. Geochem.*, *30*, 1163–1174.

Talbot, H. M., R. N. Head, R. P. Harris, and J. R. Maxwell (1999b), Steryl esters of pyropheophorbide b: A sedimentary sink for chlorophyll b, *Org. Geochem.*, *30*, 1403–1410.

Talbot, H. M., R. N. Head, R. P. Harris, and J. R. Maxwell (2000), Discrimination against 4-methyl sterol uptake during steryl chlorin ester production by copepods, *Org. Geochem.*, *31*, *871–880*.

Tani, Y., et al. (2002), Temporal changes in the phytoplankton community of the southern basin of Lake Baikal over the last 24,000 years recorded by photosynthetic pigments in a sediment core, *Org. Geochem.*, *33*, 1621–1634.

Véron, B., and C. Billard (1998), Sterolic biomarkers in marine phytoplankton. II. Free and conjugated sterols of seven species used in mariculture, *J. Phycol.*, *34*, 273–279.

Volkman, J. K. (1986), A review of sterol markers for marine and terrigenous organic matter, *Org. Geochem.*, *9*, 83–99.

Volkman, J. K., R. B. Gagosian, and G. S. Wakeham (1984), Free and esterified sterols of the marine dinoflagellate Gonyaulax polygramma, *Lipids*, *31*, 457–465.

Volkman, J. K., S. M. Barrett, G. A. Dunstan, and S. W. Jeffrey (1993), Geochemical significance of the occurrence of dinosterol and other 4-methyl sterols in a marine diatom, *Org. Geochem.*, *20*, 7–15.

Volkman, J. K., S. M. Barrett, G. A. Dunstan, and S. W. Jeffrey (1994), Sterol biomarkers for microalgae from the green algal class Prasinophyceae, *Org. Geochem.*, *21*, 1211–1218.

Volkman, J. K., S. M. Barrett, S. I. Blackburn, M. P. Mansour, E. L. Sikes, and F. Gelin (1998), Microalgal biomarkers: A review of recent research developments, *Org. Geochem.*, *29*, 1163–1179.

Wakeham, S. G. (1989), Reduction of sterols to stanols in particulate matter at oxis-anoxic boundaries in seawater, *Nature*, *342*, 787–790.

Wakeham, S. G., and J. R. Ertel (1988), Diagenesis of organic matter in suspended particles and sediments in the Cariaco Trench, *Org. Geochem.*, *13*, 815–822.

Wakeham, S. G., J. I. Hedges, C. Lee, M. L. Peterson, and P. J. Hernes (1997), Compositions and transport of lipid biomarkers through the water column and surficial sediments of the equatorial Pacific Ocean, *Deep Sea Res. Part II*, *44*, 2131–2162.

Werne, J. P., D. J. Hollander, T. W. Lyons, and L. C. Peterson (2000), Climate-induced variations in productivity and planktonic ecosystem structure from the Younger Dryas to Holocene in the Cariaco Basin, Venezuela, *Paleoceanography*, *15*, 19–29.

Withers, N. (1987), Dinoflagellate sterols, in *The Biology of Dinoflagellates*, edited by F. J. R. Taylor, *Biol. Mongr.*, vol. 21, pp. 316–359, Blackwell, Malden, Mass.

Wolff, G. A., N. A. Lamb, and J. R. Maxwell (1986), The origin and fate of 4-methyl steroids-ii. Dehydration of stanols and occurrence of C_{30} 4-methyl steranes, *Org. Geochem.*, *10*, 965–974.

K. A. Dahl, Department of Marine Geology and Geophysics, Woods Hole Oceanographic Institution, MS#22, Woods Hole, MA 02543, USA. (kdahl@whoi.edu)

R. Goericke, Marine Life Research Group, Scripps Institution of Oceanography, 9500 Gilman Dr., La Jolla, CA 92093, USA. (rgoericke@ucsd.edu)

D. J. Repeta, Department of Marine Chemistry and Geochemistry, Woods Hole Oceanographic Institution, MS#4, Woods Hole, MA 02543, USA. (drepeta@whoi.edu)

Chapter 3

Assessing the role of North Atlantic freshwater forcing in millennial scale climate variability: a tropical Atlantic perspective

This work originally appeared as:

Dahl, K. A., A. J. Broccoli, and R. J. Stouffer, Assessing the role of North Atlantic freshwater forcing in millennial scale climate variability: a tropical Atlantic perspective, Climate Dynamics, 24, 325–346, 2005.

Climate Dynamics (2005) 24: 325–346
DOI 10.1007/s00382-004-0499-5

Kristina A. Dahl · Anthony J. Broccoli
Ronald J. Stouffer

Assessing the role of North Atlantic freshwater forcing in millennial scale climate variability: a tropical Atlantic perspective

Received: 15 March 2004 / Accepted: 5 November 2004 / Published online: 22 February 2005

Abstract This study analyzes a three-member ensemble of experiments, in which 0.1 Sv of freshwater was applied to the North Atlantic for 100 years in order to address the potential for large freshwater inputs in the North Atlantic to drive abrupt climate change. The model used is the GFDL R30 coupled ocean–atmosphere general circulation model. We focus in particular on the effects of this forcing on the tropical Atlantic region, which has been studied extensively by paleoclimatologists. In response to the freshwater forcing, North Atlantic meridional overturning circulation is reduced to roughly 40% by the end of the 100 year freshwater pulse. Consequently, the North Atlantic region cools by up to 8°C. The extreme cooling of the North Atlantic increases the pole-to-equator temperature gradient and requires more heat be provided to the high latitude Atlantic from the tropical Atlantic. To accommodate the increased heat requirement, the ITCZ shifts southward to allow for greater heat transport across the equator. Accompanying this southward ITCZ shift, the Northeast trade winds strengthen and precipitation patterns throughout the tropical Atlantic are altered. Specifically, precipitation in Northeast Brazil increases, and precipitation in Africa decreases slightly. In addition, we find that surface air temperatures warm over the tropical Atlantic and over Africa, but cool over northern South America. Sea-surface temperatures in the tropical Atlantic warm slightly with larger warm anomalies developing in the thermocline. These responses are robust for each member of the ensemble, and have now been identified by a number of freshwater forcing studies using coupled OAGCMs. The model responses to freshwater forcing are generally smaller in magnitude, but have the same direction, as paleoclimate data from the Younger Dryas suggest. In certain cases, however, the model responses and the paleoclimate data directly contradict one another. Discrepancies between the model simulations and the paleoclimate data could be due to a number of factors, including inaccuracies in the freshwater forcing, inappropriate boundary conditions, and uncertainties in the interpretation of the paleoclimate data. Despite these discrepancies, it is clear from our results that abrupt climate changes in the high latitude North Atlantic have the potential to significantly impact tropical climate. This warrants further model experimentation into the role of freshwater forcing in driving climate change.

K. A. Dahl (✉)
Massachusetts Institute of Technology/
Woods Hole Oceanographic Institution Joint Program,
WHOI MS #22, Woods Hole, MA 02543, USA
E-mail: kdahl@whoi.edu
Tel.: +1-508-2892853
Fax: +1-508-4572187

A. J. Broccoli
Department of Environmental Sciences,
Rutgers University, 14 College Farm Road,
New Brunswick, NJ 08901, USA

R. J. Stouffer
Geophysical Fluid Dynamics Laboratory, P.O. 308,
Princeton, NJ 08542, USA

1 Introduction

This study examines the response of the tropical Atlantic to a freshwater input in the North Atlantic using a coupled ocean–atmosphere general circulation model. The motivation for performing freshwater forcing experiments such as this one stems from the hypothesis that millennial-scale climate changes are driven by rapid increases in freshwater input to the North Atlantic from the melting of continental ice sheets (Broecker et al. 1985, 1988). Such freshwater inputs may cause a density stratification of the water column sufficient enough to weaken the formation of North Atlantic Deep Water (NADW) and northward surface flow in the Atlantic,

thus causing a change in climate via redistributing heat normally transported by the NADW overturning cell. Tracers of deep water production support the hypothesis that changes in NADW formation are coincident with climate change during the Younger Dryas, a 1,300 year long cold event that began about 13 kyr BP (Boyle and Keigwin 1987; Keigwin et al. 1991; Bond et al. 1997), as well as during Heinrich events (Keigwin et al. 1994; Oppo and Lehman 1995; Vidal et al. 1997; Zahn et al. 1997; Curry et al. 1999). While abrupt climate change was once thought to be limited to high latitudes, there is a growing body of evidence suggesting that millennial-scale climate change affects regions around the globe (e.g. Behl and Kennett 1996; Peterson et al. 2000; Wang et al. 2001; Altabet et al. 2002).

Historically, simulations of a Younger Dryas-type event via freshwater forcing in the high-latitude North Atlantic were perceived as contradictory to paleoclimate data for the Younger Dryas because they fail to simulate large changes outside of high-latitude regions despite evidence that the Younger Dryas was a nearly global event (e.g. Cane 1998; Clement et al. 2001). The apparent disagreement between models and the paleodata, as well as the global impact of tropical interannual variability (ENSO; Wallace and Gutzler 1981; Deser and Blackmon 1995; Lau and Nath 1996; Lau 1997; Klein et al. 1999; Schmittner et al. 2000) has led some to suggest that the tropics, rather than the high latitudes, drive millennial-scale climate changes on a global scale (Cane 1998; Clement and Cane 1999; Clement et al. 2001; Yin and Battisti 2001). As the number of freshwater forcing experiments and paleoclimate reconstructions grows, however, it is important to reassess the ability of the models to simulate a Younger Dryas-type cooling.

In this paper, we explore the linkages between North Atlantic climate variability and tropical Atlantic climatology with a three-member ensemble of North Atlantic freshwater forcing experiments using the GFDL R30 coupled Ocean–Atmosphere General Circulation Model (OAGCM).

In particular, we address the following questions:

1. What is the response of the tropical Atlantic region to a cooling of the North Atlantic and a slowdown of meridional overturning circulation?
2. What are the mechanisms driving these responses?
3. How do the results of these experiments compare to paleoclimate data from the Younger Dryas cold event?
4. How sensitive are the results to slight variations in the starting conditions of the experiment?
5. How do the results of these experiments compare to freshwater forcing experiments performed using other models?

We focus on the tropical Atlantic for several reasons. The tropics have been at the center of a debate regarding the mechanisms of millennial-scale climate change (e.g. Cane 1998), yet few North Atlantic freshwater forcing studies have specifically examined the tropical response. In addition, there are many recent paleoclimate studies of the Younger Dryas that have focused on the tropical Atlantic region. This, therefore provides a strong basis for the comparison of our model results to paleoclimate data.

2 Models and methods

The model used in this study consists of coupled general circulation models of the atmosphere and the ocean, with land surface and sea-ice components also included. This model is identified as GFDL_R30_c in the nomenclature of the IPCC TAR [see Table 9.1 of Cubasch et al. (2001)]. The GFDL_R30_c model is similar to earlier versions of GFDL coupled models (e.g. Manabe et al. 1991), but with enhanced horizontal and vertical resolution. The description of the model in this section is brief and intended to emphasize the basic characteristics of the model, and the reader should refer to Delworth et al. (2002) for a more complete description.

The atmospheric component employs the spectral transform method with rhomboidal truncation at zonal wave number 30, corresponding to a transform grid spacing of approximately 2.2° latitude by 3.75° longitude. Fourteen unevenly spaced sigma coordinate levels are used for vertical differencing. Insolation at the top of the atmosphere varies seasonally, but not diurnally, and clouds are predicted whenever the relative humidity exceeds a critical threshold. The land-surface model features prognostic snow cover and soil moisture based on a simple "bucket" model. Surface temperature is determined diagnostically, based on the assumption that there is no heat stored in the soil.

The ocean component of the coupled model is based on Version 1.1 of the Modular Ocean Model (Pacanowski et al. 1991), which solves the primitive equations of motion using the Boussinesq, rigid-lid and hydrostatic approximations. The horizontal grid spacing is 2.25° latitude by 1.875° longitude, with depth as the vertical coordinate and 18 unevenly spaced levels. Sea ice is simulated by a simple thermodynamic model, in which ice is treated as a single layer with no sensible heat content. Sea ice is advected by ocean currents, but additional convergence is not permitted once the sea-ice thickness exceeds a critical value (4 m). The formation of leads is not included. The atmospheric and oceanic components of the model exchange fluxes of heat, water and momentum once a day. The heat flux consists of the radiative, sensible and latent components, and the water flux includes evaporation, sublimation, precipitation and runoff from the continents.

As the first step in initializing the fully coupled model, the atmospheric component of the coupled model is integrated using observed seasonal cycles of sea-surface temperature and sea ice as lower boundary conditions, along with a prescribed seasonal cycle of solar radiation at the top of the atmosphere.

In the second step, the ocean component of the coupled model is integrated for several thousand years starting from an isothermal, isohaline state at rest. Climatological monthly mean fluxes of heat, water, and momentum archived from the atmosphere-only integration described above are supplied to the ocean as forcing terms at the sea surface. In addition, sea-surface temperature (SST), sea-surface salinity (SSS), and sea ice are restored to an observed climatological seasonal cycle with a restoring time of 40 days. The model is run until long-term drifts in deep ocean temperature and salinity become relatively small.

Because the two component models are not necessarily in balance with each other, the SSTs computed by the ocean model generally will not match the SSTs to which they are being restored. The restoring terms in the last several hundred years of the ocean component spin-up are averaged to produce spatially and seasonally varying flux adjustment terms, which are added to the atmospheric fluxes passed to the ocean component of the coupled model. The flux adjustments are determined prior to the start of the coupled model integration and do not vary from one year to the next. Because the flux adjustments are independent of the state of the coupled model, they do not systematically damp or amplify anomalies of sea-surface temperature or sea-surface salinity. The use of flux adjustments is successful in greatly limiting the long-term drift of the model (Manabe et al. 1991).

2.1 Control run simulations

After coupling the ocean and atmosphere components of the model, a control run (CTRL1) was integrated for 900 years. A second control run (CTRL2) was integrated for 600 years starting from year 601 of CTRL1 and using the same model parameters, but on another computing system. Sea-surface temperatures from the two control runs match within 0.25°C throughout the Atlantic. Within the tropical Atlantic, the difference in SST between the two runs is generally less than 0.05°C. The precipitation patterns exhibited by the two control runs are similar for both December/January/February (hereafter DJF) and June/July/August (hereafter JJA).

The largest differences in SST and precipitation between the two control runs are significantly smaller than the anomalies that result from the freshwater forcing experiments discussed here. We therefore conclude that the differences between the two control simulations are within the range of the internal variability of each run.

Simulated and observed sea-surface temperatures agree well throughout the globe (Fig. 1). In most cases, the difference between observed and simulated temperatures is less than 1°C. Notable exceptions include patches of the Southern Ocean and the region south of Greenland. In these locations, the difference between modeled and observed SSTs is 2–3°C. The overall pattern of SST in these regions, however, is represented well by the model.

Figure 2 compares the DJF and JJA simulated precipitation with observation data from 1979–2002 (Xie and Arkin 1997). The model is able to simulate the primary features of the observed precipitation patterns. During both DJF and JJA, the model precipitation tends to overestimate precipitation over land, while underestimating precipitation over the oceans. During DJF, the model simulates excess precipitation over portions of South America and southern Africa. During JJA, the modeled precipitation over equatorial Africa is

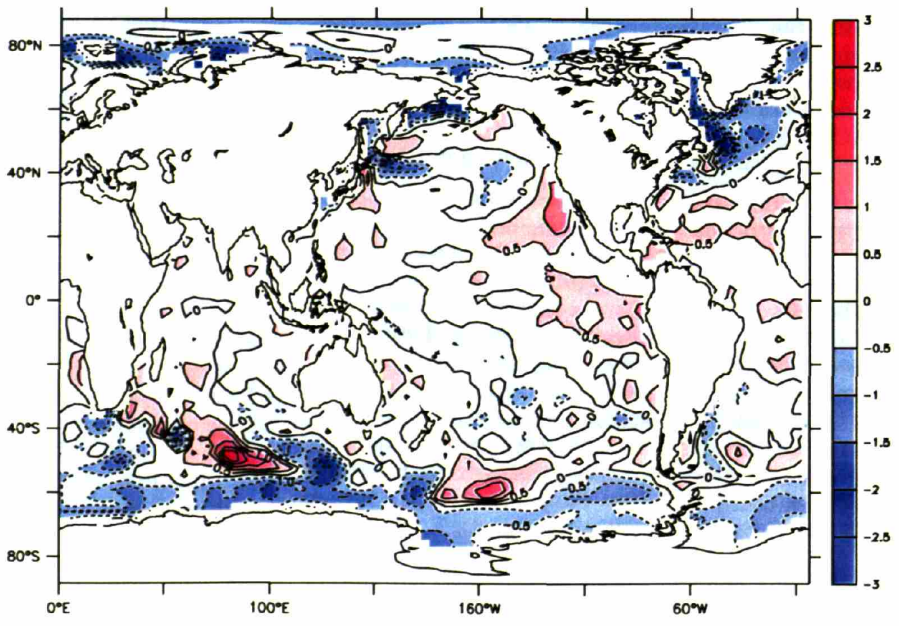

Fig. 1 Differences between simulated and observed annual sea-surface temperatures. Simulated temperatures are from years 1 to 900 of CTRL1. Observed data are from Levitus and Boyer (1994)

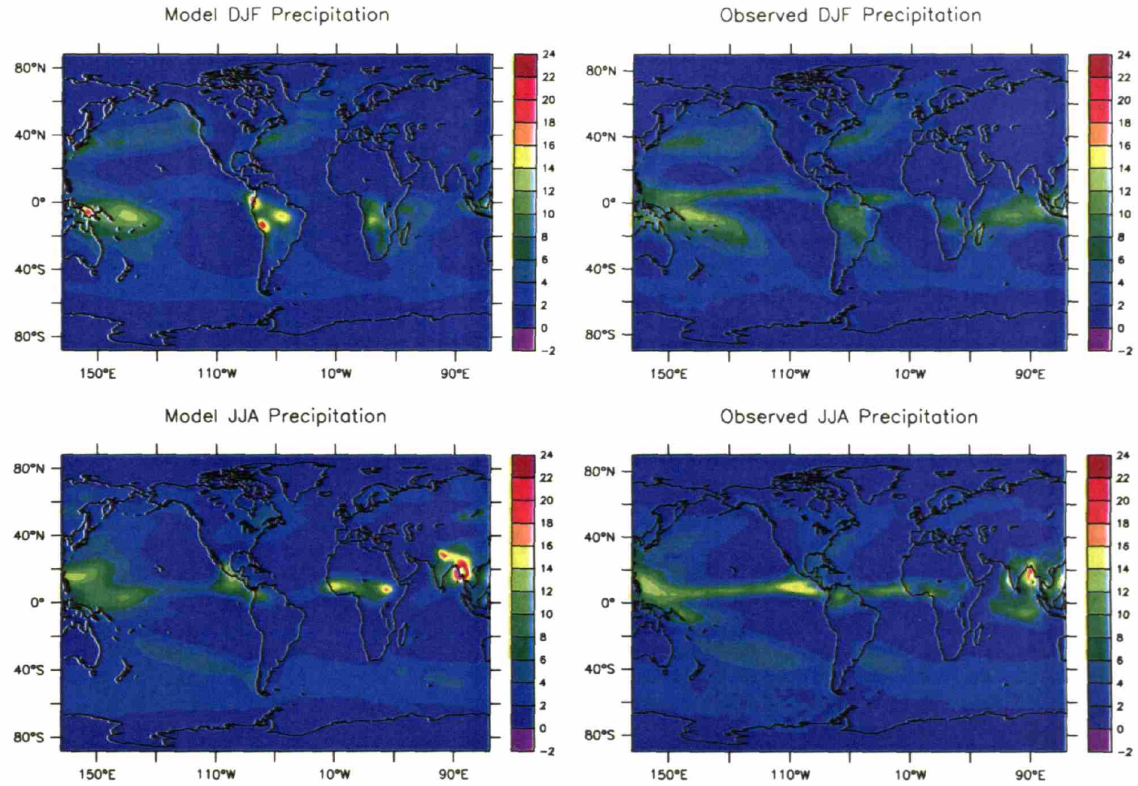

Fig. 2 Simulated and observed precipitation patterns for DJF (*top*) and JJA (*bottom*). Units are in mm day^{-1}. Simulated precipitation is from years 1 to 900 of CTRL1. Observation data are long-term averages from 1979 to 2002 (Xie and Arkin 1997)

too high. These regions of excess precipitation in both seasons correspond to the location of the Intertropical Convergence Zone (ITCZ) in each season. The position of the ITCZ in each season, however, is well captured by the model.

Simulated meridional overturning circulation (MOC) in the North Atlantic varies on multidecadal timescales between 20 Sv and 28 Sv for both CTRL1 and CTRL2. Such variability was observed in lower resolution versions of the GFDL model (Delworth et al. 1993, 1997; Delworth and Mann 2000). The mechanisms driving the variability, however, are not well understood (Delworth et al. 2002). The average value of the MOC (24.6 Sv) is somewhat stronger than current observations of NADW formation in the North Atlantic based on chlorofluorocarbon inventories (17 Sv; Smethie and Fine 2001), and direct measurements (13 Sv; Dickson and Brown 1994, and references therein).

2.2 Freshwater forcing experiments

An ensemble of three freshwater forcing experiments was performed (Table 1). The experiment FW1 was initialized from year 301 of the control run CTRL1. Experiments FW2 and FW3 were initialized from years 601 and 701 of CTRL2, respectively. In each experiment, 0.1 Sv (1 Sv = 10^6 m^3 s^{-1}) of freshwater was applied for 100 years across the Atlantic from 50°N to 70°N. The freshwater had a temperature equal to that of the ambient SST. At the end of the 100 year period, the freshwater was turned off and the recovery monitored.

Table 1 List of experiments discussed in this study

Experiment name	Forcing	Length/Description
CTRL1	Control	900 year integration
CTRL2	Control	600 year integration;Initialized from year 601 of CTRL1
FW1	0.1 Sv freshwater	100 years of freshwater forcing;140 year integration;Initialized from year 301 of CTRL1
FW2	0.1 Sv freshwater	100 years of freshwater forcing;200 year integration;Initialized from year 601 of CTRL2
FW3	0.1 Sv freshwater	100 years of freshwater forcing;200 year integration;Initialized from year 701 of CTRL2

Having three experiments with identical freshwater forcing conditions allows us to assess the robustness of relatively small responses.

The surface flux of freshwater applied during these experiments (1.6×10^{-6} cm s^{-1}) is three orders of magnitude greater than the surface salinity flux adjustment within the same box in North Atlantic (3.4×10^{-9} cm s^{-1}). The flux adjustments, which do not vary temporally or between experiments, are such that freshwater is being removed from the North Atlantic region. Because they do not vary temporally or between experiments, the flux adjustments should not systematically damp or amplify the response to freshwater forcing.

The rate of 0.1 Sv is comparable to estimates of glacial meltwater (Licciardi et al. 1999) and ice-rafted debris (MacAyeal 1993) inputs into the North Atlantic during the Younger Dryas. The duration of the freshwater pulse in these experiments is shorter than that inferred for meltwater pulse 1 A (MWP1A), which is inferred to have been associated with the Younger Dryas (Fairbanks 1989); therefore, the total freshwater input during the experiment is less than implicated for MWP1A. The discharge location of MWP1A, and its relationship to the Younger Dryas is unclear (e.g. Fairbanks 1990; Weaver et al. 2003). While we compare our results to paleoclimate data from the Younger Dryas, it should be noted that the experiments discussed here were run from modern-day boundary conditions rather than glacial or Bølling/Allerød boundary conditions. Most significantly there are no ice sheets over North America and Eurasia in our control runs, and insolation is set at modern-day levels.

Unless stated otherwise, all anomalies shown are the ensemble mean anomalies of the three FW experiments. Anomalies for FW1 were calculated using the last 25 years of the experiment run and CTRL1 while anomalies for FW2 and FW3 were calculated using the last 20 years of each experiment run and CTRL2. In each case, the time mean average of the entire available control run (i.e. 900 years for CTRL1 and 600 years for CTRL2) was used. The three individual anomalies were then averaged in order to determine the ensemble mean anomaly.

3 Results and discussion

3.1 Model results

3.1.1 Atlantic results

In each freshwater forcing experiment, North Atlantic MOC decreases by ~10 Sv by the end of the freshwater pulse (Fig. 3). MOC decreases rapidly at the onset of each freshwater forcing. The decrease continues at a slower rate throughout the remainder of the experiments, and is punctuated by a series of decadal-scale oscillations in the strength of MOC. The decrease in

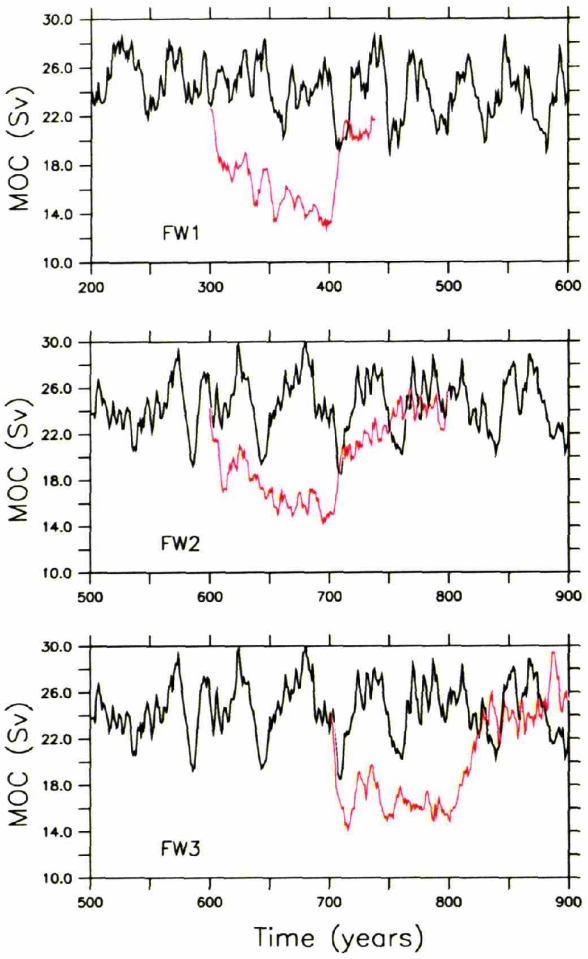

Fig. 3 Time series of North Atlantic meridional overturning circulation during the control runs (*black*) and experiments (*red*) for FW1 (*top*), FW2 (*middle*) and FW3 (*bottom*)

MOC is caused by the development of a low-salinity cap over the North Atlantic that prevents sinking and formation of deep waters (Fig. 4, top). Salinity in the North Atlantic is up to 3 psu lower during the experiments than during the control runs. Formation of Antarctic Bottom Water (AABW) increases and penetrates as far north as 40°N during the freshwater experiments. These results are generally consistent with those of other modeling studies that show a slowdown of North Atlantic Deep Water (NADW) and enhanced AABW formation in response to a North Atlantic freshwater input (Manabe and Stouffer 1995; Rahmstorf 1995; Manabe and Stouffer 1997; Schiller et al. 1997). North Atlantic MOC in each FW experiment recovers to near its initial values within 50 years of the termination of the freshwater pulse.

As a result of the decrease in MOC, North Atlantic SSTs decrease by up to 11°C (Fig. 4, middle). There is a slight cool bias in the control run (Fig. 1) where the

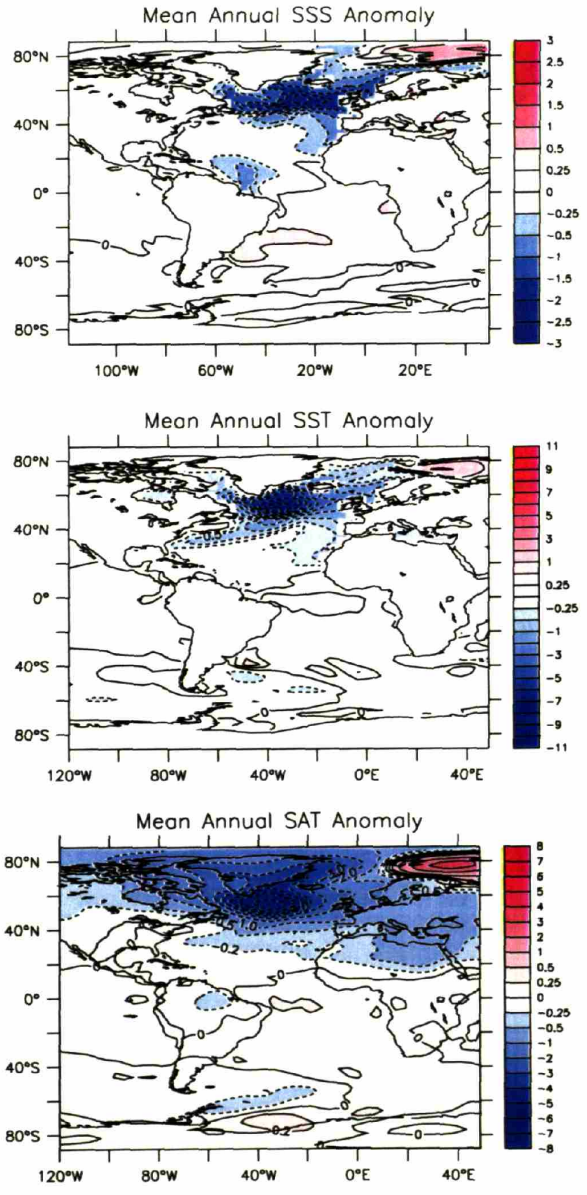

Fig. 4 Ensemble mean anomalies averaged over the last 20–25 years of each experiment. Anomalies are expressed as experiment minus control. *Top* sea-surface salinity anomaly, units are parts per thousand (ppt). *Middle* sea-surface temperature anomaly. *Bottom* surface-air temperature anomaly

greatest cooling occurs in the FW experiments that may contribute 1°C to the cool anomalies. While centered in the northern North Atlantic, the cool anomalies extend as far south as 10°N in the Atlantic. Outside of the Atlantic basin, there are no statistically significant SST anomalies. Surface-air temperatures (SATs) exhibit a similar response (Fig. 4, bottom). In the northern North Atlantic, SAT decreases by up to 8°C. This anomaly is centered just south of Greenland. The cooling extends through northern Africa. Interestingly, both the SST and SAT of the Barents Sea region warm during the freshwater forcing experiments as a result of decreased sea ice in the Barents region. The Barents Sea warming and sea ice reduction could be sensitive to the location in which the freshwater is applied, as the warming occurs north of the region into which freshwater was introduced. The pattern of sea ice anomalies produced by the freshwater forcing, namely increased sea ice south of Greenland and decreased sea ice in the Barents Sea, is reminiscent of the 9–10 year sea ice oscillations, noted by Venegas and Mysak (2000), based on century-long North Atlantic sea-ice records. The model response shows an increase in the strength of the Norwegian Current, which Venegas and Mysak (2000) identify as a likely mechanism for decreasing sea-ice concentrations in the Barents Sea.

3.1.2 Tropical Atlantic results

The cooling of the North Atlantic decreases in magnitude from high to low latitudes. The gradient of SST anomalies, with cooling to the north and warming to the south, is steep in the western tropical Atlantic and more gradual in the eastern tropical Atlantic. SSTs throughout the tropical Atlantic (5°N–20°S, 40°W–20°E) warm by 0.2°C (Fig. 5, top), with anomalies greater up to 0.4°C in the western tropical Atlantic. The magnitude of the interannual variability in tropical Atlantic SST is in the order of the anomalies exhibited during the FW experiments. However, a two-tailed *t*-test demonstrates that all of the anomalies discussed in the manuscript are significant at the 95% confidence level. The temperature anomaly increases with depth and has a maximum of 4.5°C in the thermocline off the coast of South America (Fig. 6). The warm thermocline anomaly begins to develop at the onset of the freshwater forcing and increases steadily throughout the experiment. Tropical Atlantic SSTs, however, cool for the first 20 years of the experiment before gradually warming. The SST response may be damped with respect to that of the thermocline due to air–sea processes. The warm anomalies most likely result from a decrease in the surface and thermocline return flow of warm waters from the tropics to the North Atlantic. Because the formation of deep water in the North Atlantic decreases during the freshwater forcing experiments, less water must flow northward in order to compensate for the export of deep water from the Atlantic. At the surface, northward velocity in the North Brazil Current decreases by 15–25%. In the thermocline, northward velocities, normally 1–3 cm s^{-1} in the control runs, decrease by up to 50%.

Regressing SST against North Atlantic MOC in the control runs allows us to observe the natural, unforced relationship between SST and MOC in the model. This relationship can then be compared to the anomalies generated during the FW runs. For a 1 Sv increase in MOC in the control runs, tropical Atlantic SSTs cool by up to 0.02°C (Fig. 7). Assuming that this cooling is due

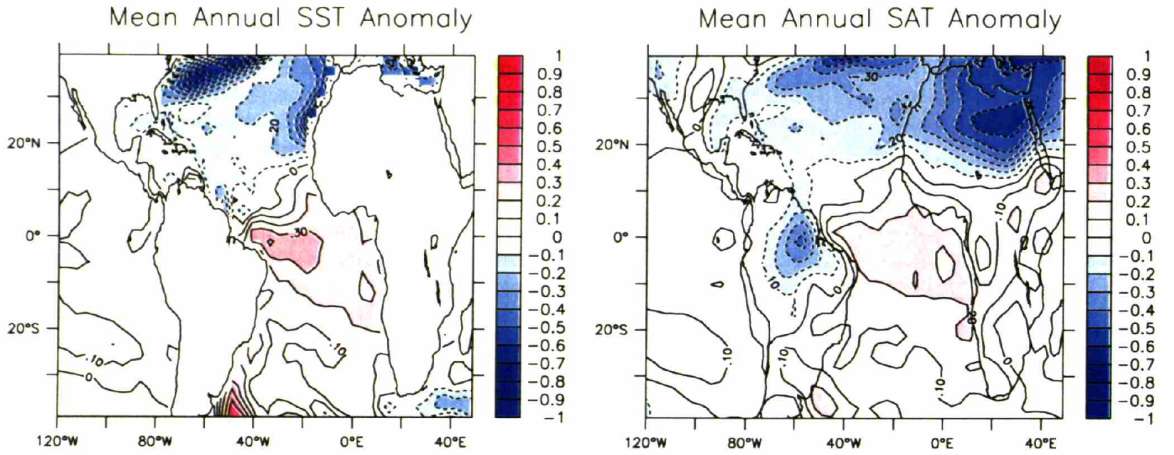

Fig. 5 Ensemble mean tropical Atlantic SST (*left*) and SAT (*right*) anomalies averaged over the last 20–25 years of each experiment Units are °C

entirely to the increase in MOC and that the relationship is linear, a 10 Sv decrease in MOC would result in a 0.1–0.2°C warming of tropical Atlantic SST. The SST anomalies that result from the freshwater forcing are therefore consistent with the relationship between tropical Atlantic SST and MOC in the control run.

Surface-air temperatures in the tropical Atlantic cool north of 10°N. The magnitude of the cooling decreases progressively southward (Fig. 5, bottom). South of 10°N, SAT decreases by up to 0.1–0.5°C over northern South America, but increases by 0.2°C over the ocean and the southern half of Africa. The dichotomy of cooling over South America and warming over Africa is the result of the precipitation changes over the two continents. As will be discussed subsequently, precipitation, and consequently soil moisture, over northern South America generally increases during the freshwater forcing experiments. As a result of the increased soil moisture, an increased proportion of incoming radiation must be devoted to evaporation of the moisture (i.e. latent heating) as opposed to heating the air (i.e. sensible heating). The net effect is, therefore, a cooling of SAT over South America. The opposite is true for Africa; i.e. the general drying of Africa allows for a decrease in latent heating and, therefore, a warming of SAT over the continent. The SAT warming over the ocean is consistent with the warming of SSTs discussed above.

During the FW experiments, the Northeast trade winds become stronger in both winter and summer while the Southeast trade winds experience little or no change

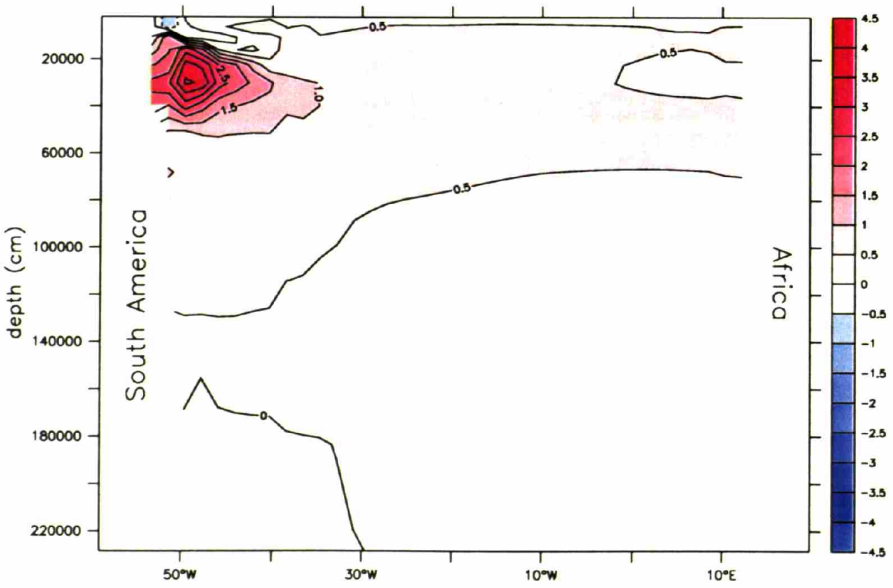

Fig. 6 Cross-sectional view (averaged from 5N to 20S) showing the ensemble mean temperature anomaly in the tropical Atlantic thermocline. Anomalies represent the ensemble mean of the three hosing experiments, averaged over the last 20–25 years of each experiment. Units are ° C

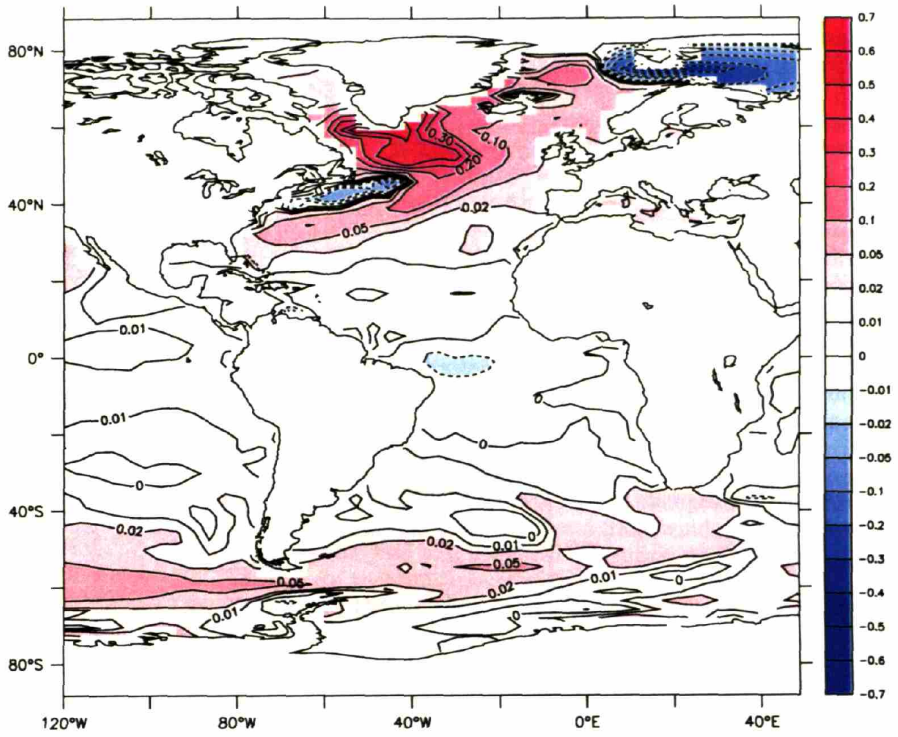

Fig. 7 Regression of SST onto North Atlantic meridional overturning circulation for years 1–900 of the control run (CTRL1). These are the SST anomalies that result from a 1 Sv increase in MOC. Units are °C

(Fig. 8). Upwelling within the upper 100 m of the water column increases in the northern tropics (5–10°N) and decreases in the southern tropics (0–10°S). These upwelling changes may help to reinforce the SST anomalies observable in Fig. 5. In association with the changes in trade wind strength, the mean position of the Intertropical Convergence Zone (ITCZ) shifts southward. In nature, the position of the ITCZ is one of the dominant controls on precipitation patterns in the Atlantic region (as well as the rest of the tropics). During the Northern Hemisphere summer, the ITCZ is at its northernmost position, residing around 10°N. During this time, there is relatively high precipitation in Central America and across the Sahel region of Africa. The ITCZ then migrates southward during Northern Hemisphere winter. Because this southward migration causes the ITCZ to fall over the continent of South America, the ITCZ becomes less latitudinally defined (Waliser and Gautier 1993). Zones within northern South America experience high precipitation during this time. In Africa, the southward migration of the ITCZ and Zaire Air Boundary (ZAB; the boundary between winds from the Atlantic and the Indian Oceans) leads to high precipitation in the southern half of the continent (Nicholson 2000).

The precipitation anomalies associated with the freshwater forcing experiments are consistent with a southward shift in the mean position of the ITCZ (Fig. 9). JJA precipitation anomalies show a decrease in the Sahel region of Africa and an increase in precipitation over coastal equatorial Africa and Northeast Brazil (NEB). These anomalies occur in a latitudinally oriented configuration, which suggests that they are driven by changes in the position of the ITCZ. The freshwater forcing induces a strong increase in precipitation in NEB during both DJF and JJA. The DJF increase is stronger than the JJA increase, likely due to increased advection of moisture from the Atlantic ocean by the strengthened NE trades. As shown in Fig. 8, the DJF wind anomalies are strongest over the equatorial Atlantic, while the JJA anomalies are strongest over the tropical–subtropical Atlantic. The strengthened DJF winds are thus gaining moisture from regions of the ocean that show a SST warming anomaly during the FW experiments. In contrast, JJA winds are blowing over higher latitude oceanic regions that undergo a cooling during the FW experiments, therefore decreasing moisture availability over the ocean. The increase in South American precipitation during DJF is associated with an increase in both high and low cloud cover (not shown) over northeast Brazil that results from the convergence of winds over northern South America (Fig. 8). In contrast, precipitation in equatorial–subequatorial Africa generally decreases during Northern Hemisphere winter. This drying may be induced by a change in the strength and direction of the winds contributing to the ZAB. During the freshwater forcing experiments, onshore winds from the Atlantic decrease slightly (5%) in strength while onshore winds from the Indian Ocean become more northerly in direction. Thus, during the freshwater forcing experi-

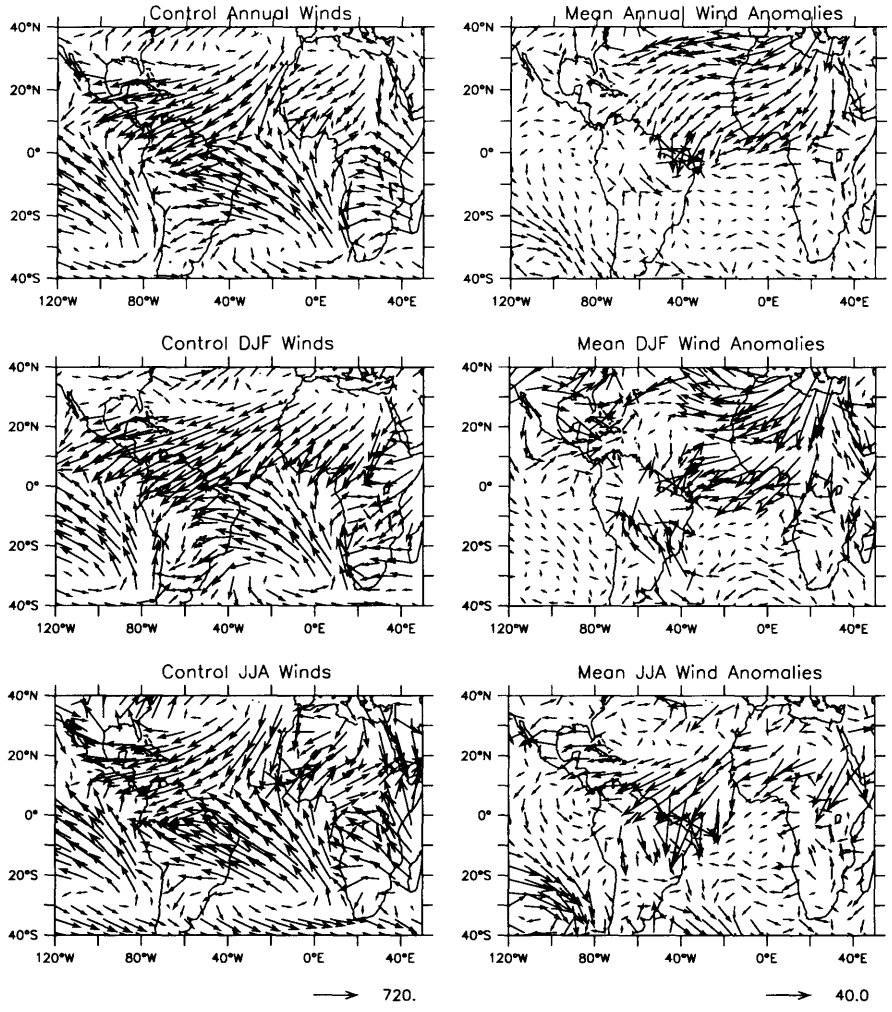

Fig. 8 Control (*left*) and anomalous (*right*) winds for ANN (*top*), DJF (*middle*), and JJA (*bottom*). Anomalies represent the ensemble mean of the three hosing experiments, averaged over the last 20–25 years of each experiment. Note the vectors for scale. Units are cm s^{-1}

ments, the convergence of the two wind systems, which is a source of DJF precipitation in the southern half of Africa, decreases. As a result, DJF rainfall decreases in this region of Africa.

The response to the southward shift of the ITCZ in the Atlantic sector is similar to the response noted by Chiang et al. (2003, hereafter CBB) in a simulation of the Last Glacial Maximum, in which insolation, CO_2, and land ice were set to their presumed 21 kyr values. They attribute the responses they observe to a "meridional mode" of atmosphere–ocean variability associated with a strengthening of the Northeast trade winds. The response of the ITCZ in the FW experiment is also accompanied by the changes in trade wind strength and the meridional SST gradient, as in CBB. To quantify this similarity, we used the anomalies of the FW experiment with respect to the control to compute the same indices of North tropical Atlantic trade wind strength and meridional SST gradient defined by CBB. The signs of these two indices in the FW experiments are consistent with CBB's LGM simulation, although the magnitudes are smaller, which suggests that a similar physical mechanism may be operative.

Some insight into the physical mechanism responsible for the southward shift of the ITCZ in the Atlantic sector in the freshwater forcing simulations can be taken from the experiments of Broccoli et al. (in preparation), who examined the response of tropical climate to extratropical thermal forcing using an atmosphere-mixed layer ocean model. The atmospheric component of this model was virtually identical to the atmospheric component of the current coupled model, but the oceanic component consisted of an isothermal, static slab of water of 50 m depth. Instead of realistic geography, two flat continents, symmetric about the equator, were used to simplify the interaction between continental configuration and climate. This simulation is hereafter identified as the SYMM integration. A second integration was also made, in which an additional heat flux of -10 W $m^{-2}$was applied to the slab ocean north of 40°N and a positive flux of the same magnitude was applied

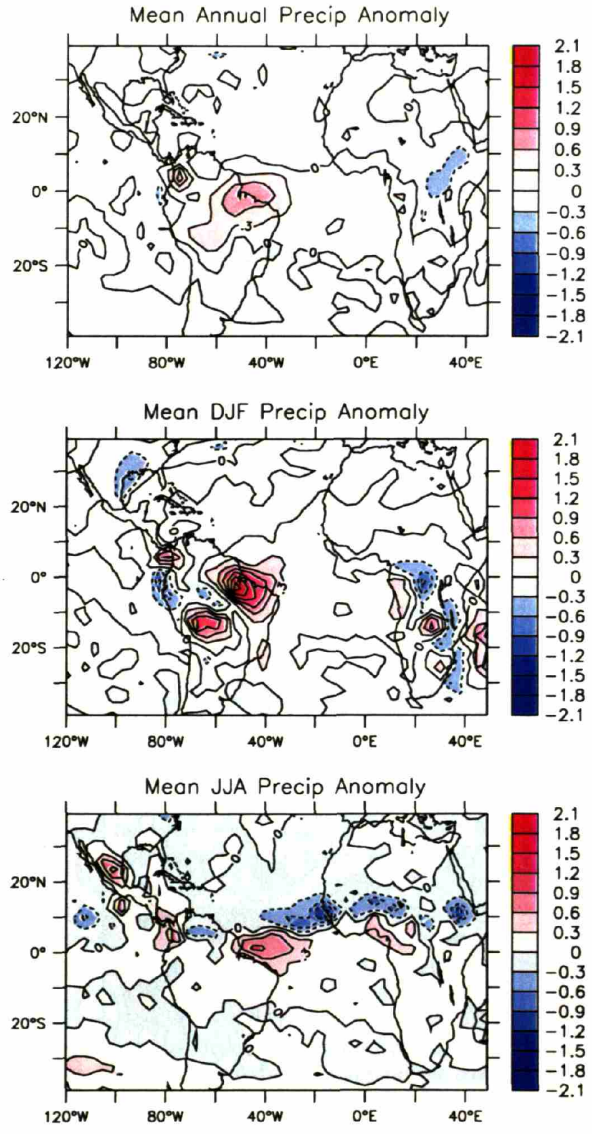

Fig. 9 Ensemble mean precipitation anomalies for ANN (*top*), DJF (*middle*), and JJA (*bottom*). The anomalies represent the last 20–25 years of each experiment. Units are mm day^{-1}

south of 40°S. This Cool North Warm South (hereafter CNWS) integration can be regarded as analogous to the FW experiments, in which a large surface cooling takes place in the extratropical North Atlantic with little systematic change in surface temperature elsewhere. For comparison, the zonally averaged heat flux anomaly north (south) of 40°N (40°S) for the cooling associated with the FW experiments is 4 W m^{-2}(0.4 W m^{-2}) and is centered in the North Atlantic with little change elsewhere. The anomalous heat fluxes prescribed for CNWS are therefore much larger than the heat flux anomalies generated during the FW experiments. In response to the extratropical thermal forcing, the ITCZ in the CNWS integration shifts southward, antisymmetric precipitation anomalies straddle the equator, and the northern trade winds are enhanced while the southern trades are weakened (Fig. 10). Each of these features is qualitatively similar to those appearing in the FW experiments in the Atlantic sector, albeit in a more exaggerated form. If one assumes that the similarity of the FW and CNWS responses is indicative of a similarity in mechanism, then the following chain of causation, described in more detail for the CNWS case by Broccoli et al. (in preparation), is responsible for the tropical Atlantic response in the FW experiments. The North Atlantic cooling that results from the weakening of the MOC strengthens the pole-to-equator temperature gradient in the Atlantic sector, causing the northern extratropics to demand more heat from the tropics. The atmospheric mean meridional circulation satisfies this increased demand by shifting southward in order to transport heat from the equator to high latitudes. The changes in ITCZ position, tropical precipitation, and trade wind strength are thus a response to a change in the mean meridional circulation of the atmosphere in the Atlantic sector.

In addition to the position of the ITCZ, tropical Atlantic SST patterns provide controls on precipitation in South America and Africa. Many studies have suggested that there is a positive correlation between rainfall in NEB and tropical Atlantic SST anomalies (Markham and McLain 1977; Hastenrath and Heller 1977; Mechoso et al. 1990) and/or the meridional SST gradient in the tropical Atlantic (Moura and Shukla 1981; Uvo et al. 1998). The extent to which tropical Atlantic SSTs influence rainfall in NEB varies on both seasonal e.g. Uvo et al. 1998) and interannual (e.g. Folland et al. 2001; Peagle and Mo 2002) timescales. Using the CTRL1 control run, we have regressed precipitation against tropical Atlantic SST averaged from 5°N–5°S across the Atlantic. An increase in tropical Atlantic SST is associated with an increase in precipitation over NEB. This relationship is particularly evident in the regressions of annually averaged precipitation onto annual SST (Fig. 11) and of DJF precipitation onto DJF SST (not shown), which is generally consistent with the findings of Uvo et al. (1998) and Peagle and Mo (2002). It is important to note that in nature, rainfall in South America is also influenced by tropical Pacific SST (e.g. Uvo et al. 1998; Pezzi and Cavalcanti 2001). Given that SST in the tropical Pacific is unchanged in response to the freshwater forcing experiments, however, it is unlikely that SST variability in the tropical Pacific is responsible for the precipitation anomalies that develop in South America. During the freshwater forcing experiment, the increase in tropical Atlantic SST may be contributing to the changes in precipitation over South America. As shown in Fig. 11, a 1°C increase in annually averaged tropical Atlantic SSTs is associated with a 0.9 mm day^{-1} increase in annually averaged NEB precipitation (30°W–50°W, 0°S–15°S). Thus the 0.3° warming of tropical Atlantic SSTs during the experiments could elevate annual pre-

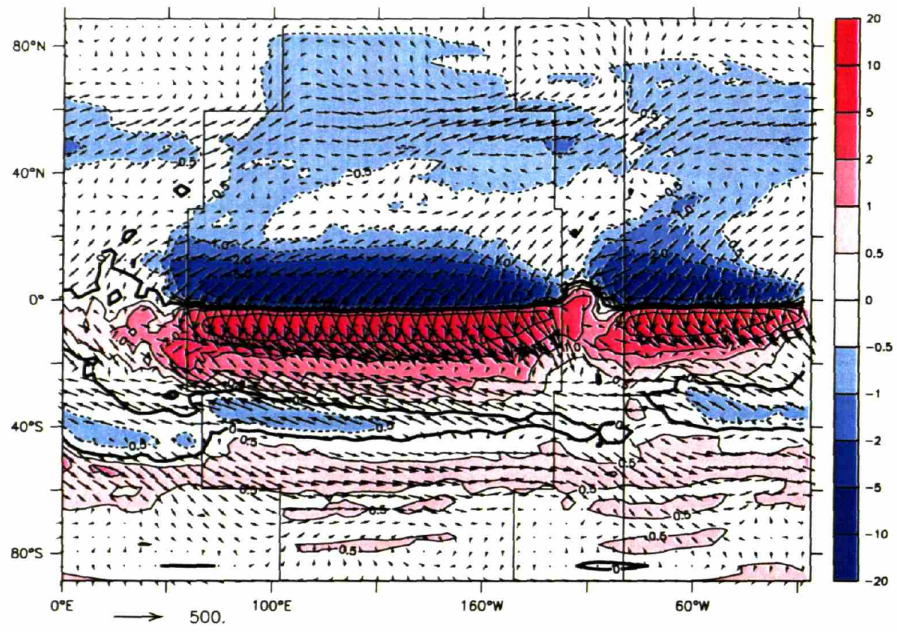

Fig. 10 Differences in annually averaged precipitation rate (colors, in mm day^{-1} and surface winds (vectors, in cm s^{-1} between the CNWS and SYMM integrations

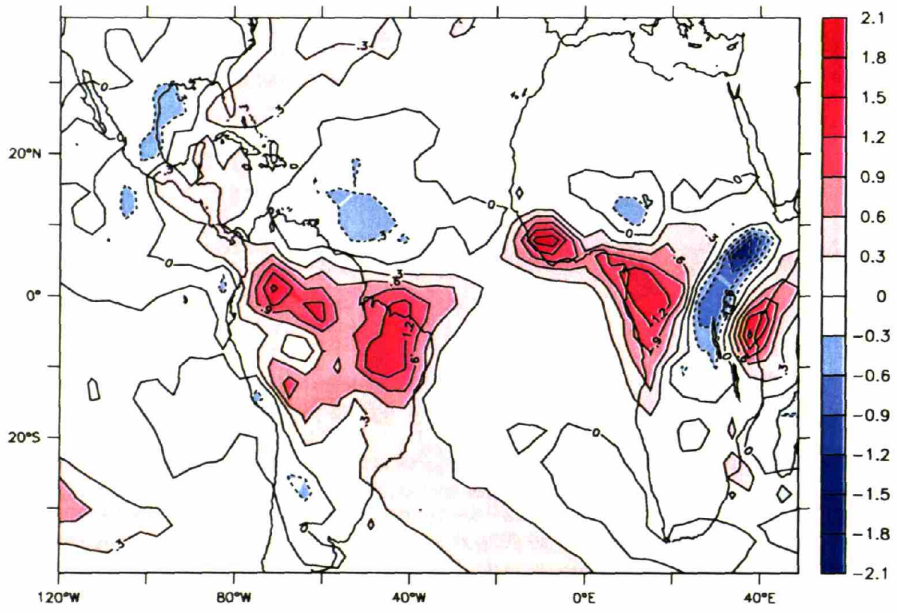

Fig. 11 Regression of annual CTRL1 precipitation against annual tropical Atlantic SST (averaged 5N–5S, 40W–0E). Units for precipitation are mm day^{-1}. The field was scaled such that the figure can be interpreted as a linear response to a 1°C increase in tropical SST

cipitation in NEB by ~0.3 mm day^{-1}, a change that is generally consistent with the results shown in Fig. 9.

Tropical Atlantic SSTs also affect precipitation patterns in Africa. Warm SSTs along the Benguela coast are associated with high coastal rainfall (Nicholson 2000). This can been seen in the control run regression of tropical Atlantic SST and precipitation. On an annual basis, a 1°C increase in tropical Atlantic SST is associated with a 1–2 mm day^{-1} increase in rainfall along the western coast of Africa (Fig. 11). The slight increase (up to 0.3 mm day^{-1}) in African coastal precipitation in response to the freshwater forcing (Fig. 9) is consistent with the 0.3°C increase in tropical Atlantic SST.

Thus, the rainfall anomalies in South America and Africa during the freshwater forcing experiments result from a combination of a southward shift in the ITCZ and an increase in tropical Atlantic SSTs. As mentioned above, the increase in tropical Atlantic SST is most likely a result of the decreased surface return flow that occurs in response to the slowdown of NADW export from the Atlantic.

3.2 Comparisons

3.2.1 Paleodata-model comparison

A growing number of studies indicate that climate variability on millennial-timescales is not limited to the North Atlantic region. Until recently, such variability was thought to be driven by rapid climate changes in the North Atlantic region, possibly caused by rapid surging of ice sheets and freshwater capping of the North Atlantic. As evidence for millennial-scale climate variability mounts from throughout the globe, however, this paradigm is being reevaluated. In essence, it is unclear whether North Atlantic climate changes can be effectively propagated throughout the globe in order to induce seemingly simultaneous climate change in remote areas (e.g. Cane 1998). Freshwater forcing experiments provide a means for testing the ability of North Atlantic-driven climate change to affect regions outside of the North Atlantic (e.g. Dong and Sutton 2002). Again, however, it must be noted that the boundary conditions for events such as the Younger Dryas were likely to have been very different from the modern day boundary conditions used in these experiments. Nevertheless, the FW experiments have a significant effect on the tropics and it is important to assess which model responses are consistent with paleoclimate data. In each of the studies discussed below, we compare the difference between Bølling/Allerød (the period preceding the Younger Dryas) and Younger Dryas climates as opposed to the difference between Holocene and Younger Dryas climate. The comparison was done in this way in hopes that a Bølling/Allerød to Younger Dryas comparison would be more analogous to the simulation of cooling from modern-day boundary conditions in the freshwater forcing experiments. The tropical Atlantic data discussed in this section are summarized in Table 2, Fig. 12, and 13.

The history of deepwater formation in the Atlantic was reconstructed using the carbon isotopic composition ($\delta^{13}C$) and Cd/Ca ratio of benthic foraminifera. Both of these proxies are sensitive to the nutrient concentration of the ambient water, which, in theory, varies with the amount of NADW versus AABW at a given site. Several North Atlantic studies of these, and other nutrient-based tracers suggest that there was a decrease in the strength, but not a shutdown, of NADW formation (Boyle and Keigwin 1987; Keigwin et al. 1991; Bond et al. 1997; Marchitto et al. 1998) during the Younger Dryas. Given that these are water-mass tracers rather than kinematic tracers, it is difficult to quantify the reduction in deepwater formation during the Younger Dryas. The direction of the changes documented by these proxies is consistent with the results obtained here.

Paleotemperature reconstructions from the North Atlantic (north of 20°N) suggest that SSTs and SATs cooled during the Younger Dryas. Although the magnitude of this cooling is location-dependent, estimates of the SST and SAT changes in the northern North Atlantic are on the order of 6–10°C (Dansgaard et al. 1989; Chappellaz et al. 1993; Kroon et al. 1997). Pollen evidence from throughout Europe also suggests a Younger Dryas cooling (e.g. Walker et al. 1994; Ammann et al. 1994; deBeaulieu et al. 1994, and references therein). For a more comprehensive map of North Atlantic sites showing a Younger Dryas cooling, refer to Broecker (1995). The limited paleoclimate data from the Barents Sea suggests that this sea was at least seasonally ice-free during the Younger Dryas (Rosell-Mele and Koc 1997). However, we know of no conclusive studies suggesting temperature changes in the Barents Sea region that would either substantiate or refute the warming response during the FW experiments.

Alkenone-derived SSTs from a well-dated core on the Iberian margin show a 3–4°C cooling during the Younger Dryas and Heinrich Event 1 (H1 Bard et al. 2000). Further south, two alkenone records from the western African margin, as well as a coral record from Barbados, show 1–2°C cooling during the Younger Dryas (Zhao et al. 1995; Guilderson et al. 2001; Kim et al. 2002). A Mg/Ca SST reconstruction from the Cariaco Basin shows a 2–3°C cooling during the Younger Dryas (Lea et al. 2003). Several studies, however, document a warming of tropical Atlantic SSTs during the Younger Dryas. These studies include sites off the coast of Grenada (~1°C, Rühlemann et al. 1999; Lea et al. 2003) along the western African Margin (Mulitza and Rühlemann 2000) and off the coast of NEB (Fig. 12, Arz et al. 1999).

Within the region that experiences warming during the FW experiments, three of the five temperature-reconstruction sites demonstrate a warming during the Younger Dryas. These sites show greater Younger Dryas warming than that generated during the FW experiments. The two sites that experience a cooling are located within upwelling regions, which may not be well simulated by our model.

Surface-air temperature reconstructions from Central and South America generally suggest that these regions cooled during the Younger Dryas (Fig. 13). Pollen-based temperature reconstructions from Costa Rica and Colombia suggest a cooling of 1–6°C. A tropical ice-core record from Huascaran, Peru, also suggests a cooling during the Younger Dryas (Thompson et al. 1995). While the FW experiments do show a cooling of SAT over northern South America, the magnitude of the cooling (less than 0.5°C is smaller than that implied by the paleoclimate data. Furthermore, the cooling of northern South America during the FW experiments is likely due to increased precipitation in the region, which may not be consistent with paleoclimate data from the Younger Dryas.

Reconstructions of aridity from the Americas suggest a pattern of reduced precipitation in northern South America, Central America, and the Caribbean and increased precipitation in southern South America (Fig. 13). Pollen data from Lake Chalco, Mexico (Flores-Diaz 1986), Haiti (Hodell et al. 1991), and Colombia

Table 2 Summary of Paleoclimate data-model comparisons

Ref#	Location	YD conditions (Type of Data)	Model results	Reference
Atlantic SST data				
1	Iberian Margin	−3–4°C (alkenone SST)	−0–2°C	Bard et al. (2000)
2	North Atlantic (37°N)	−2°C (alkenone SST)	−0.1–0.2°C	Calvo et al. (2001)
3	Northwest African Margin	−1.5°C (alkenone SST)	−0.2–+0.2°C	Zhao et al. (1995)
4	Namibian Margin	−2° C (alkenone SST)	+0.2–0.3°C	Kim et al. (2002)
5	Congo Fan	+1.5°C (alkenone SST)	+0.2–0.3°C	Mulitza and Rühlemann (2000)
6	Southwest African Coast	−1-2°C (mollusc mineralogy and $\delta^{18}O$)	+0–0.1°C	Cohen et al. (1992)
7	Barbados	−1–2°C (coral $\delta^{18}O$)	−0–0.2°C	Guilderson et al. 2001
8	Tobago Basin	+2°C (foraminifera transfer functions)	+0–0.2°C	Hüls and Zahn (2000)
9	Grenada	+1.2°C (alkenone SST)	−0–0.2°C	Ruhlemann et al. (1999)
10	Northeast Brazil Slope	+1–3°C (planktonic $\delta^{18}O$)	+0.1–0.3°C	Arz et al. (1999)
11	Cariaco Basin	−3°C (foraminifera Mg/Ca)	+0–0.2°C	Lea et al. (2003)
12	Gulf of Mexico	cooler (faunal assemblages, $\delta^{18}O$)	−0–0.2°C?	Flower and Kennett (1990)
S. American Precip, Wind, and SAT Data				
13	Ceara Rise	NE Brazil dry (Ti/Ca, Fe/Ca)	NE Brazil wet	Arz et al. (1998)
14	Amazon Fan	Amazon Basin dry (planktonic $\delta^{18}O$)	Amazon wet	Maslin and Burns (2000)
15	Cariaco Basin	northern S. America dry (Fe/Ca, Ti/Ca)	?	Haug et al. (2001)
16	Cariaco Basin	↑ trade wind strength	↑ trade wind strength	Peterson et al. (1991); Lin et al. (1997)
17	Colombia	cool, wet (pollen)	−0–0.1°C, wet	Behling and Hooghiemstra (1998)
18	Colombia	−2–4°C, dry	−0–0.1°C, wet	Van der Hammen and Hooghiemstra (1995)
19	Columbia	−1–3°C, dry	−0–0.1°C, wet	Veer et al. (2000)
20	Haiti	Dry (ostracod $\delta^{18}O$)	No response	Hodell et al. (1991)
21	Lake Chalco, Mexico	Dry (lake levels)	Wet?	Flores-Diaz (1986)
22	Costa Rica	−2–3°C (pollen)	−0–0.1°C?	Islebe et al. (1995)
23	Salar de Uyuni, Bolivia	Wet (lacustrine muds in ice core)	dry?	Baker et al. (2001)
24	Sajama, Bolivia	wet (ice core $\delta^{18}O$ and dust)	dry?	Thompson et al. (1998)
25	Huascaran, Peru	Cool and dry (ice core $\delta^{18}O$ and dust)	Cool, wet	Thompson et al. (1995)
African Precip Data				
26	Lake Victoria	Dry (lake levels)	Dry	Stager et al. (2002)
27	Ethiopia	Dry (lake levels)	Dry?	Gillespie et al. (1983); Gasse and Campo (1994)
28	Northern Sahara	Dry (carbonate $\delta^{18}O$, mineralogy)	Dry	Gasse et al. (1990)
29	Western Sahara	Dry (lake levels)	Dry?	Gasse and Campo (1994)
30	Sahel/subequatorial Africa	Dry (lake levels)	Dry?	Gasse and Campo (1994)
31	Lake Bosumtwi (Ghana)	Dry (lake levels, pollen)	Wet?	Street-Perrott and Perrott (1990); Gasse and Campo (1994)
32	Lake Barombi Mbo (Cameroon)	Dry (pollen)	Wet?	Maley and Bernac (1998)
33	Kenya	Dry (bog organic carbon content)	Dry?	Street-Perrott and Perrott (1990)
34	Lake Malawi (East Africa)	Dry (biogenic silica fluxes)	Dry?	Johnson et al. (2002)
35	Rusaka Swamp (Burundi)	Dry (organic matter and pollen)	Dry	Bonnefille et al. (1995)
36	South Africa	No discernable change (pollen)	Dry?	Scott et al. (1995)

(Van der Hammen and Hooghiemstra 1995; Veer et al. 2000) indicate that the Younger Dryas was drier than the Bølling/Allerød. The history of rainfall in the Amazon basin is poorly known for the Bølling/Allerød–Younger Dryas transition. Several reconstructions based on marine sediments, however, suggest an increase in the strength of the northeast trade winds and a drying of northern South America and the Amazon basin during the Younger Dryas (Peterson et al. 1991; Lin et al. 1997; Arz et al. 1998; Maslin et al. 2000; Haug et al. 2001). The drying likely extended at least as far south as Huascaran, Peru, where Thompson et al. (1995) find a drying during the Younger Dryas based on ice-core reconstructions. In the Bolivian Altiplano, however, studies of two tropical ice cores suggest that conditions became wetter during the Younger Dryas Thompson et al.(1998); Baker et al. (2001).

In direct contrast to the studies from northern South America, our model results suggest a strong increase in precipitation (Fig. 9) and runoff (not shown), particularly in northeast Brazil, during a Younger Dryas-type event. The reason for this difference may involve the SST increase in the tropical Atlantic (Fig. 5). As discussed above, increased Atlantic SSTs are associated with increased rainfall in northeast Brazil, both in the model and in nature. SST reconstructions for the Younger Dryas do not uniformly demonstrate a warming in the tropical Atlantic. It is therefore possible that the discrepancy between the modeled and reconstructed South American precipitation results from differences in the direction and magnitude of SST change in the tropical Atlantic during the modeled and actual event. It is also possible that the southward shift of the ITCZ produced by the FW experiments does not dis-

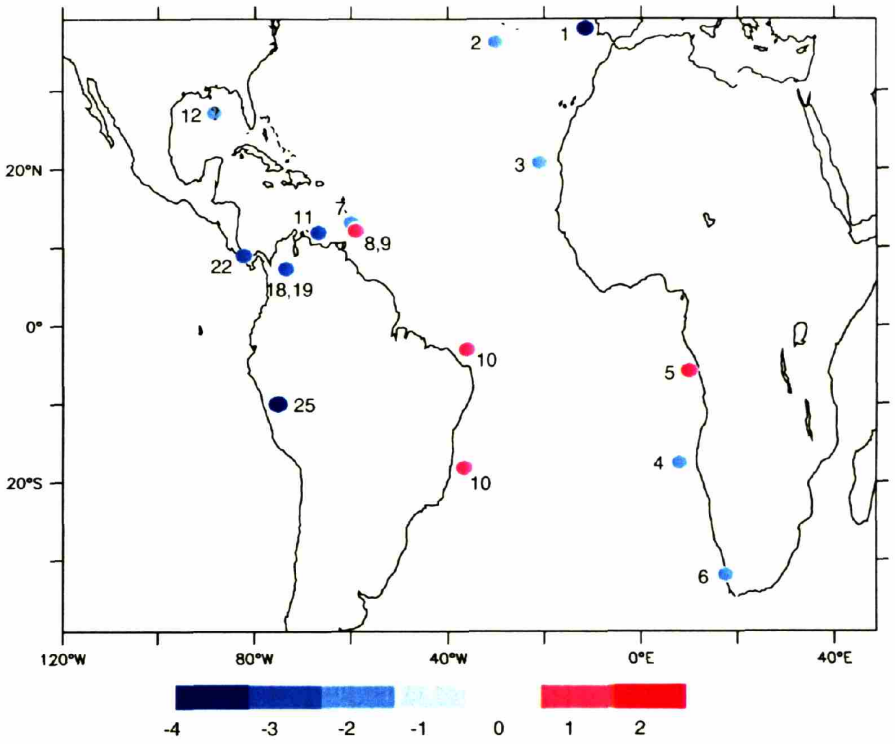

Fig. 12 Location and magnitude of SST and SAT changes associated with the Younger Dryas, as identified by paleoclimate proxies. Red tones indicate a warming, blue tones indicate a cooling. Units are °C. References (as in Table 2) are as follows: (1) Bard et al. (2000), (2) Calvo et al. (2001), (3) Zhao et al. (1995), (4) Kim et al. (2002), (5) Mulitza and Ruhlemann (2000), (6) Cohen et al. (1992), (7) Guilderson et al. (2001), (8) Hüls and Zahn (2000), (9) Rü hlemann et al. (1999), (10) Arz et al. (1999), (11) Lea et al. (2003), (12) Flower and Kennett (1990)

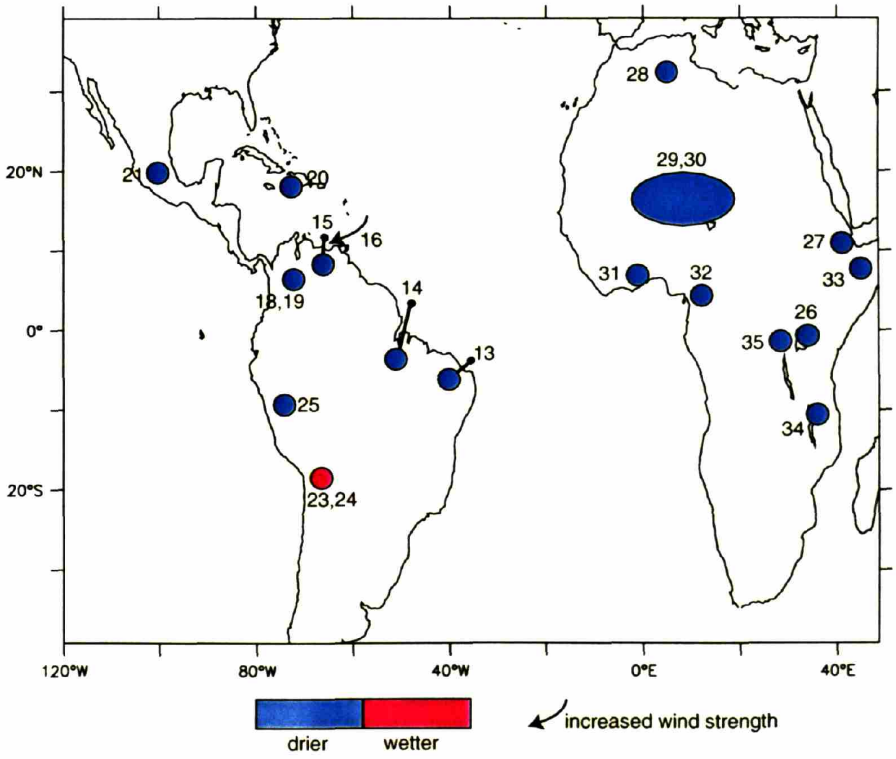

Fig. 13 Precipitation changes associated with the Younger Dryas as identified by paleoclimate proxies. Red indicates increased precipitation, blue indicates decreased precipitation. The small black dots connected by lines to larger dots indicate that the authors have used a marine sediment core to infer moisture conditions on the continent. References (as in Table 2) are as follows: (13) Arz et al. (1998), (14) Maslin and Burns (2000), (15) Haug et al. (2001), (16) Peterson et al. (1991), Lin et al.(1997), (17) Behling and Hooghiemstra (1998), (18) Van der Hammen and Hooghiemstra (1995), (19) Veer et al. (2000), (20) Hodell et al. (1991), (21) Flores-Diaz (1986), (22) Islebe et al. (1995), (23) Baker et al. (2001), (24) Thompson et al. (1998), (25) Thompson et al. (1995)

place the ITCZ as far south as it may have been during the Younger Dryas.

Lake levels decreased throughout Africa during the Younger Dryas, which indicates that the majority of Africa experienced a drying during this time (Fig. 13; Street-Perrott and Perrott 1990; Gasse and Campo 1994; Bonnefille et al. 1995; Johnson et al. 2002; Stager et al. 2002). The evidence from lake levels is supported by pollen data from Lake Bosumtwi (Ghana; Street-Perrott and Perrott 1990; Gasse and Campo 1994), Lake Barombi (Cameroon; Maley and Bernac 1998), and the Rusaka Swamp (Burundi; Bonnefille et al. 1995), as well as biogenic silica data from Lake Malawi (East Africa; Johnson et al. 2002), organic carbon data from Kenya (Street-Perrott and Perrot 1990), and carbonate $\delta^{18}O$ data from Algeria (Gasse et al. 1990). South Africa may be the exception to this widespread drying, as there is no clear evidence for changes in temperature or moisture during the Younger Dryas in this region (Scott et al. 1995).

While robust between the three experiments, the annually averaged precipitation change in the Sahel, equatorial, and subequatorial regions of Africa is small compared to the widespread drying indicated by the paleodata. Such small changes would not likely be detected in the paleoclimate record. The sense of the precipitation changes simulated by the model is in line with what the paleodata suggest; however, the magnitude of change recorded by the paleodata is much larger than the model's response. It is possible that the lack of interactive vegetation in the model could contribute to this discrepancy.

In summary, the modeled North Atlantic response is consistent with data from the Younger Dryas that suggest a cooling of North Atlantic SST and a reduction in the formation of NADW. Paleo–SST reconstructions for the tropical Atlantic suggest a heterogeneous response during the Younger Dryas. Three of the five sites within the region showing a warming during the FW experiments do exhibit a warming during the Younger Dryas. The two sites showing a Younger Dryas cooling lie within upwelling regions, which may complicate the paleoclimate data-model comparison. The warming predicted by the model is weaker than the SST reconstructions suggest for sites that underwent a warming during the Younger Dryas. Paleo–SAT data and the modeled SAT response agree in direction, but not in magnitude; i.e. the cooling of northern South America suggested by the model is weaker than that suggested by the paleoclimate data. The model response may also be affected by precipitation changes during the FW experiments that do not agree with paleoclimate data from South America. Both the model and paleoclimate data suggest that African precipitation decreased, but the modeled drying is weak compared to the changes indicated by the data. Paleoclimate data for South American precipitation changes during the Younger Dryas strongly disagree with the model response. However, this too may simply be the model not producing large enough changes, as a farther southward shift of the ITCZ could induce a drying in NEB in the model. Thus, the freshwater forcing experiments performed for this study capture the direction, but not the magnitude, of change for several parameters (tropical Atlantic SST, African precipitation, and possibly the southward extent of the ITCZ) in the tropical Atlantic region.

The potential reasons why discrepancies exist between the model results and paleoclimate data fall into three main categories: model boundary conditions and experimental design, model limitations, and limitations of the paleoclimate data. The difference in boundary conditions between themodel run (at modern boundary conditions) and the Younger Dryas could have a substantial impact on the ability of the model to simulate Younger Dryas-type climate change. As shown by Yin and Battisti (2001, ice sheets, which were likely present in some form during the Younger Dryas, act as amplifiers of subtle climate change by altering the course of storm tracks. In addition, land ice was shown by Chiang et al. (2003) to be the primary driver of the tropical Atlantic wind, precipitation, and SST response to Last Glacial Maximum boundary conditions. The presence of ice sheets during the Younger Dryas was also associated with sea levels on the order of 60 m lower than today (Fairbanks 1989). The mean climate state of the Younger Dryas was also likely to have been colder than the modern mean climate state. The sea-ice distribution, and the resulting feedbacks, was also most likely different during the Younger Dryas than it is in the model. While the model we used incorporates sea ice, a colder mean climate would enhance the sea ice–albedo feedback. If sea-ice growth in the model occurred under colder boundary conditions, the high-latitude response to FW forcing, and by extension the tropical Atlantic response, would be enhanced. It is also important to consider that, if, as suggested by Weaver et al. (2003), MWP1A originated from Antarctica and triggered the Bølling/Allerød, then the difference in climate between the Bølling/Allerød and the Younger Dryas could have been amplified relative to our "Younger Dryas" FW experiments that used modern-day boundary conditions. Finally, the duration of the forcing for the Younger Dryas was likely to have been much longer than the model freshwater forcing. Thus anomalies may have grown in strength throughout the Younger Dryas in such a way that they were unable to grow during the experiments. Despite the presumably large changes that these differing boundary conditions would have on our experiments, it is interesting to note that climate simulations that do impose Younger Dryas boundary conditions have also had difficulty simulating the changes inferred by paleoclimate data outside of the North Atlantic/Northern European region (Renssen 1997; Renssen and Isarin 1998; Renssen and Lautenschlager 2000).

Limitations of the model's climate feedbacks and architecture could also contribute to differences between the model response and paleoclimate data from the Younger Dryas. Evidence from both Greenland (GISP2)

and Antarctic (Taylor Dome) ice cores suggests that atmospheric methane levels dropped by about 200 ppbv at the Bøllng/Allerød–Younger Dryas transition (Brook et al. 2000). The additional negative radiative forcing associated with the decreased methane could have caused a cooling that was not represented with the model used in this study. In nature, vegetative feedback processes also have a significant effect on tropical climate. In mid-Holocene simulations, the terrestrial response to orbital forcing was amplified, thus becoming more realistic, when vegetation changes are included (Braconnot et al. 1999). Our model does not incorporate vegetation or atmospheric chemistry. Therefore, feedbacks associated with these processes do not contribute to the modeled response to freshwater forcing. It is also possible that an important climate forcing was not included in the experimental design. If millennial-scale variability is paced by variations in solar output, as was suggested by Bond et al. (2001), then the neglect of this component of the climate system may contribute to model–paleodata discrepancies. Precipitation patterns are relatively noisy in the model as well as in nature. While the model captures the general orographic features (and therefore rainfall patterns) associated with mountain ranges such as the Andes, it is unrealistic to expect that the simulated precipitation at a given location within the Andes will accurately reflect precipitation at that location in the real world. Similarly, the resolution of the model does not permit the accurate simulation of specialized environments, such as the Cariaco Basin. That the model's ITCZ generally overestimates precipitation over land may contribute to the discrepancies between precipitation patterns during the Younger Dryas and those that result from the freshwater forcing experiment. More specifically, the model may overestimate the precipitation increase in NEB and underestimate the drying of Africa as a result of the ITCZ's land bias. Finally, it is possible that the model's physics are not accurate enough to generate the responses indicated by the paleodata.

Uncertainties in the interpretation of paleoclimatic data could also contribute to model–paleodata differences. In terms of age control, there are uncertainties in both the measurement of ^{14}C and in the estimation of the reservoir age of a marine system through time. Furthermore, recent evidence suggests that alkenones, from which SST can be derived, are often several thousand years older than foraminifera from the same depth horizon (Ohkouchi et al. 2002). The proxy data itself is also subject to some uncertainty. For sexample, there is a strong seasonality to alkenone production; therefore alkenone-derived SSTs may reflect the temperature only during one season. Furthermore, given that alkenone-producing coccolithophorids do not live exactly at the sea surface, alkenone temperatures may be recording slightly deeper, and therefore, colder temperatures. Depending upon the specific depth habitat of the coccolithophorids, this may partially explain why alkenone-based SST reconstructions record a Younger Dryas warming closer in magnitude to the FW temperature anomalies at thermocline depths.

3.2.2 Intra-model comparison

Despite differences in computer systems, starting values of North Atlantic MOC, and control runs, the results described in this paper are robust for all three of the individual FW experiments. In order to assess the robustness of the responses, we have compared the response of each of the three FW experiments using ten indices (Fig. 14). The indices we have chosen are: North Atlantic MOC, SAT in the region south of Greenland, SAT over the Barents Sea, tropical Atlantic SST, ANN, DJF, and JJA precipitation in South America and Africa. All comparisons were made for the last 20–25 years of each experiment. The mean and range of the anomalies for each of these indices are shown in Fig. 15.

For each FW experiment, the overall decrease in North Atlantic MOC was 8–9 Sv, a ~40% decrease from the original value. The reduction for each experiment occurred within two decades. All three experiments also demonstrate multidecadal variability of the North Atlantic MOC that has a similar timescale, but a lower magnitude, to the varibility observed in the control runs.

SAT anomalies south of Greenland vary by about 1°C between the three FW experiments, with a mean cooling of about 5°C. The range in SAT anomalies for the Barents Sea region is greater: about 2°C, with a mean value of 2°C. Despite the broad range of temperature anomalies in the Barents Sea, all three experiments show a warming in this region. Tropical Atlantic SST anomalies vary by less than 0.05°C between the three runs. All three experiments show a warming of ~2°C for the region shown in Fig. 14.

Precipitation anomalies for all three FW experiments show an increase in South American precipitation during both the summer (JJA) and the winter (DJF), as well as on an annual basis. The largest anomaly, DJF, also has the greatest range in magnitude. African precipitation in all three experiments exhibits a slight decrease. Despite the mild nature of this drying, it is robust for both the annual average as well as for DJF and JJA.

3.2.3 Comparison with simulations by other models

Several modeling groups have performed experiments similar to those of this study using coupled ocean–atmosphere GCMs. Descriptions of the experiments we will consider in this section (Manabe and Stouffer 1997; Schiller et al. 1997; Rind et al. 2001; Vellinga and Wood 2002) can be found in Table 3. The deepwater response obtained with the FW experiments is qualitatively similar to those of other freshwater forcing studies, which all show decreases in North Atlantic MOC of 30–50% ~100 years after the forcing is applied. All of the models also show maximum cooling in the North Atlantic region.

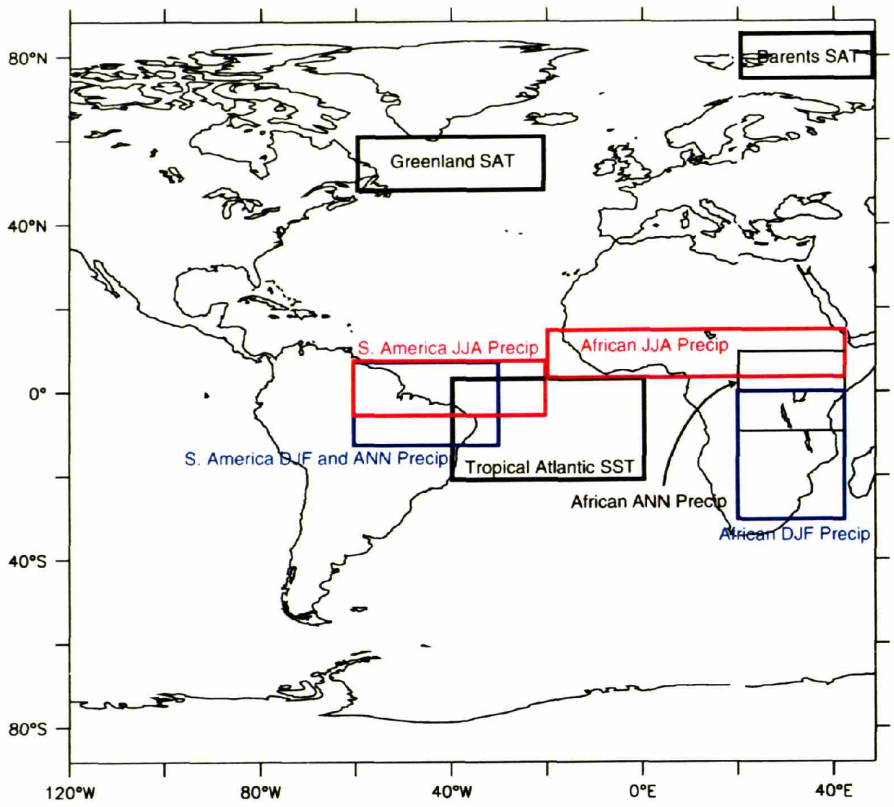

Fig. 14 Indices for intra-model comparison

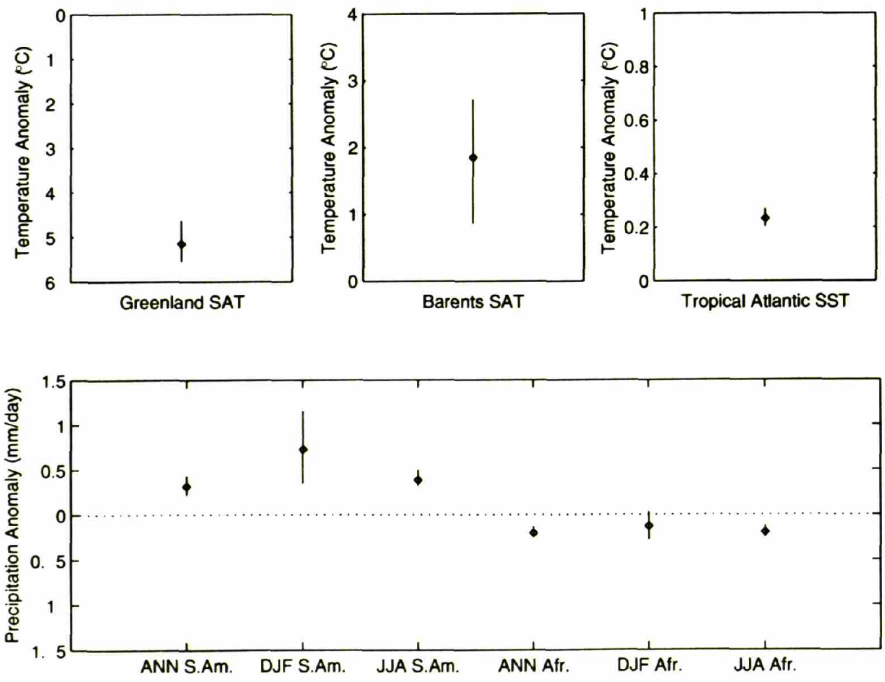

Fig. 15 Variability of the responses of the three FW experiments for various indices shown in Fig. 14. The ensemble mean anomaly is shown as an *open circle*, and the range of anomalies is shown as a *bar through the circle*

In the tropical Atlantic, the SAT response of the R30 model is similar to that of Schiller et al. (1997) and Vellinga and Wood (2002), who found a warming of up to 3.0°C over much of the tropical Atlantic Ocean. Rind et al.(2001) also find a warming response in experiments with greater freshwater forcing (32× St. Lawrence) or weaker control run thermohaline circulation (8× St. Lawrence with FLUX control run). Similar to our findings, Rind et al. (2001) document a pattern of cooling (0.1–0.5°C) over South America after 160 years. The SAT anomalies generated during the Manabe and Stouffer (1997) experiment show a widespread warming over the entire tropical Atlantic region with only isolated patches of slight cooling over eastern South America. Over Africa, the studies discussed here, with the exception of Vellinga and Wood (2002) show a patchy warming of 0.1–2.5°C.

The tropical Atlantic precipitation anomalies observed in these experiments are very similar to those observed by Manabe and Stouffer (1997) in both magnitude and location for NEB and Africa Schiller et al. (1997) and Vellinga and Wood (2002) also find large (2 mm day^{-1})increases in precipitation in northeast Brazil, although their anomalies are shifted further offshore than the anomaly found in this study. Furthermore, both Schiller et al. (1997) and Vellinga and Wood (2002) document strong drying over northwestern half of South America that we do not find here. The magnitude and spatial pattern of drying over Africa documented by Schiller et al. (1997) and our study are similar, while Vellinga and Wood (2002) find patchy increases in precipitation. Given the noisy nature of precipitation in models, we can consider Schiller et al. (1997) and our study to be in relatively good agreement with one another. With the exception of Rind et al. (2001), all of the model experiments considered here show a southward shift in the ITCZ in response to North Atlantic freshwater forcing.

In contrast, Rind et al. (2001) find little change in the precipitation in South America and an increase in precipitation of 0.1–0.5 mm day^{-1} in Eastern Africa. However, the precipitation response they find using a much greater freshwater forcing rate (0.53 Sv, 32× St. Lawrence) is generally more consistent with the results of this study.

In summary, there are several responses to North Atlantic freshwater forcing for which the majority of models concur. The value for SAT cooling in the North Atlantic seems to be converging on ~8°C. While some models show more or less cooling, the direction of the anomaly (i.e. cooling) is consistent. All of the models discussed here show some degree of warming of tropical Atlantic SAT, and four out of the five models show an increase in precipitation in Northeast Brazil. Precipitation changes over Africa are less consistent between models, with three models showing decreased African precipitation and two showing patchy increases. The differences in the magnitude of the modeled responses could be caused by a number of factors, including model architecture, different forcings, and different initial conditions. The forthcoming results of the CMIP (Coupled Model Intercomparison Project) experiments, in which many modeling groups have prescribed the same freshwater forcing, should further elucidate the relationship between model architecture and experimental outcome.

4 Conclusions

Using a coupled OAGCM, we have examined the response of the tropical Atlantic to a North Atlantic freshwater forcing event. A three-member ensemble of experiments shows that, in response to this forcing, the climate state of the Atlantic is significantly changed. The largest responses occur in the North Atlantic, where MOC decreases by 40% and SATs cool by up to ~8°C. Responses in the tropical Atlantic are more subtle. The increased meridional temperature gradient induced by the high latitude cooling causes the northern hemisphere extratropics to demand more heat from the tropics. The ITCZ therefore shifts southward and the Northeast trade winds increase in strength. As a result of the change in the winds and the position of the ITCZ, precipitation patterns throughout the Atlantic basin change. Specifically, precipitation north of 10°N decreases, while precipitation in Northeast Brazil increases substantially and Africa undergoes a mild drying. The changes in precipitation over the continents alter the amount of latent versus sensible heating of the land. Consequently, in general, South America cools while Africa warms.

The strongest tropical Atlantic temperature response occurs in the thermocline, where temperatures warm by up to 4.5°C. This warming, which was noted in previous studies (e.g. Manabe and Stouffer 1997), results from a combination of a decrease in the strength of northward-

Table 3 Other freshwater forcing experiments discussed in this study

Authors	Model	Forcing applied	Duration	Initial MOC	Recovery time
This study	GFDL R30	0.1 Sv	100 years	24 Sv	50 years
Manabe and stouffer (1997)	GFDL R15	0.1 Sv	500 years	18 Sv	250 years
Rind et al. (2001) (Run LTC1)	GISS	0.15 Sv in N. Atlantic + inputs elsewhere	160 years	20 Sv (and decreasing)	No recovery
Schiller et al. (1997)	ECHAM3	Linear increase 0–0.625 Sv	250 years	18 Sv	120 years
Vellinga and Wood (2002)	HadCM3	2 psu decrease in N. Atlantic	0	20 Sv	120 years

flowing currents in the surface and thermocline layers. Warm water is thus allowed to remain in the tropics without being exported to the north or replenished by colder waters from below. These effects occur as a result of a decreased need for surface-water compensation of waters exported from the North Atlantic via deep-water formation. It is probable that the weak (0.2–0.3°C) warming of tropical Atlantic SSTs reflects a surface damping of the response at depth.

Comparison of the model's response to paleoclimate data from the Younger Dryas reveals that, for many parameters, the freshwater forcing experiments capture the direction but underestimate the magnitude of changes indicated by the paleoclimate data. An example of this is the moderate drying of Africa in the model compared to the widespread drying indicated by a variety of aridity proxies for the Younger Dryas. These differences could result from a number of factors, the most notable of which is that the model was run using modern-day boundary conditions, whereas the boundary conditions for the Younger Dryas were likely to have been very different.

Analysis of the three ensemble members shows that, despite slight differences in initial MOC conditions, computer systems, and control runs, the responses discussed above are robust in each member of the ensemble. In no case does the range of responses exhibited by the ensemble members change the direction of the response.

The results of this study allowed us to identify a number of responses to freshwater forcing experiments that are consistent across a range of models and experimental conditions. These robust responses include an 8°C cooling of North Atlantic SAT, a moderate warming of tropical Atlantic SST and SAT, an increase in precipitation in Northeast Brazil, and, to a lesser extent, decreased precipitation in Africa. While the North Atlantic cooling and decreased African precipitation are in line with the paleoclimate data for the Younger Dryas, the widespread warming of tropical SST and SAT and the increased Northeast Brazil precipitation are not. The latter observations suggest that one or more of the following problems exist: (1) Multiple models are unable to simulate a Younger Dryas-type event or (2) The paleoclimate data, which come from a wide variety of proxies, are flawed. We suspect that the primary reason for discrepancies between the models and the paleoclimate data is that there are numerous forcings associated with the Younger Dryas, such as land ice and vegetative feedbacks that were not incorporated into many models, including the model used in this study. In order to investigate this possibility, additional freshwater forcing experiments, particularly those with Bølling/Allerød or Younger Dryas boundary conditions should be performed. In addition, the pattern of SST changes during the Younger Dryas will become clearer as more and more high-resolution SST reconstructions are carried out. Further investigation of millennial-scale variability during the Holocene may provide a more appropriate analog to freshwater forcing experiments, such as this one, performed with modern-day boundary conditions. Despite differences between paleoclimate reconstructions of the Younger Dryas and the modeled response to freshwater forcing, our results suggest that abrupt climate changes in the high latitudes can have a significant effect on tropical climate.

Acknowledgements We would like to thank Ruediger Gerdes, Rong Zhang, Delia Oppo, and two anonymous reviewers for thoughtful discussions and reviews of this manuscript. This work was funded in part by a WHOI Watson Fellowship (to kad).

References

Altabet MA, Higginson MJ, Murray DW (2002) The effect of millennial-scale changes in Arabian Sea denitrification on atmospheric CO_2. Nature 415:159–162

Ammann B, Eicher U, Gaiullard MJ, Haeberli W, Lister G, Lotter AF, Maisch M, Niessen F, Schluchter CH, Wolfarth B (1994) The Wurmian late-glacial in lowland Switzerland. J Quaternary Sci 9:119–127

Arz HW, tzold JPä, Wefer G (1998) Correlated millennial-scale changes in surface hyrography and terrigenous sediment yield inferred from last glacial marine deposits off Northeastern Brazil. Quaternary Res 50:157–166

Arz HW, Pätzold J, Wefer G (1999) The deglacial history of the western tropical Atlantic as inferred from high resolution stable isotope records off northeastern Brazil. Earth Planet Sci Lett 167:105–117

Baker PA, Rigsby CA, Seltzer GO, Frisk SC, Lowenstein TK, Bacher NP, Veliz C (2001) Tropical climate changes at millennial and orbital timescales on the Bolivian Altiplano. Nature 409:698–701

Bard E, Rostek F, Turon JL, Gendreau S (2000) Hydrological impact of Heinrich Events in the Subtropical North Atlantic. Science 289:1321–1324

Behl RJ, Kennett JP (1996) Brief interstadial events in the Santa Barbara basin, NE Pacific, during the past 60 kyr. Nature 379:243–246

Behling H, Hooghiemstra H (1998) Late Quaternary palaeoecology and palaeoclimatology from pollen records of the savannas of the Llanos Orientales in Colombia. Palaeogeogr Palaeoclim Palaeoecol 139:251–267

Bond G, Showers W, Cheseby M, Lotti R, Almasi P, deMenocal P, Priore P, Cullen H, Hajdas I, Bonani G (1997) A pervasive millennial-scale cycle in North Atlantic Holocene and glacial climates. Science 278:1257–1266

Bond G, Kromer B, Beer J, Muscheler R, Evans MN, Showers W, Hoffmann S, Lotti-Bond R, Hajdas I, Bonani G (2001) Persistent solar influence on North Atlantic climate during the Holocene. Science 294:2130–2136

Bonnefille R, Riollet G, Buchet G, Icole M, Lafont R, Arnold M, Jolly D (1995) Glacial/interglacial record from intertropical Africa, high resolution pollen and carbon data at Rusaka Burundi. Quaternary Sci Rev 14:917–936

Boyle EA, Keigwin LD (1987) North Atlantic thermohaline circulation during the last 20,000 years linked to high latitude surface temperature. Nature 330:35–40

Braconnot B, Joussaume S, Marti O, de Noblet N (1999) Synergistic feedbacks from ocean and vegetation on the African monsoon response to mid-Holocene insolation. Geophys Res Lett 26:2481–2484

Broecker WS (1995) The glacial world according to Wally. Eldigio Press, Palisades

Broecker WS, Peteet D, Rind D (1985) Does the ocean-atmosphere system have more than one stable mode of operation?. Nature 315:21–25

Broecker WS, Andree M, Wolli W, Oeschger W, Bonani G, Kennett J, Peteet DA (1988) A case in support of a meltwater diversion as the trigger for the onset of the Younger Dryas. Paleoceanography 3:1–9

Brook EJ, Harder S, Severinghaus J, Steig EJ, Sucher CM (2000) On the origin and timing of rapid changes in atmospheric methane during the last glacial period. Global Biogeochem Cycles 14:559–572

Calvo E, Villanueva J, Grimalt JO, Boelaert A, Labeyrie L (2001) New insights into the glacial latitudinal temperature gradients in the North Atlantic. Results from U37 k′ sea-surface temperatures and terrigenous inputs. Earth Planet Sci Lett 188:509–519

Cane MA (1998) A role for the tropical Pacific Science 282:59–61

Chappellaz J, Blunier T, Raynaud D, Barnola JM, Schwander J, Stauffer B (1993) Synchronous changes in atmospheric CH_4 Greenland climate between 40 and 8 kyr BP. Nature 366:443–445

Chiang JCH, Biasutti M, Battisti DS (2003) Sensitivity of the Atlantic Intertropical Convergence Zone to Last Glacial Maximum boundary conditions. Paleoceanography 18:10.1029/2003PA000916

Clement AC, Cane MA (1999) A role for the tropical Pacific coupled ocean-atmosphere system on Milankovitch and millennial timescales part I: a modeling study of tropical Pacific variability. In: Clark PU, Webb RS, Keigwin LD (eds) Mechanisms of Global Climate Change on Millennial Timescales, vol. 112. American Geophysical Union, Washington DC

Clement AC, Cane MA, Seager R (2001) An orbitally driven tropical source for abrupt climate change. J Climate 14:2369–2375

Cohen AL, Parkington JE, Brundrit JB, Van Der Merwe NJ (1992) A Holocene marine climate record in mollusc shells from the southwest African coast. Quaternary Res 38:379–385

Cubasch U, Meehl GA, Boer GR, Stouffer RJ, Dix M, Noda A, Senior CA, Raper S, Yap KS, Abe-Ouchi A, Brinkop S, Claussen M, Collins M, Evans J, Fischer-Bruns L, Flato G, Fyfe JC, Ganopolski A, Gregory JM, Hu Z-Z, Joos F, Knutson T, Knutti R, Landsea C, Mearns L, Milly C, Mitchell JFB, Nozawa T, Paeth H, Sausen RJ, Smith S, Stocker T, Timmerman A, Ulbrich U, Weaver A, Wegner J, Whetton P, Wigley T, Winton M, Zwiers F (2001) Projections of future climate change. In: Houghton JT, Ding Y, Griggs DJ, Noguer M, van der Linden PJ, Dai X, Maskell K, Johnson CA (eds) Climate change 2001: The scientific basis. Cambridge University Press, Cambridge, pp 555–582

Curry WB, Marchitto T, McManus JF, Oppo DW, Laarkamp KL (1999) Millennial-scale changes in ventilation of the thermocline, intermediate, and deep waters of the glacial North Atlantic. In: Clark PU, Webb RS, Keigwin LD (eds) Mechanisms of global climate change at millennial timescales, vol. 112. American Geophysical Union, Washington DC, pp 59–78

Dansgaard W, White JWC, Johnsen SJ (1989) The abrupt termination of the Younger Dryas climate event. Nature 339:532–533

deBeaulieu J-L, Andrieu V, Lowe JJ, Ponel P, Reille M (1994) The Weichselian late-glacial in southwestern Europe Iberian Peninsula, Pyrenees, Massif Central, Northern Appenines. J Quaternary Sci 9:101–108

Delworth TL, Mann ME (2000) Observed and simulated multidecadal variability in the Northern Hemisphere. Clim Dyn 16:661–676

Delworth T, Manabe S, Stouffer RJ (1993) Interdecadal variations of the thermohaline circulation in a coupled ocean-atmosphere model. J Climate 6:1993–2011

Delworth TL, Manabe S, Stouffer RJ (1997) Multidecadal climate variability in the Greenland Sea and surrounding regions: a coupled model simulation. Geophys Res Lett 24:257–260

Delworth TL, Stouffer RJ, Dixon KW, Spelman MJ, Knutson TR, Broccoli AJ, Kushner PJ, Wetherald RT (2002) Simulation of climate variability and change by the GFDL R30 coupled climate model. Clim Dyn 19:555–574

Deser C, Blackmon ML(1995) On the relationship between tropical and North Pacific sea-surface temperature variations. J Climate 8:1677–1680

Dickson RR, Brown J (1994) The production of North Atlantic deep water: sources, rates, and pathways. Geophys J Res 99:12319–12341

Dong BW, Sutton RT (2002) Adjustment of the coupled ocean-atmosphere system to a sudden change the thermohaline circulation. Geophys Res Lett 29:10.1029/2002GL015229

Fairbanks RJ (1989) A 17,000-year glacio-eustatic sea level record: influence of glacial melting rates on the Younger dryas event and deep-ocean circulation. Nature 342:637–642

Fairbanks RJ (1990) The age and origin of the Younger Dryas Climate Event in Greenland ice cores. Paleoceanography 5:937–948

Flores-Diaz A (1986) In: Lorenzo JL, Mirambell M (eds) Tlapacoya: 35,000 Años de Historia del Lago de Chalco Instituto Nacional de Antropologia e Historia, Mexico City, pp 109–156

Flower BP, Kennett JP (1990) The Younger Dryas cool episode in the Gulf of Mexico. Paleoceanography 5:949–961

Folland CK, Colman AW, Rowell DP, Davey MK (2001) Predictability of Northeast Brazil rainfall and real-time forcast skill 1987–98. J Climate 14:1937–1958

Gasse F, Van Campo E (1994) Abrupt post-glacial climate events in West Asia and North Africa monsoon domains. Earth Planet Sci Lett 126:435–456

Gasse F, Tehet R, Durand A, Gilbert E, Fontes JC (1990) The arid-humid transition in the Sahara and the Sahel during the last deglaciation. Nature 346:141–146

Gillespie R, Street-Perrott FA, Switsur R (1983) Post-glacial arid episodes in Ethiopia have implications for climate prediction. Nature 306:680–683

Guilderson TP, Fairbanks RG, Rubenstone JL (2001) Tropical Atlantic coral oxygen isotopes: glacial- interglacial sea-surface temperatures and climate change. Marine Geol 172:75–89

Hastenrath S, Heller L (1977) Dynamics of climate hazards in Northeast Brazil. Quart J Roy Meteor Soc 103:77–92

Haug GH, Hughen KA, Sigman DM, Peterson LC, Röhl U (2001) Southward migration of the intertropical convergence zone through the Holocene. Science 293:1304–1308

Hodell DA, Curtis JH, Jones GA, Higuera-Gundy A, Brenner M, Binford MV, Dorsey KT (1991) Reconstruction of Caribbean climate change over the past 10,500 years. Nature 352:790–793

Hüls M, Zahn R (2000) Millennial-scale sea surface temperature variability in the western tropical North Atlantic from planktonic foraminiferal census counts. Paleoceanography 15:659–678

Islebe GA, Hooghiemstra H, van der Borg K (1995) A cooling event during the Younger Dryas Chron in Costa Rica. Palaeogeogr Palaeoclim Palaeoecol 117:73–80

Johnson TC, Brown ET, McManus J, Barry S, Barker P, Gasse F (2002) A high-resolution paleoclimate record spanning the past 25,000 years in southern East Africa. Science 296:113–114

Keigwin LD, Jones GA, Lehman SJ, Boyle EA (1991) Deglacial meltwater discharge North Atlantic deep circulation and abrupt climate change. Geophys J Res 96:16811–16286

Keigwin LD, Curry WB, Lehman SJ, Johnson GS (1994) The role of the deep ocean in North Atlantic climate change between 70 and 130 kyr ago. Nature 371:323–326

Kim JH, Schneider RR, Müller PJ, Wefer G (2002) Interhemispheric comparison of deglacial sea-surface temperature patterns in Atlantic eastern boundary currents. Earth Planet Sci Lett 194:383–393

Klein SA, Soden BJ, Lau N-C (1999) Remote sea-surface temperature variations during ENSO: evidence for a tropical atmospheric bridge. J Climate 12:917–932

Kroon D, Austin WEN, Chapman MR, Ganssen GM (1997) Deglacial surface circulation changes in the northeastern Atlantic: temperature and salinity records off NW Scotland on a century scale. Paleoceanography 12:755–763

Lau N-C (1997) Interaction between global SST anomalies and the midlatitude atmospheric circulation. B Am Meteorol Soc 78:21–33

Lau N-C, Nath MJ (1996) The role of the "atmospheric bridge" in linking tropical Pacific ENSO events to extratropical SST anomalies. J Climate 9:2036–2057

Lea DW, Pak DK, Peterson LC, Hughen KA (2003) Synchroneity of tropical and high-latitude Atlantic temperatures over the last glacial termination. Science 301:1361–1364

Levitus S, Boyer T (1994) World Ocean Atlas 1994, vol. 4: Temperature vol. 13 of NOAA Atlas NESDIS US. Government Printing Office, Washington DC

Licciardi JM, Teller JT, Clark PU (1999) Freshwater routing by the Laurentide ice sheet during the last deglaciation. In: Clark PU, Webb RS, Keigwin LD (eds) Mechanisms of global climate change on millennial timescales, vol. 112. American Geophysical Union, Washington DC, pp 177–201

Lin HL, Peterson LC, Overpeck JT, Trumbore SE, and Murray DW (1997) Late Quaternary climate change from $\delta^{18}O$ records of multiple speciesof planktonic foraminifera: High-resolution records from the anoxic Cariaco Basin, Venezuela. Paleoceanography 12:415–427

MacAyeal DR (1993) Binge/purge oscillations of the Laurentide ice sheets as a cause of the North Atlantic's Heinrich events. Paleoceanography 8:775–784

Maley J, Brenac P (1998) Vegetation dynamics, palaeoenvironments and climatic changes in the forests of western Cameroon during the last 28,000 years B.P. Rev Palaeobot Palynol 99:157–187

Manabe S, Stouffer RJ (1995) Simulation of abrupt climate change induced by freshwater input to the North Atlantic Ocean. Nature 378:165–167

Manabe S, Stouffer RJ (1997) Coupled ocean-atmosphere model response to freshwater input: comparison to the Younger Dryas event. Paleoceanography 12:321–336

Manabe S, Stouffer RJ, Spelman MJ, Bryan K (1991) Transient responses of a coupled ocean–atmosphere model to gradual changes of atmospheric CO_2 part I: annual mean response. J Climate 4:785–818

Marchitto TM, Curry WB (1998) Millennial-scale changes in North Atlantic circulation since the last glaciation. Nature 393:557–661

Markham CG, McLain DR (1977) Sea-surface temperature related to rain in Ceara, northeastern Brazil. Nature 265:320–323

Maslin MA, Burns SJ (2000) Reconstruction of the Amazon Basin effective moisture availability over the past 14,000 years. Science 290:2285–2287

Mechoso CR, Lyons SW, Spahr JA (1990) The impact of sea-surface temperature anomalies on the rainfall over northeast Brazil. J Climate 3:812–826

Moura AD, Shukla J (1981) On the dynamics of droughts in Northeast Brazil: observations, theory, and numerical experiments with a general circulation model. J Atmos Sci 38:2653–2675

Mulitza S, Rühlemann CR (2000) African monsoonal precipitation modulated by interhemispheric temperature gradients. Quaternary Res 53:270–274

Nicholson SE (2000) The nature of rainfall variability over Africa on time scales of decades to millenia. Global Planet Change 26:137–158

Ohkouchi N, Eglinton TI, Keigwin LD, Hayes JM (2002) Spatial and temporal offsets between proxy records in a sediment drift. Science 298:1224–1227

Oppo DW, Lehman SJ (1995) Suborbital timescale variations of North Atlantic Deep Water during the past 135,000 years.Paleoceanography 10:901–910

Pacanowski R, Dixon K, Rosati A (1991) The GFDL Modular Ocean Model users guide version 1. GFDL Ocean Group Technical Report 2

Peagle JN, Mo KC (2002) Linkages between summer rainfall variability over South America and sea-surface temperature anomalies. J Climate 15:1389–1407

Peterson LC, Overpeck JT, Kipp NG, Imbrie J (1991) A high-resolution late quaternary upwelling record from the anoxic Cariaco Basin, Venezuela. Paleoceanography 6:99–119

Peterson LC, Haug GH, Hughen KA, Röhl U (2000) Rapid changes in the hydrologic cycle of the tropical Atlantic during the last glacial. Science 290:1947–1950

Pezzi P, Cavalcanti IFA (2001) The relative importance of ENSO and tropical Atlantic sea-surface temperature anomalies for seasonal precipitation over South America: a numerical study. Clim Dyn 17:205–212

Rahmstorf S (1995) Bifurcations of the Atlantic thermohaline circulation in response to changes in the hydrological cycle. Nature 378:145–149

Renssen H (1997) The global response to ounger Dryas boundary conditions in an AGCM simulation. Clim Dyn 13:587–599

Renssen H, Isarin RFB (1998) Surface temperature in NW Europe during the Younger Dryas: AGCM simulation compared with temperature reconstructions. Clim Dyn 14:33–44

Renssen H, Lautenschlager M (2000) The effect of vegetation in a climate model simulation of the Younger Dryas. Global Planet Change 26:423–443

Rind D, de Menocal P, Russell G, Sheth S, Collins D, Schmidt G, Teller J (2001) Effects of glacial meltwater in the GISS coupled atmosphere-ocean model 1. North Atlantic Deep Water response. J Geophys Res 106:27325–27353

Rosell-Mele A, Koc N (1997) Paleoclimatic significance of the stratigraphic occurrence of photosynthetic biomarker pigments in the Nordic seas. Geology 25:49–52

Rühlemann C, Mulitza S, Muller PJ, Wefer G, Zahn R (1999) Warming of the tropical Atlantic Ocean and slowdown of the thermohaline circulation during the last deglaciation. Nature 402:511–514

Schiller A, Mikolajewicz U, and Voss A (1997) The stability of the North Atlantic thermohaline circulation in a coupled ocean-atmosphere general circulation model. Clim Dyn 13:325–347

Schmittner A, Appenzeller C, Stocker TF Enhanced Atlantic freshwater export during an El Niño. Geophys Res Lett 27:1163–1166

Scott L, Steenkamp M, Beaumont PB (1995) Palaeoenvironmental conditions in South Africa at the Pleistocene–Holocene transition. Quaternary Sci Rev 14:937–947

Smethie WJ Jr, Fine RA (2001) Rates of North Atlantic deep water formation calculated from chlorofluorocarbon inventories. Deep Sea Res Part I 48:189–215

Stager JC, Mayewski PA, Meeker LD (2002) Cooling cycles, Heinrich event 1, and the dessication of Lake Victoria. Palaeogeogr Palaeoclim Palaeoecol 183:169–178

Street-Perrott FA, Perrott RA (1990) Abrupt climate fluctuations in the tropics: the influence of Atlantic Ocean circulation. Nature 343:607–610

Thompson LG, Mosley-Thompson E, Davis ME, Lin P-N, Henderson KA, Cole-Dai J, Bolzan JF, Liu KB (1995) Late glacial stage and Holocene tropical ice core records from Huascarán, Peru. Science 269:46–50

Thompson LG, Davis ME, Mosley-Thompson E, Sowers TA, Henderson KA, Zagorodvov VS, Lin P-N, Mikhalenko VN, Campen RK, Bolzan JF, Cole-Dai J, Francou B (1998) A 25,000-year tropical climate history from Bolivian ice cores. Science 282:1858–1864

Uvo CB, Repelli CA, Zebiak SE, Kushnir Y (1998) The relationship between tropical Pacific and Atlantic SST and Northeast Brazil monthly precipitation. J Climate 11:551–562

Van der Hammen T, Hooghiemstra H (1995) The El Abra stadial, a Younger Dryas equivalent in Colombia. Quaternary Sci Rev 14:841–851

Veer R, Islebe GA, Hooghiemstra H (2000) Climatic change during the Younger Dryas chron in northern South America: a test of the evidence. Quaternary Sci Rev 19:1821–1835

Vellinga M, Wood RA (2002) Global climatic impacts of a collapse of the Atlantic thermohaline circulation. Climatic Change 54:251–267

Venegas SA, Mysak LA (2000) Is there a dominant timescale of natural climate variability in the Arctic? J Climate 13:3412–3434

Vidal L, Labeyrie L, Cortijo E, Arnold M, Duplessy JC, Michel E, Becque S, van Weering TCE (1997) Evidence for changes in the

North Atlantic deep water linked to meltwater surges during Heinrich events. Earth Planet Sci Lett 146:13–27

Waliser DE, Gautier C (1993) A satellite-derived climatology of the ITCZ. J Climate 6:2162–2174

Walker MJC, Bohncke SJP, Coope GR, O'Connell M, Usinger H, Verbruggen C (1994) The Devensian/Weichselian late-glacial in northwest Europe (Ireland, Britain, north Belgium, the Netherlands, nortwest Germany. J Quaternary Sci 9:109–118

Wallace JM, Gutzler DS (1981) Teleconnections in the geopotential height field during the Northern Hemisphere winter. Mon Weather Rev 115:784–812

Wang YJ, Cheng H, Edwards RH, An ZS, Wu JY, Shen C-C, Dorale JA (2001) A high-resolution absolute-dated Late Pleistocene monsoon record from Hulu Cave, China. Science 294:2345–2348

Weaver AJ, Saenko OA, Clark PU, Mitrovica JX (2003) Meltwater pulse 1A from Antarctica as a trigger of the Bølling–Allerød warm interval. Science 299:1709–1713

Xie P, Arkin PA (1997) Global precipitation: a 17-year monthly analysis based on gauge observations, satellite estimates, and numerical model output. Bull. Am Meterol Soc 78:2539–2558

Yin JH, Battisti DS (2001) The importance of tropical sea-surface temperature patterns in simulations of the Last Glacial Maximum climate. J Climate 14:565–581

Zahn R, Schonfield J, Kudrass H-R, Park M-H, Erlenkeuser H, Grootes P (1997) Thermohaline instability in the North Atlantic during meltwater events: stable isotope and ice-rafted detritus records from core S075-26KL, Portuguese margin. Paleoceanography 12:696–710

Zhao M, Beveridge NAS, Shackleton NJ, Sarnthein M, Eglinton G (1995) Molecular startigraphy of cores off northwest Africa: sea-surface temperature history over the last 80 ka. Paleoceanography 10:661–675

Chapter 4

Terrigenous plant wax inputs to the Arabian Sea: Implications for the reconstruction of winds associated with the Indian Monsoon

This work originally appeared as:

Dahl, K. A., D. W. Oppo, T. I. Eglinton, K. A. Hughen, W. B. Curry, and F. Sirocko, Terrigenous plant wax inputs to the Arabian Sea: Implications for the reconstruction of winds associated with the Indian Monsoon, Geochimica et Cosmochimica Acta, 69, 2547–2558, 2005.

Geochimica et Cosmochimica Acta, Vol. 69, No. 10, pp. 2547–2558, 2005

0016-7037/05 $30.00 + .00

ELSEVIER

doi:10.1016/j.gca.2005.01.001

Terrigenous plant wax inputs to the Arabian Sea: Implications for the reconstruction of winds associated with the Indian Monsoon

KRISTINA A. DAHL,[1,*] DELIA W. OPPO,[2] TIMOTHY I. EGLINTON,[3] KONRAD A. HUGHEN,[3] WILLIAM B. CURRY,[2] and FRANK SIROCKO[4]

[1]MIT/WHOI Joint Program, Woods Hole Oceanographic Institution, WHOI MS #22, Woods Hole, MA 02543, USA
[2]Department of Geology and Geophysics, Woods Hole Oceanographic Institution, WHOI MS#23, Woods Hole, MA, 02543, USA
[3]Department of Marine Chemistry and Geochemistry, Woods Hole Oceanographic Institution, WHOI MS #4, Woods Hole, MA, 02543, USA
[4]Institut für Geowissenchaften, J. Gutenberg Universität Mainz, Johann-Joachim-Becher-Weg 21, 55099 Mainz, Germany

(*Received June* 1, 2004; *accepted in revised form January* 4, 2005)

Abstract—We have determined the accumulation rates and carbon isotopic compositions ($\delta^{13}C$) of long-chain (C_{24}–C_{32}) terrigenous plant wax fatty acids in 19 surface sediment samples geographically distributed throughout the Arabian Sea in order to assess the relationship between plant wax inputs and the surrounding monsoon wind systems. Both the accumulation rate data and the $\delta^{13}C$ data show that there are three primary eolian sources of plant waxes to the Arabian Sea: Africa, Asia, and the Arabian Peninsula. These sources correspond to the three major wind systems in this region: the summer (Southwest) monsoon, the winter (Northeast) monsoon, and the summer northwesterlies that blow over the Arabian Peninsula. In addition, plant waxes are fluvially supplied to the Gulf of Oman and the Eastern African margin by nearby rivers. Plant wax $\delta^{13}C$ values reflect the vegetation types of the continental source regions. Greater than 75% of the waxes from Africa and Asia are derived from C_4 plants. Waxes delivered by northwesterly winds reflect a greater influence (25–40%) of C_3 vegetation, likely derived from the Mesopotamian region. These data agree well with previously published studies of eolian dust deposition, particularly of dolomite derived from the Arabian Peninsula and the Mesopotamian region, in surface sediments of the Arabian Sea. The west-to-east gradient of plant wax $\delta^{13}C$ and dolomite accumulation rates are separately useful indicators of the relationship between the northwesterly winds and the winds of the Southwest monsoon. Combined, however, these two proxies could provide a powerful tool for the reconstruction of both southwest monsoon strength as well as Mesopotamian aridity.

1. INTRODUCTION

The Asian monsoon system is one of the most important components of Earth's climate today because of its broad influence in both tropical and extratropical regions. With over 60% of the planet's population living within monsoon-affected regions, it is critical that we develop an understanding of not only present-day monsoon climatology, but also potential monsoonal variability by studying the past. This study aims to assess the potential of terrestrial plant waxes as recorders of wind source and strength for winds associated with the Indian Monsoon. This is accomplished by mapping the accumulation rate and carbon isotopic composition ($\delta^{13}C$) of plant waxes in surface sediments from throughout the Arabian Sea.

The Indian monsoon system is associated with strong winds that have the potential to carry large amounts of terrestrial material to the Arabian Sea from the surrounding land masses. Seasonal changes in wind direction (Fig. 1), and therefore source region for eolian material, produce a mixture of components that are integrated into the sediment record. During boreal summer, southwesterly winds (up to 30 m s^{-1}) associated with the summer monsoon blow over Ethiopia and Somalia, potentially carrying material from Africa to the Arabian Sea (Ramage et al., 1972). These summer monsoon winds are driven a gradient of low pressure over the Asian continent and higher pressure over the Arabian Sea. Persistent northwesterly winds (2–13 m s^{-1}) over the Arabian Peninsula, which are driven by a pressure gradient between the Iranian highlands and the Arabian lowlands, also have the potential to deliver terrestrial material to the Arabian Sea during boreal summer (Ackerman and Cox, 1989). During boreal winter, northeasterly winds (2–4 m s^{-1}) associated with the Indian winter monsoon blow from Asia toward the Arabian Sea, thereby introducing material from southern Asia to the Arabian Sea (Ramage et al., 1972).

In order to reconstruct the intensity of the Indian monsoon through time, it is critical to have a means of determining the strength of the winds described above. Past wind strength can be inferred directly via the concentration of eolian material, such as dust (e.g., Sirocko et al., 2000), or indirectly via proxies for wind-induced upwelling (e.g., Overpeck et al., 1996; Anderson et al., 2002) in marine sediments. Eolian-derived plant waxes have the potential to be direct proxies for both wind strength and trajectory (e.g., Ohkouchi et al., 1997; Huang et al., 2000; Rommerskirchen et al., 2003; Schefuß et al., 2003). Sedimentary plant wax records may also reflect changes in the source area of the compounds through time. Changes in plant wax source area through time must be constrained prior to inferring changes in wind strength.

1.1. Terrestrial Plant Waxes

Terrestrial plant leaf waxes, produced by all higher plants (Gulz, 1994), contain long-chain (C_{25}–C_{36}) *n*-alkanes, *n*-alcohols, and *n*-alkanoic acids that serve as protection against

* Author to whom correspondence should be addressed (kdahl@whoi.edu).

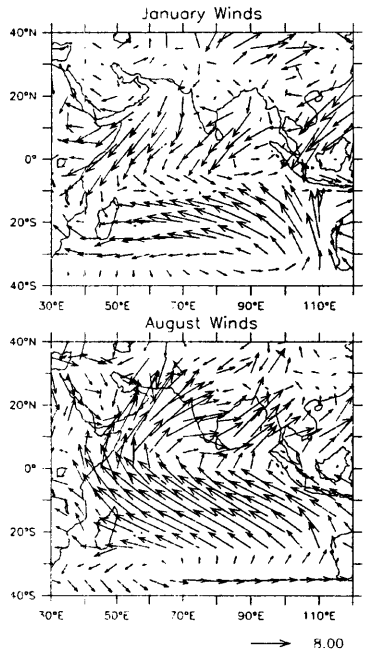

Fig. 1. Winds associated with the Indian Monsoon during January (top) and August (bottom). Data are long-term monthly averages for 1968–1996. NCEP Reanalysis Data provided by the NOAA-CIRES Climate Diagnostic Center, Boulder, Colorado, from their Web site (http://www.cdc.noaa.gov). Units are ms^{-1}.

dessication and bacterial attack (Eglinton and Hamilton, 1963; Simoneit et al., 1977; Cox et al., 1982; Brassell, 1993; Collister et al., 1994; Simoneit, 1997). These compounds are periodically ablated from living plants by wind (Hadley and Smith, 1989) and can therefore be analyzed in sediments as a means of reconstructing eolian input to the marine environment (e.g., Ohkouchi et al., 1997; Huang et al., 2000; Rommerskirchen et al., 2003). Plant waxes in marine sediments on coastal margins can also be fluvially derived (e.g., Prahl et al., 1994; Kienast et al., 2003; Pelejero, 2003; Hughen et al., 2004). It is also important to note that ancient plant waxes in soils and dessicated lakes may be delivered to the marine environment by winds or rivers (e.g., Eglinton et al., 1997, 2002).

In principle, any one of the three primary lipids groups comprising plant waxes can be used to characterize terrestrial plant wax inputs to marine sediments. As noted by Simoneit (1997) and Huang et al. (2000) in their studies of all three of these classes of lipids, the carbon isotopic composition of the *n*-alkanoic acids correlated nearly 1:1 with the carbon isotopic composition of the *n*-alkanes. This good correlation confirms what was predicted from biosynthetic considerations by Gulz (1994) as well as from observations (e.g., Collister et al., 1994; Conte and Weber, 2002; Chikaraishi et al., 2004) and reflects the fact that *n*-alkanes are biosynthesized from *n*-alkanoic acids (Cheesbrough and Kolattukudy, 1984; Post-Beittenmiler, 1996).

In terms of their abundance in marine sediments, *n*-alkanoic acids are generally as abundant as *n*-alkanes (e.g., Huang et al., 2000), if not more abundant. We have chosen to study the *n*-alkanoic acids because of their abundance in sediments and because they are not subject to contamination by fossil hydrocarbons, as *n*-alkanes commonly are (Eglinton et al., 1997; Pearson and Eglinton, 2000). Given that the Arabian Sea region is very close to regions with high abundances of petroleum, this study concentrates on *n*-alkanoic acids rather than on *n*-alkanes.

1.2. Sedimentation in the Arabian Sea

Lithogenic material is delivered to the Arabian Sea via many sources, both fluvial and eolian (Sirocko and Lange, 1991, and references therein). The primary fluvial sources of sediment are the Indus River, the Tapti and Narmada Rivers, and runoff from the Makran Margin. The primary regions providing a source of eolian material are the Arabian Peninsula, Eastern Africa, and Pakistan/Northern India. Because terrestrial plant waxes can be delivered to sediments by both winds and rivers, it is important to consider the modern potential eolian and fluvial inputs of sediment to our core locations.

The Indus Fan is the second largest deep-sea fan in the world, reflecting the high discharge of sediments from the Himalayas, which are drained by the Indus River (Kolla and Coumes, 1987; Prins et al., 2000a). A study by Prins et al. (2000a, closed square on Fig. 2) has shown that during glacial low stands during the Quaternary period, material from the Indus River was deposited on the middle fan. Between 8000 and 10,000 yr ago, however, when sea level had risen to near present-day levels, eolian dusts from the Arabian Peninsula began to dominate terrigenous sedimentation on the middle fan (Prins et al., 2000a). Indus sediments are presently deposited on the inner shelf and in the Ranns of Kutch, a subaerially exposed region within the southeast corner of the Indus Delta (Wells and Coleman, 1984; von Rad and Tahir, 1997). The outer shelf is currently characterized by a lack of deposition (von Rad and Tahir, 1997). The Murray Ridge, located to the east of site 57KL on Figure 2, prevents Indus material from being deposited in the Gulf of Oman (Wells and Coleman, 1984).

Deposition and redistribution of fluvial material is more significant on the Makran Margin than on the Indus Margin (Staubwasser and Sirocko, 2001). While sediment input from the many small rivers that drain this region was higher during glacial times than it is today, there is still active fluvial sedimentation on the Makran Margin (von Rad et al., 1999; Prins et al., 2000b). A study of the clay mineralogy of the same core-top sediments used in this study revealed that the accumulation rate of chlorite, the source of which is the Makran Margin, has a maximum in the Gulf of Oman that diminishes southeastward (Sirocko et al., 1991). Site 57KL, used in both this study and in Sirocko et al. (1991), is on the tail end of that maximum and is thus likely to have a significant fluvial influence from the Makran region (Fig. 2).

A number of small rivers draining from the Indian subcontinent into the eastern Arabian Sea also deliver fine-grained material to sediments. The largest of these rivers are the Tapti and Narmada. Deposition from these rivers occurs mainly on the continental shelf and is linked to topographic depressions on the seafloor (Sirocko et al., 1991, and references therein).

Despite the number of rivers draining into the Arabian Sea, eolian fluxes dominate lithogenic sedimentation in areas of hemipelagic, nonturbidite deposition (Sirocko and Sarnthein,

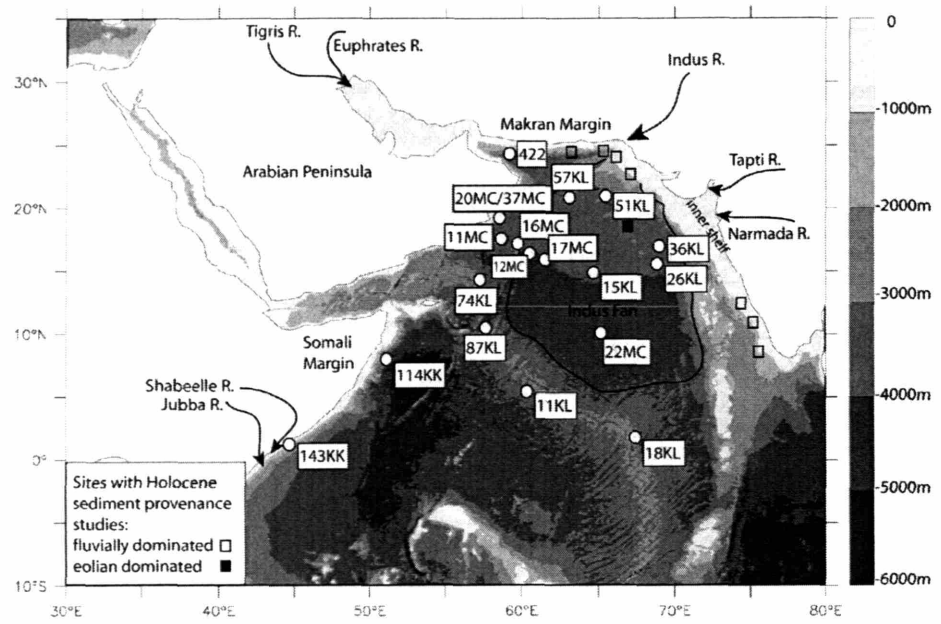

Fig. 2. Map of the Arabian Sea region. Circles indicate cores used in this study. Closed square indicates a sediment core for which Holocene sedimentation is known to be predominantly eolian (Prins et al., 2000a). Open squares indicated sediment cores for which Holocene sedimentation is known to be predominantly fluvial (Sirocko and Lange, 1991; von Rad and Tahir, 1997; von Rad et al., 1999; Prins et al., 2000b; Staubwasser and Sirocko, 2001).

1989). The main source of dust to the Arabian Sea is the Arabian Peninsula/Mesopotamia region (Tindale and Pease, 1999, and references therein). The two other primary dust sources are Eastern Africa and the Asian continent (e.g., Sirocko et al., 2000).

1.3. Compound-Specific Isotope Analysis

The carbon isotopic composition of leaf waxes is determined by several factors, including the local abundance and isotopic composition of atmospheric carbon dioxide, temperature, and aridity (Cerling et al., 1997; Street-Perrott et al., 1997; Kuypers et al., 1999; Pagani et al., 1999). These three factors are reflected in the photosynthetic pathway utilized by the plant. The two main pathways, C_3 and C_4, differ in the extent to which they discriminate against ^{13}C relative to ^{12}C. C_3 plants, found in forests and high-latitude grasslands, have carbon isotopic compositions ranging from $-25‰$ to $-30‰$ (Collister et al., 1994). The C_4 pathway is used primarily by plants in arid and semiarid environments, such as tropical grasslands. C_4 plants have a $\delta^{13}C$ of $-10‰$ to $-16‰$ (Collister et al., 1994). Lipids are depleted in ^{13}C relative to bulk plant tissue by 4 to 8‰ (Rieley et al., 1991, 1993; Collister et al., 1994; Chikaraishi et al., 2004). The compounds utilized for this study, *n*-alkanoic acids, exhibit isotopic compositions of $-38‰$ for C_3 plants and $-20‰$ for C_4 plants (Chikaraishi et al., 2004). Because the carbon isotopic compostions of C_3 and C_4 plants are offset from one another, the $\delta^{13}C$ of terrestrial plant waxes in marine sediments can be interpreted using a two end-member mixing model reflecting the relative inputs of C_3 and C_4 plants. It is important to note that the isotopic composition of long-chain fatty acids is not significantly affected by early diagenesis (Haraoka and Ishiwarati, 2000).

Sixty-six percent of the total land area in the Middle Eastern and African regions that surround the Arabian Sea has sparse or barren vegetation (Food and Agriculture Organization of the United Nations [FAO], 2002; Development Data Group, The World Bank, 2002). Shrublands, savanna, and grasslands compose 25% of the remaining land area and are the most prevalent types of vegetated land cover in these regions (Food and Agriculture Organization of the United Nations [FAO], 2002; Development Data Group, The World Bank, 2002). These vegetation types are characterized by C_4 plants (Cerling et al., 1993). The natural vegetation of India and Pakistan, the primary countries from which Asian plant waxes would be derived, is also largely shrubland and grassland (Food and Agriculture Organization of the United Nations [FAO], 2002; Development Data Group, The World Bank, 2002). The Mesopotamian region, located between the Tigris and Euphrates Rivers in modern-day Iraq, contains over 20,000 km^2 of marshlands within which reed beds of *Typha* and *Phragmites* are the main vegetation types. Both *Typha* and *Phragmites* are C_3 terrestrial emergent vascular plants (Sermolli, 1957; Cloern et al., 2002).

We hypothesized that the modern core-top accumulation rates and isotopic compositions of plant waxes in the Arabian Sea would reflect the three main potential sources of fluvial and eolian material to the Arabian Sea: Africa, the Arabian Peninsula/Mesopotamian region, and Asia. Given the abundance of C_4 vegetation throughout the Arabian Sea region, we expected that the $\delta^{13}C$ of plant waxes would reflect largely C_4 sources.

Table 1. Locations of surface sediments used in this study.

Cruise	Core	Core type	Latitude	Longitude	Water depth (m)	Sample depth (cmbsf)[a]
SO28	11KL	box	5°23.4′N	60°15.1′E	3859	0–5
SO28	18KL	box	1°54.0′N	67°20.5′E	3035	0–10
SO42	15KL	box	14°52.8′N	64°44.8′E	3920	0–5
SO42	26KL	box	15°30.9′N	68°45.6′E	3776	0–5
SO42	36KL	box	17°04.5′N	69°02.7′E	2055	0–5
SO42	51KL	box	20°57.9′N	65°33.5′E	2644	0–5
SO42	57KL	box	20°54.5′N	63°07.3′E	3422	0–5
SO42	74KL	box	14°19.3′N	57°20.8′E	3212	9–15
SO42	87KL	box	10°30.1′N	57°44.2′E	3773	0–5
IOE	114KK	piston	08°00.5′N	51°12.8′E	3843	3–8
IOE	143KK	piston	01°15.0′N	44°47.0′E	1522	12–19
Meteor5	422		24°23.4′N	59°02.5′E	2732	0–10
TN41	11MC	multi	17°26.1′N	58°47.7′E	3618	0–1
TN41	12MC	multi	16°24.1′N	60°14.2′E	4040	0–1
TN41	16MC	multi	17°13.0′N	59°36.5′E	3478	0–1
TN41	17MC	multi	15°59.7′N	61°32.0′E	3985	0–1
TN41	22MC	multi	10°02.1′N	65°05.1′E	4426	0–1
TN41	37MC	multi	19°16.1′N	58°21.1′E	784	1–1.5
TN47	20MC	multi	19°14.1′N	58°22.2′E	806	0–1

[a] Centimeters below seafloor.

2. MATERIALS AND METHODS

2.1. Surface Sediments

Many of the surface sediments used in this study (Fig. 2) came from the core-top sample set of Sirocko and Sarnthein (1989). As many of these original samples have been depleted, we have supplemented this sample set with a number of multicores from the western Arabian Sea. Two box cores were obtained during the R/V *Sonne-28* cruise in 1983. Seven 5-m-long box cores were obtained during the R/V *Sonne-42* cruise. Two piston cores were obtained during leg IOE. One core was obtained on *Meteor-5*. Core tops of seven multicores, recovered as part of the JGOFS program during cruises TN-41 and TN-47, were also analyzed. Table 1 shows a complete list of samples used in this study.

2.2. Analytical Methods

Multicore samples were freeze-dried overnight. All other samples were oven dried at 60°C. Samples were crushed gently prior to the extraction of the lipid biomarkers. A total lipid extract (TLE) was isolated using accelerated solvent extraction (ASE; 1000 psi, 100°C, 9:1 dichloromethane: methanol). The TLE was then evaporated to a small volume and applied to an aminopropyl column (Supelco LC-NH_2, 0.5 g). The nonpolar fraction was eluted with 7 mL of 9:1 dichloromethane:acetone. The polar fraction, containing the *n*-alkanoic acids, was eluted with 8 mL of 2% formic acid in dichloromethane. This latter fraction was taken to dryness and transesterified overnight at 70°C using 95:5 methanol:HCl. The methanol had a known isotopic composition of −47.25‰. The resultant fatty acid methyl esters (FAMES) were partitioned into the organic phase by adding 20 mL of Milli-Q water and 10 mL of hexane to each vial. After sonicating for 5 min to ensure that the liquid/liquid extraction was complete, the hexane fraction was applied to a sodium sulfate column to remove residual water. The liquid/liquid extraction was then repeated twice with 5-mL aliquots of hexane that were also applied to the sodium sulfate column. Samples were then taken to dryness. An aliquot of the sample was dried down, redissolved in 50:50 pyridine:bis(trimethylsilyl)trifluoroacetamide (BSTFA), and heated at 70°C for 15 min prior to analysis by gas chromatography–mass spectrometry (GC-MS).

GC-MS analyses were performed using an HP 6890 gas chromatograph fitted with a J&W DB-5 column and coupled to an HP 5973 mass-selective detector. The GC-MS temperature program was 40°C (isothermal) for 1 min, 20°C/min to 120°C, hold for 5 min, 10°C/min to 320°C, hold for 20 min. C_{22}–C_{32} FAMES eluted between 25 and 40 min. Compound-specific carbon isotope analyses were performed on the FAMES via gas chromatography–isotope ratio mass spectrometry (GC-irMS) using a Finnigan Delta^{Plus} isotope mass spectrometer coupled to an HP 6890 gas chromatograph. The temperature program for the GC-irMS was similar to that used for GC-MS. All isotope samples were run in triplicate.

2.3. Data Analysis

FAME concentrations were determined by integrating the chromatograms generated by the flame ionization detector (FID) of the GC-MS and comparing with a standard mixture of FAMES of known concentration. We consider the total plant wax concentration to be the sum of the even-numbered homologues from C_{24}–C_{32}. Isotopic compositions were determined for each individual homologue by averaging the values obtained in the three replicate analyses. Carbon isotopic values were calibrated to several CO_2 pulses of known isotopic composition. Instrument error, determined via repeated measurements of a suite of nine standards, is estimated to be 0.3‰. The average standard deviation ($\pm 1\sigma$) for triplicate analyses of the C_{30} alkanoic acid was 0.44‰. For cases in which the isotopic composition of one member of the triplicate was greater than 1‰ different from the other two members, the average of the other two values was used. By this method, members of the triplicate that were significantly different at the greater than 2σ level from the other two analyses were excluded. The isotopic composition of each homologue was then corrected for the addition of the methyl group during transesterification using a mass-balance approach.

Plant wax accumulation rates were calculated using the age models, sedimentation rates, and dry bulk densities given in Sirocko et al. (2000) for all Sonne, IOE, and Meteor cores. Sedimentation rates for all TN multicores are based on a minimum of two radiocarbon dates per multicore, with the exceptions of 17MC, for which the sedimentation rate was calculated using core TN47-01MC, located at the same site but taken during a later cruise, and 12MC, for which the sedimentation rate was estimated to be between the sedimentation rates of 16MC and 17MC. All multicore radiocarbon dates were determined at the National Ocean Sciences Accelerator Mass Spectrometry (NOSAMS) facility in Woods Hole (Table 2). Dry bulk densities of TN samples were determined by oven drying a known volume (typically ~5 cm^3) of sediment and weighing.

3. RESULTS AND DISCUSSION

3.1. Accumulation Rates

Total terrestrial plant wax fatty acid concentrations ranged from 0.054 to 11.4 μg/gdw, corresponding to accumulation

Table 2. Radiocarbon dates on cores used in this study.

Core	Depth (cm)	Species	^{14}C age	Error	NOSAMS Acc. #
TN41-11MC	1–2	mixed planktonics	490	35	39676
TN41-11MC	47–48	*G. sacculifer*[a] and *G. ruber* (white)	1620	30	39677
TN41-16MC	0–2	*G. menardii*	475	25	14411
TN41-16MC	3–4	*G. menardii*	695	40	14412
TN41-16MC	7–8	*G. menardii*	710	50	15782
TN41-16MC	13–15	*G. menardii*	1650	25	14414
TN41-16MC	19–20	*G. menardii*	2130	30	14415
TN47-01MC[b]	0–1	*G. menardii*	1490	35	14416
TN47-01MC	3–4	*G. menardii*	1170	50	14417
TN47-01MC	7–8	*G. menardii*	3060	100	14418
TN47-01MC	13–14	*G. menardii*	5160	45	14419
TN41-22MC	0–1	*G. menardii*	3720	55	14420
TN41-22MC	7–8	*G. menardii*	10,750	60	14422
TN41-22MC	13–14	*G. sacculifer*	12,000	55	14423
TN41-22MC	19–20	*G. menardii*	13,100	55	16683
TN41-37MC	0–0.5	*G. sacculifer*	3080	55	38213
TN41-37MC	43–44	*G. sacculifer*	10,250	60	38214
SO42-74KL[c]	7.5	*G. ruber*	1230	60	
SO42-74KL[c]	35	*G. ruber*	3350	100	

[a] Only sacculifers without saclike final chambers were used.
[b] This site is at the same location as TN41-17MC, the multicore used in this study. Sedimentation rates for core 01MC were used to calculate accumulation rates for 17MC.
[c] Uncalibrated ages as reported by Sirocko et al. (1993).

rates of 0.048–59.3 μg cm^{-2} kyr^{-1} (Fig. 3). The range in concentrations exhibited in the Arabian Sea is consistent with Holocene concentrations observed in a variety of other settings, including eolian-dominated sites such as the West African Margin (0.5–0.8 μg cm^2 kyr^{-1} for *n*-alkanoic acids; Huang et al., 2000), the Central Pacific (0.1–1.5 μg cm^2 kyr^{-1} for

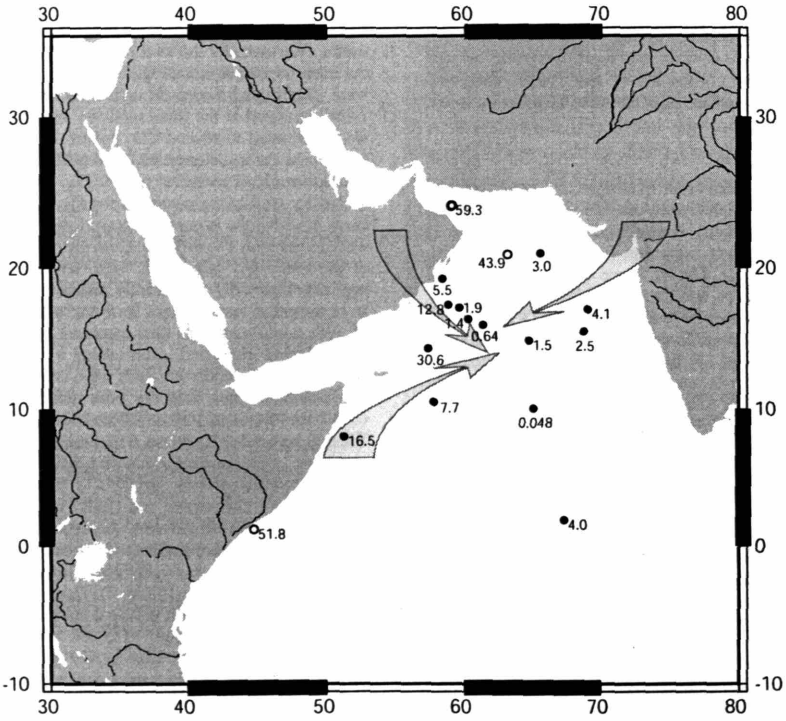

Fig. 3. Leaf wax *n*-alkanoic acid (C_{24}–C_{32}) accumulation rates. Units are μg cm^{-2} kyr^{-1}. Open circles indicate sites known to be significantly affected by fluvial sedimentation (Sirocko et al., 1991). Schematic arrows are intended to highlight gradients within the data.

n-alkanes; Ohkouchi et al., 1997), and the South China Sea (0–1.5 μg cm^2 kyr^{-1} for the C_{29}-alkane; Pelejero, 2003), as well as fluvially dominated sites such as the Cariaco Basin (3–30 μg cm^2 kyr^{-1} for *n*-alkanoic acids; Hughen et al., 2004). The spatial patterns described in this section for the total plant wax fraction also hold true for the concentrations and accumulation rates of individual homologues.

The highest plant wax accumulation rates occur within the Gulf of Oman (site 422; 59.3 μg cm^{-2} kyr^{-1}) and along the Somali Margin (site 143KK; 51.8 μg cm^{-2} kyr^{-1}), two sites where the lithogenic sedimentation is primarily fluvial (Sirocko et al., 1991). Consistent with the extent of Makran Margin–derived chlorite, accumulation rates are also very high at site 57KL, in the northwest Arabian Sea (Sirocko et al., 1991). Because these three sites are clearly affected by fluvial sedimentation, they are unlikely to be useful locations for eolian reconstructions. Given the current state of knowledge regarding present-day sedimentation in the Arabian Sea, however, plant waxes at the remaining sites are likely delivered by winds (Wells and Coleman, 1984; Sirocko and Sarnthein, 1989; von Rad and Tahir, 1997; Prins et al., 2000a).

Excluding the three sites just described, several general trends in plant wax accumulation rates can be observed in Figure 3. Accumulation rates decrease from the Somali Margin (site 114KK) toward the interior of the Arabian Sea, likely reflecting a source of plant waxes derived from Africa. A northwest-southeast gradient extends offshore of the Oman Margin, reflecting a source of plant waxes derived from the summertime northwesterly winds that blow over the Arabian Peninsula. A third, and weaker, gradient can be observed from the Indian subcontinent (sites 26KL and 36KL) to the interior of the Arabian Sea (e.g., site 15KL). As is evident in Figure 3, not all sites are consistent with these gradients. This is likely the result of the errors associated with estimation of sedimentation rates. In summary, the accumulation rate data suggest three eolian sources of plant waxes to the Arabian Sea: Africa, Asia, and the Arabian Peninsula/Mesopotamian region (hereafter APM).

The gradients observed in plant wax accumulation rates are similar to those of other studies investigating modern-day eolian dust inputs to the Arabian Sea (e.g., Tindale and Pease, 1999; Sirocko et al., 2000). Satellite, sediment trap, and surface sediment data have demonstrated that the northeast monsoon does not transport significant quantities of dust to the Arabian Sea (Sirocko and Sarnthein, 1989; Clemens, 1998; Schulz et al., 2002). However, plant wax accumulation rates at sites affected by northeast monsoon winds are lower than at sites affected by the southwest monsoon winds and roughly equal to those at sites affected by the northwesterly winds. This suggests that the winds of the northeast monsoon do provide a source of plant waxes to the Arabian Sea.

Despite their strength, the summer southwest monsoon winds are not the primary carriers of dust to the interior of the Arabian Sea because the Findlater Jet forms in the relatively dust free equatorial region near the African margin (Tindale and Pease, 1999). Nevertheless, African dust, with a characteristically high Zr/Hf ratio, has been identified in core-top sediments, which suggests that dust deposition during the southwest monsoon is significant (Sirocko et al., 2000). Furthermore, East African pollen types have been observed downwind of Somalia during the summer southwest monsoon (Van Campo, 1991). We find relatively high accumulation rates of plant waxes at site 114KK, along the Somali Margin, suggesting that southwest monsoon winds transport leaf waxes, as well as pollen and dust, from Eastern Africa to the Arabian Sea.

The main source of mineral dust to the Arabian Sea is the Arabian Peninsula, over which northwesterly winds blow during the summer (Sirocko and Sarnthein, 1989; Sirocko et al., 1991; Tindale and Pease, 1999, and references therein). The aridity and availability of desert dust in the APM region allows for efficient advection of fine material, even though the northwesterly winds are less intense than the winds of both the southwest and northeast monsoons. The Arabian Peninsula is also a source of pollen to the Arabian Sea (Van Campo, 1991). Similar to the results for dust inputs, we find that the northwesterly winds deliver a significant amount plant waxes to the Arabian Sea. As plant waxes are commonly associated with eolian dust (Simoneit et al., 1977; Cox et al., 1982; Peltzer and Gagosian, 1987; Poynter et al., 1989; Huang et al., 2000; Schefuß et al., 2003), this is to be expected.

3.2. Carbon Isotopes

Compound-specific $\delta^{13}C$ of the plant waxes (Fig. 4a) supports the notion that the compounds found in the Arabian Sea are derived from three sources. $\delta^{13}C$ values for the C_{30} alkanoic acid (hereafter $\delta^{13}C_{30}$) range from $-21‰$ to $-27‰$, reflecting contributions from both C_3 and C_4 plants throughout the region (Rieley et al., 1991, 1993; Collister et al., 1994; Chikaraishi et al., 2004). Other homologues, as well as the average values for all even-numbered homologues from C_{24}–C_{32}, show similar trends and isotopic compositions.

In order to quantify the relative contributions of C_3 and C_4 plant waxes to the total observed carbon isotopic composition for the C_{30} alkanoic acid at different sites, we have defined a two end-member model with the $\delta^{13}C$ of C_3 and C_4 *n*-alkanoic acids as $-38‰$ and $-20‰$, respectively (Chikaraishi et al., 2004). These isotopic compositions are intended to be representative rather than absolute, as *n*-alkanoic acids from both C_3 and C_4 plants exhibit a range of isotopic compositions (e.g., Chikaraishi et al., 2004). Along the Indian and African margins, $\delta^{13}C_{30}$ values of $-21‰$ to $-23.6‰$ indicate C_4 contributions of over 80%, which reflects the abundance of exposed C_4 biomass in these regions. Along the Oman Margin, the $\delta^{13}C_{30}$ exhibits much lighter values of $-25.1‰$ to $-27‰$. These values reflect C_4 contributions of 60–75% (Fig. 4b). This is somewhat surprising given the dryness of the Arabian Peninsula. However, the origin of the northwesterly winds is such that they could ablate material from the Mesopotamian region (Sirocko et al., 1991). The climate of this region is semiarid, with wet winters and hot, dry summers. Such seasonality is conducive to dust production and transport (Pye, 1989). The southern Mesopotamian plains encompass numerous shallow (<3 m) freshwater and brackish lakes as well as extensive marshes (Aqrawi, 2001) that contain C_3 plant material (e.g., *Typhus* and *Phragmites*) that could be transported to the Arabian Sea via the summertime northwesterly winds. The extent of the C_3-like $\delta^{13}C_{30}$ values is similar to the extent of high dolomite accumulation rates (Fig. 5) observed by Sirocko et al.

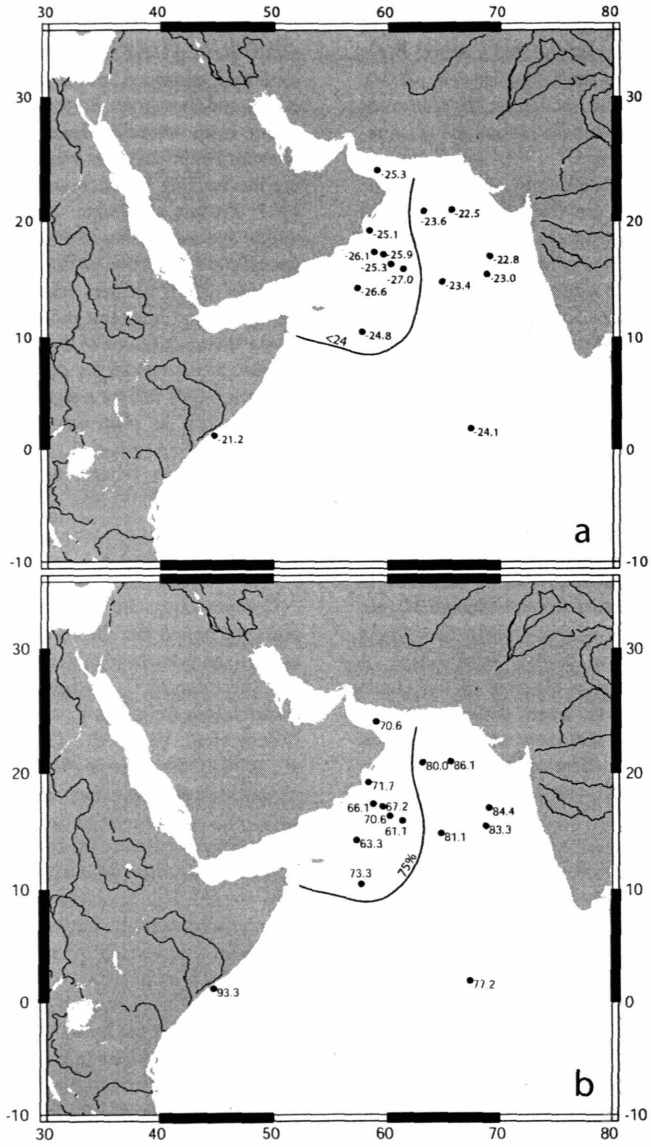

Fig. 4. (a) Carbon isotopic composition of C_{30} alkanoic acid. Units are permil. The isoline (hand drawn) is intended to distinguish sites with carbon isotopic compositions of less than 24‰ from those with carbon isotopic compositions of greater than 24‰. (b) Percentage of C4-derived plant waxes contributing to the total plant wax $\delta^{13}C$ in surface sediments. Percentages determined using a two end-member mixing model with C_4 $\delta^{13}C = -20‰$ and C_3 $\delta^{13}C = -38‰$ (Chikaraishi et al., 2004). The isoline (hand drawn) highlights sites with sites with C_4 contributions of less than 75%.

(1991). Mesopotamian dusts are known to be rich in dolomite. Both dolomite and plant waxes may therefore be derived from the Mesopotamian region. Thus, despite the weakness of the northwesterlies relative to the southwest and northeast monsoon winds, these winds are an important source of C_3 plant waxes to the Arabian Sea.

3.3. Homologue Distributions

The carbon preference index (CPI; the sum of the even carbon–numbered *n*-alkanoic acids from C_{24} to C_{32} divided by the sum odd carbon–numbered *n*-alkanoic acids from C_{23} to C_{31}) of the Arabian Sea samples ranges from 3.1 to 6.6. The CPI is a measure of the degree of degradation of the *n*-alkanoic acids, which, when unaltered, have a strong even-over-odd predominance (Brassell, 1993). There do not appear to be any geographic trends in the CPI in the Arabian Sea (data not shown), which suggests that the accumulation rate and carbon isotopic trends evidenced throughout the Arabian Sea are not significantly affected by diagenetic overprinting. CPI values calculated in this study compare

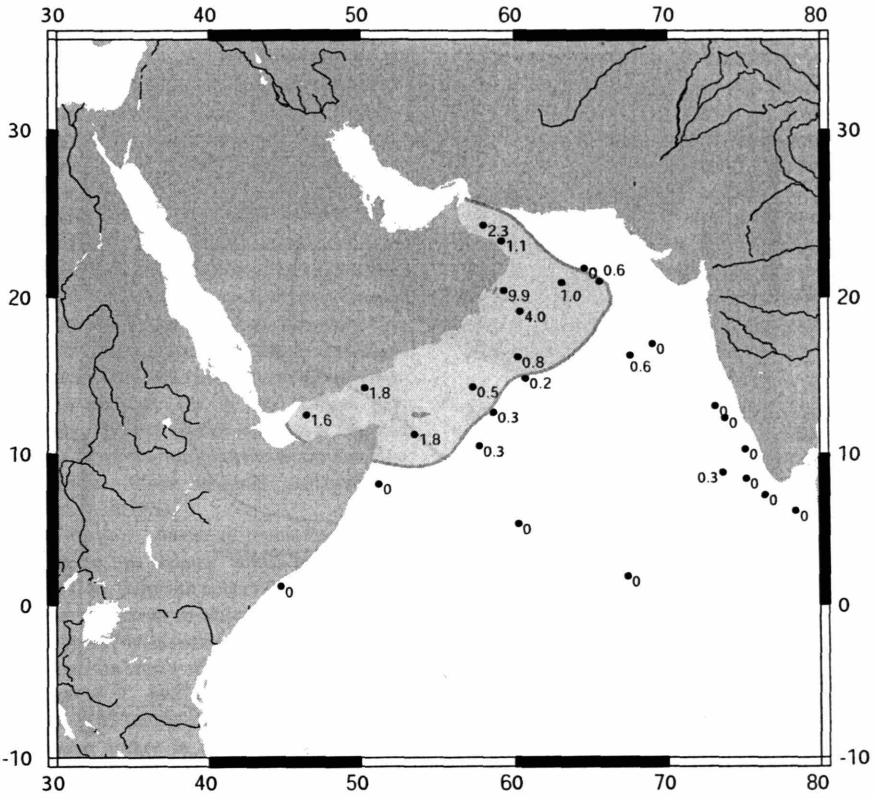

Fig. 5. Dolomite accumulation rates (g m^{-2} yr^{-1}) from Sirocko et al. (1991). The shaded area (hand drawn) highlights sites with dolomite accumulation rates of greater than 0.5 g m^{-2} yr^{-1}.

well to those observed along the west African margin by Huang et al. (2000) and Rommerskirchen et al. (2003).

We also find no evidence for a correlation between the average chain length (ACL; $\Sigma(C_i{*}i)/\Sigma C_i$, where C_i is the concentration of an *n*-alkanoic acid of chain length *i*) of *n*-alkanoic acids and their carbon isotopic composition in the Arabian Sea. Such a relationship has been noted in several studies from the west African margin and the Cariaco basin (Rommerskirchen et al., 2003; Schefuß et al., 2003; Hughen et al., 2004) using a variety of different means of calculating ACL. In contrast, ACL values from the Arabian Sea, calculated for all homologues C_{24}–C_{32} as well as subsets including only the highest abundance homologues, show no correlation to $\delta^{13}C$.

3.4. Plant Wax Ages

While the plant waxes analyzed in this study do come from core-top sediments, two concerns arise regarding the age of the waxes. First, it must be established that the surface sediments containing the waxes are, in fact, modern. Radiocarbon ages confirm that the surface sediments of all of the TN multicores are less than 4000 yr old. When a standard 400 yr reservoir correction is applied, two of these cores (11MC and 16MC) have ages of about 50 yr. Similarly, the surface sample from core 74KL has an age between 1230 and 3350 yr. The surface ages of the rest of the cores used in this study have not been determined via ^{14}C dating. However, applying the sedimentation rates reported by Sirocko et al. (1991) to the depth ranges given in Table 1 for each core shows that the age range represented by each sample is less than 2 kyr in all but two cases (11KL: 2.35 kyr and 18KL: 4 kyr). These sediments therefore encompass a relatively short timespan. Coupled with evidence from low resolution oxygen isotope records, it is unlikely that the samples used for this study contain sediments older than a few thousand years (Sirocko, 1989, 1995).

The second concern is whether the plant waxes found in modern sediments are, in fact, modern themselves, or whether they are "pre-aged." While it is generally assumed that the different components of a given sediment horizon are contemporaneous, this is not always the case. For example, plant waxes contained within eolian dust collected off Northwest Africa exhibit ^{14}C ages of ~650 yr, likely the result of a mixture of waxes derived from modern vegetation and from dessicated lake sediments and/or soils (Eglinton et al., 2002). Given that the climate of the Middle East was generally wetter prior to ~4 kyr B.P. than it is today (e.g., Cullen et al., 2000; Aqrawi, 2001, and references therein), there are potential sources of C_3 plant waxes from dessicated lake beds throughout the Arabian Sea region. In this case, it

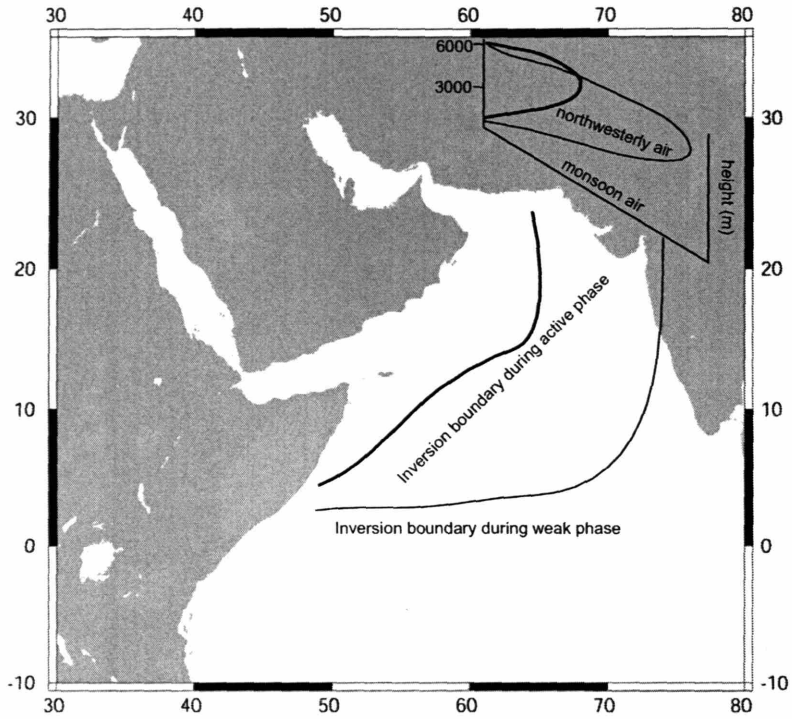

Fig. 6. Schematic of the relationship between northwesterly and southwesterly winds during active (bold line) and weak (thin line) phases. Lines represent the eastward extent of the monsoon inversion. A cross section of the air masses with height in the atmosphere is also shown. Adapted from Findlater (1969) and Narayanan and Rao (1981).

would be possible for the C_3-like $\delta^{13}C$ signature seen in core-top sediments off the coast of Oman to be derived from pre-aged plant waxes from the Arabian Peninsula rather than being derived from the modern C_3 sources within Mesopotamia. While this possibility does exist, it is unlikely for the following reason. Dessicated lake beds containing C_3 plant material should be present throughout the Arabian Sea region, not just on the Arabian Peninsula, as both East Africa (e.g., Gasse, 2000, and references therein) and southern Asia (e.g., Enzel et al., 1999) also experienced a drying during the mid-Holocene. Thus, the three major wind systems in the region could all be delivering pre-aged waxes to the Arabian Sea. If this were the case, then there would be no clear C_3 signal off of the Arabian Peninsula. The fact that this signal is so clear indicates either that lake beds containing C_3 plant material are found only on the Arabian Peninsula (unlikely given the generalized mid-Holocene aridification of the region) or that any pre-aged plant wax material from Asia and Africa is swamped by a modern C_4 signature while the signal from Mesopotamia plus the Arabian Peninsula is not. While this second option cannot be ruled out, it seems unlikely given that all three major source regions are deserts and should therefore have similar potentials for eolian deflation. These concerns could be further addressed by compound-specific ^{14}C dating of the plant waxes in core-top sediments throughout the Arabian Sea.

3.5. Controls on the Deposition of Plant Waxes in the Arabian Sea

While the transportation of plant waxes from the APM region is dependent upon the northwesterlies, the deposition of these waxes in the Arabian Sea is likely dependent upon the strength of the southwest monsoon. Eolian material is subject to both dry and wet deposition. In the absence of rainfall, fine particles can be carried over great distances (e.g., Ohkouchi et al., 1997, and references therein). In this case, the removal is dependent upon both wind strength and particle density. However, particulate material can also be removed from the air via precipitation (Duce, 1995). During the summer, when both the northwesterlies and the southwesterlies are active, the hot, dry northwesterlies overlie the moist southwesterlies (Findlater, 1969, and references therein). The height of the boundary between the two air masses, known as the monsoon inversion, increases from west to east and depends upon the strength of the southwest winds (Narayanan and Rao, 1981). When the southwest monsoon is strong, the inversion is confined to the region west of 65°E (Narayanan and Rao, 1981). The transportation of dust and other eolian material is therefore blocked from the interior of the Arabian Sea. However, when the southwest winds are weak, such as during a break period, the inversion moves eastward toward the Indian subcontinent and material contained within the northwesterly winds can be trans-

ported further out into the Arabian Sea (Fig. 6). Transportation of eolian material to the interior of the Arabian Sea is therefore strongly dependent upon the moist southwesterly winds of the summer monsoon (Tindale and Pease, 1999). Accordingly, the spatial extent of ^{13}C-depleted plant wax fatty acids (Fig. 4a) and high dolomite accumulation rates (Fig. 5) correlate well with the approximate position of the monsoon inversion during an active phase, as determined by Narayanan and Rao (1981; Fig. 6). This suggests that the west-to-east $\delta^{13}C$ gradient in the Arabian Sea can potentially be used as an indicator of the position of the monsoon inversion, and therefore of the relationship between the southwesterly and northwesterly winds, and, by extension, the intensity of the southwest monsoon. One potential complication in the interpretation of temporal changes in plant wax accumulation rate is the uncertainty of the magnitude of fluvial inputs through time. In the Arabian Sea, lowered sea level during the Last Glacial Maximum allowed for the sedimentation of Indus-derived material as far from the continent as the middle fan, where lithogenic sedimentation today is eolian (Prins et al., 2000a).

Based on the above findings, downcore reconstructions of the southwest monsoon in this manner would benefit from using a combination of both dolomite accumulation rates and plant wax $\delta^{13}C$. Alone, variations in dolomite accumulation rates could reflect changes in Mesopotamian aridity, northwesterly wind strength, and southwesterly wind strength. Within the source region, plant wax $\delta^{13}C$, unlike dolomite, responds to aridity. Thus plant wax $\delta^{13}C$ potentially can be used to infer changes in Mesopotamian aridity as well as changes in the relationship between the northwesterly and southwesterly winds. For example, if plant wax $\delta^{13}C$ along the Oman margin became less depleted and dolomite accumulation rates decreased, the cause would likely be an increase in summer monsoon wind strength. However, if plant wax $\delta^{13}C$ became less depleted and dolomite accumulation rates increased, the cause would likely be increased Mesopotamian aridity. Such an approach would ideally be complimented by the utilization of a biomarker for fluvial input, such as lignin (Goñi et al., 1998), in order to constrain changes in riverine input through time.

4. CONCLUSIONS

Based on the accumulation rate and $\delta^{13}C$ compositions of terrestrial plant wax *n*-alkanoic acids, we have determined that leaf waxes are delivered to the Arabian Sea from sources in Asia, Africa, and the Arabian Peninsula/Mesopotamian region. The carbon isotopic composition of vascular plant fatty acids in modern sediments reflects the vegetation of the land masses surrounding the Arabian Sea. Plant waxes derived from Asia and Africa reflect C_4 contributions of ~80% while plant waxes derived from the Arabian Sea/Mesopotamian region reflect a greater influence (25% or more) of C_3 plants. These data are consistent with modern-day observations of dust and pollen inputs to the Arabian Sea (Van Campo, 1991; Tindale and Pease, 1999), as well as with surface sediment dust data (Sirocko et al., 2000). The extent of the modern transport of plant waxes (as indicated by the geographic extent of plant waxes with C_3 contributions of over 25%) correlates well with the modern-day boundary between the dry northwesterly and moist southwesterly winds that develop during the summer. The transport of eolian material to the interior of the Arabian Sea via the northwesterly winds is limited by the presence of the moist southwesterly winds associated with the Indian summer monsoon. These winds effectively create a barrier that prevents dust and plant waxes carried by northwesterly winds from reaching into the central Arabian Sea. We therefore hypothesize that the west-to-east gradient in plant wax $\delta^{13}C$ across the Arabian Sea could provide a means for reconstructing the relationship between the summer northwesterly and southwesterly winds and, therefore, the strength of the southwest monsoon itself. This approach would be even more powerful when used in conjunction with dolomite accumulation rates, as both Mesopotamian aridity and southwest monsoon strength could be deduced.

Acknowledgments—We thank Sean Sylva and Carl Johnson for technical assistance. We also thank Dorinda Ostermann and Luping Zou for their assitance in the preparation of samples for radiocarbon work. The comments of three anonymous reviewers significantly improved this manuscript. This work was supported by a SGER grant from the National Science Foundation to D.O. and a Schlanger Ocean Drilling Fellowship to K.D.

Associate editor: R. H. Harvey

REFERENCES

Ackerman S. A. and Cox S. K. (1989) Surface weather observations of atmospheric dust over the southwest summer monsoon region. *Meteorol. Atmos. Phys.* **41,** 19–34.

Anderson D. M., Overpeck J. T., and Gupta A. K. (2002) Increase in the Asian southwest monsoon during the past four centuries. *Science* **297,** 596–599.

Aqrawi A. A. M. (2001) Stratigraphic signatures of climatic change during the Holocene evolution of the Tigris-Euphrates delta, lower Mesopotamia. *Global Planet. Change* **28,** 267–283.

Brassell S. C. (1993) Applications of biomarkers for delineating marine paleoclimatic fluctuations during the Pleistocene. In *Organic Geochemistry* (eds. M. H. Engel and S. A. Macko), pp. 699–737. Plenum Press.

Cerling T. E., Want Y., and Quade J. (1993) Expansion of C_4 ecosystems as an indicator of global ecological change in the late Miocene. *Nature* **361,** 344–345.

Cerling T. E., Harris J. M., MacFadden B. J., Leakey M. G., Quade J., Eisenmann V., and Ehleringer J. R. (1997) Global vegetation change through the Miocene/Pliocene boundary. *Nature* **389,** 153–158.

Cheesbrough T. M. and Kolattukudy P. E. (1984) Alkane biosynthesis by decarbonylation of aldehydes catalyzed by a particulate preparation from *Pisum sativum*. *Proc. Natl. Acad. Sci. USA* **81,** 6613–6617.

Chikaraishi Y., Naraoka H., and Poulson S. R. (2004) Hydrogen and carbon isotopic fractionations of lipid biosynthesis amount terrestrial (C3, C4, and CAM) and aquatic plants. *Phytochemistry* **65,** 1369–1381.

Clemens S. C. (1998) Dust response to seasonal atmospheric forcing: Proxy evaluation and calibration. *Paleoceanography* **13,** 471–490.

Cloern J. E., Canuel E. A., and Harris D. (2002) Stable carbon and nitrogen isotope composition of aquatic and terrestrial plants of the San Francisco Bay estruarine system. *Limnol. Oceanogr.* **47,** 713–729.

Collister J. W., Rieley G., Stern B., Eglinton G., and Fry B. (1994) Compound-specific $\delta^{13}C$ analyses of leaf lipids from plants with differing carbon dioxide metabolisms. *Org. Geochem.* **21,** 619–627.

Conte M. H. and Weber J. C. (2002) Plant biomarkers in aeorsols record isotpic discrimination of terrestrial photosynthesis. *Nature* **417,** 639–641.

Cox R. E., Mazurek M. M., and Simoneit B. R. T. (1982) Lipids in Harmattan aerosols of Nigeria. *Nature* **296,** 848–849.

Cullen H. M., deMenocal P. B., Hemming S., Hemming G., Brown F. H., Guilderson T., and Sirocko F. (2000) Climate change and the collapse of the Akkadian empire: Evidence from the deep sea. *Geology* **28,** 379–382.

Development Data Group, The World Bank. (2002) World Development Indicators 2002 online. http://publications.worldbank.org.

Duce R. A. (1995) Sources, distributions, and fluxes of mineral aerosols and their relationship to climate. In *Aerosol Forcing of Climate* (eds. R. J. Charlson and J. E. Helntzenberg), pp. 43–72. Wiley.

Eglinton G. and Hamilton R. J. (1963) The distribution of *n*-alkanes. In *Chemical Plant Taxonomy* (ed. T. Swain), pp. 187–217. Academic Press.

Eglinton T. I., Benitez-Nelson B. C., Pearson A., McNichol A. P., Bauer J. E., and Druffel E. R. M. (1997) Variability in radiocarbon ages of individual organic compounds from marine sediments. *Science* **277,** 796–799.

Eglinton T. I., Eglinton G., Dupont L., Sholkovitz E. R., Montluçon D., and Reddy C. M. (2002) Composition, age, and provenance of organic matter in NW African dust over the Atlantic Ocean. *Geochem. Geophys. Geosyst.* **3,** 10.1029/2001GC000269.

Enzel Y., Ely L. L., Mishra S., Ramesh R., Amit R., Lazar B., Rajaguru S. N., Baker V. R., and Sandler A. (1999) High-resolution Holocene environmental changes in the Thar desert, north western India. *Science* **284,** 125–128.

Findlater J. (1969) A major low-level air current near the Indian Ocean during the northern summer. *Quart. J. R. Met. Soc.* **95,** 362–380.

Food and Agriculture Organization of the United Nations (FAO). (2002) Faostat on-line statistical service. http://apps.fao.org.

Gasse F. (2000) Hyrological changes in the African tropics since the Last Glacial Maximum. *Quat. Sci. Rev.* **19,** 189–211.

Goñi M. A., Ruttenberg K. C., and Eglinton T. I. (1998) A reassessment of the sources and importance of land-derived organic matter in surface sediments from the Gulf of Mexico. *Geochim. Cosmochim. Acta* **62,** 3055–3075.

Gulz P.-G. (1994) Epicuticular leaf waxes in the evolution of the plant kingdom. *J. Plant Physiol.* **143,** 453–464.

Hadley J. L. and Smith W. K. (1989) Wind erosion of leaf surface wax in alpine timberline conifers. *Arctic Alpine Res.* **21,** 392–398.

Haraoka H. and Ishiwarati R. (2000) Molecular and isotopic abundances of long chain *n*-fatty acids in open marine sediments of the western North Pacific. *Chem. Geol.* **165,** 23–36.

Huang Y., Dupont L., Sarnthein M., Hayes J. M., and Eglinton G. (2000) Mapping of C_4 plant input from North West Africa into North East Atlantic sediments. *Geochim. Cosmochim. Acta* **64,** 3505–3513.

Hughen K. A., Eglinton T. I., Xu L., and Makou M. (2004) Abrupt tropical vegetation response to rapid climate changes. *Science* **304,** 1955–1959.

Kienast M., Hanebuth T. J. J., Pelejero C., and Steinke S. (2003) Synchroneity of meltwater pulse 1a and the Bolling warming: New evidence from the South China Sea. *Geology* **31,** 67–70.

Kolla V. and Coumes F. (1987) Morphology, internal structure, seismic stratigraphy, and sedimentation on the Indus Fan. *Am. Assoc. Petrol. Geol. Bull.* **71,** 650–677.

Kuypers M. M. M., Pancost R. D., and Sinninge-Damste J. S. (1999) A large and abrupt fall in atmospheric CO_2 concentration during Cretaceous times. *Nature* **399,** 342–345.

Narayanan M. S. and Rao B. M. (1981) Detection of monsoon inversion by TIROS-N satellite. *Nature* **294,** 546–548.

Ohkouchi N., Kawamura K., and Taira A. (1997) Molecular paleoclimatology: Reconstruction of climate variabilities in the late Quaternary. *Org. Geochem.* **27,** 173–183.

Overpeck J. T., Anderson D. M., Trumbore S., and Prell W. L. (1996) The Southwest Monsoon over the last 18,000 years. *Clim. Dyn.* **12,** 213–225.

Pagani M., Freeman K. H., and Arthur M. A. (1999) Late Miocene atmospheric CO_2 concentrations and the expansion of C_4 grasses. *Science* **285,** 876–879.

Pearson A. and Eglinton T. I. (2000) The origin of *n*-alkanes in Santa Monica Basin surface sediment: A model based on compound-specific $\Delta^{14}C$ and $\delta^{13}C$ data. *Org. Geochem.* **31,** 1103–1116.

Pelejero C. (2003) Terrigenous *n*-alkane input in the South China Sea: high-resolution records and surface sediments. *Chem. Geol.* **200,** 89–103.

Peltzer E. T. and Gagosian R. B. (1987) Sampling and quantitation of lipids in aerosols from the remote marine atmosphere. *Anal. Chim. Acta* **198,** 125–144.

Post-Beittenmiler D. (1996) Biochemistry and molecular biology of wax production in plants. *Ann. Rev. Plant Physiol. Plant Mol. Biol.* **47,** 405–430.

Poynter J. G., Farrimond P., Robinson N., and Eglinton G. (1989) Aeolian-derived higher plant lipids in the marine sedimentary record: Links with palaeoclimate. In *Paleoclimatology and Paleometeorology: Modern and Past Patterns of Global Atmospheric Transport*, Vol. 282 of NATO ASI Series, Series C (eds. M. Leinen and M. Sarnthein), pp. 435–462. Kluwer Academic Publishers.

Prahl F. G., Ertel J. R., Goñi M. A., Sparrow M. A., and Eversmeyer B. (1994) Terrestrial organic carbon contributions to sediments on the Washington margin. *Geochim. Cosmochim. Acta* **58,** 3035–3048.

Prins M. A., Postma G., Cleveringa J., Cramp A., and Kenyon N. H. (2000a) Controls on terrignous sediment supply to the Arabian Sea during the late Quaternary: The Indus Fan. *Mar. Geol.* **169,** 327–349.

Prins M. A., Postma G., and Weltje G. J. (2000b) Controls on terrignous sediment supply to the Arabian Sea during the late Quaternary: The Makran continental slope. *Mar. Geol.* **169,** 351–371.

Pye K. (1989) Processes of fine particle formation, dust source regions, and climatic changes. In *Paleoclimatology and Paleometeorology: Modern and Past Patterns of Global Atmospheric Transport*, Vol. 282 of NATO ASI Series, Series C (eds. M. Leinin and M. Sarnthein), pp. 3–30. Kluwer.

Ramage C. S., Miller F. R., and Jeffries C. (1972) *Meteorological Atlas of the International Indian Ocean Expedition: The Surface Climate of 1963, 1964.* U.S. National Science Foundation and India Meteorological Department.

Rieley G., Collister J. W., Jones D. M., Eglinton G., Eakin P. A., and Fallick A. E. (1991) Sources of sedimentary lipids deduced from stable isotope analyses of individual compounds. *Nature* **352,** 425–427.

Rieley G., Collister J. W., Stern B., and Eglinton G. (1993) Gas chromatography-isotope ratio mass spectrometry of leaf was *n*-alkanes from plants of differing carbon dioxide metabolisms. *Rapid Comm. Mass Spectrom.* **7,** 488–491.

Rommerskirchen F., Eglinton G., Dupont L., Güntner U., Wenzel C., and Rullkötter J. (2003) A north to south transect of Holocene southeast Atlantic continental margin sediments: Relationship between aerosol transport and compound-specific $\delta^{13}C$ land plant biomarker and pollen records. *Geochem. Geophys. Geosyst.* **4,**

Schefuβ E., Ratmeyer V., Stuut J.-B. W., Jansen J. H. F., and Damsté J. S. S. (2003) Carbon isotope analyses of *n*-alkanes in dust from the lower atmosphere over the central eastern Atlantic. *Geochim. Cosmochim. Acta* **67,** 1757–1767.

Schulz H., vonRad U., and Ittekkot V. (2002) Plankic foraminifera, particle flux and oceanic productivity off Pakistan, NE Arabian Sea: Modern analogues and application to the paleorecord. In *The Tectonic and Climatic Evolution of the Arabian Sea Region* (eds. P. D. Clift, D. Kroon, C. Gaedieke, and J. Craig), pp. 499–516. Special Publication 195. Geological Society, London.

Sermolli P. (1957) Una carta geobotanica dell'Africa Orientale (Eritrea, Etiopia, Somalia). *Webbia* **XIII 1,** 15–132.

Simoneit B. R. T. (1997) Compound-specific carbon isotope analyses of individual long-chain alkanes and alkanoic acids in Harmattan aerosols. *Atmos. Environ.* **31,** 2225–2233.

Simoneit B. R. T., Chester R., and Eglinton G. (1977) Biogenic lipids in particulates from the lower atmosphere over the eastern Atlantic. *Nature* **267,** 682–685.

Sirocko F. (1989) Zur akkumulation von Staubsedimenen im nördlichen Indischen Ozean: Anzeiger der Klimagerschichte Arabiens und Indiens. Ph.D. thesis, Geologisch Paläontologisches Insitut Universität Kiel.

Sirocko F (1995) Abrupt change in monsoonal climate: Evidence from the geochemical composition of Arabian Sea sediments. Habilitation thesis. Ph.D. thesis, University of Kiel.

Sirocko F. and Sarnthein M. (1989) Wind-borne deposits in the Northwestern Indian Ocean: Record of Holocene sediments versus satellite data. In *Paleoclimatology and Paleometeorology: Modern and Past Patterns of Global Atmospheric Transport*, Vol. 282 in NATO ASI Series, Series C (eds. M. Leinin and M. Sarnthein), pp. 401–433. Kluwer.

Sirocko F. and Lange H. (1991) Clay-mineral accumulation rates in the Arabian Sea during the late Quaternary. *Mar. Geol.* **97,** 105–119.

Sirocko F., Sarnthein M., Lange H., and Erlenkeuser H. (1991) Atmospheric summer circulation and coastal upwelling in the Arabian Sea during the Holocene and last glaciation. *Quat. Res.* **36,** 72–93.

Sirocko F., Sarnthein M., Erlenkeuser H., Lange H., Arnold M., and Duplessy J. C. (1993) Century-scale events in monsoonal climate over the past 24,000 years. *Nature* **364,** 322–324.

Sirocko F., Garbe-Schönberg D., and Devey C. (2000) Processes controlling trace element geochemistry of Arabian Sea sediments during the last 25,000 years. *Global Planet. Change* **26,** 217–303.

Staubwasser M. and Sirocko F. (2001) On the formation of laminated sediments on the continental margin off Pakistan: The effects of sediment provenance and sediment redistribution. *Mar. Geol.* **172,** 43–56.

Street-Perrott F. A., Huang Y., Perrott R. A., Eglinton G., Barker P., Khelifa L. B., Harkness D. D., and Olago D. O. (1997) Impact of lower atmospheric carbon dioxide on tropical mountain ecosystems. *Science* **278,** 1422–1426.

Tindale N. W. and Pease P. P. (1999) Aerosols over the Arabian Sea: Atmospheric transport pathways and concentrations of dust and sea salt. *Deep-Sea Res. II* **46,** 1577–1595.

Van Campo E. (1991) Pollen transport into Arabian Sea sediments. *Proceedings of the Ocean Drilling Program, Scientific Results,* Vol. 117 (eds. W. L. Prell, N. Niitsuma, et al.), pp. 277–280. Ocean Drilling Program.

von Rad U. and Tahir M. (1997) Late Quaternary sedimentation on the outer Indus shelf and slope (Pakistan): Evidence from high-resolution seismic data and coring. *Mar. Geol.* **138,** 193–236.

von Rad U., Schulz H., Riech V., den Dulk M., Berner U., and Sirocko F. (1999) Multiple monsoon-controlled breakdown of oxygen-minimum conditions during the past 30,000 yeasr documented in laminated sediments off Pakistan. *Palaeogeogr. Palaeoclim. Palaeoecol.* **152,** 129–161.

Wells J. T. and Coleman J. M. (1984) Deltaic morphology and sedimentology, with special references to the Indus River Delta. In *Marine Geology and Oceanography of Arabian Sea and Coastal Pakistan* (eds. B. U. Haq and J. D. Milliman), pp. 85–100. Van Nostrand Reinhold.

Chapter 5

Sea surface temperature pattern reconstructions in the Arabian Sea

This chapter has been submitted to Paleoceanography as:

Kristina A. Dahl and Delia W. Oppo, Sea surface temperature pattern reconstructions in the Arabian Sea

5.1 Abstract

Sea surface temperature (SST) and seawater $\delta^{18}O$ ($\delta^{18}O_w$) were reconstructed in a suite of sediment cores from throughout the Arabian Sea for four distinct time horizons (0 ka, 8 ka, 15 ka, and 20 ka) with the aim of understanding the history of the Indian Monsoon and the climate of the Arabian Sea region. This was accomplished through the use of paired Mg/Ca and $\delta^{18}O$ measurements of the planktonic foraminifer *Globigerinoides ruber*. By analyzing both basin–wide changes and changes in cross–basinal gradients, we assess both monsoonal and regional–scale climate changes. SST is colder than present for the majority of sites within all three paleo–time slices. The 20 ka and 15 ka time slices exhibit average negative temperature anomalies of 2.5–3.5°C, attributable, in part, to the influences of glacial atmospheric CO_2 concentrations and large continental ice sheets. The elimination of the cross–basinal SST gradient during these two time slices likely reflects a decrease in summer monsoon and an increase in winter monsoon strength. Changes in $\delta^{18}O_w$ that are unattributable to global ice volume changes reflect decreased evaporation and increased winter monsoon mixing. SSTs throughout the Arabian Sea were still cooler than present by an average of 1.4°C in the 8 ka time slice. These cool SSTs, along with lower $\delta^{18}O_w$ throughout the basin, are attributed to an increase in the strength of both the summer and the winter monsoon and increased runoff and precipitation. Both the Indian Monsoon and the regional Arabian Sea mean climate have varied substantially over over the past 20 ka. Furthermore, these results emphasize the importance of taking a spatial approach to the reconstruction of processes such as monsoon upwelling.

5.2 Introduction

Reconstructing the history of the Indian Monsoon is critical for developing an understanding of past, present, and future monsoon variability. Because Arabian Sea sea surface temperatures (SSTs) are sensitive to the strength of Indian Monsoon winds, they can be used to infer monsoon strength through time. During boreal summer, southwest winds associated with the Indian Summer Monsoon blow over the Arabian Sea (Figure 5-1). These

winds induce coastal upwelling along the Somali and Omani margins. The upwelling is reflected in the SST pattern in the Arabian Sea (Figure 5-1), which is characterized by a $\sim$ 4°C temperature gradient increasing from west (24 – 25°C) to east (28°C). During the Indian Winter monsoon, north–northeast winds from the Asian continent cause mixing and cooling of the surface waters of the northernmost Arabian Sea, north of 20°N. Sites in this region experience a 3–4°C cooling during this season. On an annually averaged basis, SST in the western Arabian Sea is $\sim$ 2°C cooler than in the eastern Arabian Sea.

In addition to being affected by Indian Monsoon winds, Arabian Sea SSTs, like SST everywhere, can be affected by a number of radiative forcing factors, including solar insolation, which varies on seasonal and orbital timescales, greenhouse gas forcing, including the concentration of CO_2, and land surface properties, particularly the extent of land ice. The strength of the monsoon itself is, in turn, dependent upon these radiative forcing factors (*e.g. Pinot et al.*, 1999; *Liu et al.*, 2003), although the relative importance of these factors in determining monsoon strength is a subject of debate (*Clemens et al.*, 1991; *Reichart et al.*, 1998; *Clemens and Prell*, 2003). Nevertheless, climate models forced with either altered solar insolation (*Liu et al.*, 2003) or altered atmospheric CO_2 and land ice (*Pinot et al.*, 1999) show large changes in Arabian Sea SST. Thus Arabian Sea SSTs can vary as a direct response to variations in radiative forcing or indirectly as a response to variations in monsoon strength.

Sea surface salinity (SSS) in the Arabian Sea is relatively high (35–36.5 psu), reflecting high evaporation rates and the input of highly saline waters from the Red Sea and Persian Gulf. SSS patterns in the basin vary as a function of season (Figure 5-1). The waters upwelled during the summer in the western Arabian Sea are marked by low salinities (*Schott et al.*, 2002). The salinity gradient during the summer monsoon season therefore increase by $\sim$0.5 psu from west to east across the basin. On an annually averaged basis, there is almost no gradient across the basin.

Historically, paleoceanographic time–series reconstructions of the Indian Monsoon have taken advantage of signals associated with summer monsoon–induced upwelling in the western Arabian Sea, such as the percentage and/or isotopic composition of specific planktonic foraminifera within the upwelling regions (*Prell*, 1984; *Naidu and Malmgren*, 1995;

Overpeck et al., 1996; *Anderson et al.*, 2002; *Gupta et al.*, 2003). In this study, we reconstruct the Arabian Sea SST pattern for four time periods (0 ka, 8 ka, 15 ka, and 20 ka). By using a suite of sediment cores from throughout the Arabian Sea, we can assess SST changes in both upwelling and non-upwelling regions, thus allowing for discrimination between SST changes induced by local upwelling and regional–scale SST changes that are unlikely to be caused by upwelling. Our SST reconstructions are accomplished using the Mg/Ca ratio of the planktonic foraminifer *Globigerinoides ruber*, which has been shown to be sensitive to SST (*e.g. Anand et al.*, 2003, and references therein). In addition, we calculate seawater δ^{18}O (hereafter $\delta^{18}O_w$) as a means of reconstructing the surface hydrology of the Arabian Sea by pairing our Mg/Ca SSTs with δ^{18}O measurements on the same samples.

5.3 Materials and Methods

The sediment cores used in this study (Figure 5-2, Table 1) include box, piston, and gravity cores collected on a number of different cruises. The modern, 8 ka, 15 ka, and 20 ka time horizons were identified in each core via a combination of oxygen isotope stratigraphies and AMS ^{14}C dates (Table 2, Supplementary Figure 1 *Sirocko*, 1989). We have recalibrated the ^{14}C dates originally published by *Sirocko* (1989) using Calib 5.0 *Stuiver and Reimer* (1993), which somewhat alters the ages of the time horizons identified by *Sirocko* (1989) and subsequently used in this study. These time slices are intended to representative of modern, Early Holocene, deglacial, and glacial conditions, respectively. While the sedimentation rates and depth ranges for each core and sample indicate that the age range does not exceed 2 ka for any of the individual samples used in this study, the full age range represented by any given time slice could be somewhat larger. For this reason, the heterogeneities in our SST and $\delta^{18}O_w$ reconstructions are likely due, in large part, to differences in ages of samples within the same time slice.

Specimens of *Globigerinoides ruber* (white) were picked from the 212–300μm size fraction. Each sample, composed of an average of 50 individuals, was then weighed and crushed gently between two glass slides in order to open the individual chambers for effec-

tive cleaning. A split of the total sample, representing approximately 10 individuals, was then removed for isotopic analysis, and the remainder was used for Mg/Ca analysis.

Samples for Mg/Ca were then subjected to a series of cleaning treatments designed to remove clays, metal oxides, and organic matter from the shells. Our cleaning procedure followed that of *Boyle and Keigwin* (1985) and subsequent revisions (*Rosenthal et al.*, 1995; *Boyle and Rosenthal*, 1996).

Mg/Ca ratios were measured with a high–resolution sector–field inductively coupled plasma mass spectrometer (ICP–MS; Finnegan Element2). Mg, Ca, and Al concentrations were determined in low resolution mode by averaging measurements from 74 scans. All ions were counted in analog mode. Because foraminifera from parts of the Arabian Sea contain stubbornly adhering clays that could potentially elevate the measured Mg/Ca (K. L. Bice et al., The application of SIMS for measuring Mg/Ca in rare, delicate, or altered planktonic foraminifera: Examples from the Holocene, Paleogene, and Cretaceous, submitted manuscript), we also monitored Al/Ca ratios. Samples with Al/Ca values greater than 30μmol/mol, twice that observed in foraminifera considered to have no detrital clay contamination, were excluded from the final data set (3 samples total; *Lea et al.*, 2003; *Schmidt et al.*, 2004). A standard, containing high–purity elements in ratios consistent with those observed in foraminifera, and a blank of 2% HNO_3 were run between every four samples. The instrumental error for Mg/Ca, calculated from repeated measurements of a series of consistency standards, is 0.03 μmol/mol.

In order to convert measured Mg/Ca ratios to SST, we used the calibration of *Rosenthal and Lohmann* (2002). This calibration incorporates shell weight in order to correct for dissolution, which preferentially removes Mg from the foraminiferal tests. This calibration accounts for the fact that our samples, which come from a wide range of depths within the Arabian Sea, likely experience differing degrees of dissolution. The combined instrumental and calibrative errors associated with our calculated Mg/Ca SST is estimated to be ± 1°C

Stable isotopes were measured using a Finnigan MAT 253 coupled to a Kiel III carbonate device. The analytical precision of this instrument for $\delta^{18}O$, as determined by replicate analyses (n=600) of the carbonate standard NBS19 is 0.07‰. $\delta^{18}O_w$ was calculated using the *G. ruber*–specific calibration of *Mulitza et al.* (2003): $\delta^{18}O_{w,VSMOW}$ = ($T_{Mg/Ca}$ -

14.2)/4.44 + $\delta^{18}O_{carbonate,VPDB}$ + 0.27

At sites for which we had both a modern and a time–slice measurement of Mg/Ca SST and $\delta^{18}O_w$, time–slice SST and $\delta^{18}O_w$ anomalies were calculated using the values from the same core. For several sites, however, we had time–slice samples without a modern sample from the same core. In these instances, SST anomalies were calculated using the time–slice sample and the nearest available core–top value. Anomalies calculated by the latter method are denoted in all the figures by open circles as opposed to filled circles.

5.4 Results and Discussion

5.4.1 0 ka

SST

With the exception of three data points, the Mg/Ca–derived SSTs for each site comprising the 0 ka time slice fall within the modern observed SST range at that site (Figures 5-3 and 5-4; *Levitus and Boyer*, 1994). At most sites, Mg/Ca SSTs are either at or slightly below the observed annual average SST, in accordance with the observation that *G. ruber* lives year round in the Arabian Sea, but experiences blooms during both monsoon seasons (*Curry et al.*, 1992; *Conan and Brummer*, 2000; *Peeters et al.*, 2002). The reconstructed west–to–east SST gradient of $2 - 4$°C is consistent with the observed annually averaged and summer SST gradients of 2°C and 4°C, respectively.

$\delta^{18}O_w$

The core top data show a west–to–east gradient in $\delta^{18}O_w$ of 0.3‰, with the west being lower than the east (Figure 5-4). The relationship between $\delta^{18}O_w$ and salinity in the Arabian Sea varies from location to location and depends heavily upon the abundance of Red Sea Waters (Figure 5-5). However, our data are consistent with modern observations of lower salinities in the western than in the eastern Arabian Sea during the summer upwelling season (*Levitus and Boyer*, 1994). In terms of absolute value, our modern $\delta^{18}O_w$ data are higher than observations by up to 1‰ (*Schmidt et al.*, 1999). This discrepancy is likely due

to a combination of sources of error including those associated with the calcification depth of, and therefore the temperature recorded by, the foraminifera, and the calibrations for the Mg/Ca–SST relationship and the SST–$\delta^{18}O_w$–$\delta^{18}O_c$ relationship. These errors are presumably temporally invariant; thus, while they affect the absolute values of the calculated $\delta^{18}O_w$, they do not affect the anomalies upon which we focus in subsequent sections.

Surface seawater $\delta^{18}O$ at a given location is determined by elements of the local hydrological cycle, including precipitation, evaporation, runoff, and advection of water from other locations. The Arabian Sea is an evaporative basin (*Oberhuber*, 1988), which results in heavy surface $\delta^{18}O_w$ values and lower subsurface $\delta^{18}O_w$ values. The modern $\delta^{18}O_w$ and observed salinity gradients in the Arabian Sea are the product of two phenomena: 1) Upwelling in the western Arabian Sea associated with the summer monsoon brings fresher water to the surface; and 2) The western Arabian Sea experiences greater convection and precipitation than the eastern Arabian Sea. Both of these processes serve to depress salinity and $\delta^{18}O_w$ in the western Arabian Sea relative to the eastern Arabian Sea.

5.4.2 20 ka

The 20ka time slice encompasses the Last Glacial Maximum (LGM). At this time, solar insolation was within $1 W m^{-2}$ of present day values (Figure 6-7; *Berger and Loutre*, 1991). Together, drastically (80 ppmv) reduced atmospheric CO_2 concentrations (*Monnin et al.*, 2001) and greater ice volume, however, were responsible for a $\sim 4 W m^{-2}$ decrease in global net radiative forcing relative to today (*Broccoli*, 2000).

SST

At the LGM, SST throughout the Arabian Sea was colder than it is today (Figure 5-7). Colder than present SSTs are evident at sites affected by monsoon upwelling and mixing (shaded regions in Figure 5-4) as well as those that are not affected by such processes (unshaded regions in Figure 5-4). The average SST anomaly relative to present was -3.6 ± 1.8°C (1σ error bars). Such a response is consistent with a climate model simulation of the LGM using an atmospheric–mixed layer ocean model (*Broccoli*, 2000). Because

there was no simulation of upwelling or other oceanic processes within this model, the 2°C Arabian Sea cooling predicted by the model resulted from atmospheric–only mechanisms, namely a prescribed lowering of CO_2 and changes in continental ice that result in changes in atmospheric circulation and, in turn, wind strength and evaporative cooling. The basin–wide cold SST anomalies as determined via our data suggests that the Arabian Sea, like much of the rest of the tropics, could have cooled as a direct result of decreased radiative forcing. It is also important to note, however, that the disappearance of the west–to–east SST gradient within this time slice implies that the strength of Indian Monsoon was altered during this time. The lack of a gradient results from larger cold anomalies in the eastern Arabian Sea than in the western Arabian Sea. This SST pattern could result from a weakened summer monsoon (and therefore decreased upwelling and a subsequent relative warming) either on its own or in conjunction with a strengthened winter monsoon (and therefore enhanced mixing and cooling of surface waters in the northern and eastern Arabian Sea). Either scenario is consistent with both climate model simulations of the LGM (*Pinot et al.*, 1999) and our theoretical understanding that external radiative forcing would cool the land more effectively than the ocean, thereby decreasing (increasing) the land–ocean temperature gradient during the summer (winter) and decreasing (increasing) the strength of the summer (winter) monsoon.

LGM comparison with alkenone and transfer function data

Based on foraminiferal transfer function reconstructions of SST, the CLIMAP study concluded that LGM SSTs in the Arabian Sea were within 1°C of present day SSTs (*CLIMAP Project Members*, 1981). Since then, a number of investigations employing the use of alkenones (*Emeis et al.*, 1995; *Bard et al.*, 1997; *Rostek et al.*, 1997; *Sonzogni et al.*, 1998; *Higginson et al.*, 2004) and foraminiferal abundances (*Cayre and Bard*, 1999; *Naidu and Malmgren*, 2005) have suggested that LGM SSTs were in fact on the order of 3°C cooler than present. With the exception of *Sonzogni et al.* (1998), these studies have utilized a time series approach, thus giving a temporal, rather than spatial, history of SST. As noted by *Sonzogni et al.* (1998), alkenone–derived SSTs are systematically lower than estimates derived from transfer functions and/or the modern analog technique at the same site. Mg/Ca

and alkenone data from nearby cores suggest that Mg/Ca–derived SSTs may be still lower than alkenone SSTs, although both proxies suggest a basin–wide negative SST anomaly of ~2–4°C for the LGM. Unlike our Mg/Ca data, the spatially distributed alkenone data of *Sonzogni et al.* (1998) show a similar magnitude of cold anomalies in both the eastern and western parts of the Arabian Sea. Offsets between alkenone and Mg/Ca SST estimates may result from differences in the seasonality of the production of alkenone–producing coccoliths and foraminifera. Nonetheless, the Mg/Ca data presented here provides further evidence for a greater cooling in the Arabian Sea than had been originally suggested by CLIMAP.

$\delta^{18}O_w$

Globally, $\delta^{18}O_w$ was approximately 1‰ higher at the LGM than it is today (*Fairbanks*, 1989; *Schrag et al.*, 2002, and references therein). Although $\delta^{18}O_w$ at most sites in the Arabian Sea was higher than present at the LGM, the increase at most sites was considerably less than 1‰ (Figure 5-7). Sites within the western Arabian Sea experienced increases of 0.4–0.7‰ while sites in the eastern Arabian Sea experienced almost no change in $\delta^{18}O_w$ relative to today. The results suggest a reversal of the $\delta^{18}O_w$ gradient observed in our 0 ka samples such that, during the LGM, the eastern Arabian Sea was characterized by lower values than the western Arabian Sea.

The dampened increase in $\delta^{18}O_w$ relative to the global mean could be the result of a number of factors. Given the cool SSTs in the Arabian Sea at this time, evaporation was likely lower. Today, evaporation results in a positive $\delta^{18}O_w$ gradient of 0.1–0.3‰ from the surface to 100 m depth (W. Curry, unpublished data). A decrease in evaporation would therefore decrease surface $\delta^{18}O_w$ values. Such a decrease could partially offset the global increase in $\delta^{18}O_w$. The reversal of the modern gradient implies that changes in the strength of the summer and winter monsoons could also be affecting $\delta^{18}O_w$ values. More specifically, weaker than present summer monsoon upwelling and stronger than present in winter monsoon mixing could be responsible for the fact that the positive western Arabian Sea $\delta^{18}O_w$ anomaly increase was significantly larger than that of the eastern Arabian Sea. It is also possible that a decrease in the outflow of highly saline waters from the Red Sea,

as has been proposed by *Locke and Thunell* (1988) and *Naqvi and Fairbanks* (1996), could cause a relative freshening of Arabian Sea waters.

5.4.3 15 ka

Insolation conditions at 30°N at 15 ka BP were markedly different from those at 20 ka (Figure 6-7). Between 20 ka and 15 ka, annually averaged insolation increased by 6 Wm^{-2} (*Berger*, 1978). However, global ice volume was still higher than at present (*Fairbanks*, 1989; *Bard et al.*, 1996), and CO_2 was still at near–glacial values (200 ppmv; *Monnin et al.*, 2001).

SST

All sites included in this study had cooler SSTs at 15 ka than they do today (Figure 5-8). The average negative temperature anomaly for this time slice is 2.9 ± 2.2°C. The greatest anomalies occur at sites that lie outside of the modern summer upwelling region. That this time slice is generally cold in our study is consistent with the fact that temperatures in the North Atlantic at 15 ka were colder than during the LGM (*Waelbroeck et al.*, 1998; *Bard et al.*, 2000). This cold period in the North Atlantic is known as Heinrich Event 1 (H1). The chronology for our cores is not sufficient enough to state for certain that we have captured H1. However, it seems likely given the cold SSTs observed within this time slice. That SST remained cold at this time despite greatly increased solar insolation suggests that the influence of glacial boundary conditions outweighed the influence of solar insolation. If, in fact, this time slice does capture H1, the data are consistent with the hypothesis that the Asian monsoon system is subject to downstream effects from the North Atlantic region (*Kutzbach et al.*, 1993).

Again, insight into the impact of the Indian Monsoon on SST during this time can be gained by evaluating the SST gradient across the Arabian Sea. SST anomalies for the western Arabian Sea sites are heterogeneous, ranging from -0.5°C to -4.3°C. Given this heterogeneity, it appears that the west–to–east SST gradient was either nonexistent or reversed during this time. This implies an increase in the strength of the winter monsoon (and

a greater cooling of SST in the northeastern Arabian Sea via mixing) and a decrease in the strength of the summer monsoon (and a relative warming of western Arabian Sea SSTs via reduced upwelling) relative to today.

$\delta^{18}O_w$

At 15 ka, $\delta^{18}O_w$ in the Arabian Sea was higher than it is today by an average of 0.73‰ (Figure 5-8). This positive anomaly is close to that of the global mean of 0.75‰ (*Fairbanks*, 1989), which implies that ice volume changes are largely responsible for the higher conditions exhibited in this time slice. While the data, like the SST data for this time slice, are heterogeneous, the average positive anomaly in the west is greater than that in the east by 0.3‰. Thus, as was the case for the 20 ka time slice, the core–top $\delta^{18}O_w$ gradient was reversed during this time. This gradient reversal likely reflects the same trends that were evident at 20 ka: an increase in the winter monsoon, and a decrease in the summer monsoon relative to today.

5.4.4 8 ka

Annually averaged insolation at 8 ka was similar to that at 15 ka (Figure 6-7). CO_2 and ice volume, however, were near their present day values, thus significantly altering radiative forcing conditions relative to the 15 ka and 20 ka time slices (*Bard et al.*, 1996; *Petit et al.*, 1999, and references therein). At 8 ka, perihelion, the point at which Earth is closest to the sun, occurred during August while today perihelion occurs during January. Thus, at 8 ka, Northern Hemisphere seasonality was enhanced relative to today and to the 15 ka and 20 ka time slices. In the absence of lowered CO_2 and greater ice volume as forcing factors, the importance of insolation was likely greater at 8 ka than at 15 ka and 20 ka.

SST

At 8 ka, SSTs throughout the Arabian Sea were cooler than today by an average of 1.4 ± 1.3°C (Figure 5-9). Thus, from 15 ka to 8 ka, the Arabian Sea experienced a 1.5°C warming associated with the deglaciation. Sites in the eastern Arabian Sea exhibit larger

cold anomalies than those in the western Arabian Sea, resulting in a decrease in the strength of the SST gradient across the basin.

Our finding that SSTs throughout the basin were cooler than present at 8 ka is corroborated by two Arabian Sea sites with Holocene alkenone–SST records that demonstrate that SSTs were cooler at 7 ka than they are today (*Kim et al.*, 2004). While the Arabian Sea warmed from the early Holocene to today, sites throughout the subtropical North Atlantic and Mediterranean regions cooled (*Marchal et al.*, 2002; *Kim et al.*, 2004, and references therein). This cooling trend is commonly attributed to decreasing solar insolation. In the Arabian Sea region, however, modeling studies indicate that the enhanced seasonality during this time would result in an increase in both the summer and winter monsoons (*Kutzbach and Gallimore*, 1988; *Prell and Kutzbach*, 1992; *Liu et al.*, 2003). The colder SSTs during this time is therefore likely the result of stronger than present summer monsoon upwelling in the western Arabian Sea and winter monsoon mixing in the northeastern Arabian Sea. A number of studies, most of which utilize the percentage of the planktonic foraminifer *Globigerina bulloides* as a monsoon upwelling indicator, have indicated that this time period was one of greater summer monsoon strength (*Prell*, 1984; *Naidu and Malmgren*, 1995; *Overpeck et al.*, 1996; *Fleitmann et al.*, 2003; *Gupta et al.*, 2003). Given the negative SST anomalies we observe outside of the summer monsoon upwelling region, however, our data suggest that an increase in summer monsoon intensity must have been accompanied by an increase in winter monsoon intensity. Thus, while the basin–wide cold anomalies observed in the 20 and 15 ka time slices were likely due, in large part, to the influence of glacial boundary conditions, the basin–wide cold anomalies in the 8 ka time slice resulted from greater seasonality and strengthened winter and summer monsoons associated with solar insolation conditions.

$\delta^{18}\mathbf{O}_w$

Throughout the basin $\delta^{18}O_w$ was, on average, 0.5‰ lower at 8 ka than it is today (Figure 5-9). The light anomalies are larger in the eastern Arabian Sea than in the western Arabian Sea, thereby reducing the cross basinal gradient that is observed today. Increased transport of subsurface waters to the surface during both monsoon seasons could account

for the overall decrease in $\delta^{18}O_w$. In this case, the decreased gradient would require that the increase in winter monsoon mixing was greater than the increase in summer monsoon upwelling. Alternatively, increased precipitation and runoff associated with a strengthened summer monsoon contributed to the $\delta^{18}O_w$ decrease. Sites in the eastern Arabian Sea would be more affected by increased runoff than sites in the west given the distribution of rainfall and rivers in the region, consistent with our results.

5.5 Summary and Conclusions

We have constructed Arabian Sea SST and $\delta^{18}O_w$ maps for four time periods in order to gain an understanding of the history of the Indian Monsoon. The occurrence of basin–wide SST changes in the 8 ka, 15 ka, and 20 ka time slices suggests that long–term variations in the SST pattern in this region are a function not just of monsoon–induced upwelling, but of other factors as well. Consistent with modeling studies, we find that glacial boundary conditions have a profound influence on Arabian Sea SST that is irrespective of monsoon upwelling (*Broccoli*, 2000). Lowered CO_2 and increased ice volume contributed to basin–wide cold anomalies relative to today in the Arabian Sea at 15 ka and 20 ka via direct radiative forcing. Superimposed upon the cold anomalies are changes in the SST pattern that imply an increase (decrease) in winter (summer) monsoon strength relative to today. Absolute SSTs, as well as the SST pattern, at the 8 ka time slice reflect the relaxation of glacial boundary conditions and enhanced Northern Hemisphere seasonality. The $\delta^{18}O_w$ patterns for these time slices are consistent with our interpretation of the SST analyses. Additionally, we interpret the $<1‰$ increases in $\delta^{18}O_w$ during the 15 ka and 20 ka time slices as reflecting weaker than present evaporation, possibly in concert with changes in the strength of both the summer and winter monsoons. Lower than present $\delta^{18}O_w$ in the 8 ka time slice may be due to increased precipitation and/or runoff into the Arabian Sea along with changes in upper oceanic dynamics.

Mg/Ca–derived SSTs at the LGM suggest lower SSTs than originally reconstructed by the CLIMAP study (*CLIMAP Project Members*, 1981). These results add to a growing body of evidence of alkenone and foraminiferal abundance derived SST estimates implying

that SSTs in the Arabian Sea were $2 - 4$°C cooler than present at the LGM (*Emeis et al.*, 1995; *Bard et al.*, 1997; *Rostek et al.*, 1997; *Sonzogni et al.*, 1998; *Cayre and Bard*, 1999; *Higginson et al.*, 2004; *Naidu and Malmgren*, 2005).

Our interpretations of temperature and $\delta^{18}O_w$ changes presume that there were no large changes in the temperature or $\delta^{18}O_w$ of Arabian Sea source waters over the past 20,000 years. Waters upwelled in the Arabian Sea originate in the subtropical Indian Ocean and are markedly colder and fresher than the surface waters of the Arabian Sea (*Schott et al.*, 2002). Changes in the properties and/or the flux of these source waters could affect the surface properties of the Arabian Sea, particularly within upwelling regions.

The primary radiative forcing factors (CO_2, ice volume, and solar insolation) appear to exert differing degrees of influence on Arabian Sea climate over the past 20ka. Sea surface conditions at 15 ka and 20 ka in the Arabian Sea were very similar, despite very different solar insolation conditions. Conversely, conditions recorded by the 8 ka and 15 ka time slices are very different, despite similar insolation conditions during the two time periods. This suggests that, during glacial periods, lowered CO_2 and increased ice volume are the dominant radiative forcing factors for this region. During interglacial periods, however, solar insolation dominates the radiative forcing.

5.6 Acknowledgments

We would like to thank Rose Came, Simon Thorrold, and Scot Birdwhistell for laboratory assistance and technical support with the ICP–MS as well as Rindy Ostermann for technical support with the carbonate mass spectrometer. We also thank Yair Rosenthal, and Suzanne Perron–Cashman for analyses of the 0 ka samples. Frank Sirocko, Andreas Lückge, and Bill Curry kindly provided the samples and JGOFS data for this study. Analyses were funded by a SGER grant from the National Science Foundation (OCE03–34598). Funding was also provided by a Schlanger Ocean Drilling Program Fellowship (to K.A.D.) and NSF Grant OCE02–20776 (to D.W.O.).

Table 1. Locations of sediment samples used in this study

Cruise	Core	Time Slices	Latitude	Longitude	Water depth (m)	Sample depth (cmbsf)[a]
SO28	5KL	20	6°39.8'N	61°8.0'E	3335	30–33
SO28	11KL	0, 8, 15, 20	5°23.4'N	60°15.1'E	3859	0–5/11–14/41–44/65–69
SO28	18KL	0, 8, 15, 20	1°54.0'N	67°20.5'E	3035	0–10/17–21/33–37/43–47
SO42	15KL	8, 20	14°52.8'N	64°44.8'E	3920	16–20/50–54
SO42	26KL	0, 8, 15, 20	15°30.9'N	68°45.6'E	3776	0–5/15–19/78–82/103–107
SO42	36KL	0, 8, 15, 20	17°04.5'N	69°02.7'E	2055	0–5/8–12/26–30/43–47
SO42	51KL	8, 15, 20	20°57.9'N	65°33.5'E	2644	28–32/78–82/130–134
SO42	57KL	0, 8, 15, 20	20°54.5'N	63°07.3'E	3422	0–5/28–32/78–82/118–122
SO42	64KL	8, 15, 20	19°4.6'N	64°41.0'E	3281	8–12/58–62/96–100
SO42	70KL	8, 15, 20	17°30.7'N	61°41.8'E	3810	18–22/58–62/82–86
SO42	71KL	8,15	16°14.2'N	60°15.3'E	4029	38–40/70–74
SO42	74KL	0, 8, 15, 20	14°19.3'N	57°20.8'E	3212	9–15/62–66/138–142/200-204
SO42	79KL	8, 15	14°19.3'N	58°19.6'E	4351	38–42/79–83
SO42	82KL	8, 15, 20	12°41.1'N	58°40.6'E	4416	8–10/58–62/100-105
SO42	87KL	0, 15, 20	10°30.1'N	57°44.2'E	3773	0–5/94–98/118–122
SO90	39KG	0	24°50.0'N	65°55.0'E	704	0–2
SO130	211KG	0	24°52.9'N	63°1.6'E	691	0–2
SO130	282KG	0	23°32.3'N	65°19.0'E	988	0–1
SO130	285MC	0	23°5.8'N	66°29.0'E	778	0–1
IOE	105KK	15, 20	11°16.0'N	53°32.5'E	3535	111–119/138–143
IOE	114KK	20	08°00.5'N	51°12.8'E	3843	137–141
IOE	143KK	0, 20	01°15.0'N	44°47.0'E	1522	12–19/253–258
TN47	6GGC	0, 8, 15, 20	17°22.9'N	58°47.7'E	3652	5–6/66–66.5/122–122.5/208–208.5
TN41	32MC	0	19°30.1'N	58°28.1'E	0–1	

(a) centimeters below sea floor

Table 2. Previously unreported ^{14}C dates

Cruise	Core	Depth (cmbsf)[a]	Method	Foram. species	^{14}C age (yr)	SD (yr)	Cal. Age (yr)[b]
TN47	6GGC	5–6	AMS	mixed planktonics	755	35	270
TN47	6GGC	37–38	AMS	mixed planktonics	1730	40	1090
TN47	6GGC	80–81	AMS	*G. ruber*, *G. sacculifer*[c]	10,000	70	10,660
TN47	6GGC	130–131	AMS	*G. ruber*	13,950	80	15,830
TN47	6GGC	203–204	AMS	mixed planktonics	18,000	90	20,520
TN47	6GGC	219–219.5	AMS	mixed planktonics	19,100	140	22,090

(a) centimeters below sea floor;
(b) Calibrated with a reservoir age of 600 years using Calib 5.0 (*Stuiver and Reimer*, 1993);
(c) without sac-like final chamber

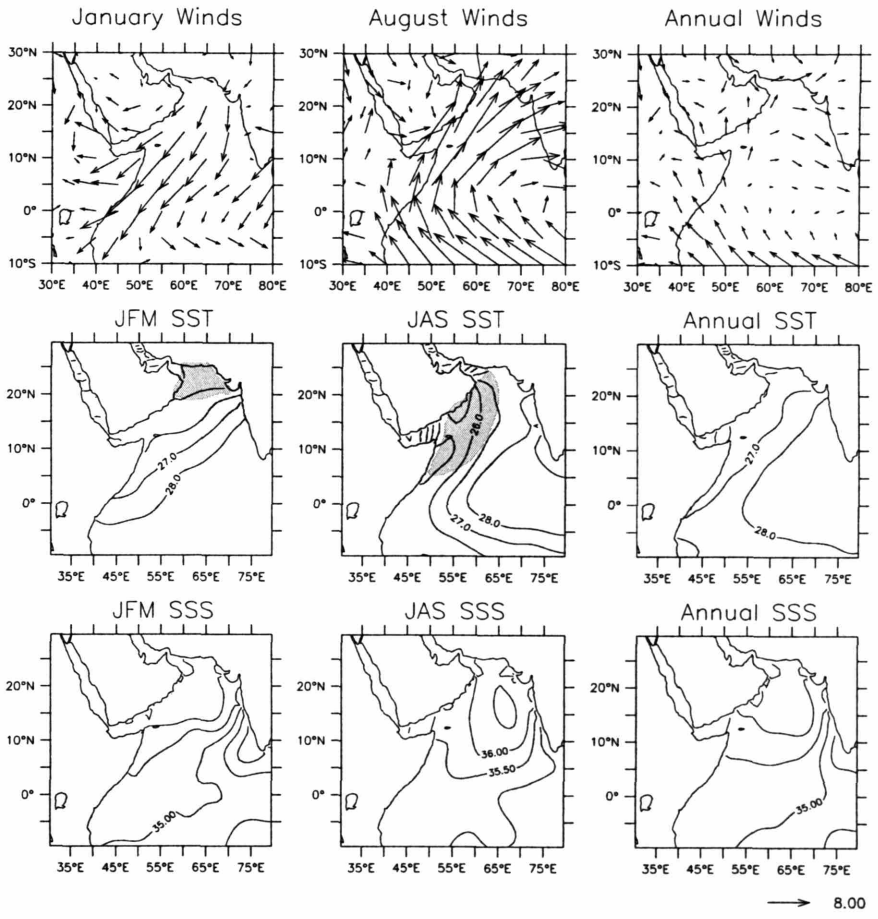

Figure 5-1: Arabian Sea climatology for winter (December–January–February; left), summer (June–July–August; middle), and annual average (right). SST and SSS data are from *Levitus and Boyer* (1994). SSS units are psu. Shading indicates regions of winter monsoon mixing and summer monsoon upwelling. Wind data provided by the NOAA–CIRES Climate Diagnostic Center, Boulder Colorado (http://www.cdc.noaa.gov). Units are ms^{-1}.

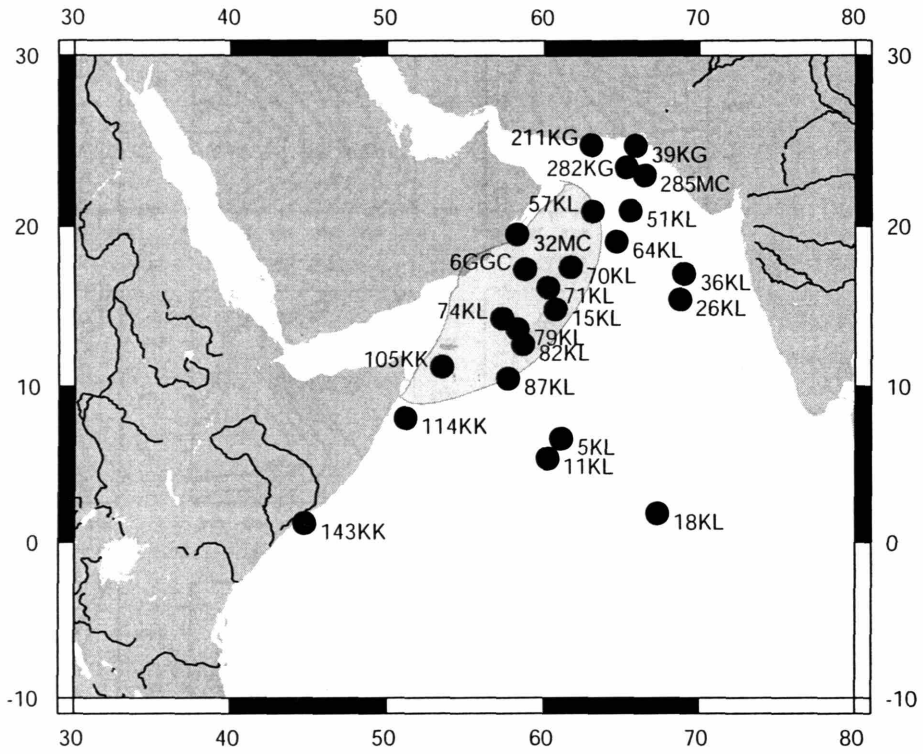

Figure 5-2: Locations of cores used in this study. Shading indicates the region currently affected by summer monsoon upwelling.

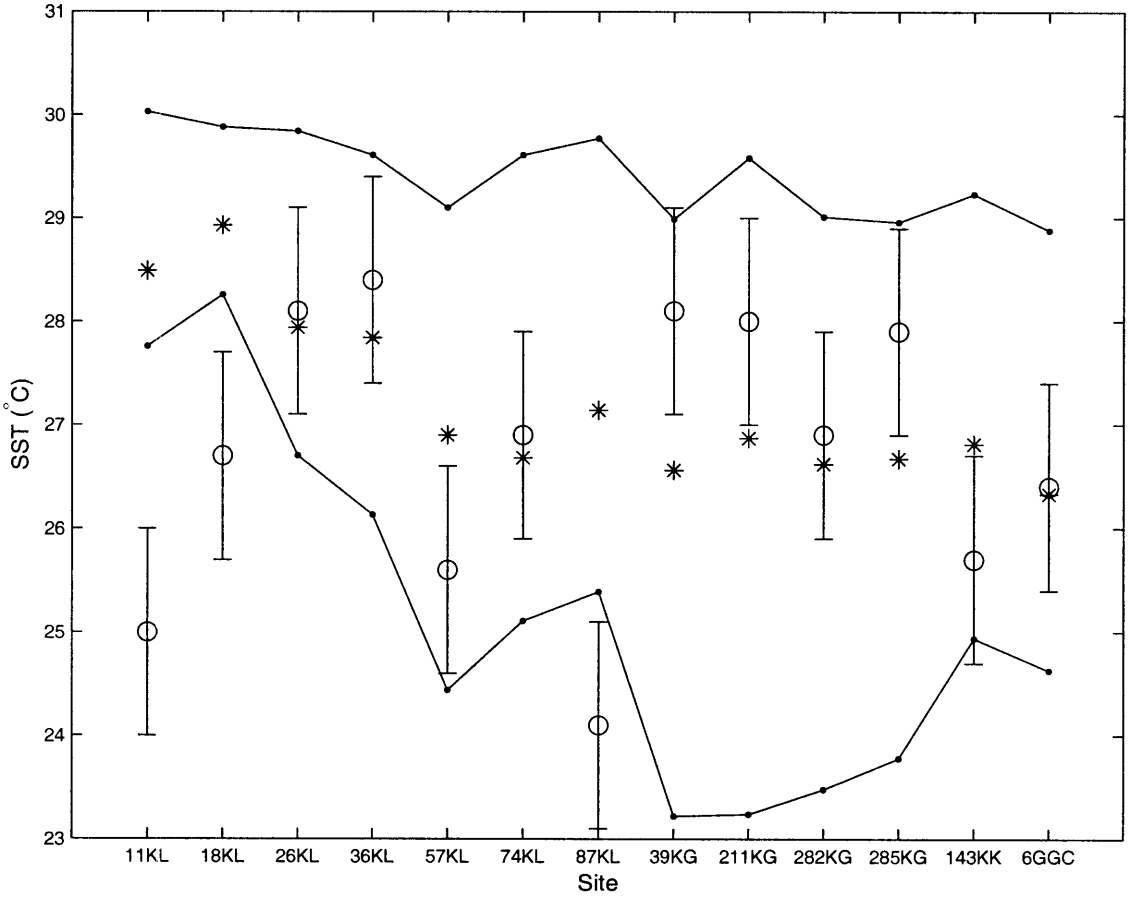

Figure 5-3: Mg/Ca SST derived from core tops throughout the Arabian Sea (open circles) compared to the SST range experienced at each site (solid lines) and the annual average observed SST (asterisks). Observational data from *Levitus and Boyer* (1994).

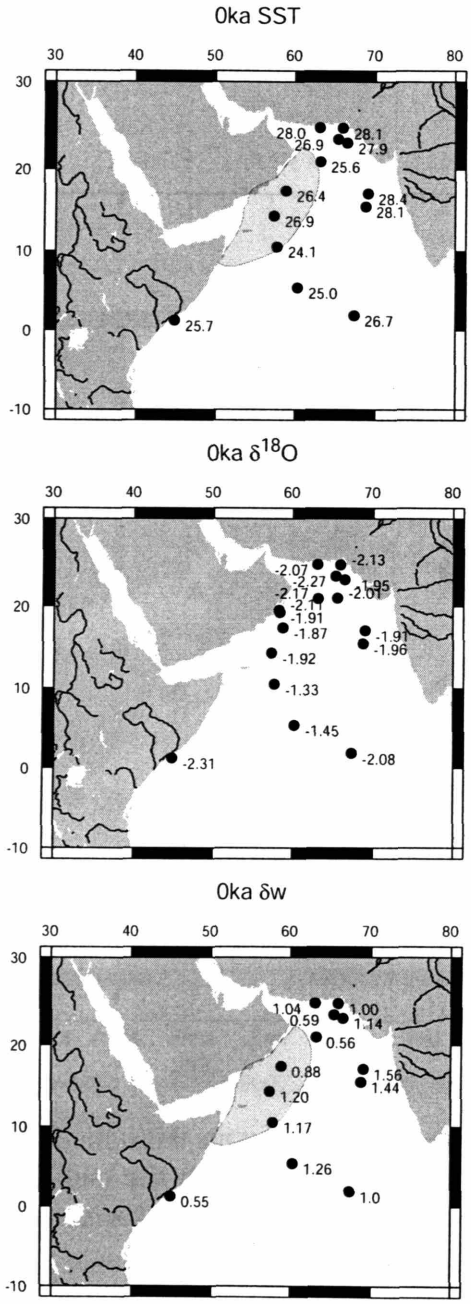

Figure 5-4: Surface conditions reconstructed from core–top (0 ka) sediments. (top) Mg/Ca SST; (middle) δ^{18}O; (bottom) $\delta^{18}O_w$. Shading is as for Figure 5-2.

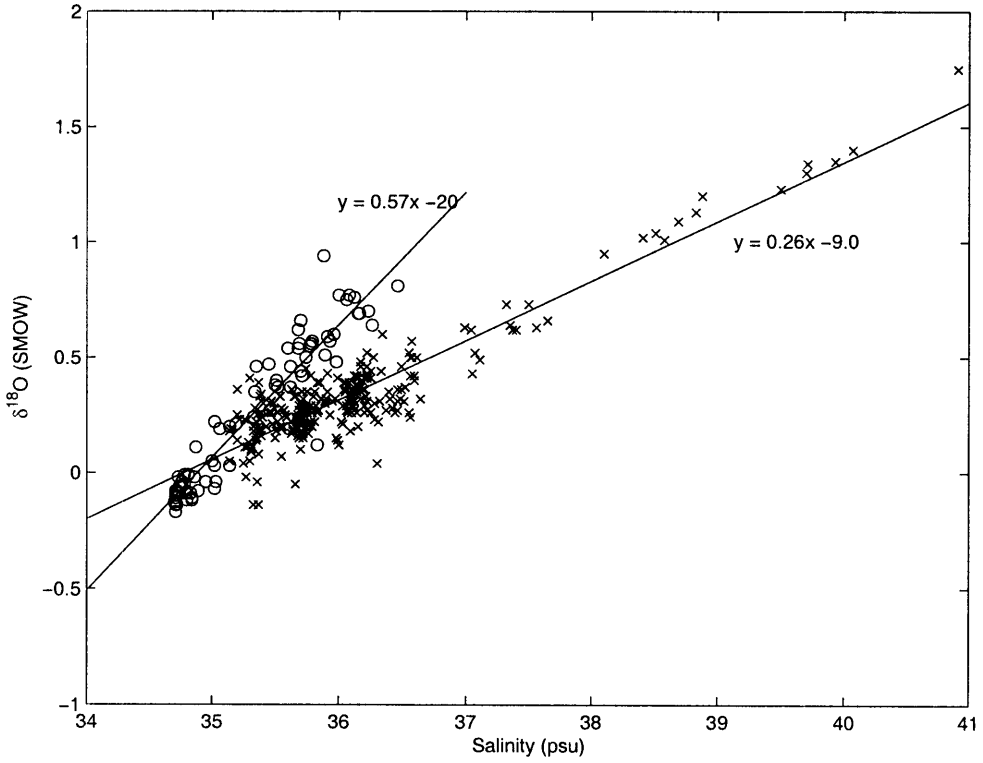

Figure 5-5: Salinity–$\delta^{18}O_w$ relationships for the Arabian Sea. Crosses denote surface data from *Delaygue et al.* (2001) (r2=0.85). This dataset is heavily sampled in the Gulf of Aden region and likely reflects a great deal of influence of Red Sea Water. Circles denote full water column data from this study obtained during JGOFS cruises TN–041 and TN–047 (1994 and 1995, respectively; r^2=0.90). This dataset includes stations in the western, central, and eastern Arabian Sea. Note that the two datasets overlap significantly, but that the slopes defining the salinity–$\delta^{18}O_w$ relationships differ.

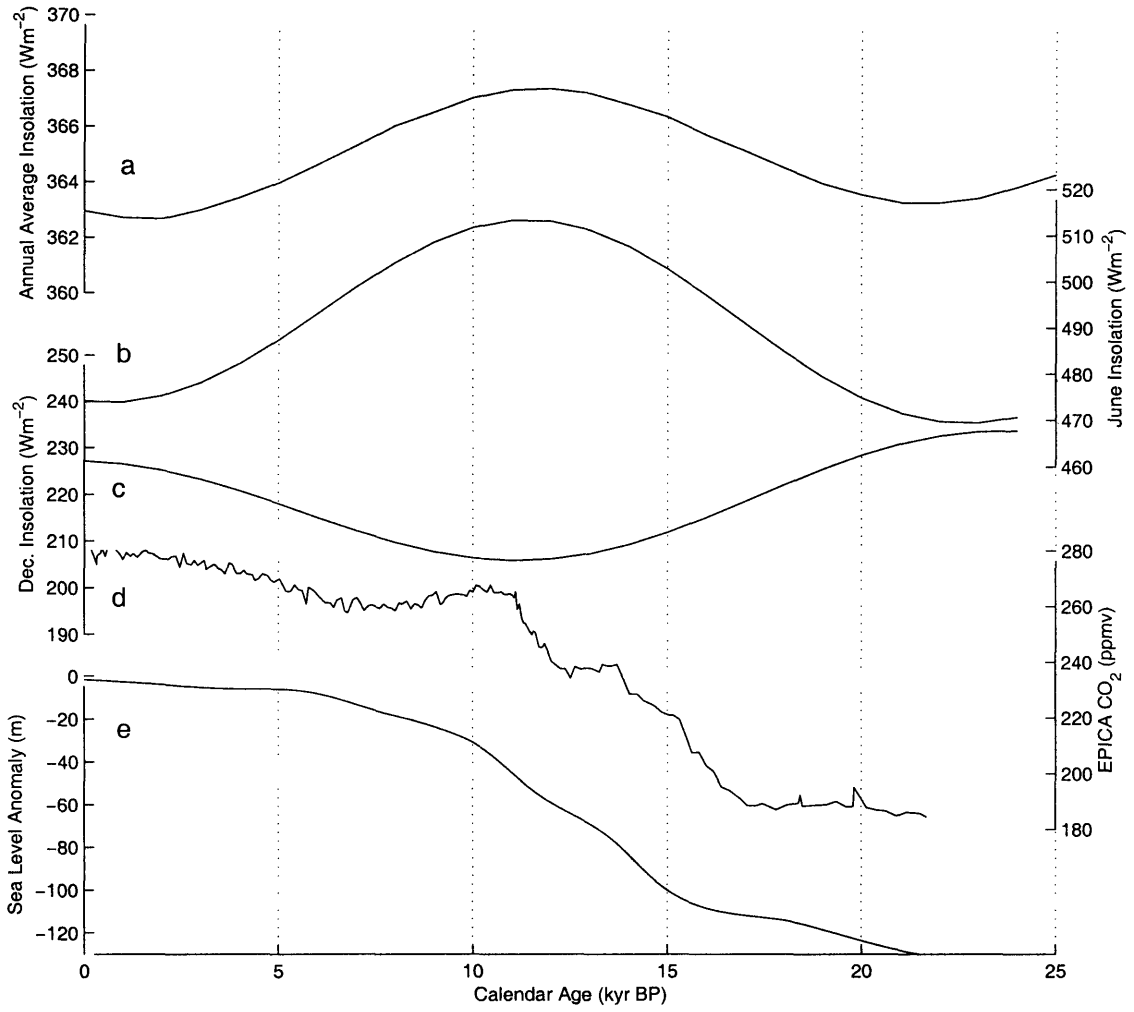

Figure 5-6: Insolation at 30°N for (a) annual average; (b) June; (c) December (*Berger*, 1978; *Berger and Loutre*, 1991). (d) Atmospheric CO_2 in the EPICA Dome C ice core (*Monnin et al.*, 2001). (e) Sea level as determined from Barbados corals (*Fairbanks*, 1989).

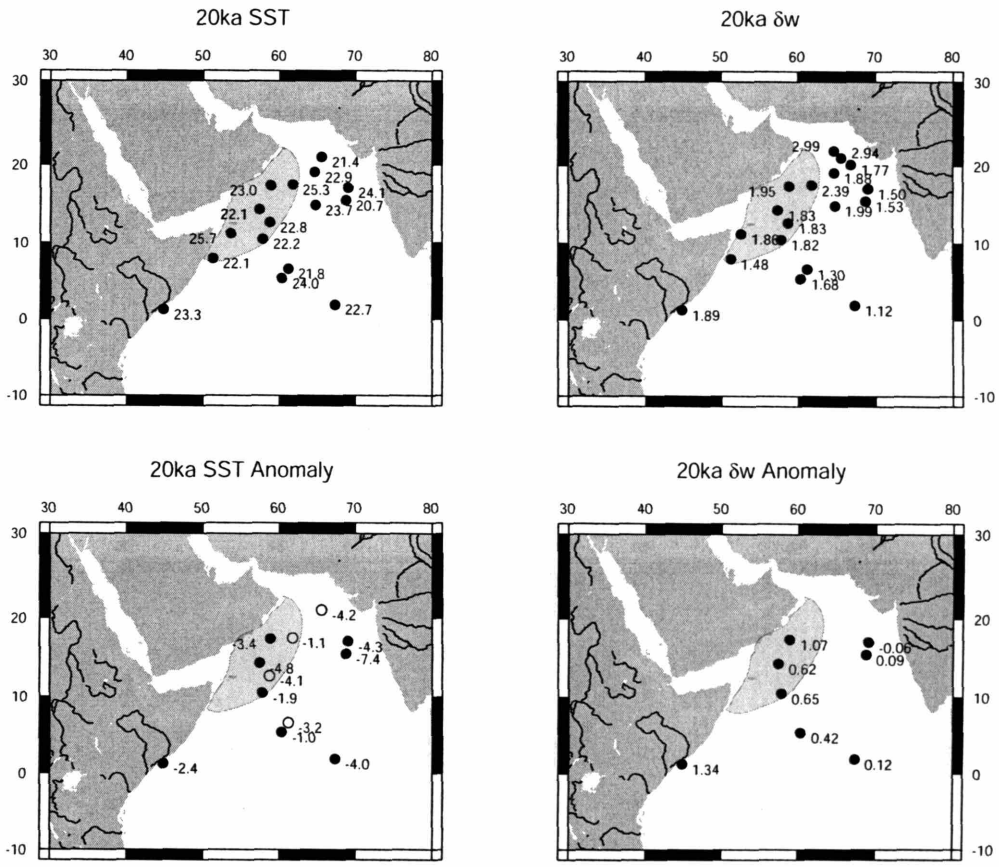

Figure 5-7: Surface conditions at 20 ka. (top) Mg/Ca sea surface temperature and $\delta^{18}O_w$ (bottom) SST and $\delta^{18}O_w$ anomalies relative to the 0ka time slice. Solid circles represent cores for which a modern and a time slice sample were available. Open circles represent cores for which anomalies were calculated using the time slice sample and the nearest modern core–top sample. Shading is as for Figure 5-2.

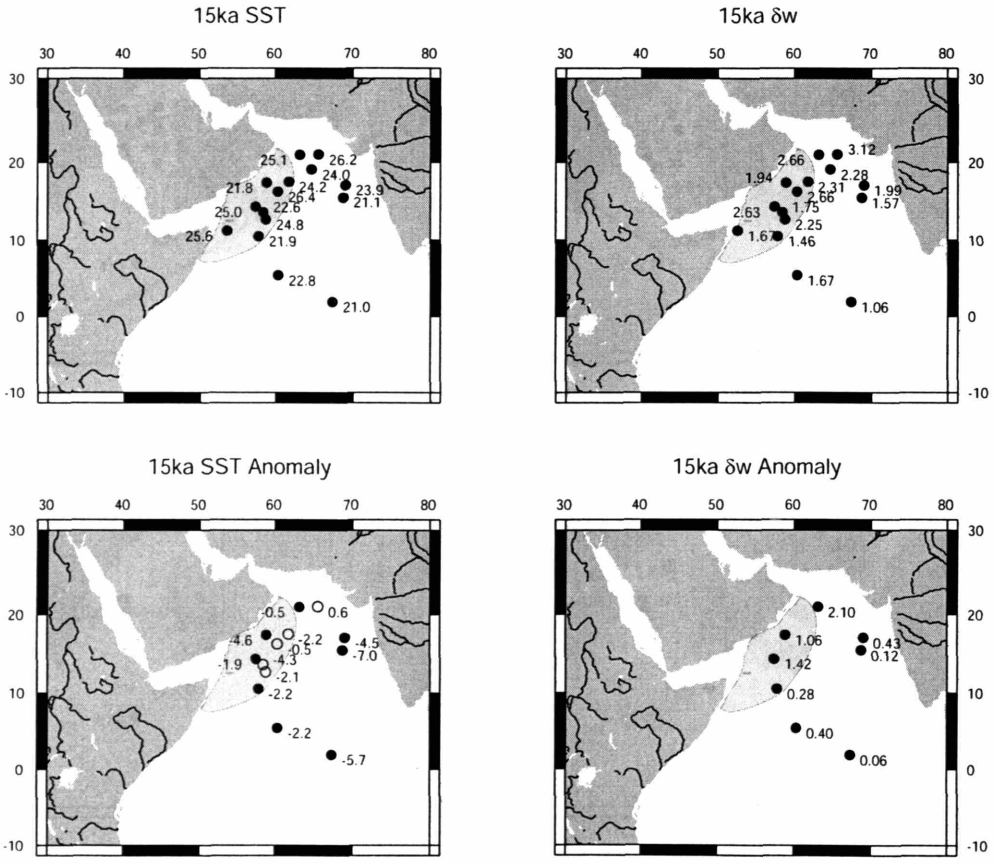

Figure 5-8: Surface conditions at 15 ka. (top) Mg/Ca SST and $\delta^{18}O_w$ (bottom) SST and $\delta^{18}O_w$ anomalies relative to the 0ka time slice. Symbols are as for Figure 5-7, shading is as for Figure 5-2.

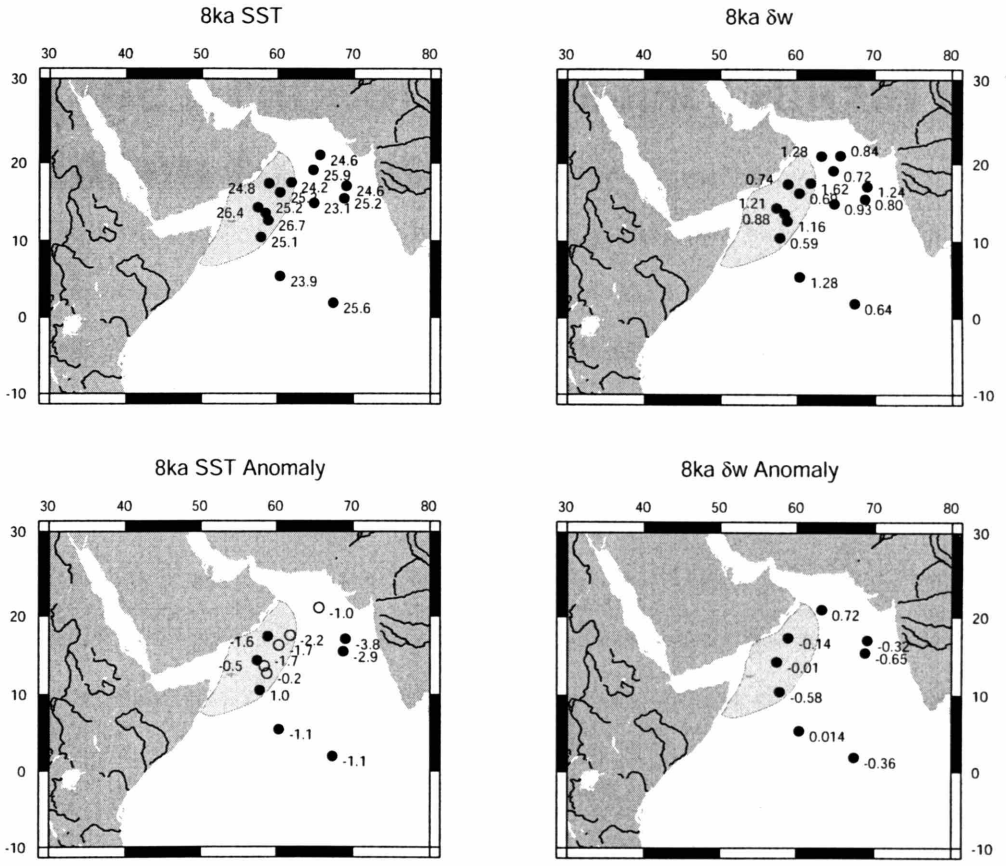

Figure 5-9: Surface conditions at 8 ka. (top) Mg/Ca SST and $\delta^{18}O_w$ (bottom) SST and $\delta^{18}O_w$ anomalies relative to the 0ka time slice.Symbols are as for Figure 5-7, shading is as for Figure 5-2.

Chapter 6

Sea surface temperature reconstructions from the Arabian Sea: Last Glacial Maximum to present

6.1 Abstract

Sea surface temperature (SST) and the oxygen isotopic composition of seawater ($\delta^{18}O_w$) were reconstructed at ODP Site 723B on the Oman Margin for the time period from the Last Glacial Maximum (LGM, ~20,000 years ago) to the present and at Site 39KG/56KA on the Pakistan Margin from 5,000 years ago (5 ka) to the present. This was accomplished using paired Mg/Ca and $\delta^{18}O$ analyses on two species of planktonic foraminifera, *Globigernoides ruber* and *Globigerina bulloides*. At Site 723B we find low SSTs during the Early Holocene, implying stronger than present summer monsoon upwelling, and a gradual increase in SSTs after 6 ka, implying a weakening of summer monsoon upwelling during this time. Comparison of our Mg/Ca SST results with other published SST records from this site reveals a consistent LGM to Holocene warming of $2-3°C$; however, the Holocene temperature trends suggested by the different records vary greatly. These differences are likely a function of differences in the seasonality of proxy production. In contrast to the Oman Margin records, our Mg/Ca record from the Pakistan Margin agrees well with a previously published alkenone record from the same site (*Doose-Rolinski et al.*, 2001), with both proxies suggesting a long term increase in SST (and therefore a decrease in winter monsoon strength) from 5 ka to the present. As SST at these sites can be an indicator of the strength of the Indian Monsoon, it is critical that we consider and understand the inherent seasonality of our SST proxies.

6.2 Introduction

With climatological effects spanning both the tropics and the extratropics, the Indian Monsoon is among the most important climate processes on Earth. This dramatic phenomenon dominates the climate of the Arabian Sea region. During boreal summer, sensible heating of the Asian continent causes a warming of the land that is stronger than the warming of the Arabian Sea due to differences in heat capacity. This differential heating sets up a pressure gradient (with higher pressures over the ocean) that drives onshore winds from the southwest. These winds bear marine moisture that falls as heavy precipitation, thus releasing latent heat to the troposphere and intensifying the circulation (*Hastenrath*

and Greischar, 1993). During this season, the strong southwesterly winds induce coastal upwelling along the Oman Margin. The pressure gradient is reversed during boreal winter and drives dry winds from the north–northeast over the Arabian Sea. The cold air advected with these winds cools the northernmost Arabian Sea.

The importance of understanding the history of the Indian Monsoon has been recognized for several decades. Through both climate modeling and paleoceanographic reconstructions along the Oman Margin of the abundance of *G. bulloides*, a planktonic foraminifer whose abundance has been correlated to low SSTs caused by summer monsoon–induced upwelling (*Prell*, 1984), the pioneering work of Warren Prell and John Kutzbach helped to shape a canonical view of the response of the monsoon to changes in insolation and global climate (*Prell and Curry*, 1981; *Prell*, 1984; *Prell and Kutzbach*, 1987). This view, which is consistent with our theoretical understanding of monsoon dynamics (*Webster et al.*, 1998), suggests that the summer Indian Monsoon was weaker than present during the Last Glacial Maximum (LGM, ~20 ka) and stronger than present during the Early Holocene (11–8 ka).

Because of its close association with summer monsoon upwelling, SST in the western Arabian Sea continues to be used as the most common marine proxy for summer monsoon strength. Subsequent studies of the abundance of *G. bulloides* in cores from upwelling areas in the Arabian Sea (*Naidu and Malmgren*, 1995; *Overpeck et al.*, 1996; *Gupta et al.*, 2003) have provided further support for the views put forth by *Prell and Kutzbach* (1987, and references therein).

In recent years, a number of time series records have been published that utilize quantitative proxies for SST, such as alkenones and artificial neural networks (*Emeis et al.*, 1995; *Doose-Rolinski et al.*, 2001; *Higginson et al.*, 2004; *Naidu and Malmgren*, 2005). These quantitative SST records often disagree with the SSTs implied by the percent *G. bulloides* records. Thus, while more quantitative, these records are difficult to reconcile with the canonical view of monsoon history since the LGM.

In this study, we first present time series of SST and the oxygen isotopic composition of seawater ($\delta^{18}O_w$) for two planktonic foraminifera, *G. ruber* and *G. bulloides*, at ODP Site 723B on the Oman Margin. In addition to providing a new record of SST from an upwelling

site on the Oman Margin, the $\delta^{18}O_w$ records provide insight into the upwelling history of the region by providing constraints on the properties of the upwelled water through time. We then compare our records to previously published SST records from the same site as a means of understanding the history of both the summer and winter Indian Monsoons. Insight regarding different proxies and the information they provide about monsoon history can be gained by looking at multiproxy records from other sites as well. We therefore also present new Mg/Ca SST and $\delta^{18}O_w$ records from Site 39KG/56KA on the Pakistan Margin, for which there is a published alkenone SST record (*Doose-Rolinski et al.*, 2001). Comparison of these records from different regions of the Arabian Sea aids in distinguishing signals of regional temperature change from those of monsoon–induced temperature change.

6.3 Study Sites

6.3.1 Oman Margin: Site 723B

ODP Site 723B is located along the Oman Margin in the western Arabian Sea (18°3'N, 57°4'E, 805 m water depth, Figure 6-1) and was recovered during Leg 117 of the Ocean Drilling Program. 1 cm thick samples were taken every 5 cm from 0–520 cm, corresponding to one sample every ~150–200 years [1].

Site 723B lies within the Oman upwelling region and is therefore strongly affected by changes in upwelling associated with the Indian Monsoon. SST at this site ranges from 23–29°C (Figure 6-2a). The coldest temperatures occur during the summer monsoon season, when cold water is upwelled as a result of strong southwesterly winds. A secondary SST minimum occurs during the winter monsoon season as a result of the advection of cold air by northeasterly winds and subsequent deepening of the mixed layer. Salinities at this site are high due to the presence of highly saline waters from the Red Sea and Persian Gulf. During the summer monsoon, however, salinity decreases, reflecting the relative freshness

[1]Note that high resolution samples from nearby box core RC2730 will be analyzed in order to fill in the time period from 2 ka to the present. If these results are obtained prior to 5/20/05, this chapter will be revised accordingly and committee members will receive a revised version.

of the upwelled waters (Figure 6-2b). As determined by both sediment trap and satellite observations, productivity in the western Arabian Sea has maxima during both monsoon seasons, with the summer monsoon productivity maximum being much larger than the winter monsoon maximum (*Honjo et al.*, 1999; *Banse and English*, 2000, and references therein). *G. bulloides* is only present at this site during the summer upwelling season (*e.g. Curry et al.*, 1992). While *G. ruber* is present year round, its abundance increases during both the summer and winter monsoon seasons (*e.g. Curry et al.*, 1992).

6.3.2 Pakistan Margin: Site 39KG/56KA

We also present data from cores SO90–39KG and SO90–56KA (hereafter 56KA), a box core–kasten core pair from the Pakistan Margin (24°50'N, 65°55'E, 695 m water depth, Figure 6-1). This site is located in the heart of an oxygen minimum zone (OMZ) and contains laminated sediments throughout the Holocene. A very high–resolution alkenone record from these cores was published by *Doose-Rolinski et al.* (2001). For this study, we generated data on samples at 10 cm intervals, corresponding to one sample every ~100 years. The two cores are spliced together at 30 cm. Data above this depth is derived from box core 39KG.

Sea surface temperatures at site 56KA also vary seasonally with the Indian Monsoon. Here, however, SST is coldest (23-24°C) during the winter monsoon season as a result of northeasterly wind–induced mixed layer deepening (Figure 6-2c). This region does not experience summer monsoon–induced upwelling; hence, summer SSTs are relatively warm (27–28°C). The annual cycle of salinity at this site is characterized by a minimum during the summer monsoon season, when continental precipitation to the northeast of the core site is at a maximum (Figure 6-2d; *Levitus and Boyer*, 1994). A secondary salinity minimum occurs during the winter monsoon season, when precipitation on the Makran margin, located north and northwest of the core site, is highest. The salinity variations here are small relative to those at Site 723B. Like the Oman Margin, the Pakistan Margin experiences a peak in productivity during the summer monsoon (*Codispoti*, 1991; *Banse*, 1994; *Andruleit et al.*, 2000). Rather than being linked to upwelling, this productivity peak is due to the advection of nutrient–rich waters from the western Arabian Sea (*Schulz et al.*, 1996).

A secondary productivity maximum occurs during the winter monsoon season.

6.4 Methods

For site 723B, eleven AMS ^{14}C dates, chosen at approximately 50 cm depth intervals, were obtained on planktonic foraminifera (Table 1). When possible, a single species was used for dating. For several dates, however, multiple planktonic species were pooled to obtain enough material for dating. Dates were obtained at the National Ocean Sciences Accelerator Mass Spectrometry Facility in Woods Hole, Massachusetts. ^{14}C ages were converted to calendar age using Calib 5.0 (*Stuiver and Reimer*, 1993) and a reservoir age of 600 yr (ΔR=200; *Dutta et al.*, 2001; *Southon et al.*, 2002).

The age model for Site 723B reveals that there are no recorded age reversals in the portion of this core on which we focus (Figure 6-3). The highest average sedimentation rates in the core ($\sim$45cm/kyr) occur between 14 and 9 ka. Sedimentation rates are lower during the Holocene ($\sim$30cm/kyr), and still lower during the last glacial period ($\sim$20cm/kyr).

The age model for cores 39KG and 56KA was published by *von Rad et al.* (1999). This age model is based on varve counts that have been calibrated by ^{14}C measurements on planktonic foraminifera. As determined by this chronology, sedimentation rates at this site can be in excess of 100 cm/kyr.

For Mg/Ca and δ^{18}O analyses, specimens of *G. ruber* (white) and *G. bulloides* were picked from the 212–300μm and 250–350μm size fractions, respectively. Each sample, composed of an average of 50 individuals, was then sonicated briefly to remove clays, weighed, and crushed gently between two glass slides in order to open individual chambers for effective cleaning. A split of the total sample, representing approximately 10 individuals, was then removed for isotopic analysis, and the remainder was used for Mg/Ca analysis.

Samples for Mg/Ca were subjected to a series of cleaning treatments designed to remove clays, metal oxides, and organic matter from the shells. Our cleaning procedure followed that of *Boyle and Keigwin* (1985) and subsequent revisions (*Rosenthal et al.*, 1995; *Boyle and Rosenthal*, 1996).

Mg/Ca ratios were measured with a high–resolution sector–field inductively coupled plasma mass spectrometer (ICP–MS; Finnegan Element2). Mg, Ca, Mn, and Al intensities were determined in low resolution mode (with the exception of Al, determined in medium resolution mode) by averaging measurements from 74 scans. All ions were counted in analog mode. Because foraminifera from parts of the Arabian Sea contain stubbornly adhering clays that could potentially elevate the measured Mg/Ca (K. L. Bice et al., The application of SIMS for measuring Mg/Ca in rare, delicate, or altered planktonic foraminifera: Examples from the Holocene, Paleogene, and Cretaceous, submitted manuscript), we also monitored Al/Ca ratios. Samples with Al/Ca values greater than 30μmol/mol, twice that observed in foraminifera considered to have no detrital clay contamination, were excluded from the final data set (14 out of 210 total samples; *Lea et al.*, 2003; *Schmidt et al.*, 2004). Mn/Ca was monitored to detect the presence of metal oxides, particularly relevant for 56KA, where redox conditions may have varied over the studied time period (*Schulz et al.*, 1998). However, no significantly elevated Mn/Ca values were obtained. A standard, containing high–purity elements in ratios consistent with those observed in foraminifera, and a blank of 2% HNO_3 were run between every four samples. The instrumental error for Mg/Ca, calculated from repeated measurements of a series of consistency standards, is 0.03 μmol/mol.

In order to convert measured *G. ruber* Mg/Ca ratios to SST, we used the calibration of *Rosenthal and Lohmann* (2002). This calibration incorporates shell weight in order to correct for dissolution, which preferentially removes Mg from the foraminiferal tests. There is no available shell weight corrected calibration for *G. bulloides*; we therefore used the calibration of *Elderfield and Ganssen* (2000) in order to convert *G. bulloides* Mg/Ca ratios to SST.

Stable isotopes were measured using a Finnigan MAT 253 coupled to a Kiel III carbonate device. The analytical precision of this instrument for δ^{18}O, as determined by replicate analyses (n=600) of the carbonate standard NBS19 is 0.07‰. $\delta^{18}O_w$ was calculated using the calibration of *Mulitza et al.* (2003): $\delta^{18}O_{w,VSMOW}$ = ($T_{Mg/Ca}$ - 14.2)/4.44 + $\delta^{18}O_{carbonate,VPDB}$ + 0.27. All $\delta^{18}O_w$ values are reported relative to VSMOW. The global ice volume effect on $\delta^{18}O_w$ was subtracted from the $\delta^{18}O_w$ thus resulting in $\delta^{18}O_{residual}$,

which reflects the local hydrological balance at each site. This subtraction was done by interpolating the *Fairbanks* (1989) sea level curve into 100–year intervals and using a conversion to $\delta^{18}O$ of 0.0076‰/meter (*Fairbanks*, 1989; *Schrag et al.*, 2002)[2].

6.5 Oman Margin Results

6.5.1 δ^{18}O

The oxygen isotopic composition of planktonic foraminifera ($\delta^{18}O$) is a function of both temperature (SST) and the oxygen isotopic composition of seawater ($\delta^{18}O_w$). An increase in δ^{18}O implies a decrease in SST and/or an increase in $\delta^{18}O_w$. Downcore $\delta^{18}O$ values *G. ruber* and *G. bulloides* within 723B range from -2‰ to 0.5‰ (Figure 6-4c,d). The highest values for both foraminifera are found from 450 to 500 cm, corresponding to late glacial ages. δ^{18}O values exhibit a decrease of $1 - 1.5$‰ associated with the deglaciation from 450–340 cm. During this deglacial interval, several reversals from the overall decreasing trend can be observed. Most notably, after decreasing between 450 and 425 cm, δ^{18}O values for both species briefly increase again by $\sim$ 0.5‰. After this brief return to heavy values, $\delta^{18}O$ values decrease rapidly by 1‰, where they plateau for ~50 cm. Values then decrease once again, marking the end of the deglaciation at ~11 ka. $\delta^{18}O$ values continue to decrease, albeit more gradually after the more dramatic deglacial decreases. Both *G. ruber* and *G. bulloides* exhibit $\delta^{18}O$ decreases of nearly 0.5‰ from 325–200 cm. $\delta^{18}O$ values for both foraminifera increase again by 0.5‰ in the upper 100–150 cm studied in this core. Typical Holocene values for *G. ruber* range from -1.5 to -2.0‰. Values for *G. bulloides* are slightly higher at -1 to -1.5‰.

6.5.2 Mg/Ca

Mg/Ca values for *G. ruber* and *G. bulloides* vary from 2.5–5.5 and 4-6 mmol/mol, respectively (Figure 6-4a,b). Average shell weights (not shown) for individual specimens

[2]Note that replicate analyses of approximately half of the *G. ruber* Mg/Ca samples from 723B will be performed prior to the submission of this manuscript for publication. In addition, replicate $\delta^{18}O$ analyses will be performed. If these analyses can be completed prior to 5/20/05, the results and text will be revised accordingly, and committee members will receive a revised version of this chapter.

vary from 8–11 μg for *G. ruber* and 5–8 μg for *G. bulloides*. There appears to be no correlation between shell weight and Mg/Ca as was observed by *Rosenthal and Lohmann* (2002).

The Mg/Ca trends of *G. ruber* and *G. bulloides* generally parallel one another. Both *G. ruber* and *G. bulloides* exhibit increases in Mg/Ca from 450 to 320 cm corresponding to the transition from glacial to interglacial conditions. Following this increase, Mg/Ca values decrease gradually to minima centered at ~125 cm (for *G. ruber*) and ~190 cm (for *G. bulloides*). *G. ruber* Mg/Ca values then increase once again while *G. bulloides* Mg/Ca values are highly variable in the top 200 cm of the core.

The Mg/Ca records exhibit both similarities and differences when compared to their respective δ^{18}O records. For example, the deglacial decrease in δ^{18}O is accompanied by increases in the Mg/Ca of both foraminifera, suggesting that SST at this site warmed during the deglaciation. The Holocene Mg/Ca and δ^{18}O trends, however, are rather different, with both Mg/Ca and δ^{18}O values decreasing gradually between 300 and 175 cm. This difference suggests a substantial $\delta^{18}O_w$ influence on the δ^{18}O record. By converting the Mg/Ca to SST and using these data to calculate $\delta^{18}O_{residual}$, we can begin to separate the SST and $\delta^{18}O_{residual}$ changes experienced at this site since the LGM.

6.5.3 SST

The SST records for *G. ruber* and *G. bulloides* (Figure 6-5b,c) strongly resemble their raw Mg/Ca counterparts. While the absolute value of the SST calculated from the Mg/Ca record depends heavily upon the Mg/Ca–SST calibration used, the nature and magnitude of the trends exhibited in the SST records do not change when alternative calibrations are applied.

Late glacial (19 to 17 ka) SSTs as recorded by *G. ruber* were $3-4$°C cooler than at 2 ka. *G. bulloides* SSTs also suggest cooler conditions than present during the late glacial. Additional data points and replicates are required to confirm these cold anomalies. The lowest temperatures recorded by both species during the studied time period occur around 16 ka ($\sim$ 22°C for *G. ruber*, $18.5°C$ for *G. bulloides*). Both species record a deglacial warming of $4 - 4.5°C$; however, the warming trends recorded by the two species differ in terms of

their timing. *G. ruber* SSTs stay low through the onset of Bølling/Allerød (~14.5 ka; BA) and begin to warm prior to the onset of the Younger Dryas (~13 ka; YD). This warming is interrupted by a brief pause (or, perhaps a 1.5°C cold reversal) that occurs at the onset of the YD, but ends prior to the end of the YD as recorded at GISP2 (Figure 6-5a). A second warming occurs simultaneously with the Preboreal warming in GISP2. The deglacial warming recorded by *G. bulloides* occurs more gradually and continuously between 16 and 11 ka.

Both *G. ruber* and *G. bulloides* record maxima in SST in the early Holocene between 11 ka and 10 ka. After this maximum, both species exhibit a sustained cooling event lasting 3 kyr (2 kyr) for *G. ruber* (*G. bulloides*). *G. ruber* SSTs then undergo further cooling until 6 ka. Minimum Holocene *G. ruber* temperatures of 24° occur at 6 ka and are followed by a substantial warming of $3 - 4°C$ between 6 ka and 2 ka. The early to mid–Holocene cooling and subsequent warming trends are also evident in the *G. bulloides* record, albeit in a muted form. After ~3 ka, the SST records for the two species diverge, however, with *G. ruber* recording a warming and *G. bulloides* recording a cooling.

6.5.4 $\delta^{18}O_{residual}$

Despite similarities in their recorded SSTs, the $\delta^{18}O_{residual}$ records for *G. ruber* and *G. bulloides* (Figure 6-5d,e) are significantly different from one another. *G. ruber* $\delta^{18}O_{residual}$ values vary between 0.5 and 2‰. Values of ~ 1.5‰ at 2 ka are up to 1‰ higher than observed $\delta^{18}O_{residual}$ values in the Arabian Sea (*Schmidt et al.*, 1999, and references therein). The discrepancy between observations and modern sedimentary $\delta^{18}O_w$ values calculated by this method was noted by Dahl and Oppo, 2005 (Sea surface temperature pattern reconstructions in the Arabian Sea, submitted manuscript, hereafter *Dahl and Oppo, submitted manuscript*) and is likely the result of uncertainties in Mg/Ca–SST calibration and the depth habitat of *G. ruber*. These uncertainties are unlikely to vary through time. Thus, while the absolute value of the $\delta^{18}O_{residual}$ values reported in this study may be shifted up or down, the nature and magnitude of the trends are robust. The heaviest *G. ruber* $\delta^{18}O_{residual}$ values ($1.5 - 2$‰) are found during the LGM and H1; however, the $\delta^{18}O_{residual}$ decreases between 19 and 15 ka preceding signs of deglaciation in Greenland (Figure 6-5a). During

the BA, $\delta^{18}O_{residual}$ returns to higher values in an event that lasts from 15 ka to 13.5 ka. This heavy event ends abruptly prior to the start of the YD. Late BA and YD $\delta^{18}O_{residual}$ values are variable, but centered about a mean of $\sim$ 1.25‰. After the YD, $\delta^{18}O_{residual}$ values steadily increase until the mid–Holocene, when values as light as 0.5‰ are reached. The $\delta^{18}O_{residual}$ then decreases between 6 ka and 2 ka. The Holocene trend mirrors that of the *G. ruber* SST trend, reflecting the influence of the long–term SST trends without correlative trends in calcite $\delta^{18}O$.

While the *G. bulloides* $\delta^{18}O_{residual}$ record does show variability, the long–term trends evident in the *G. ruber* record are conspicuously absent. Instead, $\delta^{18}O_{residual}$ values vary about a mean value of 0.54‰, close to modern observations of $\delta^{18}O_w$ throughout the Arabian Sea (*Schmidt et al.*, 1999). There is little change between glacial and interglacial values. While there is no discernible deglacial signal during the BA or the YD, $\delta^{18}O_{residual}$ values do decrease prior to the onset of the BA from glacial values of 0.75‰ to almost 0‰. This trend is similar in timing, but smaller in magnitude to the pre–BA trend in the *G. ruber* record.

6.6 Pakistan Margin Results

6.6.1 δ^{18}O

G. ruber $\delta^{18}O$ values at Site 56KA vary between -1‰ and -2.5‰ (Figure 6-6b). From 5 ka to present, the $\delta^{18}O$ composition is relatively stable, with the exception of a $\sim$500 year excursion to heavy values from 2200 to 1750 years B.P., and a shorter, possibly less severe event at 3 ka.

6.6.2 Mg/Ca and SST

Mg/Ca values at 56KA vary from 3.7 to 4.9 mmol/mol (Figure 6-6a) and show no correlation with shell weight, which varies between 7 and 10 μg per individual (not shown). Overall, there is a trend of increasing Mg/Ca ratios from 5 ka to the present. The heavy $\delta^{18}O$ excursion noted between 2.2 and 1.75 years B.P. corresponds to a period of slightly lower Mg/Ca values, which would imply a lowering of SST during this time.

These Mg/Ca values correspond to SSTs of 26 – 29°C calculated using the calibration of *Rosenthal and Lohmann* (2002) (Figure 6-6c). As with Site 723B, the particular Mg/Ca–SST calibration chosen changes the absolute SST estimates, but does not change the nature and magnitude of the trends described here. Throughout the record, SSTs are highly variable; however, a long–term warming trend spans the period from 4 ka to the present. Superimposed upon this warming are several events of note. The coldest SSTs recorded occur between 4 and 3.75 ka as the culmination of a cooling trend beginning at 4.7 ka. SSTs during this event reach a minimum values of $\sim$ 26°C before rebounding to nearly 28°C by 3.6 ka. A second major cooling event occurs between $\sim$2.5 ka. SSTs are also depressed during the major $\delta^{18}O$ excursion at 2.2–1.75 ka.

6.6.3 $\delta^{18}O_{residual}$

The $\delta^{18}O_{residual}$ record at this site generally follows the *G. ruber* $\delta^{18}O$, indicating that $\delta^{18}O_w$ is the primary control on $\delta^{18}O$ here (Figure 6-6d). In contrast to the Mg/Ca and SST records from this site, there does not appear to be a long term trend in the $\delta^{18}O_{residual}$. Heavy excursions are noted at 3 ka and 2.2–1.75 ka, coincident with the large positive $\delta^{18}O$ excursions.

6.7 Discussion

6.7.1 Oman Margin

Sea surface temperature variability at Site 723B today is dominated by the summer monsoon upwelling season, with a secondary cooling of SST during the winter monsoon season. Factors such as direct solar insolation forcing and the concentration of CO_2 in the atmosphere also play a role in determining SST. Thus changes in SST at Site 723B through time reflect varying degrees of influence of a number of parameters that affect SST.

Our understanding of the history of the monsoon, based on both model simulations and numerous paleoclimate records, is that summer monsoon strength was lower during the LGM (and stadial events such as the Younger Dryas, $\sim$13–12 ka) and higher during the Early Holocene (and interstadial events such as the Bølling/Allerød, $\sim$14.5–13 ka) than it is

today (*e.g. Prell and Kutzbach*, 1987; *Overpeck et al.*, 1996; *Schulz et al.*, 1998; *Fleitmann et al.*, 2003; *Liu et al.*, 2003). The winter monsoon is thought to have been stronger than present at the LGM (due to greater cooling on land than over the ocean) as well as during the Early Holocene, when Northern Hemisphere seasonality was larger than today (Figure 6-7; *Liu et al.*, 2003). Summer monsoon strength is thought to have decreased from the Early Holocene to the present (*e.g. Gupta et al.*, 2003). Variations in monsoon strength can be attributed several factors, including solar insolation and downstream effects from the North Atlantic (*e.g. Liu et al.*, 2003; *Schulz et al.*, 1998).

Given our understanding of the monsoon, one would expect that, at Site 723, summer monsoon upwelling would have been reduced during the LGM and enhanced during the Early Holocene with respect to today. Such changes in upwelling would presumably increase SST during the LGM and decrease SST during the Early Holocene. Convective cooling associated with the winter monsoon would have been greater during both the LGM and the Early Holocene and could have cooled temperatures at Site 723 relative to today. The combined effects of the two monsoon seasons implies a net cooling during the Early Holocene and a range of possible SST responses for the LGM depending on the relative strengths of the winter monsoon increase and the summer monsoon decrease.

In order to better understand the relationship between monsoon strength and the SST and $\delta^{18}O_{residual}$ recorded by *G. ruber* and *G. bulloides*, it is important to understand the specific season and conditions that the two species are capturing. The difference between the $\delta^{18}O_{residual}$ as recorded by *G. ruber* and *G. bulloides* provides a clue as to the specific monsoon–related process that each species is recording. That the *G. bulloides* $\delta^{18}O_{residual}$ is relatively invariant suggests that this species is solely recording the properties of the upwelled water. Given this interpretation, it is clear that the mean $\delta^{18}O_{residual}$ of the upwelled waters did not change since the LGM, although millennial–scale changes may have occurred. In contrast, the temporally variant $\delta^{18}O_{residual}$ recorded by *G. ruber* likely reflects an annually averaged signal that is affected to greater or lesser degrees by the fresh upwelled waters. The SST records provided by each species also likely reflect this seasonal difference, with *G. bulloides* recording the temperature of the upwelled water during the summer, as it does today. In contrast, *G. ruber* records an annual signal that is likely biased

toward the cold ambient temperatures the occur during its peaks in production during the summer and winter monsoon seasons. Because the SST and $\delta^{18}O_{residual}$ recorded by *G. bulloides* are more likely to be a reflection of the properties of the upwelled water than to reflect the strength of monsoon upwelling, we focus primarily on the SST and $\delta^{18}O_{residual}$ records provided by *G. ruber*.

The expected correlation between North Atlantic climate and SST on the Oman Margin is such that warm temperatures in the North Atlantic should be correlated with cold SST (due to a strong summer monsoon associated with increased upwelling). From 20 ka to 10 ka, however, Site 723B SSTs are not inversely correlated with GISP2, as one would expect if upwelling was the sole control on SST. In addition, our Holocene record demonstrates two SST minima: one in the Early Holocene and one in the mid–Holocene. Thus, despite the great influence of summer upwelling on the determination of SST at 723B today, it is clear that other factors are involved in setting SST on long timescales.

The LGM–Holocene SST change of $\sim$ 2°C at Site 723B reflects both the direct and indirect influences of glacial boundary conditions. As shown by *Broccoli* (2000), the prescription of glacial boundary conditions, particularly large continental ice sheets and lowered CO_2, in an atmospheric–only model can cause a lowering of SST in the Arabian Sea region by 2°C. The mechanism for this cooling is solely atmospheric and does not involve processes such as upwelling. Furthermore, as shown by *Sonzogni et al.* (1998) and *Dahl and Oppo, 2005, submitted manuscript*, sites throughout the Arabian Sea, including sites both affected and unaffected by upwelling today, were $2 - 3$°C cooler than present at the LGM. Given that this cooling signal is regionally coherent and can be attributed largely to processes unrelated to upwelling, it is likely that the direct radiative cooling caused by the glacial boundary conditions played a more important role in determining Arabian Sea SST than did the Indian Monsoon during this time. It is possible, however, that some of the cooling could be attributed to an increase in winter monsoon strength.

During the deglaciation (14.5 ka–11 ka), SST at Site 723B generally warms, reflecting the transition from glacial to interglacial boundary conditions. While changes in global boundary conditions are driving the overall warming trend over this time period, the absence of strong SST signals associated with the BA and YD events suggests that local pro-

cesses are also affecting SST. During the BA, SST at Site 723B remains cold rather than following the warming that occurred in the North Atlantic. These cool SSTs likely reflect an increase in summer monsoon strength and a consequent cooling of SST that opposed the Northern Hemisphere warming trend. The warming trend exhibited during the YD at Site 723B suggests that the summer monsoon decreased in strength (thereby decreasing summer upwelling) during this time as a response to the cooling in the Northern Hemisphere. Thus, in contrast to the glacial period, when glacial boundary conditions were the dominant factor forcing SST in the western Arabian Sea, deglacial SSTs were determined by the easing of glacial boundary conditions as well as by local processes, namely upwelling.

Solar insolation and seasonality at 30°N reached maxima at 11 ka (Figure 6-7). While these insolation conditions were optimal for the development of strong summer and winter monsoons, maximum summer monsoon strength did not develop until 10–8 ka. This time lag between insolation and monsoon strength is consistent with lags observed in several studies of long time–series from the Arabian Sea (*Clemens and Prell*, 1990; *Shimmield et al.*, 1990; *Clemens et al.*, 1991; *Murray and Prell*, 1992; *Altabet et al.*; *Reichart et al.*, 1998). This lag has been attributed to a number of different factors, including the timing of maximum cross–equatorial heat transport (*Clemens and Prell*, 2003, and references therein), changes in the intensity of insolation late in the upwelling season (*Reichart et al.*, 1998), and changes in the position and structure of the Findlater Jet (*Anderson and Prell*, 1993). For the case of the Early Holocene, the lag could also be attributed to a suppression of maximum monsoon strength by lingering cold conditions in the North Atlantic. As implied by the GISP2 δ^{18}O record (Figure 6-5a), North Atlantic temperatures at 11 ka were reduced relative to Early Holocene temperatures. As North Atlantic temperatures warmed, the summer monsoon was able to strengthen, thus causing a lowering of SST at Site 723B (Figure 6-5b). The low SSTs, particularly evident in the *G. ruber* record, imply high summer monsoon strength from 10–8 ka. As would be expected from modern upwelling conditions, this period of strong summer monsoon upwelling is also recorded as a period of decreasing $\delta^{18}O_{residual}$ (Figure 6-5d). The summer monsoon suppression prior to 10 ka is also evident in a record of precipitation in Oman as recorded by the δ^{18}O of a speleothem (*Fleitmann et al.*, 2003). This record shows a strong increase in precipitation

beginning at 10.5 ka, after the insolation maximum and coincident with a lowering of SST at 723B (Figure 6-5f).

At 8 ka, following the Early Holocene summer monsoon maximum, an increase in *G. ruber* SST and a decrease in *G. ruber* $\delta^{18}O_{residual}$ suggest a brief decrease in upwelling strength. However, decreasing SST after 8 ka suggests that the decreased upwelling was not sustained but was rather replaced by a continued increase in upwelling until 6 ka. Subsequent warming of SST as recorded by *G. ruber* is indicative of a decrease in the strength of the summer monsoon from 6 ka to the present. Between 6 ka and today, these trends are somewhat consistent with decreasing precipitation in Oman (*Fleitmann et al.*, 2003) and decreasing fluxes of planktonic foraminifera on the Oman Margin (*Naidu and Malmgren*, 1995). Between 8 ka and 6 ka, however, the records differ in that the decreasing precipitation trend in Oman had already begun (indicating weakening of summer monsoon strength) while the flux of planktonic foraminifera was increasing (indicating strengthening of summer monsoon strength and consistent with our record). This difference in timing may be due to changes in the spatial pattern of the Indian Monsoon. After 8 ka, the summertime position of the ITCZ over the Arabian Peninsula (determined by the strength of summer monsoon winds) likely migrated offshore gradually; thus, the land–based record of *Fleitmann et al.* (2003) would have been affected by the decrease in summer monsoon strength prior to the marine sites just offshore. Evidence suggests that many sites throughout the Middle Eastern region experienced a drying during this time (*Arz et al.*, 2003, and references therein). The trend of decreasing summer monsoon strength from 6 ka to the present is therefore likely a part of this broader, regional–scale aridification (*Joussaume et al.*, 1999; *Liu et al.*, 2004, and references therein).

6.7.2 Other Site 723 records

Previous research on Site 723 has yielded several other SST reconstructions to which we can compare our own. We will be focusing on three previously published records from Site 723. These records utilize three different SST reconstruction methods. The first is a record of the percentage of the planktonic foraminifer *Globigerina bulloides*, published by *Gupta et al.* (2003). While the percentage of *G. bulloides* is not strictly a proxy for

SST, it has been historically used in this region as an indicator of the strength of summer monsoon upwelling, as the foraminifer is only present during the upwelling season today (*e.g. Curry et al.*, 1992). The second record is an alkenone SST reconstruction published by *Higginson et al.* (2004). Like Mg/Ca, alkenones provide a quantitative estimate of SST. The third and final record is that of *Naidu and Malmgren* (2005). In this study, *Naidu and Malmgren* (2005) used a relatively new technique, artificial neural networks (ANNs) to reconstruct summer, winter, and annually averaged SST. The ANN method relies upon the abundances of members of a suite of planktonic foraminifera in order to provide quantitative SST information. A description of this technique can be found in *Malmgren and Nordlund* (1997).

The records of *Gupta et al.* (2003) and *Naidu and Malmgren* (2005) are from Site 723A, a companion core to 723B. The *Higginson et al.* (2004) record is from 723B. We consider all of these records on the timescales on which they were originally published. Timescales for the 723A records are based on more than 10 AMS ^{14}C dates. The *Higginson et al.* (2004) timescale for 723B is based on a correlation between their $\delta^{15}N$ record from this site and the GISP2 δ^{18}O record with one tie point in the interval from 20 ka to present.

Description of Records

Sea surface temperatures, as determined by *G. ruber* and *G. bulloides* Mg/Ca (Figure 6-8b,c) and annual and winter ANN (Figure 6-8d,e), underwent a $1 - 2$°C cooling between 17 and 16 ka. Alkenone SSTs (Figure 6-8g) also show a cooling at this time, although it is smaller in magnitude (0.5°C). This cooling may be a manifestation of Heinrich Event 1 in the North Atlantic. All of the records then suggest a warming of SST coincident with the initial warming associated with the BA in GISP2 (Figure 6-8a). Our *G. ruber* Mg/Ca record and the annual and winter ANN records of *Naidu and Malmgren* (2005) show two warm phases during the early BA between 16 and 14 ka, after which temperatures return to cold, pre–BA values during the middle of the BA ($\sim$14 ka). With the exception of the *Higginson et al.* (2004) alkenone record, all of the records imply an abrupt deglacial warming at $\sim$14 ka. Following this coherent warming, the clearest evidence for a YD cooling event at Site 723 comes from the ANN winter SST reconstruction, which shows a

cooling of nearly 1°C that is sustained between 13 and 12 ka. A brief cooling, coincident with that of the ANN record, occurs in the *G. ruber* Mg/Ca record, but is not sustained for the duration of the YD. The other records may show coolings at the onset of the YD; however, the signal is small and potentially determined from a single data point. A second deglacial warming event begins at 12 ka in the *G. ruber* Mg/Ca and the annual and winter ANN records and at 13 ka in the *G. bulloides* Mg/Ca record. This warming, which does not have an analog in the ANN summer or alkenone records, continues until 10–11 ka.

The greatest differences between the records occur during the Holocene. Our Mg/Ca SST records for both *G. ruber* and *G. bulloides* have maxima at 11 ka and suggest an early to mid–Holocene cooling trend followed by a warming that lasts until at least 3 ka. The ANN records for winter, summer, and the annual average also show maxima in SST at 10–11 ka and may show some evidence for an Early Holocene cooling such as that seen in our records. The timing of the transitions into and out of this event are synchronous between our records and the ANN records. However, the cooling is not sustained in the ANN records as it is in the Mg/Ca records. Following the Early Holocene cooling and subsequent warming until 8 ka, all three ANN records suggest a gradual cooling of SST that continues from 8 ka to the present. Thus, the ANN records do not corroborate the mid to late–Holocene warming evident in our records. Nor do they provide evidence for the long term decrease in monsoon strength suggested by previous studies (*e.g. Fleitmann et al.*, 2003). In contrast to both the ANN records and our records, the alkenone SST record does not have a maximum in the early Holocene. Rather, this record demonstrates a long–term, gradual warming of $1 - 1.5$°C from 10 ka to the present. The *G. bulloides* percentage record corroborates the alkenone record in that the percentage of *G. bulloides* decreases throughout the Holocene, which suggests decreasing upwelling and, therefore, increasing SST.

Seasonality Issues

Because surface water conditions in the western Arabian Sea vary greatly throughout the annual cycle, it is likely that differences in the season of production of each of the proxies discussed above contribute to the discrepancies in Holocene temperature trends.

However, different temperature trends are exhibited by proxies that are presumed to be recording the same season. For example, *G. ruber* Mg/Ca and ANN annual reconstructions are both thought to reflect conditions on an annual basis, yet the two records show different Holocene temperature trends. Perhaps a more striking example is that of the summer SST proxies: *G. bulloides* Mg/Ca, *G. bulloides* percentage, alkenones, and the ANN summer reconstruction. Each of these proxies conveys a different message regarding summer monsoon strength throughout the Holocene, with the percentage of *G. bulloides* and alkenones suggesting a long–term warming in the Holocene, ANN summer SSTs suggesting a long–term cooling, and *G. bulloides* Mg/Ca suggesting a cooling until 6 ka followed by a warming. Interestingly, the SST range recorded by each of these summer proxies is dampened relative to the proxies for annual and winter SST. This may suggest that the summer proxies are all indeed recording a more limited season; however, it is clear that, even with that constraint, there is considerable variability between proxies.

Disagreements between SST proxies have been noted in several other paleoceanographic studies. For six cores within the Arabian Sea, *Sonzogni et al.* (1998) note that there is no simple relationship between the percentage of *G. bulloides* and alkenone SSTs. Nor is percentage of *G. bulloides* simply related to its flux (*Naidu and Malmgren*, 1995). Within an upwelling zone on the western African Margin, foraminiferal assemblage SST reconstructions suggest significant warming at the end of the African Humid Period at 6 ka while alkenone SST reconstructions yield relatively stable SSTs across this transition (*deMenocal et al.*, 2000; *Zhao et al.*, 2000). These issues also hamper multiproxy SST reconstructions outside of upwelling areas. For example, alkenone and foraminiferal faunal assemblage SST reconstructions from three North Atlantic cores were found to disagree systematically, with alkenones suggesting a long–term cooling from 6 ka to present that was not apparent in the faunal data (*Marchal et al.*, 2002, and references therein).

Thus, the discrepancies between Holocene SST trends implied by different proxies at Site 723 are not unique to this site, nor are they unique to upwelling areas. The number of sites for which highly resolved multiproxy SST data are available is small but growing. As more and more such records are developed, it may be possible to assess systematic differences in the signals recorded by each proxy. In addition to studying the relationship

between SST records for the past, it is critical that we attain a better understanding of the modern seasonality and quality of our SST proxies.

6.7.3 Pakistan Margin

On an annual basis, SST at 56KA is relatively uniform with the exception of a strong cooling associated with the cold advection during the winter monsoon season. The SST variability we observe at this site through time can be interpreted as a record of the strength of the winter Indian monsoon. In this context, the long–term warming we observe in Mg/Ca SST from 5 ka to the present likely reflects a decrease in the strength of the winter monsoon and its associated cooling effects.

Given this decrease in winter monsoon strength and the decrease in summer monsoon strength from 5 ka to present implied by the Site 723B Mg/Ca record, we might expect to see a long– term increase in the $\delta^{18}O_{residual}$ at 56KA, as both the summer and winter monsoons serve to lower salinity (and therefore $\delta^{18}O_{residual}$) at this site. As shown in Figure 6-6d, however, there is no discernible long term $\delta^{18}O_{residual}$ trend in this record. This likely reflects the fact that the lowering of salinity associated with the monsoons is on the order of 0.5 psu, a decrease of only 1–2%. Using a salinity:$\delta^{18}O_w$ relationship of 0.3‰/p.s.u., the $\delta^{18}O_w$ decrease during the winter monsoon would be only 0.17‰ (*Delaygue et al.*, 2001). In contrast, there is a nearly 20% decrease in temperature during the winter monsoon. Thus, SST is a much more sensitive recorder of monsoon strength than $\delta^{18}O_w$ on the Pakistan Margin, and it is not surprising that we do not see a long–term trend in the $\delta^{18}O_{residual}$ over this time period.

6.7.4 Other Site 56KA Records

The Mg/Ca SST trends we observe at 56KA correspond well to those observed in a high–resolution alkenone SST record from the same core (Figure 6-9; *Doose-Rolinski et al.*, 2001). While the resolution of the two records is disparate, the two main periods of extended cool temperatures (4.7–3.5 ka and 3–2.25 ka) are evident in both records. In addition, both records imply a long–term warming from 4 ka to the present. The absolute values of the SST estimates provided by the two proxies are offset from one another by

$1 - 1.5$°C, with Mg/Ca estimates consistently warmer than alkenone estimates. Reanalysis of the alkenone samples, however, suggests that the original *Doose-Rolinski et al.* (2001) data may be, on average, 1°C too cold, thus bringing the Mg/Ca and alkenone SST estimates into better agreement (*Lückge et al.*, 2004).

The positive excursion in $\delta^{18}O$ and $\delta^{18}O_{residual}$ observed in our records between 2.2 and 1.75 ka is coincident with an decrease in the Ti/Al ratio at this site, indicating a decrease in fluvial input at this time (*Lückge et al.*, 2001). The $\delta^{18}O_{residual}$ record therefore likely reflects the decrease in fluvial input (and therefore a local salinification) at this site. Based on the Ti/Al data as well as K/Al ratios, *Lückge et al.* (2001) interpret this decrease in fluvial input as an indication of decreasing winter monsoon strength.

That the alkenone and Mg/Ca records at this site demonstrate coherent trends suggests that the two proxies are recording the same season and, therefore, the same process. Because SST variability at this site is dominated by a single process (*i.e.* the winter monsoon) it is likely that both SST proxies are reflecting changes in the strength of winter monsoon cold advection. It is perhaps because of the relative simplicity of the annual SST cycle at this site in comparison to Site 723 that the two SST proxies agree with one another. As more multiproxy SST records are developed, sites such as 56KA, where two proxies agree, will provide important insights into the general behavior patterns of different SST proxies.

6.7.5 Comparison between Oman and Pakistan Margins

Over the time period for which our records from sites 723B and 56KA overlap (5–2 ka), the *G. ruber* and alkenone records from the two sites show similar SST trends. Both sites experience a warming over this time period. The warming at 723B is greater than that at 56KA; however, the lack of data after 2 ka at 723B may influence this outcome. Given the difference in resolution of records from the two sites, it is not possible to compare higher frequency variability with any confidence.

The regionally coherent warming trend suggested by these two sites could be indicative of several processes. If we consider SST at the two sites to be independent, then the warmings at 723B and 56KA separately suggest a decrease in summer monsoon upwelling and a decrease in winter monsoon cold advection, respectively. Alternatively, the coinci-

dent warming at the two sites could be the result of a regional SST trend, in which case other SST records from throughout the Arabian Sea would record a warming over this time period. However, given the evidence for a decrease in summer monsoon precipitation over this time period (Figure 6-5f; *Fleitmann et al.*, 2003), it is likely that the SST records are recording changes in monsoon strength.

6.8 Conclusions

We have presented planktonic foraminiferal Mg/Ca sea surface temperature, $\delta^{18}O$, and $\delta^{18}O_{residual}$ records from two sites within the Arabian Sea with the aim of understanding the history of the Indian Monsoon and its associated upwelling patterns. At ODP Site 723B on the Oman Margin, we find an LGM to Holocene warming of $2-3$°C that is likely due to the relaxation of glacial boundary conditions either directly (via an increase in net radiative forcing) or indirectly (via changes in monsoon circulation). Holocene SSTs show a 2 kyr long minimum in the Early Holocene associated with strong summer monsoon upwelling. A gradual warming, indicating a decrease in summer monsoon strength, occurs after 6 ka, in concert with a general drying of the Middle Eastern region (*Arz et al.*, 2003, and references therein). These SST changes concur with the trends in $\delta^{18}O_{residual}$, which show decreases associated with increases in summer monsoon intensity. At Site 56KA on the Pakistan Margin, SSTs gradually increased from 5 ka to the present while $\delta^{18}O_{residual}$ values show no long–term trend. The SST trend at this site suggests that the winter monsoon was decreasing in strength over this time period. Comparison of our Mg/Ca records to previously published SST records generated using different proxies reveals that, at Site 723, Holocene SST trends are highly proxy–dependent while at Site 56KA, different proxies agree well with one another. Because our understanding of the history of the Indian Monsoon relies heavily on our ability to reconstruct and interpret Arabian Sea SST, it is critical that continue to develop our understanding of the nature of the SST proxies commonly applied in the field of paleoceanography.

6.9 Acknowledgments

We would like to thank Rose Came, Luping Zou, Simon Thorrold, and Scot Birdwhistell for laboratory assistance. David Murray and Andreas Lückge kindly provided samples for this work. Analyses were funded by a SGER Grant from the National Science Foundation (OCE03–34598). Funding was also provided by a Schlanger Ocean Drilling Program Fellowship (to K.A.D.) and NSF Grant OCE02–20776 (to D.W.O.).

Table 2. Previously unreported ^{14}C dates

Core	Depth[a]	Method	Foram. species	^{14}C age (yr)	1σ (yr)	Cal. Age (yr)[b]	1σ (yr)
ODP–723B	45.5	AMS	mixed planktonics	1900	65	1250	59
ODP–723B	145.5	AMS	G. ruber	4740	45	4750	64
ODP–723B	200.5	AMS	G. ruber + G. sacculifer	7060	55	7370	53
ODP–723B	240.5	AMS	G. ruber + G. sacculifer	8190	70	8450	71
ODP–723B	290.5	AMS	G. ruber	9010	60	9480	48
ODP–723B	335.5	AMS	G. ruber + G. sacculifer	10,150	140	10,900	188
ODP–723B	370.5	AMS	G. ruber + G. sacculifer	11,700	90	13,000	78
ODP–723B	390.5	AMS	mixed planktonics	11,950	75	13,220	65
ODP–723B	430.5	AMS	mixed planktonics	13,200	85	14,830	204
ODP–723B	450.5	AMS	mixed planktonics	14,300	80	16,300	210
ODP–723B	521.5	AMS	mixed planktonics	18,850	160	21,740	281

(a) centimeters below sea floor; (b) Calibrated with a reservoir age of 600 years using Calib 5.0 (*Stuiver and Reimer*, 1993).

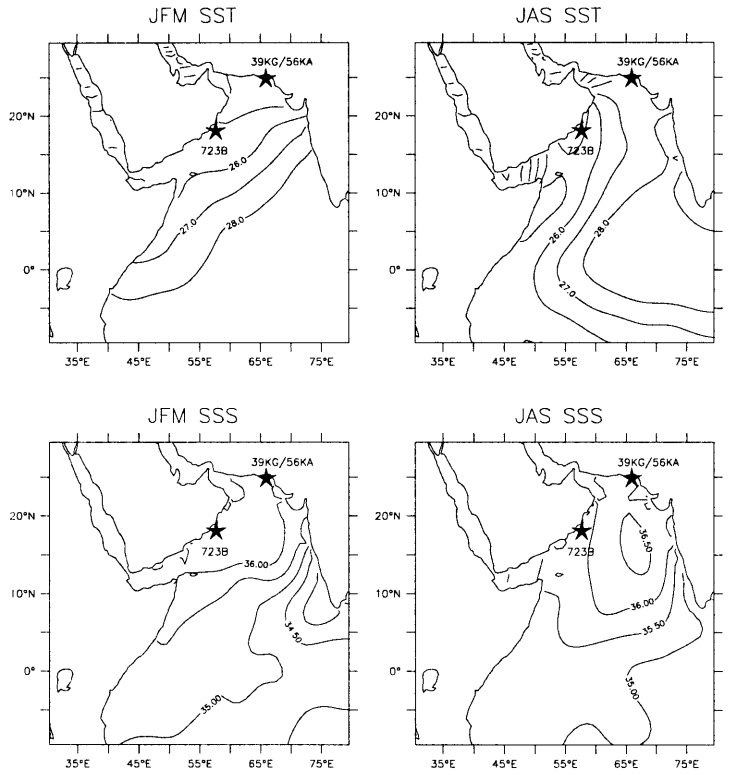

Figure 6-1: Sea surface temperature (SST, top, units are $°C$) and sea surface salinity (SSS, bottom, units are psu) for winter (JFM) and summer (JAS). Also shown are the locations of cores used in this study: Oman Margin core 723B and Pakistan Margin cores 39KG/56KA (*Levitus and Boyer*, 1994).

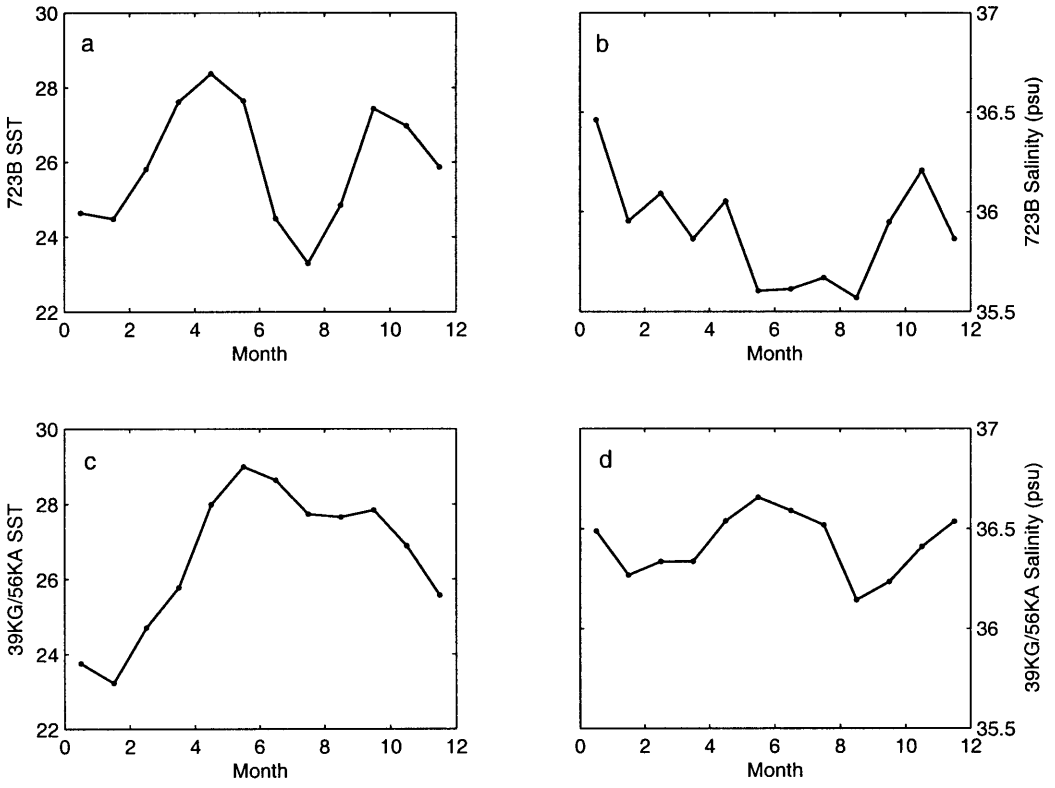

Figure 6-2: The annual cycle of sea surface temperature (left) and salinity (right) at ODP Site 723B. Data are from *Levitus and Boyer* (1994).

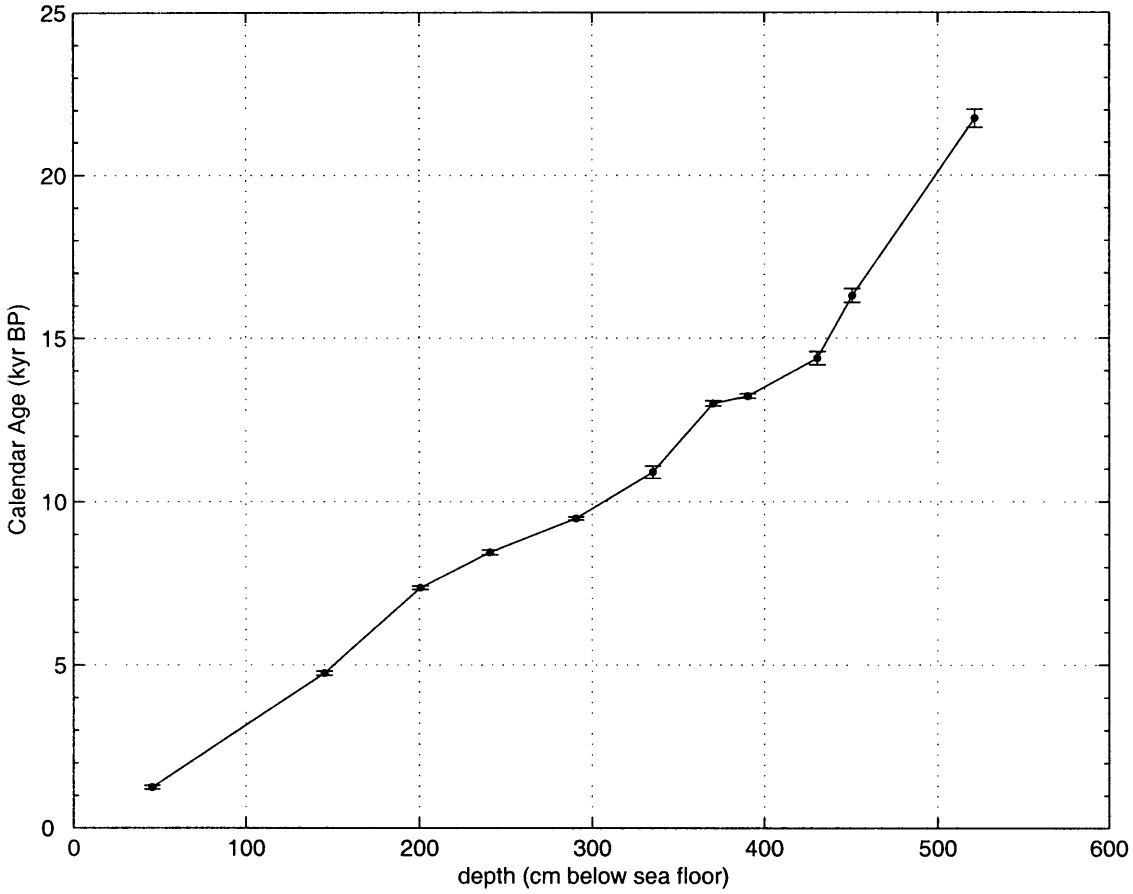

Figure 6-3: Age model for ODP Site 723B using dates shown in Table 1.

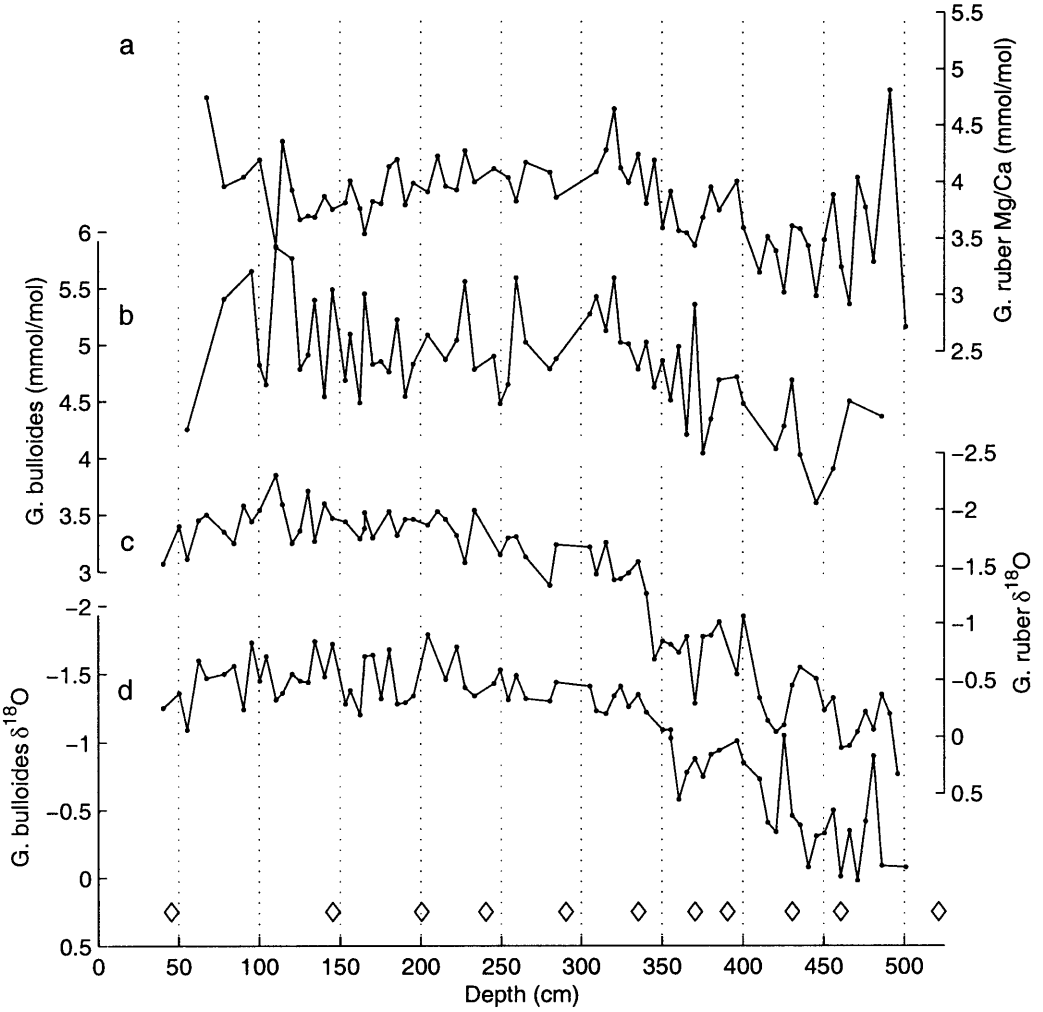

Figure 6-4: Raw Mg/Ca (in mmol/mol) and δ^{18}O (‰, VPDB) from site 723B. a) *G. ruber* Mg/Ca; b) *G. bulloides* Mg/Ca; c) *G. ruber* $\delta^{18}O$; d) *G. bulloides* $\delta^{18}O$. Calibrated ^{14}C dates are shown in open diamonds.

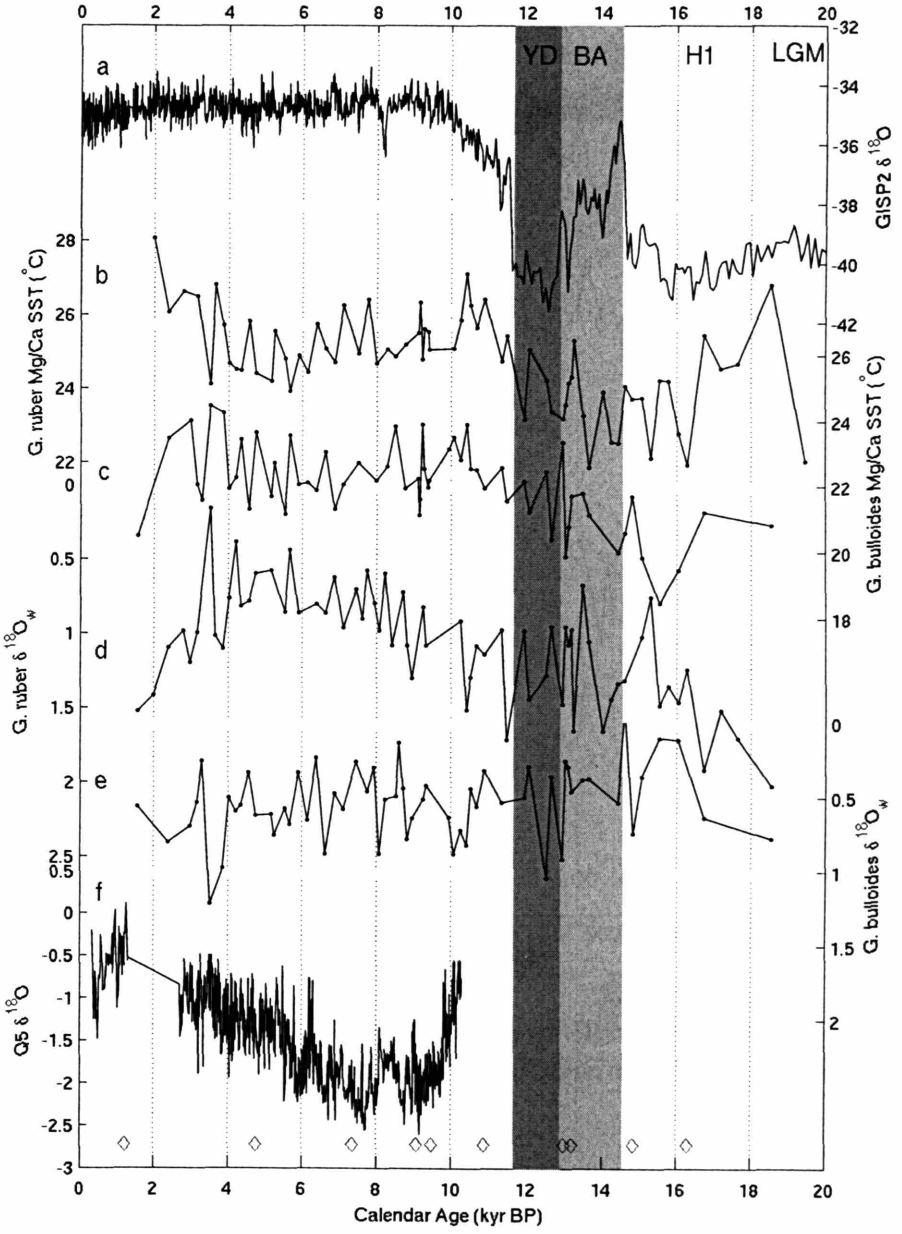

Figure 6-5: Comparison of site 723B SST (°C) and $\delta^{18}O_{residual}$ (‰, SMOW) results with records of Greenland climate and Oman precipitation. a) GISP2 $\delta^{18}O$ (*Grootes et al.*, 1993; *Grootes and Stuiver*, 1997); b) *G. ruber* Mg/Ca SST; c) *G. bulloides* Mg/Ca SST; d) *G. ruber* $\delta^{18}O_{residual}$; e) *G. bulloides* $\delta^{18}O_{residual}$; f) δ^{18}O of a stalagmite from Oman with lower δ^{18}O indicating higher precipitation (*Fleitmann et al.*, 2003).Calibrated ^{14}C dates for Site 723B are shown in open diamonds.

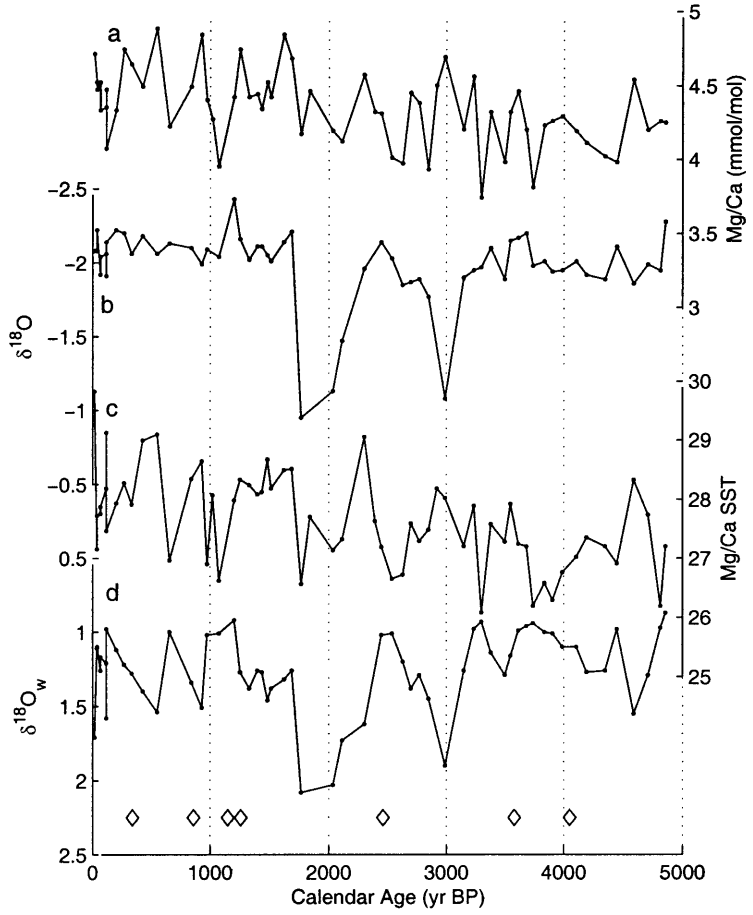

Figure 6-6: a) Mg/Ca (mmol/mol); b) $\delta^{18}O$ (‰, VPDB); c) SST (°C); and d) $\delta^{18}O_{residual}$ (‰, SMOW) at Pakistan Margin Site 56KA as determined from measurements on *G. ruber*.

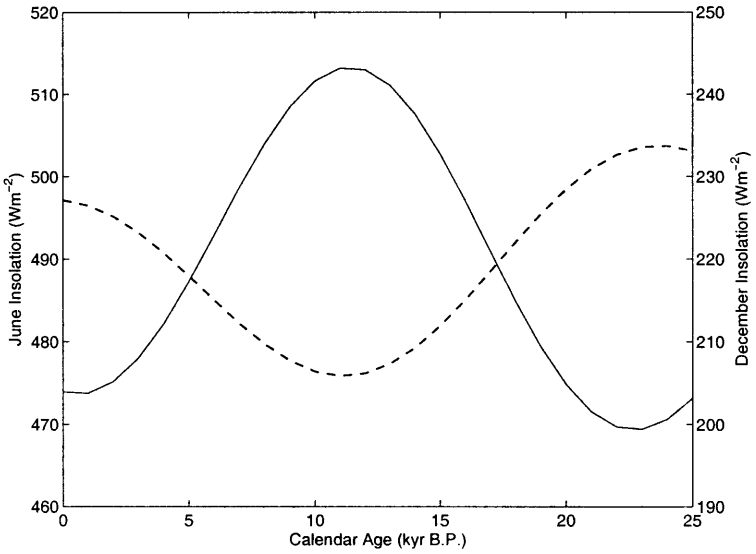

Figure 6-7: June (solid line) and December (dashed line) insolation at 30°N (*Berger and Loutre*, 1991).

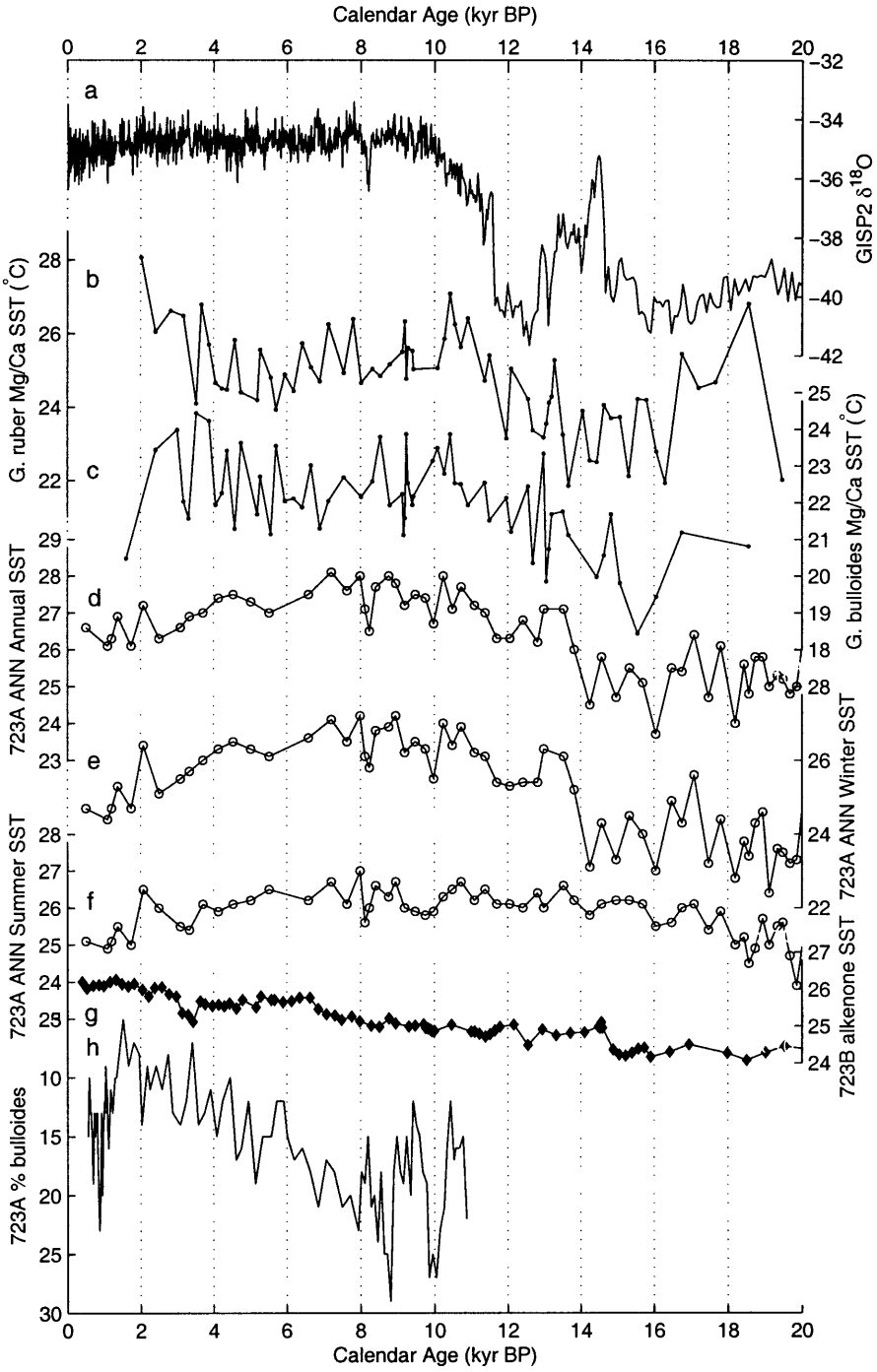

Figure 6-8: Comparison of SST records from Site 723. a) GISP2 $\delta^{18}O$ (*Grootes et al.*, 1993; *Grootes and Stuiver*, 1997); b) 723B *G. ruber* Mg/Ca SST (this study); c) 723B *G. bulloides* Mg/Ca SST (this study); d) 723A Artificial Neural Networks Annual SST (*Naidu and Malmgren*, 2005); e) 723A Artificial Neural Networks Winter SST (*Naidu and Malmgren*, 2005); f) 723A Artificial Neural Networks Winter SST (*Naidu and Malmgren*, 2005); g) 723B Alkenone SST (*Higginson et al.*, 2004); h) 723A % bulloides (note that y–axis is reversed; *Gupta et al.*, 2003). Note that all timescales are as published by the original authors and that y–axes, with the exeption of the % bulloides record, are scaled the same.

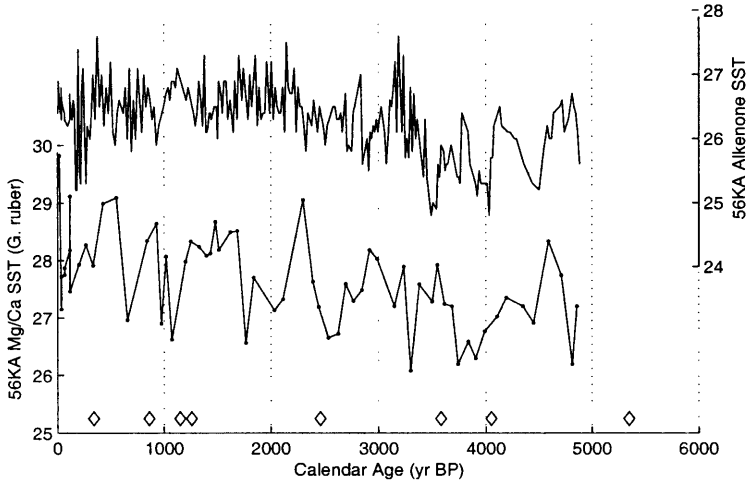

Figure 6-9: Comparison of SST records from Pakistan Margin core 56KA. a) Alkenone SST (*Doose-Rolinski et al.*, 2001); b) Mg/Ca SST (this study). Calibrated AMS ^{14}C dates are shown in open diamonds (*von Rad et al.*, 1999). Note that the age model for this core, determined by *von Rad et al.* (1999) has been calibrated with varve chronology.

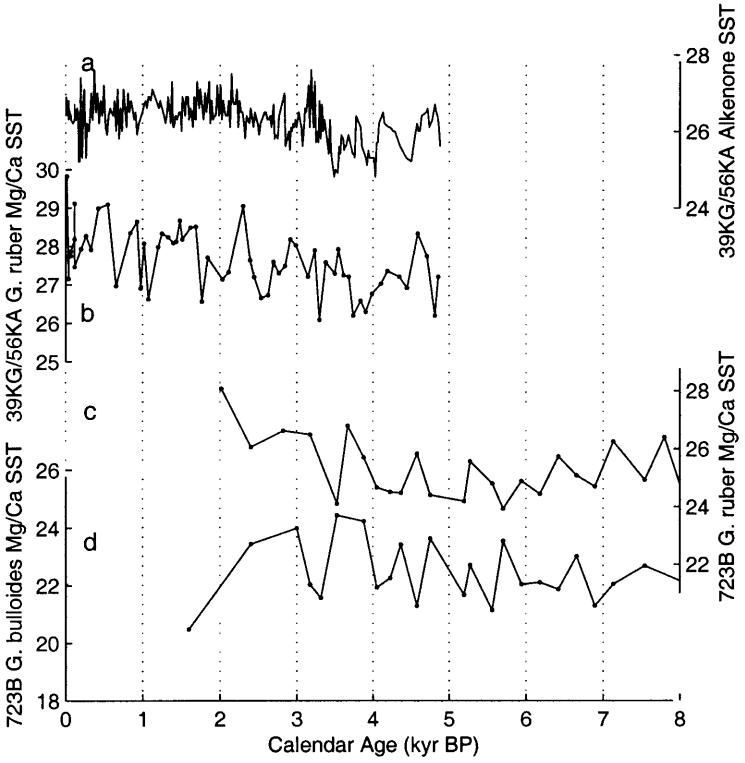

Figure 6-10: Comparison of SST records from 723B and 56KA. a) Alkenone SST at 56KA (*Doose-Rolinski et al.*, 2001); b) *G. ruber* Mg/Ca SST at 56KA; c) *G. ruber* Mg/Ca SST at 723B; d) *G. bulloides* Mg/Ca SST at 723B.

Bibliography

Ackerman, S. A., and S. K. Cox, Surface weather observations of atmospheric dust over the southwest summer monsoon region, *Meteorol. Atmos. Phys.*, *41*, 19–34, 1989.

Altabet, M. A., R. Francois, D. W. Murray, and W. L. Prell, Climate-related variations in denitrification in the Arabian Sea from sediment 15N/14N ratios, *Nature*, *373*, 506–509.

Anand, P., H. Elderfield, and M. H. Conte, Calibration of Mg/Ca thermometry in planktonic foraminifera from a sediment trap time series, *Paleoceanography*, *18*, 10.1029/2002PA00,846, 2003.

Anderson, D. M., and W. L. Prell, A 300 kyr record of upwelling off Oman during the late Quaternary: Evidence of the Asian southwest monsoon, *Paleoceanography*, *8*, 193–208, 1993.

Anderson, D. M., J. T. Overpeck, and A. K. Gupta, Increase in the Asian southwest monsoon during the past four centuries, *Science*, *297*, 596–599, 2002.

Andruleit, H. A., U. von Rad, A. Bruns, and V. Ittekkot, Coccolithophore fluxes from sediment traps in the northeastern Arabian Sea off Pakistan, *Marine Micropaleontology*, *38*, 285–308, 2000.

Aqrawi, A. A. M., Stratigraphic signatures of climatic change during the Holocene evolution of the Tigris–Euphrates delta, lower Mesopotamia, *Global Planet. Change*, *28*, 267–283, 2001.

Arz, H. W., F. Lamy, J. Pätzold, P. J. Müller, and M. Prins, Mediterranean moisture source for an Early–Holocene humid period in the Northern Red Sea, *Science*, *300*, 118–121, 2003.

Banse, K., On the coupling of hydrography, phytoplankton, zooplankton, and settling organic particles offshore in the Arabian Sea, in *Biogeochemistry of the Arabian Sea*, edited by D. Lal, vol. 103, pp. 125–161, Proceedings of the Indian Academy of Sciences (Earth and Planetary Sciences), 1994.

Banse, K., and D. C. English, Geographical differences in seasonality of CZCS–derived phytoplankton pigment in the Arabian Sea for 1978–1986, *Deep–Sea Research II*, *47*, 1623–1677, 2000.

Bard, E., B. Hamelin, M. Arnold, L. Montaggioni, G. Cabioch, G. Faure, and F. Rougerie, Deglacial sea–level record from Tahini corals and the timing of global meltwater discharge, *Nature*, *382*, 241–244, 1996.

Bard, E., F. Rostek, and C. Sonzogni, Interhemispheric synchrony of the last deglaciation inferred from alkenone palaeothermometry, *Nature*, *385*, 707–710, 1997.

Bard, E., F. Rostek, J.-L. Turon, and S. Gendreau, Hydrological impact of Heinrich Events in the Subtropical North Atlantic, *Science*, *289*, 1321–1324, 2000.

Berger, A., and M. F. Loutre, Insolation values for the climate of the last 10 million years, *Quat. Sci. Rev.*, *10*, 297–317, 1991.

Berger, A. L., Long-term variations of caloric insolation resulting from the Earth's orbital variations, *Quat. Res.*, *9*, 139–167, 1978.

Boyle, E. A., and L. D. Keigwin, Comparison of Atlantic and Pacific paleochemical records for the last 250,000 years: changes in deep ocean circulation and chemical inventories, *Earth Planet. Sci. Lett.*, *76*, 135–150, 1985.

Boyle, E. A., and Y. Rosenthal, Chemical hydrography of the South Atlantic during the last glacial maximum: δ^{13}C versus Cd, in *The South Atlantic: Present and Past Circulation*, edited by G. Wefer and et al., pp. 423–443, Springer–Verlag, New York, 1996.

Brassell, S. C., Applications of biomarkers for delineating marine paleoclimatic fluctuations during the Pleistocene, in *Organic Geochemistry*, edited by M. H. Engel and S. A. Macko, pp. 699–737, Plenum Press, New York, 1993.

Broccoli, A. J., Tropical cooling at the Last Glacial Maximum: An atmosphere-mixed layer ocean model simulation, *J. Climate*, *13*, 951–976, 2000.

Broccoli, A. J., K. A. Dahl, and R. J. Stouffer, Extratropical influences on interhemispheric asymmetry of tropical climate, *in prep.*, *xxx*, xxx, 2005.

Broecker, W. S., D. Peteet, and D. Rind, Does the ocean-atmosphere system have more than one stable mode of operation?, *Nature*, *315*, 21–25, 1985.

Broecker, W. S., M. Andree, W. Wolli, H. Oeschger, G. Bonani, J. Kennett, and D. Peteet, A case in support of a meltwater diversion as the trigger for the onset of the Younger Dryas, *Paleoceanography*, *3*, 1–9, 1988.

Cane, M. A., A role for the tropical Pacific, *Science*, *282*, 59–61, 1998.

Cayre, O., and E. Bard, Planktonic foraminiferal and alkenone records of the last deglaciation from the Eastern Arabian Sea, *Quat. Res.*, *52*, 337–342, 1999.

Cerling, T. E., Y. Want, and J. Quade, Expansion of C_4 ecosystems as an indicator of global ecological change in the late Miocene, *Nature*, *361*, 344–345, 1993.

Cerling, T. E., J. M. Harris, B. J. MacFadden, M. G. Leakey, J. Quade, V. Eisenmann, and J. R. Ehleringer, Global vegetation change through the Miocene/Pliocene boundary, *Nature*, *389*, 153–158, 1997.

Cheesbrough, T. M., and P. E. Kolattukudy, Alkane biosynthesis by decarbonylation of aldehydes catalyzed by a particulate preparation from *Pisum sativum*, *Proceedings of the National Academy of Sciences of the United States of America*, *81*, 6613–6617, 1984.

Chikaraishi, Y., H. Naraoka, and S. R. Poulson, Hydrogen and carbon isotopic fractionations of lipid biosynthesis amount terrestrial (C3, C4, and CAM) and aquatic plants, *Phytochemistry*, *65*, 1369–1381, 2004.

Clemens, S., W. Prell, D. Murray, G. Shimmield, and G. Weedon, Forcing mechanisms of the Indian Ocean monsoon, *Nature*, *353*, 720–725, 1991.

Clemens, S. C., Dust response to seasonal atmospheric forcing: Proxy evaluation and calibration, *Paleoceanography*, *13*, 471–490, 1998.

Clemens, S. C., and W. L. Prell, Late Pleistocene variability of Arabian Sea summer monsoon winds and continental aridity: Eolian records from the lithogenic components of deep–sea sediments, *Paleoceanography*, *5*, 109–145, 1990.

Clemens, S. C., and W. L. Prell, A 350,000 year summer–monsoon multi–proxy stack from the Owen Ridge, Northern Arabian Sea, *Marine Geology*, *201*, 35–51, 2003.

Clement, A. C., and M. A. Cane, A role for the tropical Pacific coupled ocean-atmosphere system on Milankovitch and millennial timescales. Part I: A modeling study of tropical Pacific variability, in *Mechanisms of Global Climate Change on Millennial Timescales*, edited by R. S. W. P. U. Clark and L. D. Keigwin, vol. 112, American Geophysical Union,, Washington, D. C., 1999.

Clement, A. C., M. A. Cane, and R. Seager, An orbitally driven tropical source for abrupt climate change, *J. Climate*, *14*, 2369–2375, 2001.

CLIMAP Project Members, Seasonal reconstruction of the Earth's surface at the Last Glacial Maximum, *Geological Socity of America Map and Chart Series*, *MC-36*, 1981.

Cloern, J. E., E. A. Canuel, and D. Harris, Stable carbon and nitrogen isotope composition of aquatic and terrestrial plants of the San Francisco Bay estruarine system, *Limnology and Oceanography*, *47*, 713–729, 2002.

Codispoti, L. A., Primary productivity and carbon and nitrogen cycling in the Arabian Sea, in *U. S. JGOFS Planning Report*, pp. 75–85, 1991.

Collister, J. W., G. Rieley, B. Stern, G. Eglinton, and B. Fry, Compound–specific δ^{13}C analyses of leaf lipids from plants with differing carbon dioxide metabolisms, *Org. Geochem.*, *21*, 619–627, 1994.

Conan, S. M.-H., and G.-J. A. Brummer, Fluxes of planktic foraminifera in response to monsoonal upwelling on the Somalia Basin margin, *Deep-Sea Research II*, *47*, 2207–2227, 2000.

Conte, M. H., and J. C. Weber, Plant biomarkers in aeorsols record isotpic discrimination of terrestrial photosynthesis, *Nature*, *417*, 639–641, 2002.

Cox, R. E., M. M. Mazurek, and B. R. T. Simoneit, Lipids in Harmattan aerosols of Nigeria, *Nature*, *296*, 848–849, 1982.

Cullen, H. M., P. B. deMenocal, S. Hemming, G. Hemming, F. H. Brown, T. Guilderson, and F. Sirocko, Climate change and the collapse of the Akkadian empire: Evidence from the deep sea, *Geology*, *28*, 379–382, 2000.

Curry, W. B., D. R. Ostermann, M. V. S. Guptha, and V. Ittekkot, Foraminiferal production and monsoonal upwelling in the Arabian Sea: evidence from sediment traps, in *Upwelling Systems: Evolution Since the Early Miocene*, edited by C. P. Summerhayes, W. L. Prell, and K. C. Emeis, no. 64 in Geological Society Special Publication, pp. 93–106, London, 1992.

de Miro, M. D., Los foraminiferos vivos y sedimentados del margen continental de Venezuela (resumen), *Acta Geol. Hisp.*, *4*, 102–106, 1971.

Delaygue, G., E. Bard, C. Rollion, J. Jouzel, M. Stievenard, and J.-C. Duplessy, Oxygen isotope/salinity relationship in the northern Indian Ocean, *Paleoceanography*, *106*, 4565–4574, 2001.

deMenocal, P., J. Ortiz, T. Guilderson, and M. Sarnthein, Coherent high- and low-latitude climate variability during the Holocene warm period, *Science*, *288*, 2198–2202, 2000.

Development Data Group, The World Bank, World Development Indicators 2002 online, *http://publications.worldbank.org*, 2002.

Doose-Rolinski, H., U. Rogalla, G. Scheeder, A. Lückge, and U. von Rad, High–resolution temperature and evaporation changes during the late Holocene in the northeastern Arabian Sea, *Paleoceanography*, *16*, 358–367, 2001.

Duce, R. A., Sources, distributions, and fluxes of mineral aerosols and their relationship to climate, in *Aerosol Forcing of Climate*, edited by R. J. Charlson and J. E. Heintzenberg, pp. 43–72, Wiley, New York, 1995.

Dutta, K., R. Bhushan, and B. L. K. Somayajulu, δR values for the northern Indian Ocean, *Radiocarbon*, *43*, 483–488, 2001.

Eglinton, G., and R. J. Hamilton, The distribution of *n*–alkanes, in *Chemical Plant Taxonomy*, edited by T. Swain, pp. 187–217, Academic Press, 1963.

Eglinton, T. I., B. C. Benitez-Nelson, A. Pearson, A. P. McNichol, J. E. Bauer, and E. R. M. Druffel, Variability in radiocarbon ages of individual organic compounds from marine sediments, *Science*, *277*, 796–799, 1997.

Eglinton, T. I., G. Eglinton, L. Dupont, E. R. Sholkovitz, D. Montluçon, and C. M. Reddy, Composition, age, and provenance of organic matter in NW African dust over the Atlantic Ocean, *Geochemistry, Geophysics, Geosystems*, *3*, 10.1029/2001GC000,269, 2002.

Elderfield, H., and G. Ganssen, Past temperature and $\delta^{18}o$ of sufrace ocean waters inferred from foraminiferal Mg/Ca, *Nature*, *405*, 442–445, 2000.

Emeis, K.-C., D. M. Anderson, H. Doose, D. Kroon, and D. Schulz-Bull, Sea-surface temperatures and the history of monsoon upwelling in the Northwest Arabian Sea during the last 500,000 years, *Quat. Res.*, *43*, 355–361, 1995.

Enzel, Y., L. L. Ely, S. Mishra, R. Ramesh, R. Amit, B. Lazar, S. N. Rajaguru, V. R. Baker, and A. Sandler, High–resolution Holocene environmental changes in the Thar desert, north–western India, *Science*, *284*, 125–128, 1999.

Fairbanks, R. G., A 17,000-year glacio-eustatic sea level record: influence of glacial melting rates on the younger dryas event and deep-ocean circulation, *Nature*, *342*, 637–642, 1989.

Ferraz-Reyes, E., Estudio del fitoplankton el la cuenta Tuy–Cariaco, Venezuela, *Bol. Inst. Oceanogr. Univ. Oriente*, *22*, 111–124, 1983.

Findlater, J., A major low–level air current near the Indian Ocean during the northern summer, *Quart. J. R. Met. Soc.*, *95*, 362–380, 1969.

Fleitmann, D., S. J. Burns, M. Mudelsee, U. Neff, J. Kramers, A. Mangini, and A. Matter, Holocene forcing of the Indian Monsoon recorded in a stalagmite from Southern Oman, *Science*, *300*, 1737–1739, 2003.

Food and Agriculture Organization of the United Nations (FAO), Faostat on–line statistical service, *http://apps.fao.org*, 2002.

Gasse, F., Hyrological changes in the African tropics since the Last Glacial Maximum, *Quat. Sci. Rev.*, *19*, 189–211, 2000.

Goñi, M. A., K. C. Ruttenberg, and T. I. Eglinton, A reassessment of the sources and importance of land–derived organic matter in surface sediments from the Gulf of Mexico, *Geochim. Cosmochim. Acta*, *62*, 3055–3075, 1998.

Grootes, P. M., and M. Stuiver, Oxygen 18/16 variability in Greenland snow and ice with 10^{-3}–10^{-5}–year time resolution, *J. Geophys. Res.*, *102*, 26,455–26,470, 1997.

Grootes, P. M., M. Stuiver, J. W. C. White, S. J. Johnsen, and J. Jouzel, Comparison of oxygen isotope records from the GISP2 and GRIP Greenland ice cores, *Nature*, *366*, 552–554, 1993.

Gulz, P.-G., Epicuticular leaf waxes in the evolution of the plant kingdom, *J. Plant Physiol.*, *143*, 453–464, 1994.

Gupta, A. K., D. M. Anderson, and J. T. Overpeck, Abrupt changes in the Asian southwest monsoon during the Holocene and their links to the North Atlantic Ocean, *Nature*, *421*, 354–357, 2003.

Hadley, J. L., and W. K. Smith, Wind erosion of leaf surface wax in alpine timberline conifers, *Arctic Alpine Res.*, *21*, 392–398, 1989.

Haraoka, H., and R. Ishiwarati, Molecular and isotopic abundances of long chain *n*–fatty acids in open marine sediments of the western North Pacific, *Chemical Geology*, *165*, 23–36, 2000.

Hastenrath, S., and L. Greischar, The monsoonal heat–budget of the hydrosphere–atmosphere system in the Indian Ocean sector, *J. Geophys. Res.*, *98*, 6869–6881, 1993.

Haug, G. H., T. F. Pedersen, D. M. Sigman, S. E. Calvert, B. Nielsen, and L. C. Peterson, Glacial/interglacial variations in production and nitrogen fixation in the Cariaco Basin during the last 580 kyr, *Paleoceangraphy*, *13*, 427–432, 1998.

Haug, G. H., K. A. Hughen, D. M. Sigman, L. C. Peterson, and U. Röhl, Southward migration of the Intertropical Convergence Zone through the Holocene, *Science*, *293*, 1304–1308, 2001.

Higginson, M. J., M. A. Altabet, L. Wincze, T. D. Herbert, and D. W. Murray, A solar (irradiance) trigger for millennial–scale abrupt changes in the southwest monsoon?, *Paleoceanography*, *19*, PA3015,doi:10.1029/2004PA001,031, 2004.

Honjo, S., J. Dymond, W. Prell, and V. Ittekkot, Monsoon–controlled export fluxes to the interior of the Arabian Sea, *Deep–Sea Research II*, *46*, 1859–1902, 1999.

Hostetler, S. W., and A. C. Mix, Reassessment of ice-age cooling of the tropical ocean and atmosphere, *Nature*, *399*, 673–676, 1999.

Huang, Y., L. Dupont, M. Sarnthein, J. M. Hayes, and G. Eglinton, Mapping of C_4 plant input from North West Africa into North East Atlantic sediments, *Geochim. Cosmochim. Acta*, *64*, 3505–3513, 2000.

Hughen, K. A., J. T. Overpeck, L. C. Peterson, and S. Trumbore, Rapid climate changes in the tropical Atlantic region during the last deglaciation, *Nature*, *380*, 51–54, 1996.

Hughen, K. A., T. I. Eglinton, L. Xu, and M. Makou, Abrupt tropical vegetation response to rapid climate changes, *Science*, *304*, 1955–1959, 2004.

Joussaume, S., et al., Monsoon changes for 6000 years ago: Results of 18 simulations from the Paleoclimate Modeling Intercomparison Project, *Geophys. Res. Lett.*, *26*, 859–862, 1999.

Kienast, M., T. J. J. Hanebuth, C. Pelejero, and S. Steinke, Synchroneity of meltwater pulse 1a and the Bølling warming: New evidence from the South China Sea, *Geology*, *31*, 67–70, 2003.

Kim, J.-H., N. Rimbu, S. J. Lorenz, G. Lohmann, S.-I. Nam, S. Schouten, C. Rühlemann, and R. R. Schneider, North Pacific and North Atlantic sea–surface temperature variability during the Holocene, *Quat. Sci. Rev.*, *23*, 2141–2154, 2004.

Klein, S. A., B. J. Soden, and N.-C. Lau, Remote sea surface temperature variations during ENSO: Evidence for a tropical atmospheric bridge, *J. Climate*, *12*, 917–932, 1999.

Kolla, V., and F. Coumes, Morphology, internal structure, seismic stratigraphy, and sedimentation on the Indus Fan, *Am. Assoc. Petrol. Geol. Bull.*, *71*, 650–677, 1987.

Kutzbach, J. E., and R. G. Gallimore, Sensitivity of a coupled atmosphere/mixed layer ocean model to changes in orbital forcing at 9000 years B.P., *J. Geophys. Res.*, *93*, 803–821, 1988.

Kutzbach, J. E., P. J. Guetter, P. J. Behling, and R. Selin, Simulated climate changes: results of the COHMAP climate–model experiments, in *Global Climates since the Last Glacial Maximum*, edited by H. E. Wright Jr., J. E. Kutzbach, T. Webb III, W. F. Ruddiman, F. A. Street-Perrott, and P. J. Bartlein, pp. 24–93, University of Minnesota Press, Minneapolis, 1993.

Kuypers, M. M. M., R. D. Pancost, and J. S. Sinninge-Damste, A large and abrupt fall in atmospheric CO_2 concentration during Cretaceous times, *Nature*, *399*, 342–345, 1999.

Lau, N.-C., and M. J. Nath, The role of the "atmospheric bridge" in linking tropical Pacific ENSO events to extratropical SST anomalies, *J. Climate*, *9*, 2036–2057, 1996.

Lea, D. W., D. K. Pak, L. C. Peterson, and K. A. Hughen, Synchroneity of tropical and high–latitude Atlantic temperatures over the last glacial termination, *Science*, *301*, 1361–1364, 2003.

Levitus, S., and T. Boyer, *World Ocean Atlas 1994 Volumne 4: Temperature*, vol. 13 of *NOAA Atlas NESDIS*, U.S. Government Printing Office,, Washington, D.C., 1994.

Lin, H.-L., L. C. Peterson, J. T. Overpeck, S. E. Trumbore, and D. W. Murray, Late Quaternary climate change from δ^{18}O records of multiple species of planktonic foraminifera: High-resolution records from the anoxic Cariaco Basin, Venezuela, *Paleoceanography*, *12*, 415–427, 1997.

Liu, Z., B. Otto-Bleisner, J. Kutzback, L. Li, and C. Shields, Coupled climate simulation of the evolution of global monsoons in the Holocene, *J. Climate*, *16*, 2472–2490, 2003.

Liu, Z., S. P. Harrison, J. Kutzbach, and B. Otto-Bleisner, Global monsoons in the mid–Holocene and oceanic feedback, *Clim. Dyn.*, *22*, 10.1007/s00,382–003–0372–y, 2004.

Locke, S., and R. C. Thunell, Paleoceanographic record of the last glacial/interglacial cycle in the Red Sea and Gulf of Aden, *Palaeogeogr. Palaeoclim. Palaeoecol.*, *64*, 163–187, 1988.

Lückge, A., H. Doose-Rolinski, A. A. Khan, H. Schulz, and U. von Rad, Monsoonal variability in the northeastern Arabian Sea during the past 5000 years: geochemical evidence from laminated sediments, *Palaeogeogr. Palaeoclim. Palaeoecol.*, *167*, 273–286, 2001.

Lückge, A., M. Staubwasser, H. Doose-Rolinski, and G. Scheeder, High–resolution Holocene SST changes in the NE Arabian Sea reveal a complex monsoon history, *Eos Trans. AGU*, *85(47), Fall Meet. Suppl.*, Abstract PP13A–0592, 2004.

Malmgren, B. A., and U. Nordlund, Application of artificial neural networks to paleoceanographic data, *Palaeogeogr. Palaeoclim. Palaeoecol.*, *136*, 359–373, 1997.

Marchal, O., et al., Apparent long–term cooling of the sea surface in the northeast Atlantic and Mediterranean during the Holocene, *Quat. Sci. Rev.*, *21*, 455–483, 2002.

Monnin, E., A. Indermühle, A. Dällenbach, J. Flückiger, B. Stauffer, T. F. Stocker, D. Raynaud, and J.-M. Barnola, Atmospheric CO_2 concentrations over the last glacial termination, *Science*, *291*, 112–114, 2001.

Mulitza, S., D. Bolotovskoy, B. Donner, H. Meggers, A. Paul, and G. Wefer, Temperature:δ^{18}O relationships of planktonic foraminifera collected from surface waters, *Palaeogeogr. Palaeoclim. Palaeoecol.*, *202*, 143–152, 2003.

Muller-Karger, F., et al., Annual cycle of primary production in the Cariaco Basin: Response to upwelling and implications for vertical export, *J. Geophys. Res.*, *106*, 4527–4542, 2001.

Murray, D. W., and W. L. Prell, Late Pliocene and Pleistocene climatic oscillations and monsoon upwelling recorded in sediments from the Owen Ridge, northwestern Arabian Sea, in *Upwelling Systems: Evolution Since the Early Miocene*, edited by C. P. Summerhayes, W. L. Prell, and K. C. Emeis, no. 64 in Geol. Soc. Spec. Publ., pp. 301–321, 1992.

Naidu, P. D., and B. A. Malmgren, A 2,200 year periodicity in the Asian monsoon system, *Geophys. Res. Lett.*, *22*, 2361–2364, 1995.

Naidu, P. D., and B. A. Malmgren, Seasonal sea surface temperature contrast between the Holocene and last glacial period in the western Arabian Sea (Ocean Drilling Project Site 723A): Modulated by monsoon upwelling, *Paleoceanography*, *20*, doi:10.1029/2004PA001,078, 2005.

Naqvi, W. A., and R. G. Fairbanks, A 27,000 year record of Red Sea Outflow: Implication for timing of post–glacial monsoon intensification, *Geophys. Res. Lett.*, *23*, 1501–1504, 1996.

Narayanan, M. S., and B. M. Rao, Detection of monsoon inversion by TIROS–N satellite, *Nature*, *294*, 546–548, 1981.

Oberhuber, J. M., An atlas based on the COADS data set: the budget of heat, buoyancy and turbulent kinetic energy at the surface of the global ocean, *Tech. rep.*, Max Plank–Institut für Meteorologie Report 15, 1988.

Ohkouchi, N., K. Kawamura, and A. Taira, Molecular paleoclimatology: reconstruction of climate variabilities in the late Quaternary, *Org. Geochem.*, *27*, 173–183, 1997.

Overpeck, J. T., D. M. Anderson, S. Trumbore, and W. L. Prell, The Southwest Monsoon over the last 18,000 years, *Clim. Dyn.*, *12*, 213–225, 1996.

Pagani, M., K. H. Freeman, and M. A. Arthur, Late Miocene atmospheric CO_2 concentrations and the expansion of C_4 grasses, *Science*, *285*, 876–879, 1999.

Pearson, A., and T. I. Eglinton, The origin of *n*–alkanes in Santa Monica Basin surface sediment: a model based on compound–specific $\Delta^{14}C$ and $\delta^{13}C$ data, *Org. Geochem.*, *31*, 1103–1116, 2000.

Peeters, F. J. C., G. A. Brummer, and G. Ganssen, The effect of upwelling on the distribution and stable isotope composition of Globigerina bulloides and Globigerinoides ruber (planktic foraminifera) in modern surface waters of the NW Arabian Sea, *Global and Planetary Change*, *34*, 269–291, 2002.

Pelejero, C., Terrigenous *n*–alkane input in the South China Sea: high–resolution records and surface sediments, *Chemical Geology*, *200*, 89–103, 2003.

Peltzer, E. T., and R. B. Gagosian, Sampling and quantitation of lipids in aerosols from the remote marine atmosphere, *Analytica Chimica Acta*, *198*, 125–144, 1987.

Petit, J. R., et al., Climate and atmospheric history of the past 420,000 years from the Vostok ice core, Antarctica, *Nature*, *399*, 429–436, 1999.

Pinot, S., G. Ramstein, S. P. Harrison, I. C. Prentice, J. Guiot, M. Stute, and S. Joussame, Tropical paleoclimates of the Last Glacial Maximum: comparison of Paleoclimate Modeling Intercomparison Project (pmip) simulations and paleodata, *Clim. Dyn.*, *15*, 857–874, 1999.

Porter, S. C., and Z. An, Correlation between climate events in the North Atlantic and China during the last deglaciation, *Nature*, *375*, 305–308, 1995.

Post-Beittenmiler, D., Biochemistry and molecular biology of wax production in plants, *Annual Reviews of Plant Physiology and Plant Molecular Biology*, *47*, 405–430, 1996.

Poynter, J. G., P. Farrimond, N. Robinson, and G. Eglinton, Aeolian–derived higher plant lipids in the marine sedimentary record: links with palaeoclimate, in *Paleoclimatology and Paleometeorology: Modern and Past Patterns of Global Atmospheric Transport*, edited by M. Leinen and M. Sarnthein, vol. 282 of *NATO ASI series, Series C*, pp. 435–462, Kluwer Academic Publishers, Dordrecht, 1989.

Prahl, F. G., J. R. Ertel, M. A. Goni, M. A. Sparrow, and B. Eversmeyer, Terrestrial organic carbon contributions to sediments on the Washington margin, *Geochim. Cosmochim. Acta*, *58*, 3035–3048, 1994.

Prell, W. L., Variation of monsoonal upwelling: a response to changing solar radiation, in *Climate Processes and Climate Sensitivity*, edited by J. Hansen and T. Takahashi, vol. 5 of *Maurice Ewing Series*, pp. 48–57, American Geophysical Union, Washington, D.C., 1984.

Prell, W. L., and W. B. Curry, Faunal and isotopic indices of monsoonal upwelling: Western Arabian Sea, *Oceanologica Acta*, *4*, 91–98, 1981.

Prell, W. L., and J. E. Kutzbach, Monsoon variability over the past 150,000 years, *J. Geophys. Res.*, *92*, 8411–8425, 1987.

Prell, W. L., and J. E. Kutzbach, Sensitivity of the Indian monsoon to forcing parameters and implications for its evolution, *Nature*, *360*, 647–651, 1992.

Prins, M. A., G. Postma, J. Cleveringa, A. Cramp, and N. H. Kenyon, Controls on terrignous sediment supply to the Arabian Sea during the late Quaternary: the Indus Fan, *Marine Geology*, *169*, 327–349, 2000a.

Prins, M. A., G. Postma, and G. J. Weltje, Controls on terrignous sediment supply to the Arabian Sea during the late Quaternary: the Makran continental slope, *Marine Geology*, *169*, 351–371, 2000b.

Pye, K., Processes of fine particle formation, dust source regions, and climatic changes, in *Paleoclimatology and Paleometeorology: Modern and Past Patterns of Global Atmo-*

spheric Transport, edited by M. Leinin and M. Sarnthein, no. C 282 in NATO ASI Series, pp. 3–30, Kluwer, Dordrecht/Boston/London, 1989.

Ramage, C. S., F. R. Miller, and C. Jeffries, Meteorological Atlas of the International Indian Ocean Expedition. The Surface Climate of 1963, 1964, *US National Science Foundation and India Meteorological Department*, 1972.

Reichart, G. J., L. J. Lourens, and W. J. Zachariasse, Temporal variability in the northern Arabian Sea oxygen minimum zone (OMZ) during the last 225,000 years, *Paleoceanography*, *13*, 607–621, 1998.

Rieley, G., J. W. Collister, D. M. Jones, G. Eglinton, P. A. Eakin, and A. E. Fallick, Sources of sedimentary lipids deduced from stable isotope analyses of individual compounds, *Nature*, *352*, 425–427, 1991.

Rieley, G., J. W. Collister, B. Stern, and G. Eglinton, Gas chromatography–isotope ratio mass spectrometry of leaf wax *n*-alkanes from plants of differing carbon dioxide metabolisms, *Rapid Communications in Mass Spectrometry*, *7*, 488–491, 1993.

Rommerskirchen, F., G. Eglinton, L. Dupont, U. Güntner, C. Wenzel, and J. Rullkötter, A north to south transect of Holocene southeast Atlantic continental margin sediments: Relationship between aerosol transport and compound–specific δ^{13}C land plant biomarker and pollen records, *Geochemistry Geophysics Geosystems*, *4*, doi: 10.1029/2003GC000,541, 2003.

Rosenthal, Y., and G. P. Lohmann, Accurate estimation of sea surface temperatures using dissolution–corrected calibrations for Mg/Ca paleothermometry, *Paleoceanography*, *17*, 10.1029/2001PA000,749, 2002.

Rosenthal, Y., E. A. Boyle, L. Labeyrie, and D. Oppo, Glacial enrichments of authigenic Cd and U in Subantarctic sediments: A climatic control on the elements' oceanic budget?, *Paleoceanography*, *10*, 395–413, 1995.

Rostek, F., E. Bard, L. Beaufort, C. Sonzogni, and G. Ganssen, Sea surface temperature

and productivity records for the past 240 kyr in the Arabian Sea, *Deep–Sea Research II*, *44*, 1461–1480, 1997.

Schefuß, E., V. Ratmeyer, J.-B. W. Stuut, J. H. F. Jansen, and J. S. S. Damsté, Carbon isotope analyses of *n*–alkanes in dust from the lower atmosphere over the central eastern Atlantic, *Geochim. Cosmochim. Acta*, *67*, 1757–1767, 2003.

Schmidt, G. A., G. R. Bigg, and E. J. Rohling, Global seawater oxygen–18 database, *http://www.giss.nasa.gov/data/018data*, 1999.

Schmidt, M. W., H. J. Spero, and D. W. Lea, Links between salinity variation in the Caribbean and North Atlantic thermohaline circulation, *Nature*, *428*, 160–163, 2004.

Schott, F. A., M. Dengler, and R. Schoenefeldt, The shallow overturning circulation of the Indian Ocean, *Progress in Oceanography*, *53*, 57–103, 2002.

Schrag, D. P., J. F. Adkins, K. McIntyre, J. L. Alexander, D. A. Hodell, C. D. Charles, and J. F. McManus, The oxygen isotopic composition of seawater during the Last Glacial Maximum, *Quat. Sci. Rev.*, *21*, 331–342, 2002.

Schulz, H., U. von Rad, and U. von Stackelberg, in *Paleoclimatology and Paleoceanography from Laminated Sediments*, edited by A. E. S. Kemp, no. 116 in Geological Society Special Publication, pp. 185–207, Blackwell Scientific, Oxford, 1996.

Schulz, H., U. von Rad, and H. Erlenkeuser, Correlation between Arabian Sea and Greenland climate oscillations of the past 110,000 years, *Nature*, *393*, 54–57, 1998.

Schulz, H., U. vonRad, and V. Ittekkot, Plankic foraminifera, particle flux and oceanic productivity off Pakistan, NE Arabian Sea: modern analogues and application to the paleorecord, in *The Tectonic and Climatic Evolution of the Arabian Sea Region*, edited by P. D. Clift, D. Kroon, C. Gaedicke, and J. Craig, no. 195 in Geol. Soc. Spec. Publ., pp. 499–516, The Geological Society, London, 2002.

Sermolli, P., Una carta geobotanica dell'Africa Orientale (Eritrea, Etiopia, Somalia), *Webbia XIII*, *1*, 15–132, 1957.

Shimmield, G. B., S. R. Mowbray, and G. P. Weedon, A 350 ka history of the Indian southwest monsoon: Evidence from deep–sea cores, northwest Arabian Sea, *Trans. R. Soc. Edinburgh Earth Sci.*, *81*, 289–299, 1990.

Simoneit, B. R. T., Compound–specific carbon isotope analyses of individual long–chain alkanes and alkanoic acids in Harmattan aerosols, *Atmos. Environ.*, *31*, 2225–2233, 1997.

Simoneit, B. R. T., R. Chester, and G. Eglinton, Biogenic lipids in particulates from the lower atmosphere over the eastern Atlantic, *Nature*, *267*, 682–685, 1977.

Sirocko, F., Zur akkumulation von Staubsedimenen im nördlichen Indischen Ozean: Anzeiger der Klimagerschichte Arabiens und Indiens, Ph.D. thesis, Geologisch–Paläontologisches Insitut Universität Kiel, 1989.

Sirocko, F., Abrupt change in monsoonal climate: evidence from the geochemical composition of Arabian Sea sediments. Habilitation Thesis, Ph.D. thesis, University of Kiel, 1995.

Sirocko, F., and H. Lange, Clay–mineral accumulation rates in the Arabian Sea during the late Quaternary, *Marine Geology*, *97*, 105–119, 1991.

Sirocko, F., and M. Sarnthein, Wind–borne deposits in the Northwestern Indian Ocean: Record of Holocene sediments versus satellite data, in *Paleoclimatology and Paleometeorology: Modern and Past Patterns of Global Atmospheric Transport*, edited by M. Leinin and M. Sarnthein, no. C 282 in NATO ASI Series, pp. 401–433, Kluwer, Dordrecht/Boston/London, 1989.

Sirocko, F., M. Sarnthein, H. Lange, and H. Erlenkeuser, Atmospheric summer circulation and coastal upwelling in the Arabian Sea during the Holocene and last glaciation, *Quat. Res.*, *36*, 72–93, 1991.

Sirocko, F., M. Sarnthein, H. Erlenkeuser, H. Lange, M. Arnold, and J. C. Duplessy, Century–scale events in monsoonal climate over the past 24,000 years, *Nature*, *364*, 322–324, 1993.

Sirocko, F., D. Garbe-Schönberg, and C. Devey, Processes controlling trace element geochemistry of Arabian Sea sediments during the last 25,000 years, *Global and Planetary Change*, *26*, 217–303, 2000.

Sonzogni, C., E. Bard, and F. Rostek, Tropical sea–surface temperatures during the last glacial period: A view based on alkenones in Indian Ocean sediments, *Quat. Sci. Rev.*, *17*, 1185–1201, 1998.

Southon, J., M. Kashgarian, M. Fontugne, B. Metivier, and W. W.-S. Yim, Marine reservoir corrections for the Indian Ocean and Southeast Asia, *Radiocarbon*, *44*, 167–180, 2002.

Staubwasser, M., and F. Sirocko, On the formation of laminated sediments on the continental margin off Pakistan: the effects of sediment provenance and sediment redistribution, *Marine Geology*, *172*, 43–56, 2001.

Street-Perrott, F. A., Y. Huang, R. A. Perrott, G. Eglinton, P. Barker, L. B. Khelifa, D. D. Harkness, and D. O. Olago, Impact of lower atmospheric carbon dioxide on tropical mountain ecosystems, *Science*, *278*, 1422–1426, 1997.

Stuiver, M., and P. J. Reimer, Extended C–14 data–base and revised Calib 3.0 C–14 age calibration program, *Radiocarbon*, *35*, 215–230, 1993.

Talbot, H. M., R. N. Head, R. P. Harris, and J. R. Maxwell, Distribution and stability of steryl chlorin esters in copepod faecal pellets from diatom grazing, *Org. Geochem.*, *30*, 1163–1174, 1999a.

Talbot, H. M., R. N. Head, R. P. Harris, and J. R. Maxwell, Discrimination against 4-methyl sterol uptake during steryl chlorin ester production by copepods, *Org. Geochem.*, *31*, 871–880, 2000.

Tindale, N. W., and P. P. Pease, Aerosols over the Arabian Sea: Atmospheric transport pathways and concentrations of dust and sea salt, *Deep–Sea Research II*, *46*, 1577–1595, 1999.

Trenberth, K. E., G. W. Branstator, D. Karoly, A. Kumar, N.-C. Lau, and C. Ropelewski, Progress during TOGA in understanding and modeling global teleconnections associated with tropical sea surface temperatures, *J. Geophys. Res.*, *103*, 14,291–14,324, 1998.

Van Campo, E., Pollen transport into Arabian Sea sediments, in *Proceedings of the Ocean Drilling Program, Scientific Results*, edited by W. L. Prell, N. Niitsuma, and et al., vol. 117, pp. 277–280, Ocean Drilling Program, College Station, 1991.

von Rad, U., and M. Tahir, Late Quaternary sedimentation on the outer Indus shelf and slope (Pakistan): evidence from high–resolution seismic data and coring, *Marine Geology*, *138*, 193–236, 1997.

von Rad, U., H. Schulz, V. Riech, M. den Dulk, U. Berner, and F. Sirocko, Multiple monsoon-controlled breakdown of oxygen-minimum conditions during the past 30,000 yeasr documented in laminated sediments off Pakistan, *Palaeogeogr. Palaeoclim. Palaeoecol.*, *152*, 129–161, 1999.

Waelbroeck, C., L. Labeyrie, J. C. Duplessy, J. Guiot, M. Labracherie, H. Leclaire, and J. Duprat, Improving past sea surface temperature estimates based on planktonic fossil faunas, *Paleoceanography*, *13*, 272–283, 1998.

Wang, Y. J., H. Cheng, R. L. Edwards, Z. S. An, J. Y. Wu, C.-C. Shen, and J. A. Dorale, A high-resolution absolute-dated Late Pleistocene monsoon record from Hulu Cave, China, *Science*, *294*, 2345–2348, 2001.

Webster, P. J., The variable and interactive monsoon, in *Monsoons*, edited by J. S. Fein and P. L. Stephens, John Wiley & Sons, 1987.

Webster, P. J., V. O. M. na, T. N. Palmer, J. Shukla, R. A. Tomas, M. Yanai, and T. Yasunari, Monsoons: Processes, predictability and the prospects for prediction, *J. Geophys. Res.*, *103*, 14,451–14,510, 1998.

Wells, J. T., and J. M. Coleman, Deltaic morphology and sedimentology, with special references to the Indus River Delta, in *Marine Geology and Oceanography of Arabian Sea*

and Coastal Pakistan, edited by B. U. Haq and J. D. Milliman, pp. 85–100, Van Nostrand Reinhold Company Inc., New York, 1984.

Zhao, M., G. Eglinton, S. K. Haslett, R. W. Jordan, M. Sarnthein, and Z. Zhang, Marine and terrestrial biomarker records for the last 35,000 years at ODP site 658C off NW Africa, *Org. Geochem.*, *31*, 919–930, 2000.